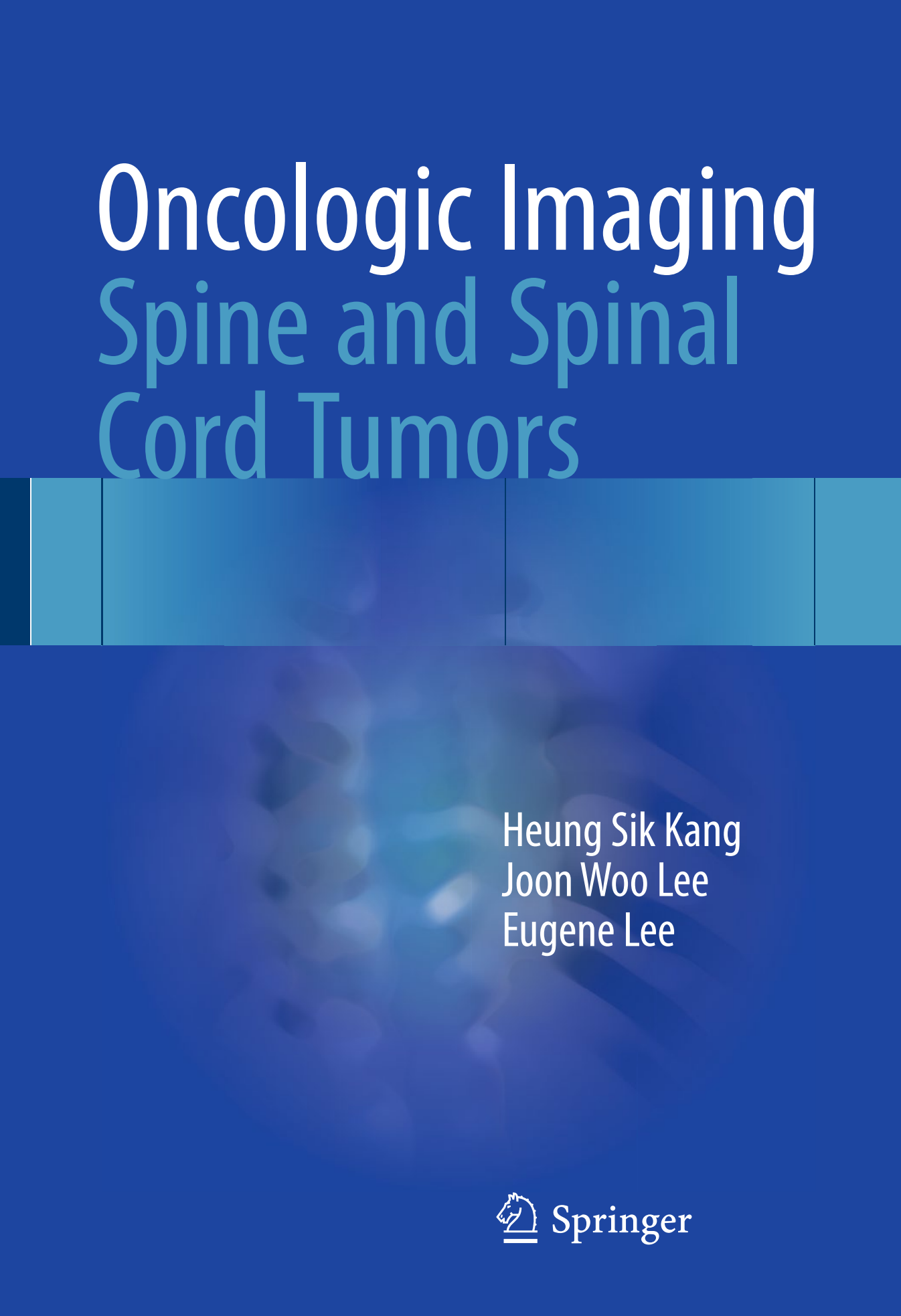


Oncologic Imaging Spine and Spinal Cord Tumors



Heung Sik Kang
Joon Woo Lee
Eugene Lee

 Springer

Oncologic Imaging: Spine and Spinal Cord Tumors

Heung Sik Kang
Joon Woo Lee • Eugene Lee

Oncologic Imaging: Spine and Spinal Cord Tumors



Heung Sik Kang, MD
Department of Radiology
Seoul National University College
of Medicine
Seoul National University Bundang
Hospital
Seongnam
South Korea

Joon Woo Lee, MD
Department of Radiology
Seoul National University College
of Medicine
Seoul National University Bundang
Hospital
Seongnam
South Korea

Eugene Lee, MD
Department of Radiology
Seoul National University Bundang
Hospital
Seongnam
South Korea

ISBN 978-981-287-699-7
DOI 10.1007/978-981-287-700-0

ISBN 978-981-287-700-0 (eBook)

Library of Congress Control Number: 2017931640

© Springer Science+Business Media Singapore 2017

This work is subject to copyright. All rights are reserved by the Publisher, whether the whole or part of the material is concerned, specifically the rights of translation, reprinting, reuse of illustrations, recitation, broadcasting, reproduction on microfilms or in any other physical way, and transmission or information storage and retrieval, electronic adaptation, computer software, or by similar or dissimilar methodology now known or hereafter developed.

The use of general descriptive names, registered names, trademarks, service marks, etc. in this publication does not imply, even in the absence of a specific statement, that such names are exempt from the relevant protective laws and regulations and therefore free for general use.

The publisher, the authors and the editors are safe to assume that the advice and information in this book are believed to be true and accurate at the date of publication. Neither the publisher nor the authors or the editors give a warranty, express or implied, with respect to the material contained herein or for any errors or omissions that may have been made.

Printed on acid-free paper

This Springer imprint is published by Springer Nature
The registered company is Springer Nature Singapore Pte Ltd.
The registered company address is: 152 Beach Road, #22-06/08 Gateway East, Singapore
189721, Singapore

To my co-authors, Joon Woo Lee and Eugene Lee, who proved their excellence and hard work through the publishing process of this book.

Heung Sik Kang

*To God, for his eternal love and support.
To my wife, Cho, for her love and support.*

Joon Woo Lee

To my parents, Lee and Chun, whom I love and respect most in the world.

Thanks to the two respected teachers, Kang and Lee, for their warm heart and understanding.

Eugene Lee

Preface

Tumors of the spine and spinal cord can be neurologically and systemically devastating, and can manifest as nonspecific back pain, making their correct diagnosis crucial for effective prognosis.

However, only a limited number of textbooks are available for clinicians and radiology trainees who are interested in embarking upon a self-learning course in imaging interpretations of spine and spinal cord tumors. With this point in mind, this book consists of three sections: warm-up part of basic concepts, tumor details, and practical tips for differential diagnosis. To enhance the readers' understanding, a total of 538 illustrations have been included.

There are several characteristic features of *Oncologic Imaging: Spine and Spinal Cord Tumors*. First, we describe the compartmental approach and histological basis of imaging appearances and then suggest the systemic approach to image interpretation for spine and spinal cord tumors in Part I. This section will be very useful for trainees in understanding the basic concepts of imaging interpretation for spine and spinal cord tumors. Second, we show the top three tumors for each compartment (e.g., intramedullary) or special condition (e.g., childhood), based on their incidence and clinical impact. For these top three tumors, we provide several cases for the readers to fully understand the imaging characters. Third, we attempt to cover all spine and spinal cord tumors that have been reported until recently according to Google search results, and we present these tumors in an alphabetical order with representative cases. This section will be useful as a quick reference when encountering difficult cases during routine practice. Finally, this book presents common confusing tumors with practical tips for differential diagnoses and case illustrations.

This book is intended for physicians and radiologists caring for patients with spine and spinal cord tumors. We hope that the readers will find this self-learning journey as richly rewarding as it has been for the authors over the course of its preparation.

Finally, we would like to thank Dr. Le Roy Chong for his assistance in editing the manuscript and our clinical fellows (Hoseok Lee, Yun Hee Cho, Yeon Jee Ko, Jiwoon Seo, Chi Young Park, and Yeon Hong Yoon) for their assistance in case preparation.

Seongnam, South Korea

Heung Sik Kang
Joon Woo Lee
Eugene Lee

Contents

Part I Warm-Up: Basic Concepts

1 Compartmental Approach to Spinal Tumors.....	3
1.1 Extradural Versus Intradural Tumor.....	3
1.2 Intradural Extramedullary Versus Intramedullary Tumor	4
1.3 Illustrations: Compartmental Approach to Spinal Tumors	5
1.3.1 Four Compartments of the Spine.....	5
1.3.2 Extradural Versus Intradural Tumor	6
1.3.3 Intradural Extramedullary Versus Intramedullary Tumor.....	8
Bibliography	10
2 Histologic Basis for Imaging Appearances of Spinal Tumors.....	11
2.1 Tumors with Fatty Component	11
2.2 Red Marrow Component	12
2.3 Tumors with Vascular Component.....	12
2.4 Tumors with High Cellularity	12
2.5 Tumors with Hemorrhagic Component	12
2.6 Tumors with Calcification/Ossification	12
2.7 Illustrations: Histologic Basis for Imaging Appearances of Spinal Tumors	13
2.7.1 Tumors with Fatty Component	13
2.7.2 Red Marrow Component	15
2.7.3 Tumors with Vascular Component.....	17
2.7.4 Tumors with High Cellularity	20
2.7.5 Tumors with Hemorrhagic Component	22
2.7.6 Tumors with Calcification/Ossification	23
Bibliography	24
3 Systematic Approach for Image Interpretation of Spinal Tumors.....	25
3.1 Intraosseous Tumors	25
3.1.1 Incidence-Based Approach for Intraosseous Tumors	26
3.1.2 Age-Based Approach for Intraosseous Tumors.....	26

3.1.3	Location-Based Approach for Intraosseous Tumors	26
3.1.4	Imaging Pattern-Based Approach for Intraosseous Tumors	26
3.2	Extradural Non-osseous Spinal Tumors	26
3.2.1	Incidence-Based Approach for Extradural Non-osseous Tumors	26
3.2.2	Imaging Pattern-Based Approach for Extradural Non-osseous Tumors	26
3.3	Intradural Extramedullary (IDEM) Tumors	27
3.3.1	Incidence-Based Approach for IDEM Tumors	27
3.3.2	Age-Based Approach for IDEM Tumors	27
3.3.3	Location-Based Approach for IDEM Tumors	27
3.3.4	Imaging Pattern-Based Approach for IDEM Tumors	27
3.4	Intramedullary (IM) Tumors	27
3.4.1	Incidence-Based Approach of IM Tumors	27
3.4.2	Age-Based Approach for IM Tumors	27
3.4.3	Location-Based Approach for IM Tumors	27
3.4.4	Imaging Pattern-Based Approach for IM Tumors	27
3.4.5	IM Tumors Versus Non-tumorous Myelopathy	28
3.5	Infant/Childhood Spinal Tumors	28
	Bibliography	28

Part II Advanced Steps: Tumor Details

4	Top 3 Spinal Tumors of Each Compartment	31
4.1	Intraosseous Tumors	31
4.1.1	Hemangioma	31
4.1.1.1	Illustrations: Hemangioma	33
4.1.2	Metastasis	35
4.1.2.1	Illustrations: Metastasis	36
4.1.3	Multiple Myeloma	40
4.1.3.1	Illustrations: Multiple Myeloma	41
4.2	Extradural Non-osseous Tumors or Tumorlike Lesions	43
4.2.1	Schwannoma	43
4.2.1.1	Illustrations: Schwannoma	44
4.2.2	Neurofibroma	47
4.2.2.1	Illustrations: Neurofibroma	48
4.2.3	Herniated Intervertebral Disc (HIVD) (Sequestration)	51
4.2.3.1	Illustrations: HIVD (Sequestration)	52
4.3	Intradural Extramedullary (IDEM) Tumors	55
4.3.1	Schwannoma	55
4.3.1.1	Illustrations: Schwannoma	56
4.3.2	Meningioma	59
4.3.2.1	Illustrations: Meningioma	60
4.3.3	Myxopapillary Ependymoma	62
4.3.3.1	Illustrations: Myxopapillary Ependymoma	63

4.4	Intramedullary (IM) Tumors	66
4.4.1	Ependymoma	66
4.4.1.1	Illustrations: Ependymoma.....	67
4.4.2	Astrocytoma.....	70
4.4.2.1	Illustrations: Astrocytoma.....	71
4.4.3	Hemangioblastoma	74
4.4.3.1	Illustrations: Hemangioblastoma	75
4.5	Multi-compartment Tumors.....	77
4.5.1	Lymphoma	77
4.5.1.1	Illustrations: Lymphoma.....	78
4.5.2	Leukemia	80
4.5.2.1	Illustrations: Leukemia	81
4.5.3	Hemangioma	84
4.5.3.1	Illustrations: Hemangioma	85
4.6	Infant/Childhood Spinal Tumors	86
4.6.1	Sacrococcygeal Teratoma	86
4.6.1.1	Illustrations: Sacrococcygeal Teratoma	87
4.6.2	Langerhans Cell Histiocytosis	89
4.6.2.1	Illustrations: Langerhans Cell Histiocytosis	90
4.6.3	Ewing's Sarcoma	93
4.6.3.1	Illustrations: Ewing's Sarcoma	94
	Bibliography	96
5	Common Spinal Tumors Outside the Top 3 Lists	
	(in Alphabetical Order)	99
5.1	Aneurysmal Bone Cyst (ABC)	99
5.1.1	Illustrations: Aneurysmal Bone Cyst (ABC).....	100
5.2	Benign Notochordal Cell Tumor (BNCT)	101
5.2.1	Illustrations: Benign Notochordal Cell Tumor (BNCT)	102
5.3	Bone Island	105
5.3.1	Illustrations: Bone Island.....	106
5.4	Cavernous Malformation (Intramedullary Cavernous Hemangioma, Cavernoma)	109
5.4.1	Illustrations: Cavernous Malformation	110
5.5	Chondrosarcoma	114
5.5.1	Illustrations: Chondrosarcoma.....	115
5.6	Chordoma.....	119
5.6.1	Illustrations: Chordoma	120
5.7	Giant Cell Tumor	123
5.7.1	Illustrations: Giant Cell Tumor	124
5.8	Lipoma.....	128
5.8.1	Illustrations: Lipoma	129
5.9	Osteoblastoma	132
5.9.1	Illustrations: Osteoblastoma.....	133
5.10	Osteochondroma	136
5.10.1	Illustrations: Osteochondroma.....	137

5.11 Osteoid Osteoma	140
5.11.1 Illustrations: Osteoid Osteoma	141
5.12 Osteosarcoma	144
5.12.1 Illustrations: Osteosarcoma	145
5.13 Plasmacytoma	147
5.13.1 Illustrations: Plasmacytoma	148
Bibliography	151
6 Rare But Interesting Spinal Tumors (in Alphabetical Order)	153
6.1 Angiolipoma	153
6.1.1 Illustrations: Angiolipoma	154
6.2 Atypical Teratoid/Rhabdoid Tumor (ATRT)	155
6.2.1 Illustrations: Atypical Teratoid/Rhabdoid Tumor (ATRT)	156
6.3 Chondroblastoma	157
6.3.1 Illustrations: Chondroblastoma	158
6.4 Epidural Hemangioma	159
6.4.1 Illustrations: Epidural Hemangioma	160
6.5 Epithelioid Angiosarcoma	163
6.5.1 Illustrations: Epithelioid Angiosarcoma	164
6.6 Epithelioid Hemangioendothelioma	166
6.6.1 Illustrations: Epithelioid Hemangioendothelioma	167
6.7 Ganglioglioma	168
6.7.1 Illustrations: Ganglioglioma	169
6.8 Ganglioneuroma	170
6.8.1 Illustrations: Ganglioneuroma	171
6.9 Undifferentiated Pleomorphic Sarcoma	172
6.9.1 Illustrations: Undifferentiated Pleomorphic Sarcoma	173
6.10 Malignant Peripheral Nerve Sheath Tumor	175
6.10.1 Illustrations: Malignant Peripheral Nerve Sheath Tumor	176
6.11 Oligodendroglioma	177
6.11.1 Illustrations: Oligodendroglioma	178
6.12 Paraganglioma	179
6.12.1 Illustrations: Paraganglioma	180
6.13 Primitive Neuroectodermal Tumor (PNET)	181
6.13.1 Illustrations: Primitive Neuroectodermal Tumor (PNET)	182
6.14 Solitary Fibrous Tumor (Hemangiopericytoma)	183
6.14.1 Illustrations: Solitary Fibrous Tumor (Hemangiopericytoma)	184
6.15 Teratoma	186
6.15.1 Illustrations: Teratoma	187
Bibliography	188

7 Other Tumor-like Lesions	191
7.1 Epidural Abscess	191
7.1.1 Illustrations: Epidural Abscess	193
7.2 Arachnoid Cyst	195
7.2.1 Illustrations: Arachnoid Cyst	196
7.3 Arachnoiditis	198
7.3.1 Illustrations: Arachnoiditis	199
7.4 Cysticercosis	200
7.4.1 Illustrations: Cysticercosis	201
7.5 Discal Cyst	202
7.5.1 Illustrations: Discal Cyst	203
7.6 Echinococcosis	204
7.7 Extramedullary Hematopoiesis	204
7.7.1 Illustrations: Extramedullary Hematopoiesis	205
7.8 (Vertebral Tophaceous) Gout	207
7.8.1 Illustrations: (Vertebral Tophaceous) Gout	208
7.9 Idiopathic Hypertrophic Pachymeningitis	209
7.9.1 Illustrations: Idiopathic Hypertrophic Pachymeningitis	210
7.10 Perineural (Root Sleeve) Cyst	212
7.10.1 Illustrations: Perineural (Root Sleeve) Cyst	213
7.11 Pigmented Villonodular Synovitis (PVNS)	214
7.11.1 Illustrations: Pigmented Villonodular Synovitis (PVNS)	215
7.12 (Focal) Red Marrow (Hematopoietic Marrow)	216
7.12.1 Illustrations: (Focal) Red Marrow (Hematopoietic Marrow)	217
7.13 Retro-odontoid (Periodontoid) Pseudotumor	218
7.13.1 Illustrations: Retro-odontoid (Periodontoid) Pseudotumor	219
7.14 Facet Synovial Cyst	220
7.14.1 Illustrations: Facet Synovial Cyst	221
7.15 Tuberculosis	223
7.15.1 Illustrations: Tuberculosis	224
7.16 Ventriculus Terminalis	225
7.16.1 Illustrations: Ventriculus Terminalis	226
Bibliography	227

Part III Final Steps: Differential Diagnosis

8 Practical Tips for Differential Diagnosis	231
8.1 Focal Red Marrow Versus Metastasis	232
8.2 Hemangioma Versus Benign Notochordal Cell Tumor (BNCT)	233
8.3 Aggressive Hemangioma Versus Metastasis	234
8.4 Hemangioma Versus Focal Fat Deposition	235

8.5	Metastasis Versus Schmorl's Node	236
8.6	Osteoblastic Metastasis Versus Bone Island	237
8.7	Ependymoma Versus Astrocytoma	238
8.8	Multiple Myeloma Versus Lymphoma.	239
8.9	Intramedullary Metastasis Versus Ependymoma.	240
8.10	Hemangioblastoma Versus Vascular Malformation.	241
8.11	Schwannoma Versus Meningioma.	242
8.12	Herniated Intervertebral Disc (Sequestration) Versus Schwannoma	243
8.13	Sacral Tumors: Chordoma Versus Giant Cell Tumor	244
8.14	Spinal Cord Tumor Versus Non-tumorous Myelopathy	245
8.15	Osteoblastoma Versus Osteosarcoma	246
8.16	Chondrosarcoma Versus Osteosarcoma.	247
8.17	Primary Versus Secondary Aneurysmal Bone Cyst (ABC).	248

Part I

Warm-Up: Basic Concepts

Compartmental Approach to Spinal Tumors

Contents

1.1	Extradural Versus Intradural Tumor	3
1.2	Intradural Extramedullary Versus Intramedullary Tumor	4
1.3	Illustrations: Compartmental Approach to Spinal Tumors	5
1.3.1	Four Compartments of the Spine	5
1.3.2	Extradural Versus Intradural Tumor	6
1.3.3	Intradural Extramedullary Versus Intramedullary Tumor	8
	Bibliography	10

The first step in the compartmental approach to spinal tumors is to determine if the lesion is intraosseous, extradural, intradural extramedullary (IDEM), or intramedullary (IM) in location. The possible differential diagnoses and optimal surgical approaches of these tumors are different depending on their compartmental location. In most cases it is not difficult to identify the compartment in which these tumors are situated on MRI, although it can be confusing in some instances. In the chapter, we will discuss radiological clues that can be helpful in localizing the compartment to which these tumors belong.

1.1 Extradural Versus Intradural Tumor

The main clues favoring an extradural tumor are extrinsic dural sac compression and tumor extension into the neural foramen. With severe tumor compression of the dural sac, however, it can be difficult to tell if the dural/cord compression is extrinsic (by an extradural tumor) or due to a space occupying lesion within the dura (by an intradural tumor). The clue that points toward an extradural tumor lies in the appearance of the subarachnoid space at the margin of the tumor; due to extrinsic compression of the dura, the subarachnoid space between the dura and spinal cord is obliterated at its margin of the tumor. With an intradural tumor, the dura bulges out instead with

a convex appearance, while the cord is compressed by the tumor, resulting in widening of the subarachnoid space at the edge of the tumor.

1.2 Intradural Extramedullary Versus Intramedullary Tumor

The clue that can be used to differentiate an extramedullary from an intramedullary tumor lies in the appearance of the outer contour of the spinal cord at the margin of the tumor. With an extramedullary tumor, the outer contour of the spinal cord at the interface with the tumor is indented upon and compressed by the tumor

resulting in widening of the subarachnoid space, whereas with an intramedullary tumor the outer contour of the spinal cord has a convex bulge resulting in narrowing of the subarachnoid space.

Exophytic intramedullary tumors can occasionally be confusing and mimic appearances of extramedullary tumors, especially in the lower thoracic spinal cord and conus medullaris. In such cases, the axial images have to be reviewed carefully. With intramedullary tumors part of the tumor can be shown to be contiguous with the spinal cord, and if this can be established, it can be concluded that the tumor originates from the spinal cord.

1.3 Illustrations: Compartmental Approach to Spinal Tumors

1.3.1 Four Compartments of the Spine

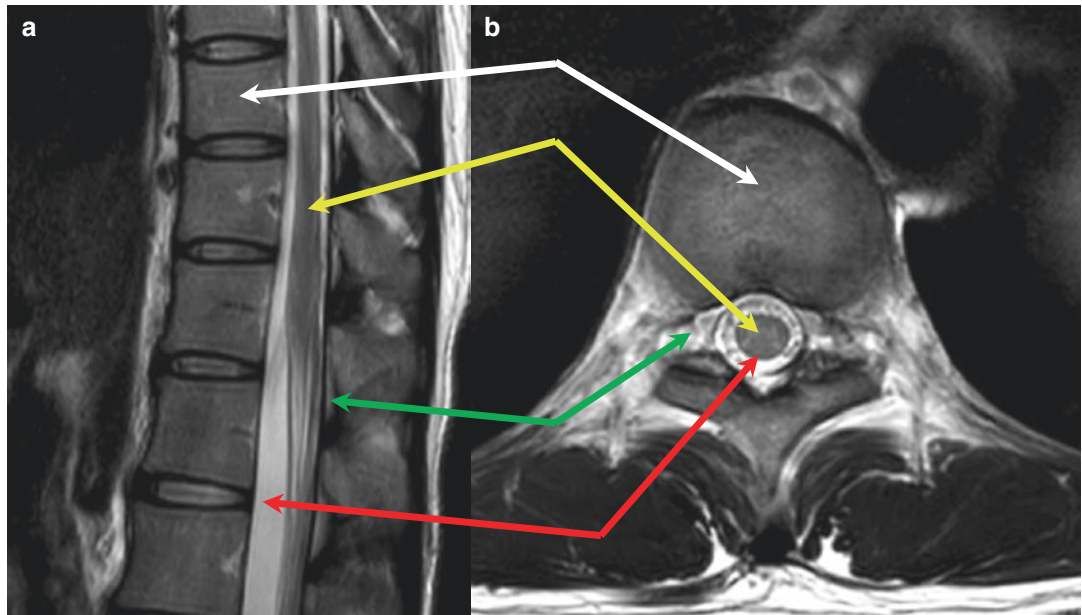


Fig. 1.1 The concept of compartmental locations of the spine on the T2-weighted magnetic resonance (MR) images, sagittal (**a**) and axial (**b**) scans. The compartments are

composed of four different locations: intraosseous (*white arrow*), intramedullary (IM, *yellow arrow*), extradural space (*green arrow*), and intradural extramedullary (*red arrow*)

1.3.2 Extradural Versus Intradural Tumor

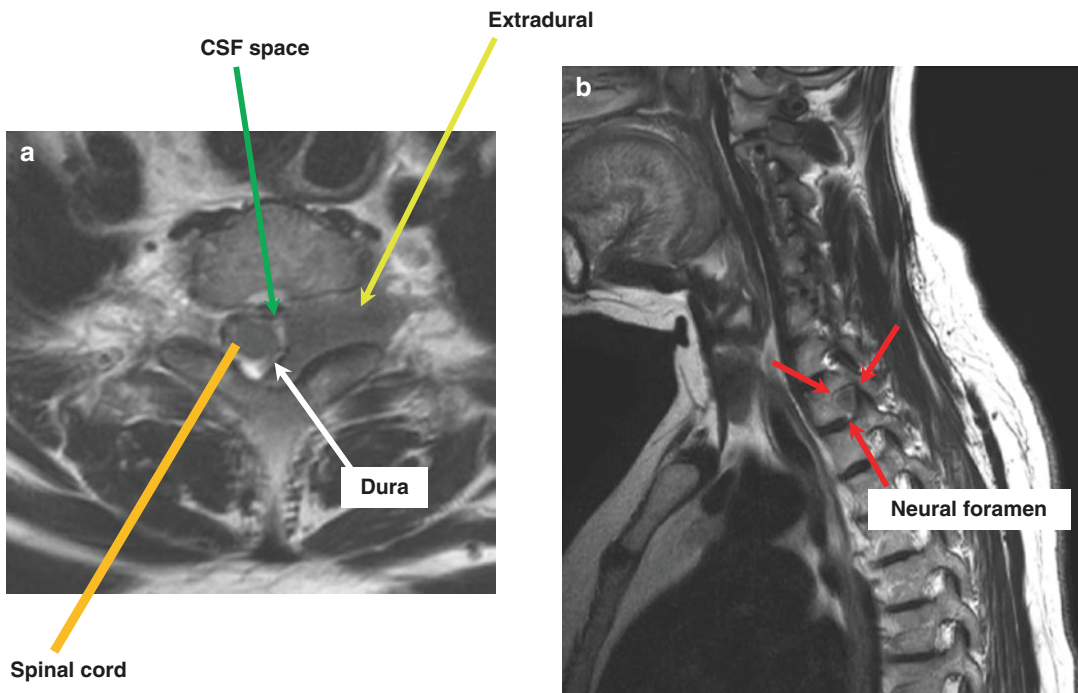


Fig. 1.2 An approximately 2 cm extradural mass encasing the left T1 nerve root in a 58-year-old female. The axial T2-weighted image (**a**) shows extrinsic dural sac compression (white arrow) and tumor extension to the neural foramen (yellow arrow). The subarachnoid

space between the dura and spinal cord (green arrow) is obliterated at the margin of the tumor due to extrinsic compression by the tumor. The sagittal T2-weighted image (**b**) shows widening of the neural foramen due to tumor extension

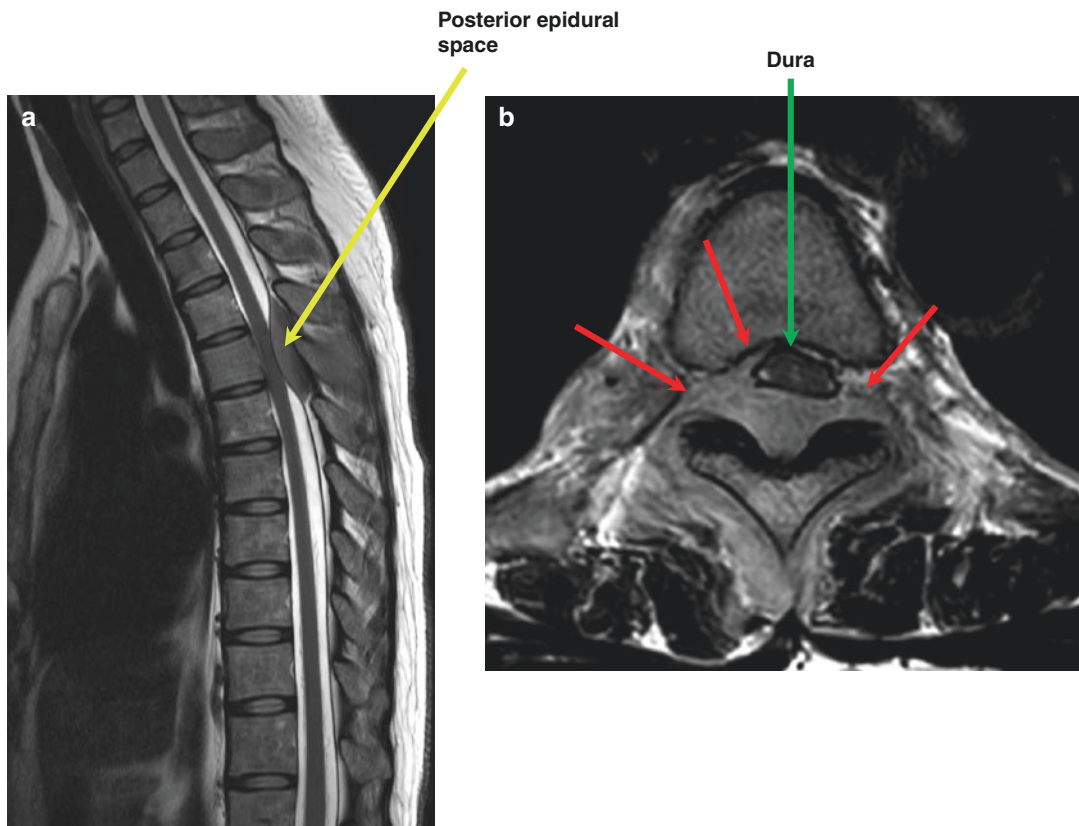


Fig. 1.3 Known B-lymphoblastic lymphoma involvement of the extradural space from T4 to T6 in a 48-year-old female. (a) Tumor is mainly located in the posterior epidural space with dural sac compression (yellow arrow). The subarachnoid space is obliterated anteroposteriorly

with mild cord compression. (b) Axial T2-weighted MR image shows severe tumor compression of the dural sac (green arrow). Tumor also extends into the bilateral neural foramen and anterior epidural space (red arrows)

1.3.3 Intradural Extramedullary Versus Intramedullary Tumor

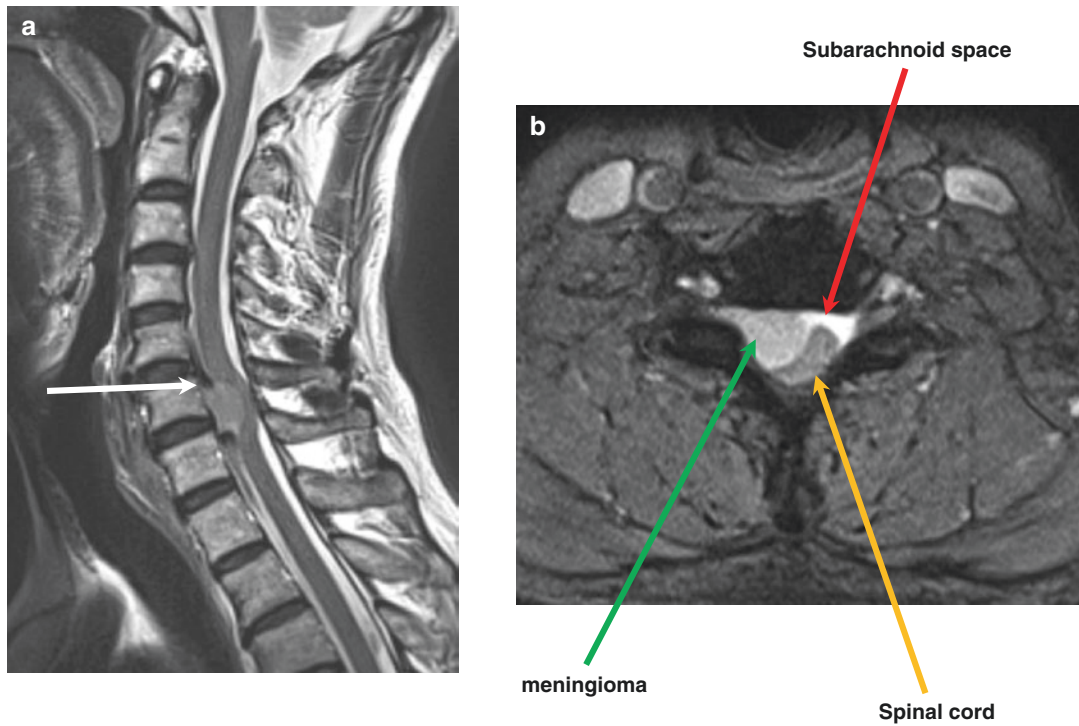


Fig. 1.4 An approximately 1.5 cm intradural extramedullary (IDEM) mass at C6–C7 spinal level in a 63-year-old female. (a) The sagittal T2-weighted image shows a high signal intensity mass with “dural tail sign” (white arrow) combined with craniocaudal flow artifact. There is severe cord compression by the tumor. (b) On the axial T2-weighted MR image, there is left-sided cord deviation

with signal change indicating compressive myelopathy (yellow arrow). The outer contour of the spinal cord at the interface with the tumor is indented and compressed by the tumor resulting in widening of the subarachnoid space (red arrow). All these findings (a, b) are compatible with an intradural extramedullary tumor, such as a meningioma

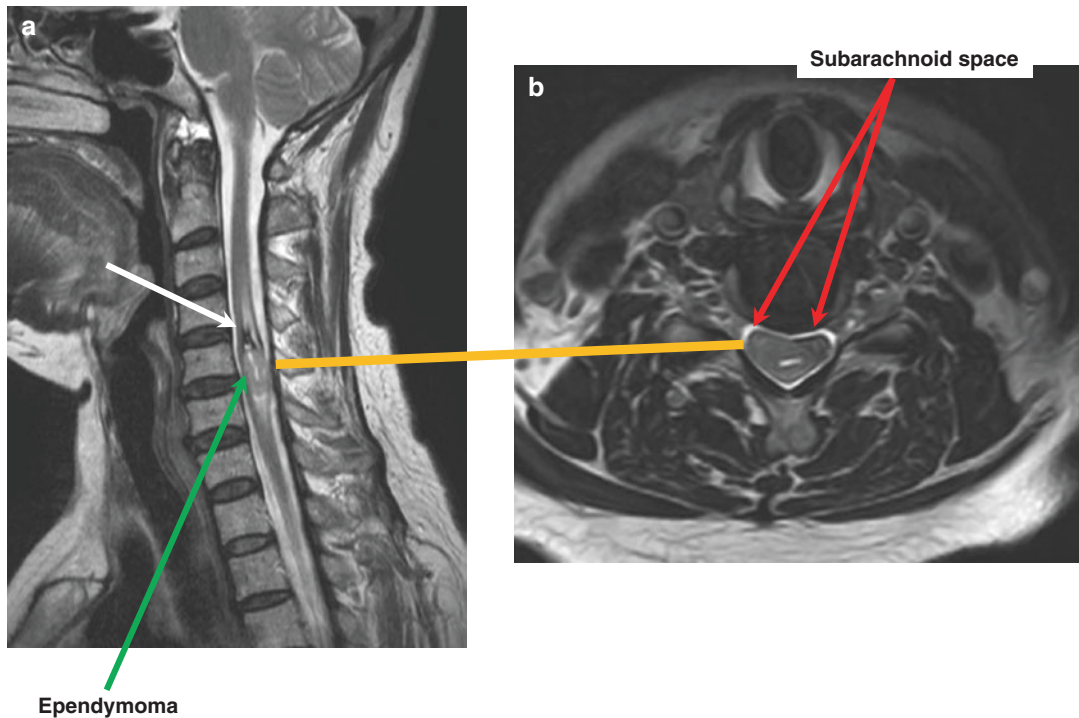


Fig. 1.5 Intramedullary ependymoma at C5–C6 spinal level (green arrow) in a 37-year-old female. (a) The sagittal T2-weighted MR image shows a 1.5 cm well-defined intramedullary mass with surrounding cord edema and hemosiderin deposition (“hemosiderin cap”) at its cranial

aspect (white arrow). (b) The axial T2-weighted MR image shows that the outer contour of the spinal cord has a convex bulge resulting in narrowing of the subarachnoid space (red arrow)

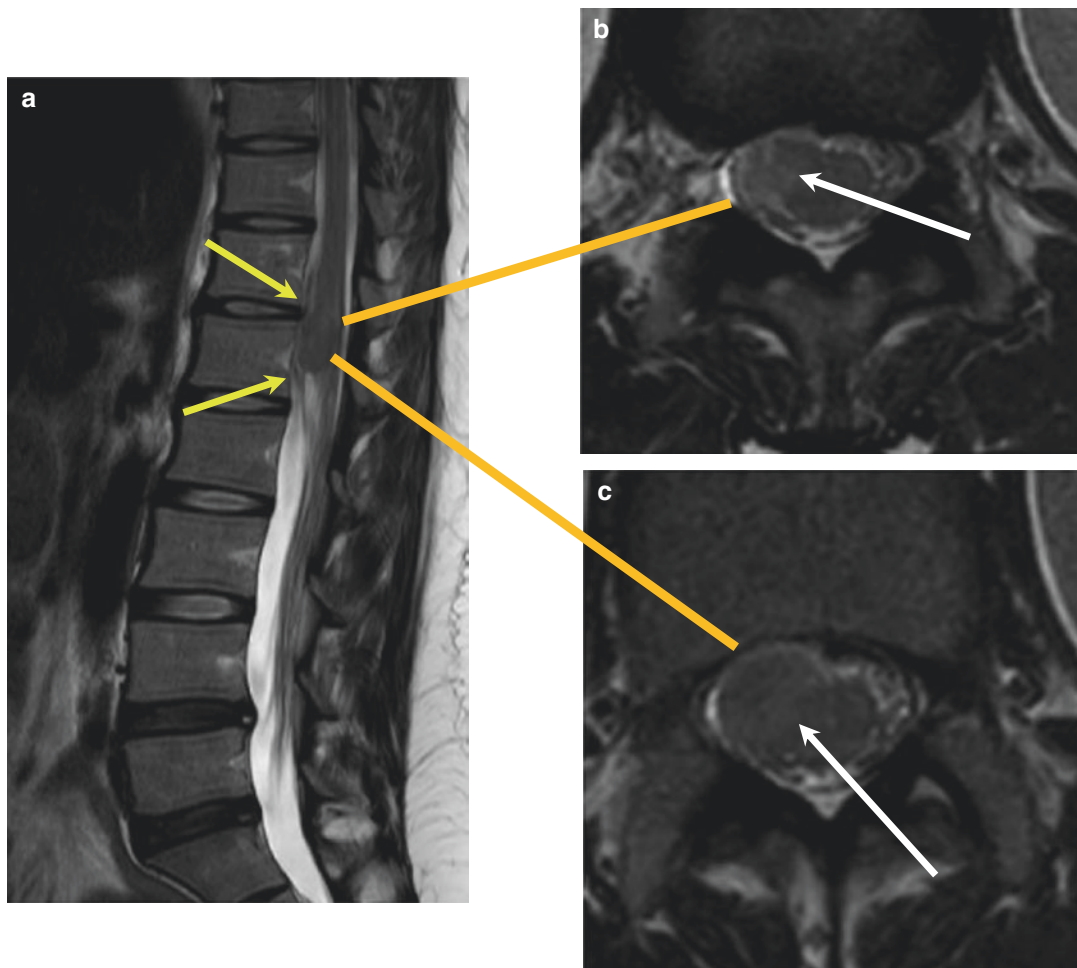


Fig. 1.6 Exophytic intramedullary tumor at the conus medullaris in a 46-year-old female. (a) On the sagittal T2-weighted image, the tumor mimics appearance of an intradural extramedullary tumor with cord compression

(yellow arrow). (b, c) The axial T2-weighted MR images show that part of the tumor is contiguous with the spinal cord (white arrows), and it can be concluded that the tumor originates from the spinal cord

Bibliography

- Kang HS, Lee JW, Kwon JW. Radiology illustrated: spine. Heidelberg: Springer Science & Business Media; 2014.
 Kim DH, Chang U-K, Kim S-H, Bilsky MH. Tumors of the spine. Philadelphia: Elsevier Health Sciences; 2008.

Merhimer Z, Stosic-Opincal T, Thurnher MM. Neuroimaging of spinal tumors. Magn Reson Imaging Clin N Am. 2016;24(3):563–79. doi:[10.1016/j.mric.2016.04.007](https://doi.org/10.1016/j.mric.2016.04.007).

Ross JS, Moore KR. Diagnostic imaging: spine. Philadelphia: Elsevier Health Sciences; 2015.

Cramer GD, Darby SA. Clinical anatomy of the spine, spinal cord, and ANS. Philadelphia: Elsevier Health Sciences, 2013.

Histologic Basis for Imaging Appearances of Spinal Tumors

2

Contents

2.1	Tumors with Fatty Component	11
2.2	Red Marrow Component	12
2.3	Tumors with Vascular Component	12
2.4	Tumors with High Cellularity	12
2.5	Tumors with Hemorrhagic Component	12
2.6	Tumors with Calcification/Ossification	12
2.7	Illustrations: Histologic Basis for Imaging Appearances of Spinal Tumors	13
2.7.1	Tumors with Fatty Component	13
2.7.2	Red Marrow Component	15
2.7.3	Tumors with Vascular Component	17
2.7.4	Tumors with High Cellularity	20
2.7.5	Tumors with Hemorrhagic Component	22
2.7.6	Tumors with Calcification/Ossification	23
	Bibliography	24

It is important to understand the histologic basis for the imaging appearances of spinal tumors in order to arrive at the correct diagnosis or formulate reasonable differential diagnoses. For example, hemangiomas in the vertebral bodies commonly contain fatty stroma and reveal high T1 and T2 signal on MR imaging, which is the main clue for its diagnosis. Highly cellular tumors such as lymphomas show intermediate signal intensity on T2-weighted images, which is also a clue for its diagnosis.

2.1 Tumors with Fatty Component

Fatty components within tumors show high signal on T1-weighted and T2-weighted MR images and can be suppressed with fat suppression MR techniques. The most common tumor containing fatty component is a hemangioma. If we see a fat-containing tumor in the vertebral body, the most probable diagnosis is that of a hemangioma. However, note that in contrast to vertebral hemangiomas, epidural hemangiomas do not show fatty signal in most cases. The most common fat-containing tumor in the epidural space is an angioliopoma, while the most common fat-containing tumors in the paravertebral muscles are lipomas and liposarcomas.

2.2 Red Marrow Component

Red marrow hyperplasia can mimic bony metastasis. Red marrow can show intermediate signal on T1-weighted images with patchy areas of slight enhancement. The signal of red marrow should be isointense or hyperintense to that of the intervertebral disc on T1-weighted images. Similar signal can be seen in multiple myeloma; however, multiple myelomas show strong enhancement in most cases.

2.3 Tumors with Vascular Component

Vascular components of spinal tumors show strong enhancement similar to those seen in venous structures on MRI. Usually, these vascular components show high signal intensity on T2-weighted images; however, in cases of intratumoral hemorrhage areas of low signal intensity can be seen on T2-weighted images. Common vascular tumors of the bony vertebrae include hemangiomas, telangiectatic osteosarcomas, and aneurysmal bone cysts. The common vascular tumors in the epidural space are hemangiomas and angilipomas. The most common vascular tumor in the intradural extramedullary space is a paraganglioma, and the most common vascular tumor in the spinal cord is a hemangioblastoma.

2.4 Tumors with High Cellularity

Highly cellular components of tumors show intermediate signal intensity on T2-weighted images and demonstrate enhancement. This is often seen in lymphomas and meningiomas and can be found in some highly cellular metastases or sarcomas.

2.5 Tumors with Hemorrhagic Component

Hemorrhagic components within tumors can show variable signal intensity depending on the stage of bleeding. Chronic repetitive bleeding can result in hemosiderin deposition within or around the tumor. Hemosiderin is of dark signal on T1-weighted and T2-weighted images. Such signal change can be exaggerated on gradient echo images due to susceptibility blooming artifacts.

2.6 Tumors with Calcification/Ossification

Calcification/ossification can be more easily and reliably detected on CT compared to MR images, demonstrating high attenuation on CT images while on MRI showing low signal intensities on all sequences. Intratumoral calcifications can be seen in chondrosarcomas and meningiomas, while intratumoral ossification can be found in osteoblastomas and osteosarcomas.

2.7 Illustrations: Histologic Basis for Imaging Appearances of Spinal Tumors

2.7.1 Tumors with Fatty Component

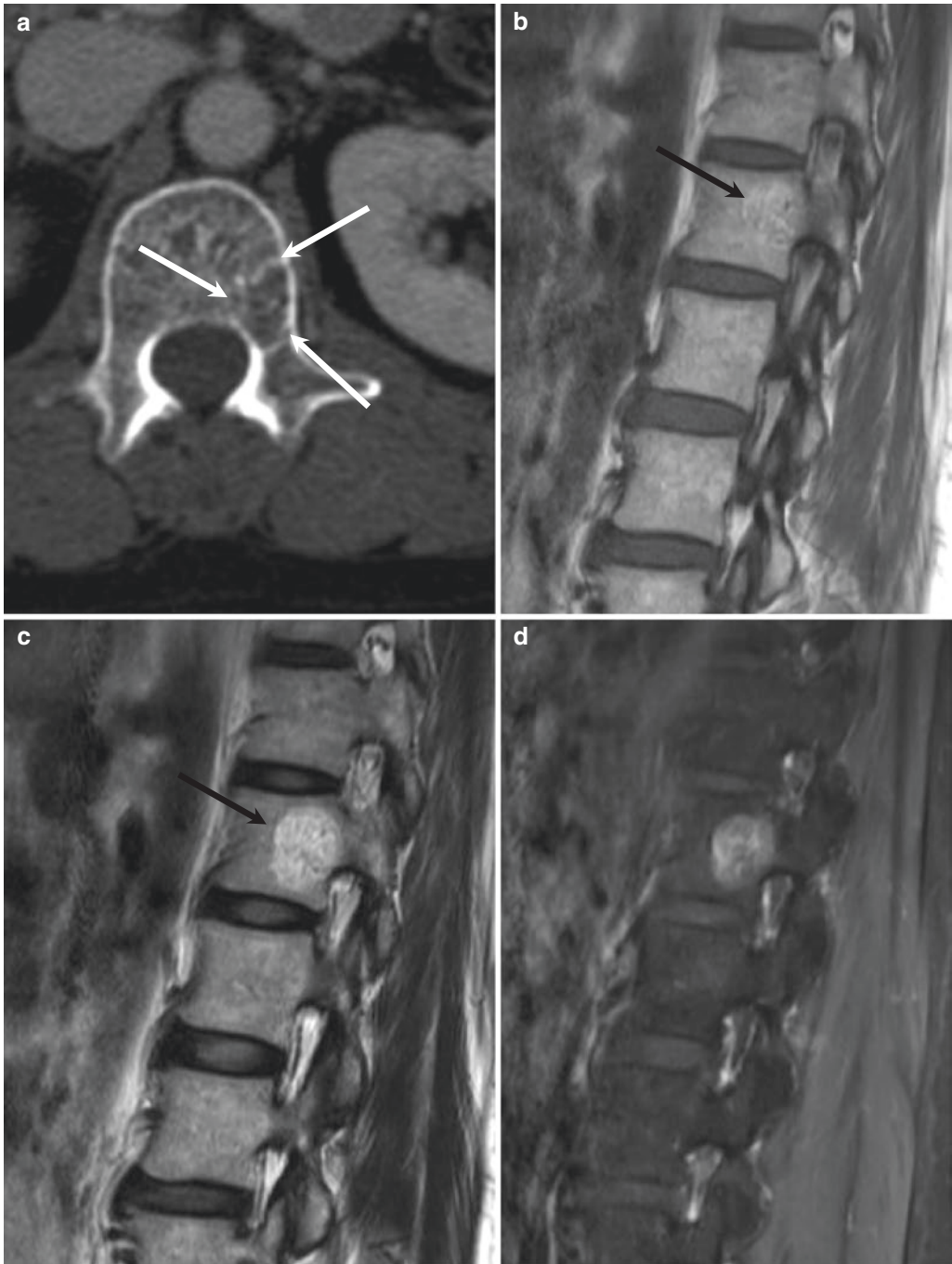


Fig. 2.1 Hemangioma at L1 vertebra in a 57-year-old woman. Axial CT scan of lumbar spine (a) shows an osteolytic lesion in the left posterior corner of the vertebral body with internal dot-like trabeculation (white arrows). T1-weighted sagittal

(b) and T2-weighted sagittal (c) MR images show high signal intensities indicating internal fat component with preserved coarse trabeculation (black arrows). Contrast-enhanced T1-weighted sagittal MR image (d) shows avid enhancement

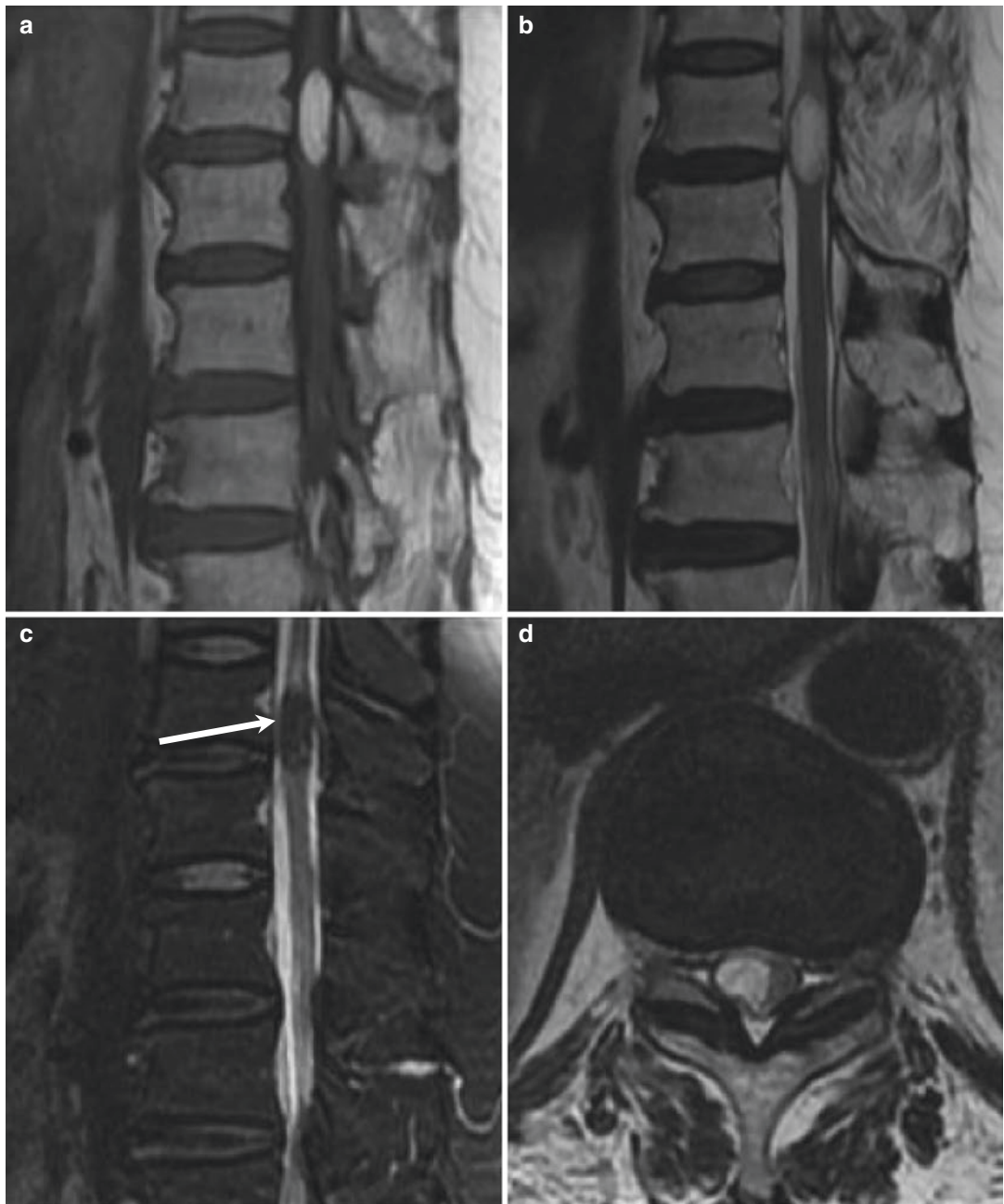


Fig. 2.2 Thoracic intradural lipoma in a 63-year-old woman. T1- and T2-weighted sagittal images (a, b) of the lower thoracic spine show a hyperintense intradural lipoma. On fat-suppressed T2-weighted sagittal image (c),

the mass shows signal dropout suggesting internal fat component (white arrow). T2-weighted axial image (d) shows an intradural lipoma adherent to the dorsolateral thoracic spinal cord

2.7.2 Red Marrow Component



Fig. 2.3 Focal red marrow of the T1 vertebral body in a 60-year-old woman with a history of ovarian cancer. T2-weighted (a) and T1-weighted sagittal MR images show a slightly low signal lesion in the posterosuperior aspect of the T9 vertebral body (whited arrows). On the

T1-weighted image (b), the lesion shows higher signal than the intervertebral disc. Mild contrast enhancement is also noted on contrast-enhanced T-weighted sagittal image (c). After 4 years follow-up MR (d), the contrast enhancement disappeared

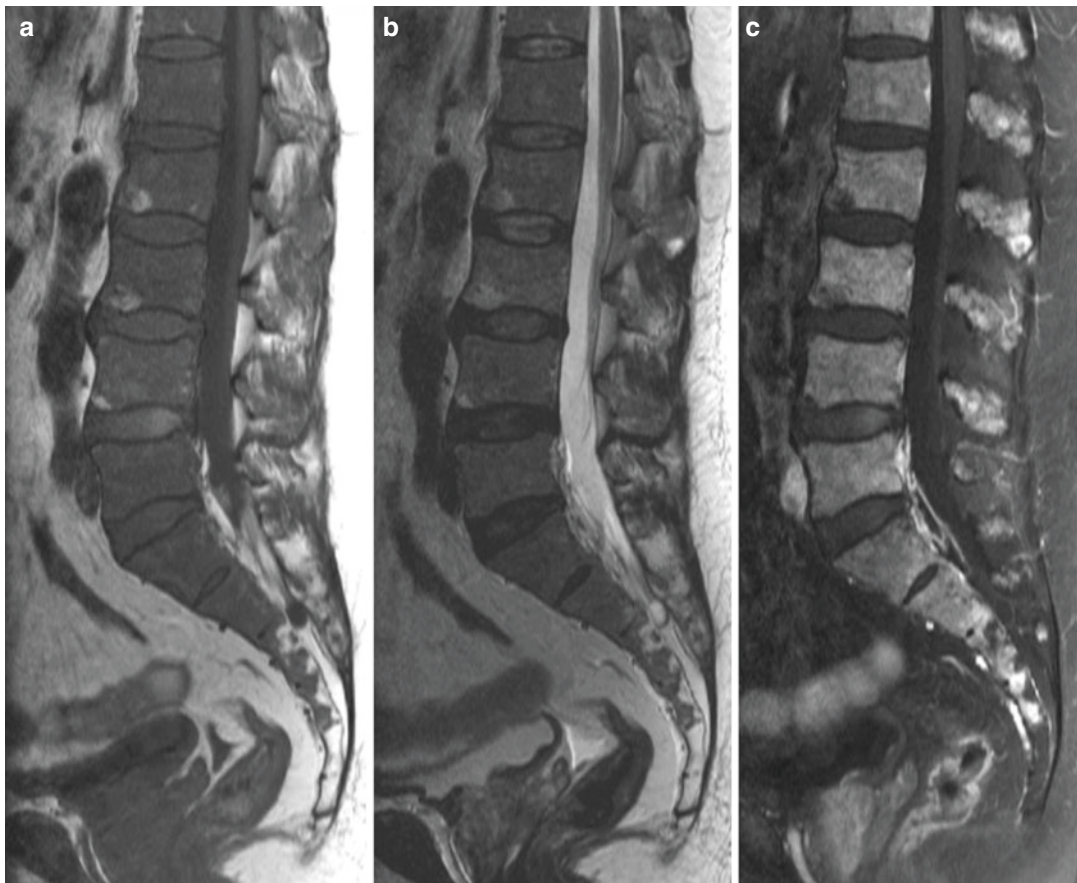


Fig. 2.4 Spine involvement of multiple myeloma in a 72-year-old man. T1-weighted sagittal (a) and T2-weighted (b) MR images of lumbar spine show diffuse low signal intensity involving the entire vertebrae, of

relatively lower signal intensity than the intervertebral discs. Contrast-enhanced T1-weighted sagittal MR image (c) shows diffuse homogeneous enhancement

2.7.3 Tumors with Vascular Component

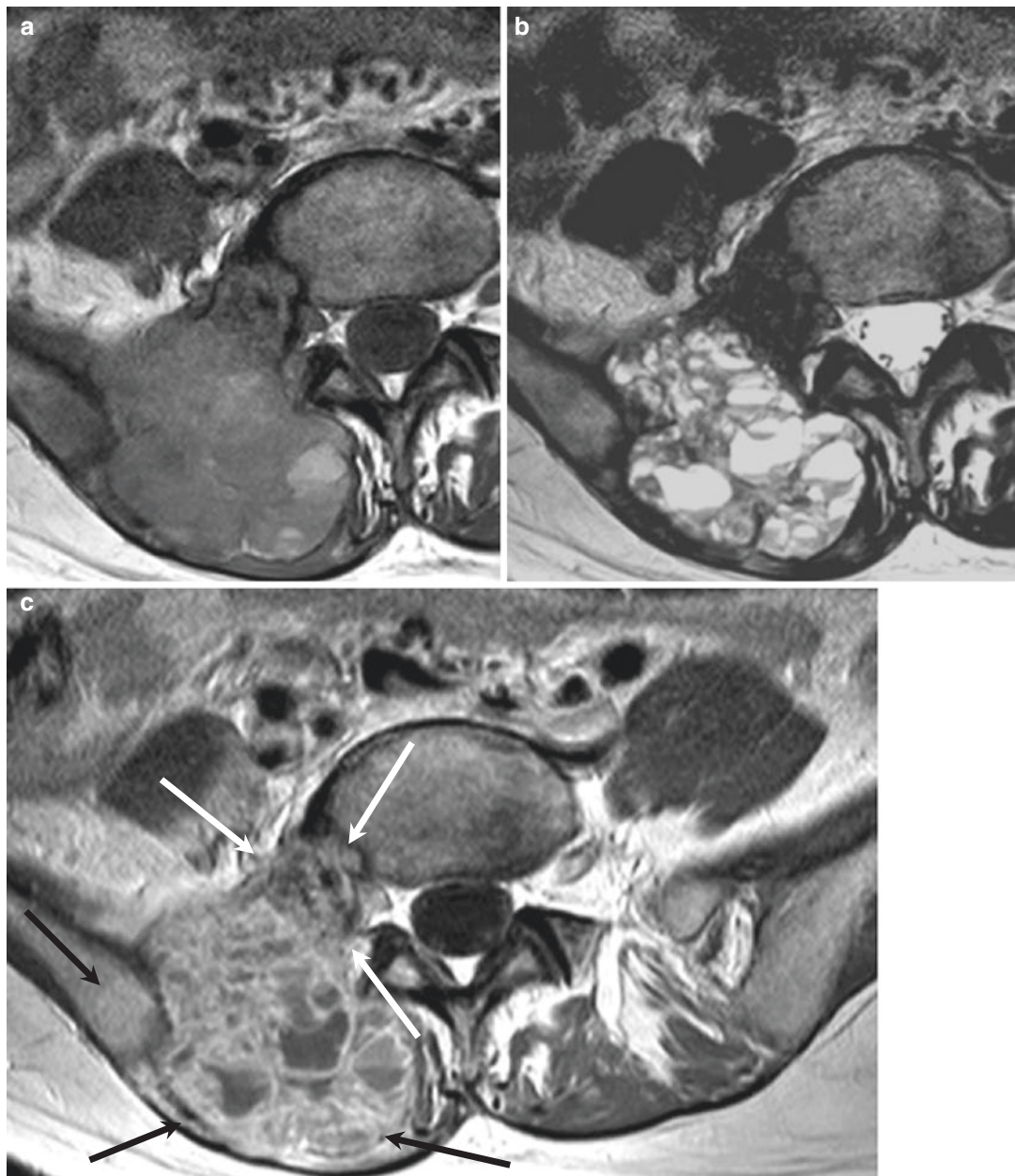


Fig. 2.5 Primary vertebral telangiectatic osteosarcoma in a 21-year-old woman. Axial T1-weighted (a) and T2-weighted (b) MR images at the level of L5 vertebra show a mainly multiloculated cystic, expansile mass with internal fluid-fluid levels due to hemorrhage, originating from the right pedicle, right articular process, and a

portion of the vertebral body. Axial contrast-enhanced T1-weighted fat-saturated MR image (c) at the same level shows a small enhancing solid component near the vertebral body (white arrows) and thin septal enhancement. Ipsilateral back muscles and iliac promontory involvement are also observed (black arrows)

Fig. 2.6 Epidural hemangioma in a 17-year-old man presented with bilateral hand weakness. T2-weighted sagittal MR image (a) shows a multi-lobular mass containing a low signal intensity internal tortuous vessel-like structure in the posterior epidural space of the upper thoracic spine (white arrows). Contrast-enhanced T1-weighted sagittal MR image (b) shows strong enhancement of the lesion



Fig. 2.7 Paraganglioma in a 51-year-old woman. T2-weighted (a) and contrast-enhanced T1-weighted fat suppression (b) sagittal MR images show a large bulky hypervascular intradural mass from L1 to L4 level. The mass shows cystic changes with internal fluid-fluid levels at the top and bottom of the tumor (black arrows). There are extensive enlarged vessels within and around the tumor (white arrows)





Fig. 2.8 Hemangioblastoma in a 22-year-old man. Fat-saturated T1-weighted sagittal image with contrast enhancement (a) and T2-weighted sagittal image (b) show an avidly enhancing mass with extensive syrinx formation

throughout the spinal cord. There are multiple flow voids within the mass and prominent dilated tortuous vessels along the posterior cord surface (*white arrows*)

2.7.4 Tumors with High Cellularity

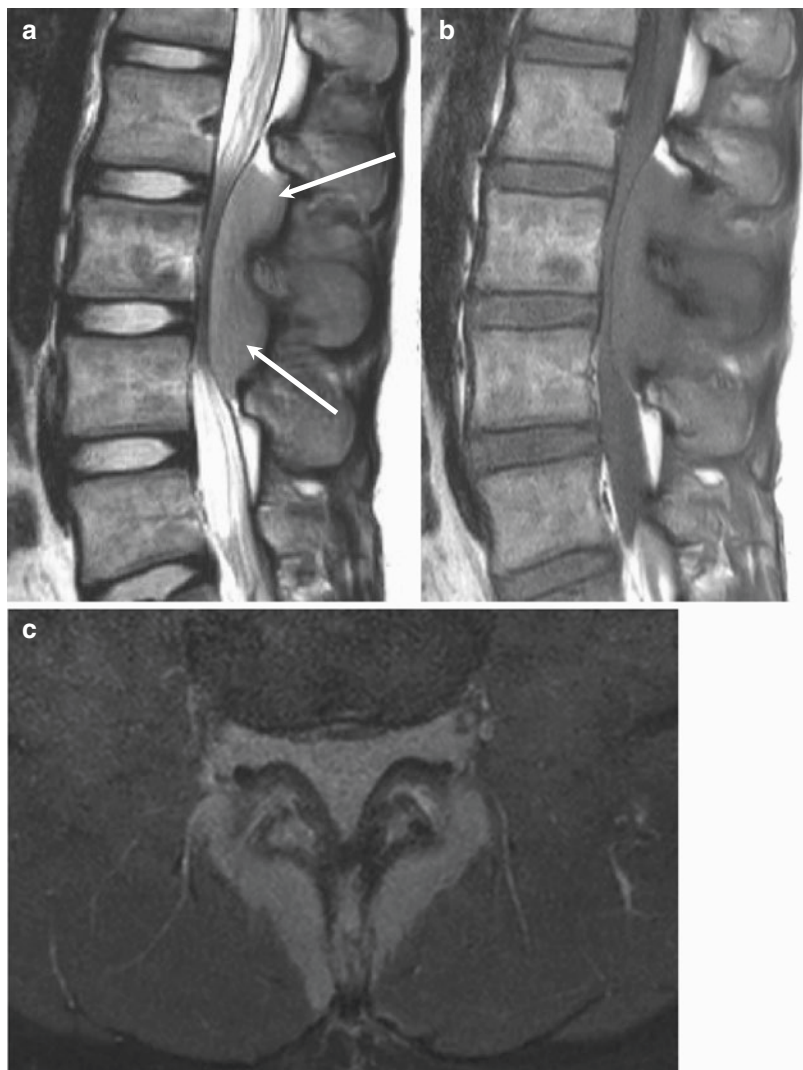


Fig. 2.9 Lymphoma of the lumbar spine in a 19-year-old man. T2- and T1-weighted sagittal MR images (**a, b**) show a diffuse intermediate signal intensity soft tissue mass at the L3 posterior epidural space compressing the dural sac. Note the intermediate T2 signal intensity of the tumor

suggesting highly cellular components (white arrows). Contrast-enhanced T1-weighted fat-suppressed axial MR image (**c**) shows the lesion involving the posterior epidural space, paravertebral muscles, and both lamina and spinous process with homogenous contrast enhancement

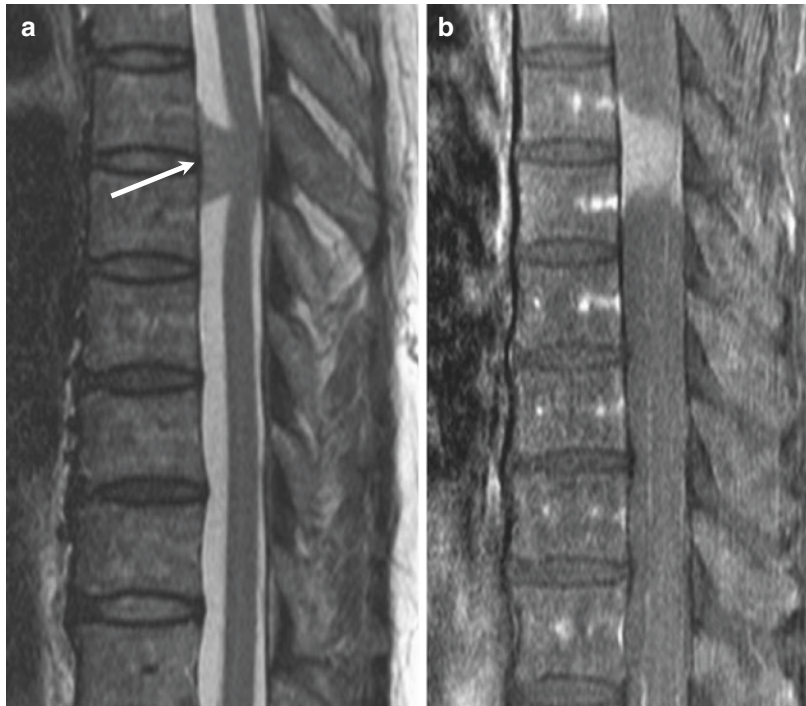


Fig. 2.10 Meningioma at T6/7 level in a 50-year-old woman. T2-weighted sagittal MR image (a) shows a dural-based mass with intermediate signal intensity and cord compression at T6/T7 level. Note the intermediate T2

signal intensity of the tumor suggesting highly cellular components (white arrow). Contrast-enhanced T1-weighted sagittal MR image (b) shows avid enhancement with dural enhancement near the mass (dural tail sign)

2.7.5 Tumors with Hemorrhagic Component

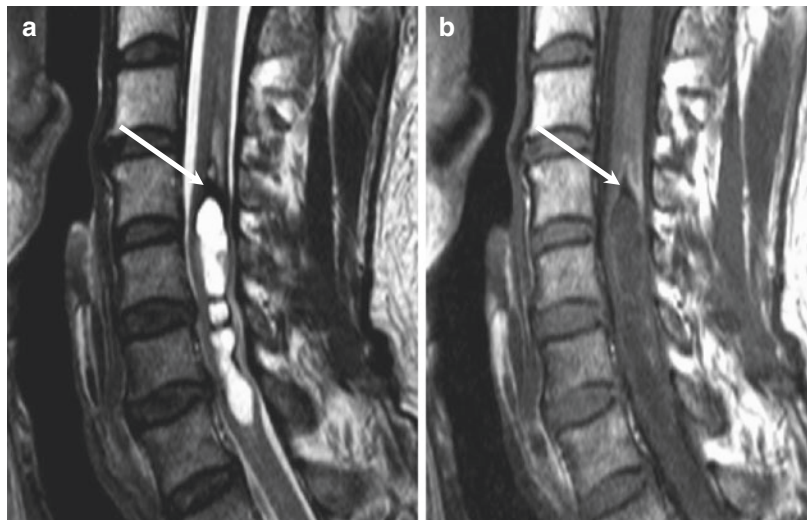


Fig. 2.11 Cellular ependymoma in a 51-year-old man. T2- and T1-weighted sagittal MR images (**a**, **b**) show a large lobulated cystic mass in the cervical spinal cord.

Prominent hemosiderin deposition (dark signal on T2- and T1-weighted images) at the cranial aspect of the tumor is noted (*white arrows*)

2.7.6 Tumors with Calcification/Ossification

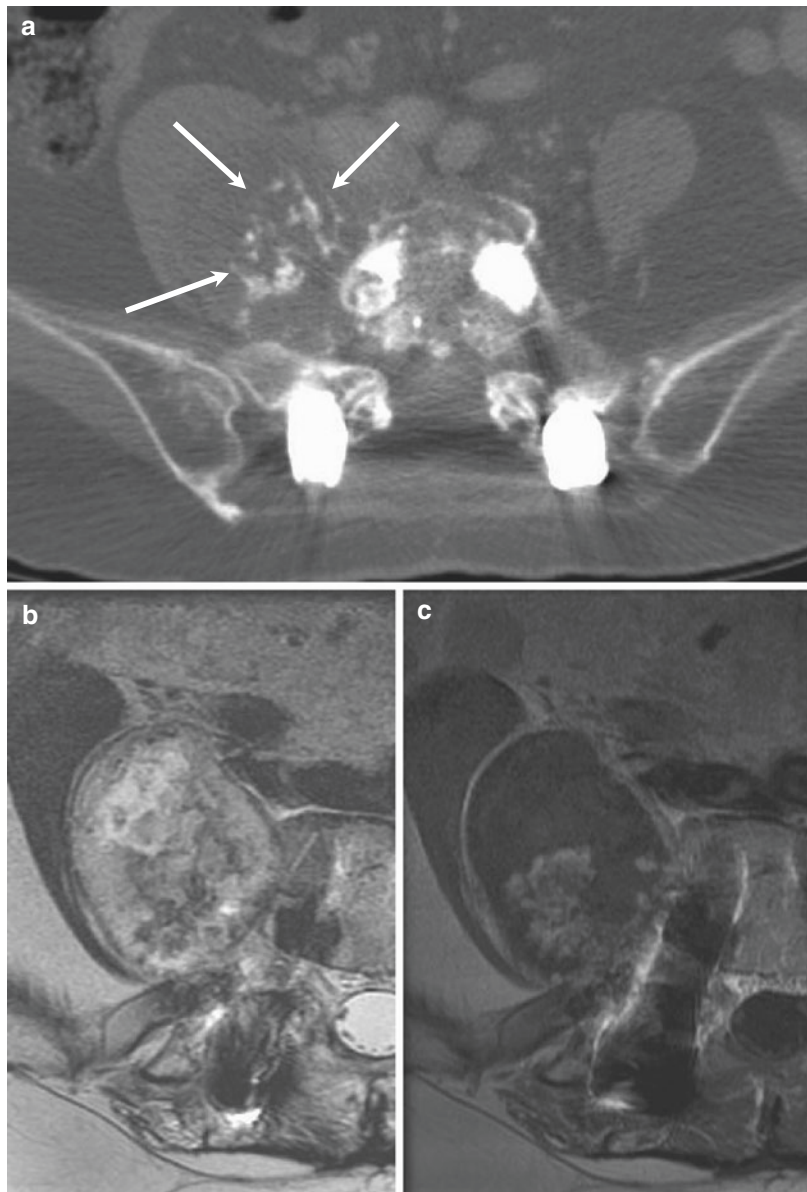


Fig. 2.12 Chondrosarcoma at the right side of L4-L5-S1 vertebral body levels in a 68-year-old woman. Axial CT scan of the lumbar spine (a) shows an oval mass containing ring and stippled calcifications (chondroid matrix) at the right side of the vertebral body (white arrows) with suspicious bony connections to the vertebral body.

Surgical screws of the lumbar spine are seen. T2-weighted axial MR image (b) shows heterogeneous high signal intensity of the lesion. Contrast-enhanced T1-weighted axial MR image (c) shows internal irregular enhancement and some internal septal enhancement

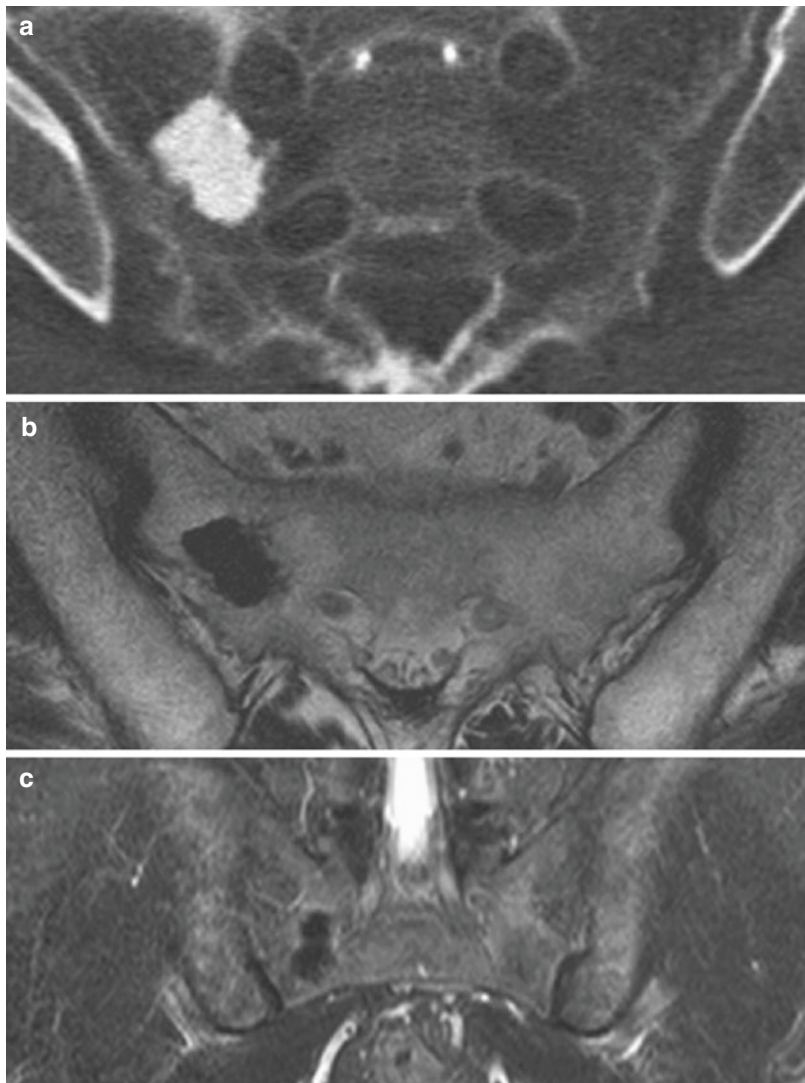


Fig. 2.13 Sacral bone island in a 66-year-old man. Sacral CT axial image (a) shows the dense sclerotic character of the bone island. T2-weighted axial MR image (b) shows a

dark signal intensity lesion of the right sacral wing. Contrast-enhanced T1-weighted coronal image (c) shows no enhancement of the lesion

Bibliography

- Kang HS, Lee JW, Kwon JW. Radiology illustrated: spine. Heidelberg: Springer Science & Business Media; 2014.
 Kim DH, Chang U-K, Kim S-H, Bilsky MH. Tumors of the spine. Philadelphia: Elsevier Health Sciences; 2008.
 Merhimer Z, Stosic-Opincal T, Thurnher MM. Neuroimaging of spinal tumors. Magn Reson Imaging Clin N Am. 2016;24(3):563–79. doi:[10.1016/j.mric.2016.04.007](https://doi.org/10.1016/j.mric.2016.04.007).

- Rodallec MH, Feydy A, Larousserie F, Anract P, Campagna R, Babinet A, et al. Diagnostic imaging of solitary tumors of the spine: what to do and say. Radiographics Rev Publ Radiol Soc N Am Inc. 2008;28(4):1019–41. doi:[10.1148/rg.284075156](https://doi.org/10.1148/rg.284075156).
 Ross JS, Moore KR. Diagnostic imaging: spine. Philadelphia: Elsevier Health Sciences; 2015.
 Cramer GD, Darby SA. Clinical anatomy of the spine, spinal cord, and ANS. Philadelphia: Elsevier Health Sciences, 2013.

Systematic Approach for Image Interpretation of Spinal Tumors

3

Contents

3.1	Intraosseous Tumors	25	3.4.4	Imaging Pattern-Based Approach for IM Tumors	27
3.1.1	Incidence-Based Approach for Intraosseous Tumors	26	3.4.5	IM Tumors Versus Non-tumorous Myelopathy	28
3.1.2	Age-Based Approach for Intraosseous Tumors	26	3.5	Infant/Childhood Spinal Tumors	28
3.1.3	Location-Based Approach for Intraosseous Tumors	26		Bibliography	28
3.1.4	Imaging Pattern-Based Approach for Intraosseous Tumors	26			
3.2	Extradural Non-osseous Spinal Tumors	26			
3.2.1	Incidence-Based Approach for Extradural Non-osseous Tumors	26			
3.2.2	Imaging Pattern-Based Approach for Extradural Non-osseous Tumors	26			
3.3	Intradural Extramedullary (IDEM) Tumors	27			
3.3.1	Incidence-Based Approach for IDEM Tumors	27			
3.3.2	Age-Based Approach for IDEM Tumors	27			
3.3.3	Location-Based Approach for IDEM Tumors	27			
3.3.4	Imaging Pattern-Based Approach for IDEM Tumors	27			
3.4	Intramedullary (IM) Tumors	27			
3.4.1	Incidence-Based Approach of IM Tumors	27			
3.4.2	Age-Based Approach for IM Tumors	27			
3.4.3	Location-Based Approach for IM Tumors	27			

3.1 Intraosseous Tumors

Intraosseous tumors present as osteolytic or osteoblastic lesions on plain X-ray or CT images. On MRI, intraosseous tumors are best detected on T1-weighted or fat-suppressed T2-weighted images. Diffuse tumor marrow infiltration and involvement (such as may be seen in multiple myeloma) can be missed because of its ill-defined nature. The clue pointing toward diffuse bone marrow involvement is the signal of the bone marrow on T1-weighted images compared with the intervertebral discs; if the signal of the bone marrow is hypointense to intervertebral discs, diffuse marrow infiltrative tumors have to be considered.

In analyzing tumors to arrive at logical differential diagnoses, clinical factors such as patient age and tumor incidence are considered, following which tumor location and imaging pattern are evaluated.

3.1.1 Incidence-Based Approach for Intraosseous Tumors

Most common benign bone tumor	Hemangioma
Most common malignant bone tumor	Metastasis

3.1.2 Age-Based Approach for Intraosseous Tumors

Pediatric (< 20 years)	Eosinophilic granuloma (EG), osteoid osteoma, osteoblastoma, Ewing's sarcoma, leukemia
Young adult (20–39 years)	Giant cell tumor, osteosarcoma, osteoblastoma, lymphoma
Middle age (40–59 years)	Metastasis, plasmacytoma
Elderly (> 60 years)	Metastasis, multiple myeloma, chondrosarcoma

3.1.3 Location-Based Approach for Intraosseous Tumors

Vertebral body	Giant cell tumor, hemangioma, benign notochordal cell tumors (BNCT), Langerhans cell histiocytosis
Posterior elements	Sarcoma, osteoid osteoma, osteoblastoma
Diffuse	Metastasis, multiple myeloma, lymphoma, leukemia

3.1.4 Imaging Pattern-Based Approach for Intraosseous Tumors

Benign appearing osseous lesions	Hemangioma, BNCT, EG, fibrous dysplasia
Radiodense tumor on X-ray	Blastic metastases, osteosarcoma, fibrous dysplasia, BNCT, Hodgkin's lymphoma, multiple myeloma
Multi-compartmental lesions	Lymphoma, hemangioma, leukemia, metastases
Extensive reactive change	Osteoid osteoma, osteoblastoma
Fluid-fluid levels	Aneurysmal bone cyst (primary or secondary), telangiectatic osteosarcoma

3.2 Extradural Non-osseous Spinal Tumors

The distinction between extradural and intradural extramedullary tumors is determined by the relationship with the dura. Extradural tumors are located in the epidural space outside the dura. The epidural space contains fat and venous plexuses, which show high signal intensities on T1-weighted images and can demonstrate enhancement. Extradural tumors may extend into the paravertebral space via the neural foramina. Extradural tumors may originate from nerves, fat, and vessels.

3.2.1 Incidence-Based Approach for Extradural Non-osseous Tumors

Most common	Benign nerve sheath tumor (schwannomas, neurofibromas), herniated intervertebral disc (as a tumor mimic)
Rare	Angiolipomas, extradural arachnoid cyst, malignant peripheral nerve sheath tumors (MPNST)

3.2.2 Imaging Pattern-Based Approach for Extradural Non-osseous Tumors

Cystic tumors	Schwannoma, extradural arachnoid cyst, synovial cyst, discal cyst
Tumors with lobular contours	Hemangioma, angiolioma, teratoma
Tumors with hemorrhage	Hemangioma, solitary fibrous tumor
Strong heterogeneous enhancement	Hemangioma, solitary fibrous tumor, paraganglioma
Moderate homogeneous enhancement	Lymphoma, leukemia
Peripheral enhancement	Schwannoma, herniated intervertebral disc
Fatty component	Angiolipoma

3.3 Intradural Extramedullary (IDEM) Tumors

Intradural extramedullary (IDEM) tumors are located within the dura but outside the spinal cord (medulla) and are thus usually found in the subarachnoid space. IDEM tumors can compress the spinal cord easily and can be symptomatic even if the tumor is small. IDEM tumors can originate from nerves (including nerve sheath), meninges, or vessels.

3.3.1 Incidence-Based Approach for IDEM Tumors

Most common	Benign nerve sheath tumor
Second most common	Meningioma

3.3.2 Age-Based Approach for IDEM Tumors

Pediatric	Lipoma, teratoma
Young	Benign nerve sheath tumor
Adult	Meningioma

3.3.3 Location-Based Approach for IDEM Tumors

Cervical	Benign nerve sheath tumor
Thoracic	Meningioma
Lumbar	Benign nerve sheath tumor, myxopapillary ependymoma, paraganglioma

3.3.4 Imaging Pattern-Based Approach for IDEM Tumors

Tumors with high cellularity	Meningioma, lymphoma
Tumors with intralesional calcifications	Meningioma
Hypervascular tumors with AV shunt or superficial siderosis	Ependymoma, paraganglioma, meningeal melanocytoma

Tumors near the conus medullaris or cauda equina	Ependymoma, paraganglioma
Multiple IDEM tumors	Benign nerve sheath tumor, ependymoma, leptomeningeal seeding/metastasis

3.4 Intramedullary (IM) Tumors

Intramedullary tumors are situated within the spinal cord. Intramedullary tumors are true CNS tumors like those found in the brain parenchyma. Intramedullary tumors can cause acute neurologic symptoms if the tumor bleeds.

3.4.1 Incidence-Based Approach of IM Tumors

Most common	Ependymoma
Second most common	Astrocytoma
Third most common	Hemangioblastoma

3.4.2 Age-Based Approach for IM Tumors

Pediatric	Astrocytoma (most common)
Adult	Ependymoma (most common)

3.4.3 Location-Based Approach for IM Tumors

Central	Ependymoma
Eccentric	Astrocytoma
Posterior subpial	Hemangioblastoma

3.4.4 Imaging Pattern-Based Approach for IM Tumors

Tumors with cystic change	Astrocytoma, hemangioblastoma
Tumors with hemorrhage	Ependymoma, cavernous hemangioma, metastasis

Tumors with surrounding extensive cord edema	Metastasis
Multiple IM tumors	Hemangioblastoma

3.4.5 IM Tumors Versus Non-tumorous Myelopathy

IM tumor	Myelitis
Extensive cord swelling	Mild cord swelling
Progression of edema or mass effect	Resolution of edema
Areas of intermediate T2 signal intensity	No areas of intermediate T2 signal intensity
Enhancement in the center of the lesion	Enhancement in the periphery of the lesion
Surrounding syrinx or hemosiderin	No syrinx or hemosiderin

3.5 Infant/Childhood Spinal Tumors

Bone tumors	Eosinophilic granuloma, Ewing's sarcoma, neuroblastoma metastases
-------------	---

Intradural extramedullary tumors	Nerve sheath tumor, ganglioneuroma, lipoma, teratoma
Intramedullary tumors	Pilocytic astrocytoma

Bibliography

- Kang HS, Lee JW, Kwon JW. Radiology illustrated: spine. Heidelberg: Springer Science & Business Media; 2014.
- Kim DH, Chang U-K, Kim S-H, Bilsky MH. Tumors of the spine. Philadelphia: Elsevier Health Sciences; 2008.
- Merhimer Z, Stosic-Opinicai T, Thurnher MM. Neuroimaging of spinal tumors. Magn Reson Imaging Clin N Am. 2016;24(3):563–79. doi:[10.1016/j.mric.2016.04.007](https://doi.org/10.1016/j.mric.2016.04.007).
- Rodallec MH, Feydy A, Larousserie F, Anract P, Campagna R, Babinet A, et al. Diagnostic imaging of solitary tumors of the spine: what to do and say. Radiographics Rev Publ Radiol Soc N Am Inc. 2008;28(4):1019–41. doi:[10.1148/radiographics.284075156](https://doi.org/10.1148/radiographics.284075156).
- Ross JS, Moore KR. Diagnostic imaging: spine. Philadelphia: Elsevier Health Sciences; 2015.
- Cramer GD, Darby SA. Clinical anatomy of the spine, spinal cord, and ANS. Philadelphia: Elsevier Health Sciences, 2013.

Part II

Advanced Steps: Tumor Details

Top 3 Spinal Tumors of Each Compartment

Contents

4.1 Intraosseous Tumors	31	4.5.1.1 Illustrations: Lymphoma	78
4.1.1 Hemangioma	31	4.5.2 Leukemia	80
4.1.1.1 Illustrations: Hemangioma	33	4.5.2.1 Illustrations: Leukemia	81
4.1.2 Metastasis	35	4.5.3 Hemangioma	84
4.1.2.1 Illustrations: Metastasis	36	4.5.3.1 Illustrations: Hemangioma	85
4.1.3 Multiple Myeloma	40	4.6 Infant/Childhood Spinal Tumors	86
4.1.3.1 Illustrations: Multiple Myeloma	41	4.6.1 Sacrococcygeal Teratoma	86
4.2 Extradural Non-osseous Tumors or Tumorlike Lesions	43	4.6.1.1 Illustrations: Sacrococcygeal Teratoma	87
4.2.1 Schwannoma	43	4.6.2 Langerhans Cell Histiocytosis	89
4.2.1.1 Illustrations: Schwannoma	44	4.6.2.1 Illustrations: Langerhans Cell Histiocytosis	90
4.2.2 Neurofibroma	47	4.6.3 Ewing's Sarcoma	93
4.2.2.1 Illustrations: Neurofibroma	48	4.6.3.1 Illustrations: Ewing's Sarcoma	94
4.2.3 Herniated Intervertebral Disc (HIVD) (Sequestration)	51	Bibliography	96
4.2.3.1 Illustrations: HIVD (Sequestration)	52		
4.3 Intradural Extramedullary (IDEM) Tumors	55		
4.3.1 Schwannoma	55		
4.3.1.1 Illustrations: Schwannoma	56		
4.3.2 Meningioma	59		
4.3.2.1 Illustrations: Meningioma	60		
4.3.3 Myxopapillary Ependymoma	62		
4.3.3.1 Illustrations: Myxopapillary Ependymoma	63		
4.4 Intramedullary (IM) Tumors	66		
4.4.1 Ependymoma	66		
4.4.1.1 Illustrations: Ependymoma	67		
4.4.2 Astrocytoma	70		
4.4.2.1 Illustrations: Astrocytoma	71		
4.4.3 Hemangioblastoma	74		
4.4.3.1 Illustrations: Hemangioblastoma	75		
4.5 Multi-compartment Tumors	77		
4.5.1 Lymphoma	77		

4.1 Intraosseous Tumors

4.1.1 Hemangioma

1. Epidemiology
 - Peak incidence: 30–50 years old, tendency to increase in size with age
 - Asymptomatic: M = F
 - Symptomatic: M < F
2. Location
 - Thoracic spine (60%) > lumbar spine (29%) > cervical spine (6%) > sacrum (5%)
 - Vertebral body >> posterior elements

3. Characteristic imaging findings

- Well-defined round or lobular intraosseous masses
- Thickened trabeculation on X-ray, CT, MR
- High signal on T1-weighted and T2-weighted images
- Avid enhancement

4. Spectrum of imaging findings

- Low signal on T1-weighted images in vascular (aggressive, symptomatic) hemangioma
- Poor enhancement in sclerosing hemangioma
- Both epidural and vertebral body involvement

5. Differential diagnosis

- Benign notochordal cell tumor
 - Sclerosis on CT
 - Low signal on T1-weighted images
 - No enhancement
- Metastasis
 - Cortical destruction
 - Low signal on T1-weighted images
- Focal fat
 - Irregular shape
 - No enhancement

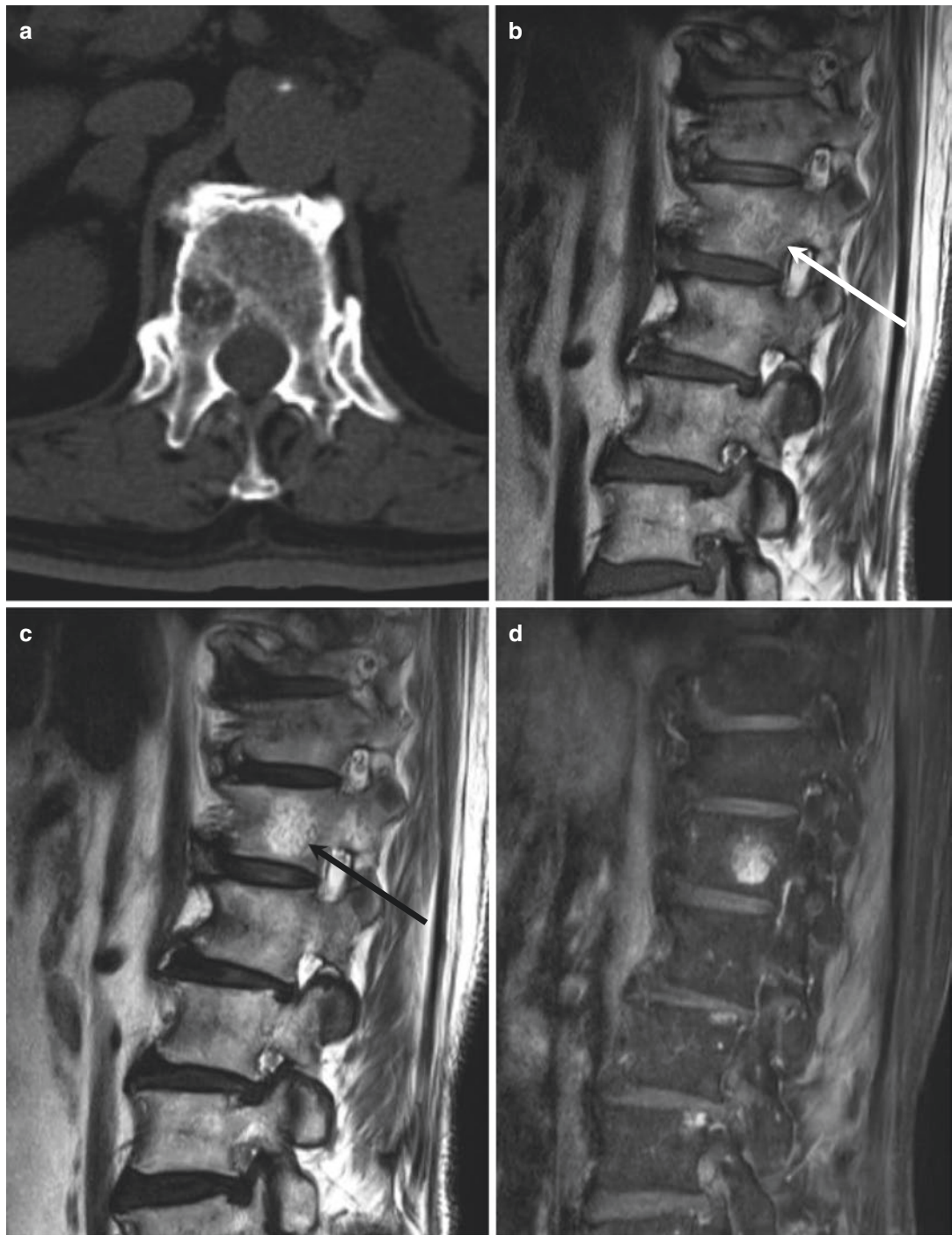
4.1.1.1 Illustrations: Hemangioma

Fig. 4.1 Hemangioma of the T12 vertebra in a 76-year-old woman. Axial CT scan of the lumbar spine (a) shows small osteolytic lesion in the right posterior corner of the vertebral body. T1-weighted sagittal MR image (b) shows subtle low signal intensity with a hyperintense rim (white

arrow). T2-weighted sagittal MR image (c) shows high signal intensity with preserved internal trabeculation (black arrow). Contrast-enhanced T1-weighted sagittal MR image (d) shows enhancement

Fig. 4.2 Hemangioma of the L1 vertebra in a 78-year-old woman. Axial CT scan of the lumbar spine (**a**) shows an osteolytic lesion involving the entire vertebral body with internal dot-like trabeculation. T1-weighted sagittal (**b**) and T2-weighted sagittal (**c**) MR images show a heterogeneous low signal intensity lesion with preserved coarse trabeculations (white arrows). Contrast-enhanced T1-weighted sagittal MR image (**d**) shows avid enhancement



4.1.2 Metastasis

1. Epidemiology

- Middle age and elderly (can be seen in all ages)
- Men: from prostate cancer, lung cancer
- Women: from breast cancer, lung cancer

2. Location

- Thoracic spine (70%), lumbar spine (20%), cervical spine (10%)
- Common in vertebral body

3. Characteristic imaging findings

- Osteolytic (70%), osteoblastic (9%), mixed (21%) pattern
- Osteolytic masses
 - With cortical destruction and paravertebral extension
 - Malignant compression fracture: complete replacement of the bone marrow
 - Different signal characteristics and aggressiveness depending on primary tumors
- Osteoblastic mass with peripheral enhancement
 - Common in breast cancer and prostate cancer
 - Irregular sclerotic mass on X-ray and CT with endplate depression
 - Hypointense signal on T1-weighted and T2-weighted MR images
 - Peripheral enhancement
- Mixed pattern
 - Osteolytic and osteoblastic masses in the spine

4. Spectrum of imaging findings

- Malignant compression fracture.
 - Complete replacement of the bone marrow signal in the vertebral body
 - Convex posterior margin of vertebral body
 - Hypointense signal on T1-weighted images

- Strong enhancement or internal irregular non-enhancing areas

- Epidural mass with biconcavity due to midline septum

- Single lesion can be possible.

- Sclerotic rim around the tumors can be seen.

- Slow-growing metastases in thyroid cancer.

- Direct invasion from retroperitoneal or mediastinal metastasis.

5. Differential diagnosis

- Aggressive hemangioma
 - Thickened trabeculation
- Red marrow hyperplasia/red marrow reconversion
 - Isointense or hyperintense signal than intervertebral disc on T1-weighted images
 - Patchy enhancement
- Schmorl's node (intravertebral disc herniation)
 - Cortical depression on T1-weighted image or CT
 - Same signal as intervertebral disc
- Multiple myeloma
 - Diffuse or variegated involvement
 - Benign osteoporotic pattern of compression fracture
- Lymphoma
 - Multi-compartment without definable cortical breakage
 - Homogeneous signal character
 - Younger age
- Tuberculosis
 - Subligamentous extension
 - Intraosseous rim-like enhancement
- Polyostotic fibrous dysplasia
 - Ground glass opacity
 - Bony overgrowth or remodeling
- Lymphangiomatosis
 - Cystic nature
 - No interval change

4.1.2.1 Illustrations: Metastasis

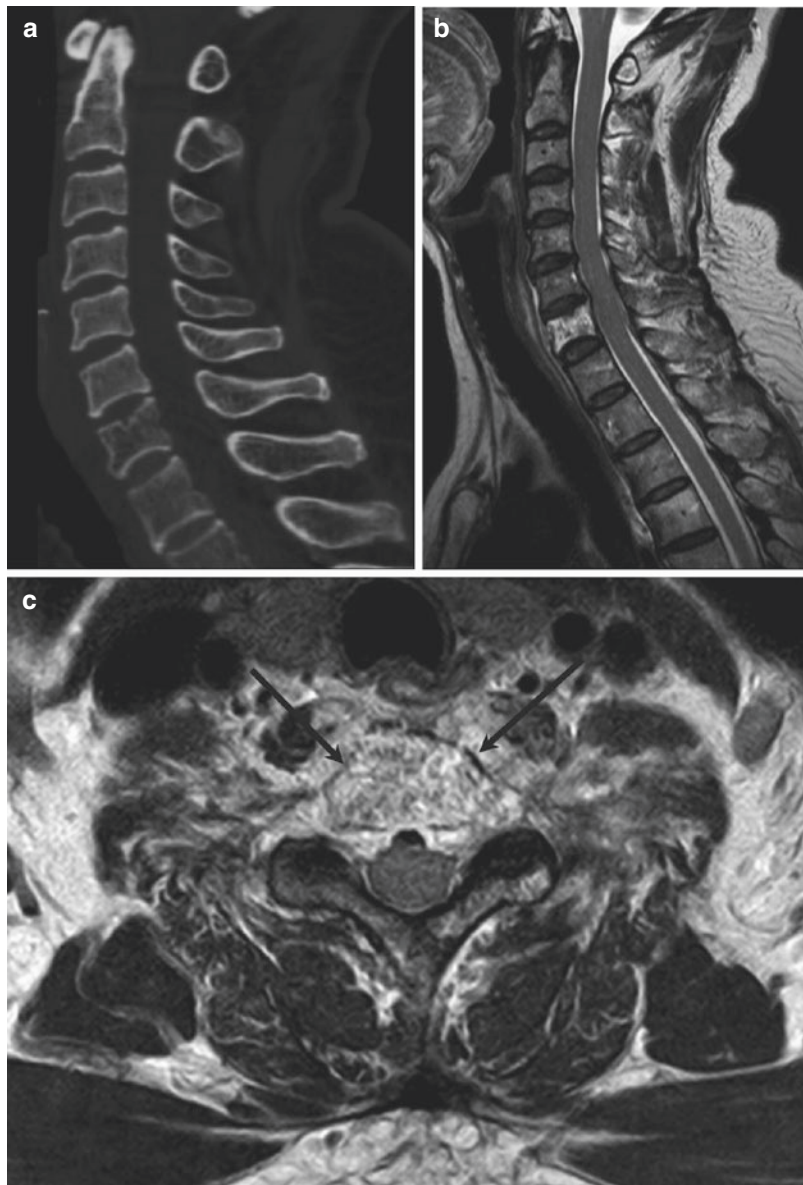


Fig. 4.3 Metastasis of C7 in a 76-year-old woman with underlying pancreatic adenocarcinoma. Sagittal CT scan of cervical spine (a) shows an ill-defined osteolytic lesion involving the entire vertebral body. T2-weighted sagittal (b) and axial (c) MR images show a heterogeneous high signal intensity lesion with paravertebral and epidural

extension (*black arrows*). T1-weighted sagittal MR image (d) shows low signal intensity involving the whole vertebral body, of relatively lower signal intensity than that of the intervertebral disc. Contrast-enhanced T1-weighted sagittal MR image (e) shows faint enhancement with avid paravertebral and epidural soft tissue enhancement



Fig. 4.3 (continued)

Fig. 4.4 Metastases of the L2, L3, and L4 vertebrae in a 35-year-old woman with breast cancer. Coronal CT scan of the lumbar spine (a) shows an osteoblastic L2 vertebral body lesion. T1-weighted sagittal MR image (b) shows heterogeneous low signal intensity foci involving the L2, L3, and L4 vertebral bodies (white arrows). T2-weighted sagittal MR image (c) shows heterogeneous low signal intensity areas. Contrast-enhanced T1-weighted sagittal MR image (d) shows heterogeneous enhancement

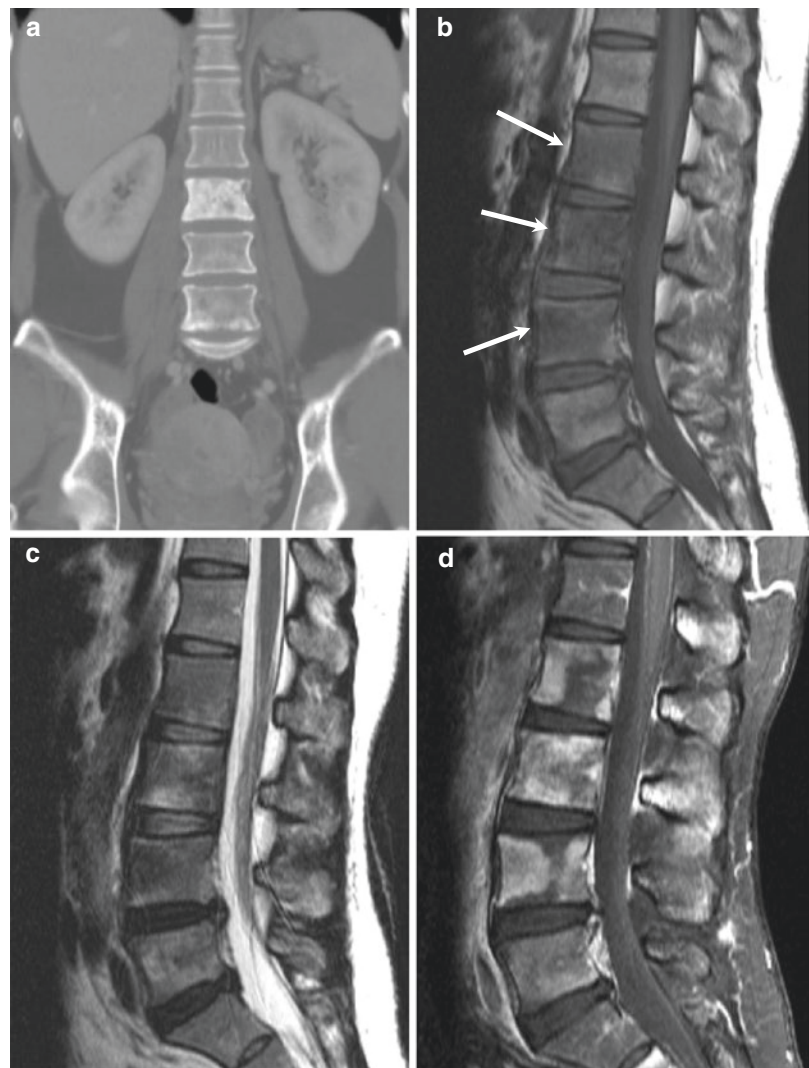
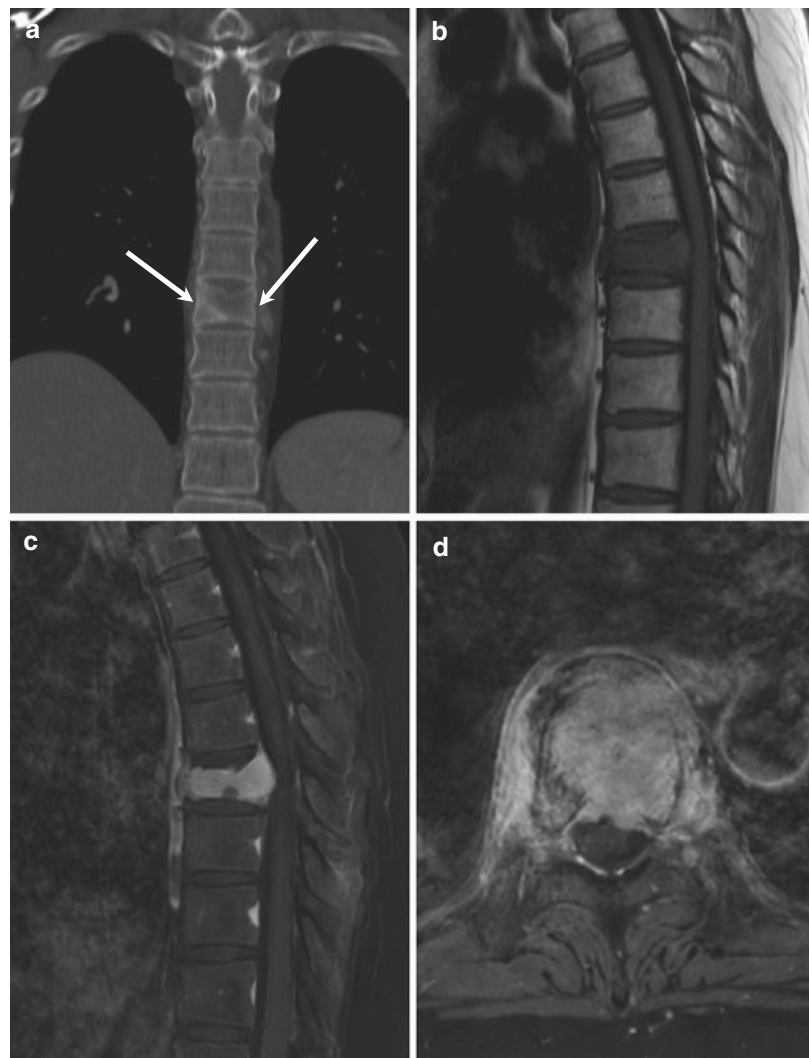


Fig. 4.5 Metastasis of the T8 vertebra in a 48-year-old woman with renal cell carcinoma. Coronal CT scan of the thoracic spine (**a**) shows an osteolytic lesion in the left side of the T8 vertebral body with decreased vertebral height (white arrows). T1-weighted sagittal MR image (**b**) shows diffuse low signal intensity involving the entire T8 vertebral body in keeping with a pathologic compression fracture, of relatively lower signal intensity than the intervertebral disc. Contrast-enhanced T1-weighted sagittal (**c**) and axial (**d**) MR images show diffuse homogeneous enhancement with paravertebral and epidural extension



4.1.3 Multiple Myeloma

1. Epidemiology

- 50–60 years old
- M > F

2. Location

- Diffuse involvement
- Compression fracture: 87% in T6 ~ L4

3. Characteristic imaging findings

- Variegated pattern
 - Salt-and-pepper appearance
 - Tiny, innumerable T1-hypointense nodules in the whole spine: strong enhancement even within tiny nodules
- Diffuse pattern
 - Diffuse T1-hypointensity of the bone marrow involving the whole spine
 - Lower signal than intervertebral disc on T1-weighted image
- Multinodular pattern
 - Similar character as multiple metastases
- Benign osteoporotic pattern of compression fractures

4. Spectrum of imaging findings

- Sclerotic mass in the vertebral body.
- One of the features in POEMS syndrome (M-spike = multiple myeloma).

- Normal bone marrow pattern is possible.
- Single lesion: plasmacytoma.

5. Differential diagnosis

- Red marrow hyperplasia/red marrow reconversion
 - Isointense or hyperintense signal to intervertebral disc on T1-weighted images
 - Patchy enhancement
- Lymphoma
 - Multi-compartment: bone, epidural, leptomeningeal
 - Homogeneous signal
 - Stronger enhancement
- Metastases
 - Multiple nodular masses
 - Heterogeneous enhancement
 - Cortical destruction
- Osteoporosis in elderly
 - Patchy areas of marrow inhomogeneity due to fatty deposition and red marrow hyperplasia
 - Low signal area of bone marrow
 - Irregular shape
 - Same or higher signal than intervertebral disc

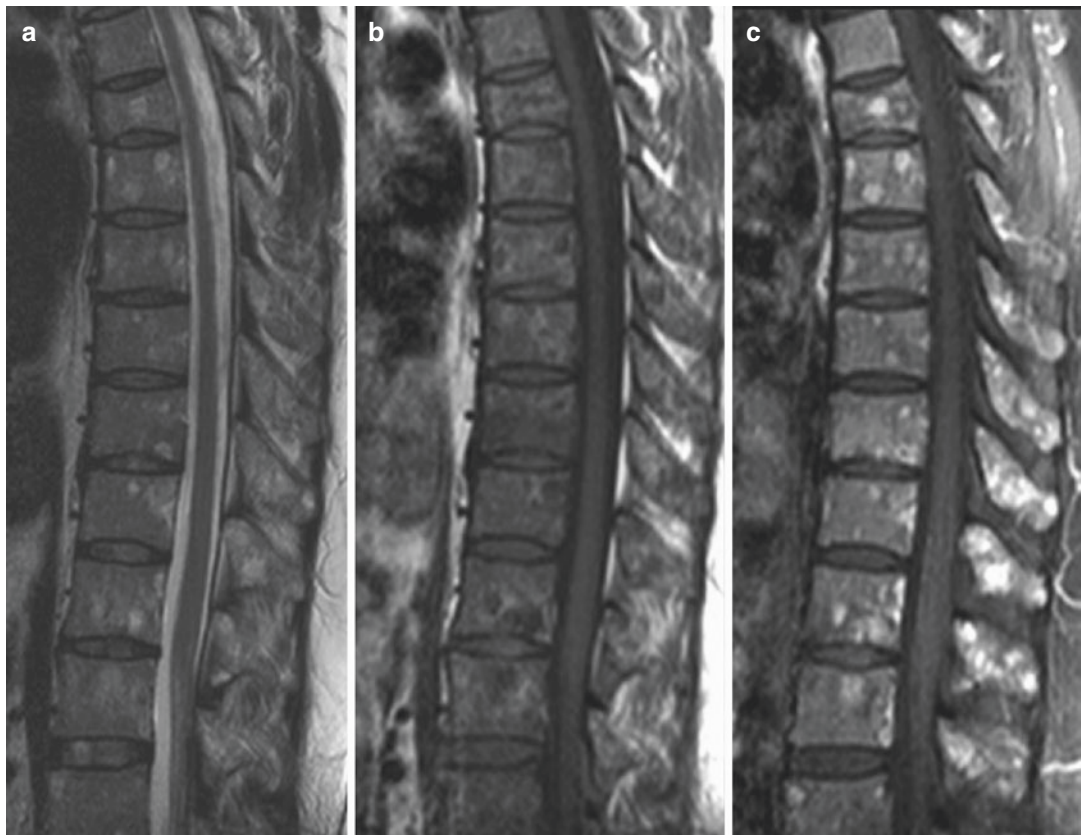
4.1.3.1 Illustrations: Multiple Myeloma

Fig. 4.6 Spine involvement from multiple myeloma in a 43-year-old man. T1-weighted sagittal MR image (a) of the thoracic spine shows multiple small low signal intensity nodules. T2-weighted sagittal MR image (b) shows high signal intensity foci. Contrast-enhanced T1-weighted sagittal MR image (c) shows strong enhancement of these nodules

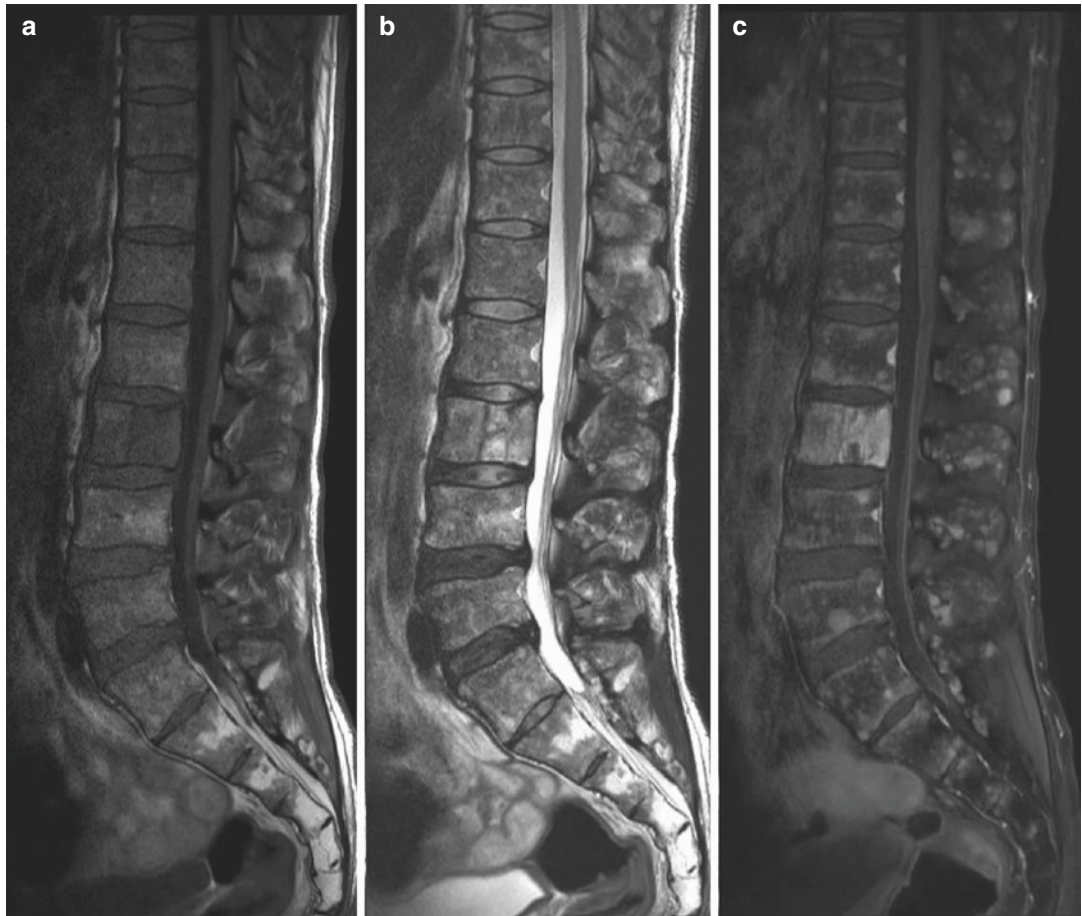


Fig. 4.7 Spine involvement from multiple myeloma in a 47-year-old man. T1-weighted sagittal (a) and T2-weighted (b) MR images of the lumbar spine show tiny, innumerable

hypointense nodules throughout the whole spine. Contrast-enhanced T1-weighted sagittal MR image (c) shows strong enhancement of these tiny nodules

4.2 Extradural Non-osseous Tumors or Tumorlike Lesions

4.2.1 Schwannoma

1. Epidemiology
 - 30–60 years old
 - M = F
2. Location
 - Thoracic > lumbar, cervical
3. Characteristic imaging findings
 - Well-defined, lobular contoured, extradural mass
 - Foraminal widening, bony scalloping
 - High signal on T2-weighted image, homogeneous or peripheral irregular enhancement
4. Spectrum of imaging findings
 - Intradural extension (dumbbell shape)
 - Cystic degeneration: peripheral irregular enhancement, central bright T2-hyperintensity
5. Differential diagnosis
 - Neurofibroma

- Fusiform shape
- Target sign: peripheral high signal + central low signal on T2-weighted images
- Herniated disc (sequestration)
 - Low signal on T2-weighted images
 - No enhancement/peripheral enhancement with central T2-hypointensity
 - Protrusion at the base of the adjacent intervertebral disc
- Abscess
 - Thin peripheral enhancement
 - Bone marrow edema of the adjacent vertebral body
- Angiolipoma
 - T1-hyperintensity
- Epidural hemangioma
 - Cystic or solid mass with homogeneous enhancement
 - Lobular shape
- Epidural hematoma
 - No enhancement, foci of T1-hyperintensity or T2-hypointensity

4.2.1.1 Illustrations: Schwannoma

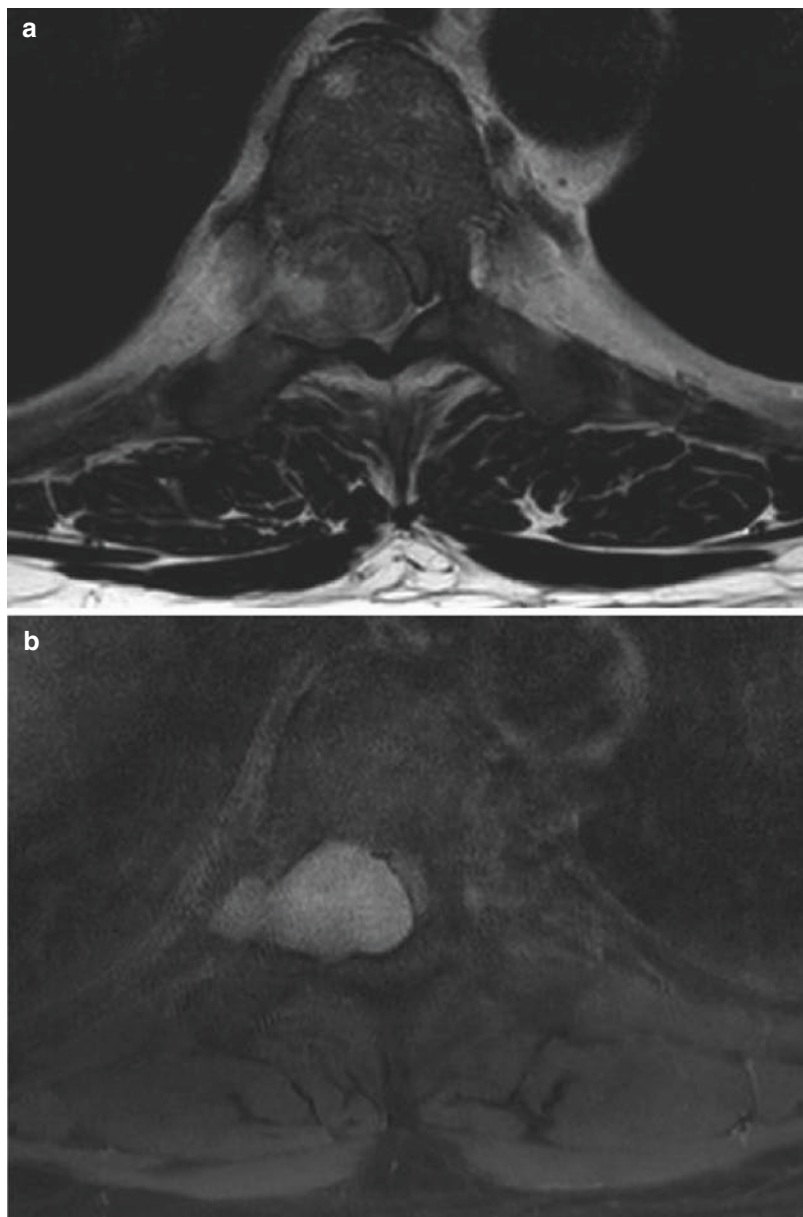


Fig. 4.8 Extradural schwannoma in a 50-year-old man. T2-weighted axial MR image (**a**) shows a heterogeneous signal intensity extradural soft tissue mass involving the right T8/T9 neural foramen. Marked compression and

left-sided deviation of the spinal cord is noted. Contrast-enhanced T1-weighted axial MR image (**b**) shows homogeneous enhancement

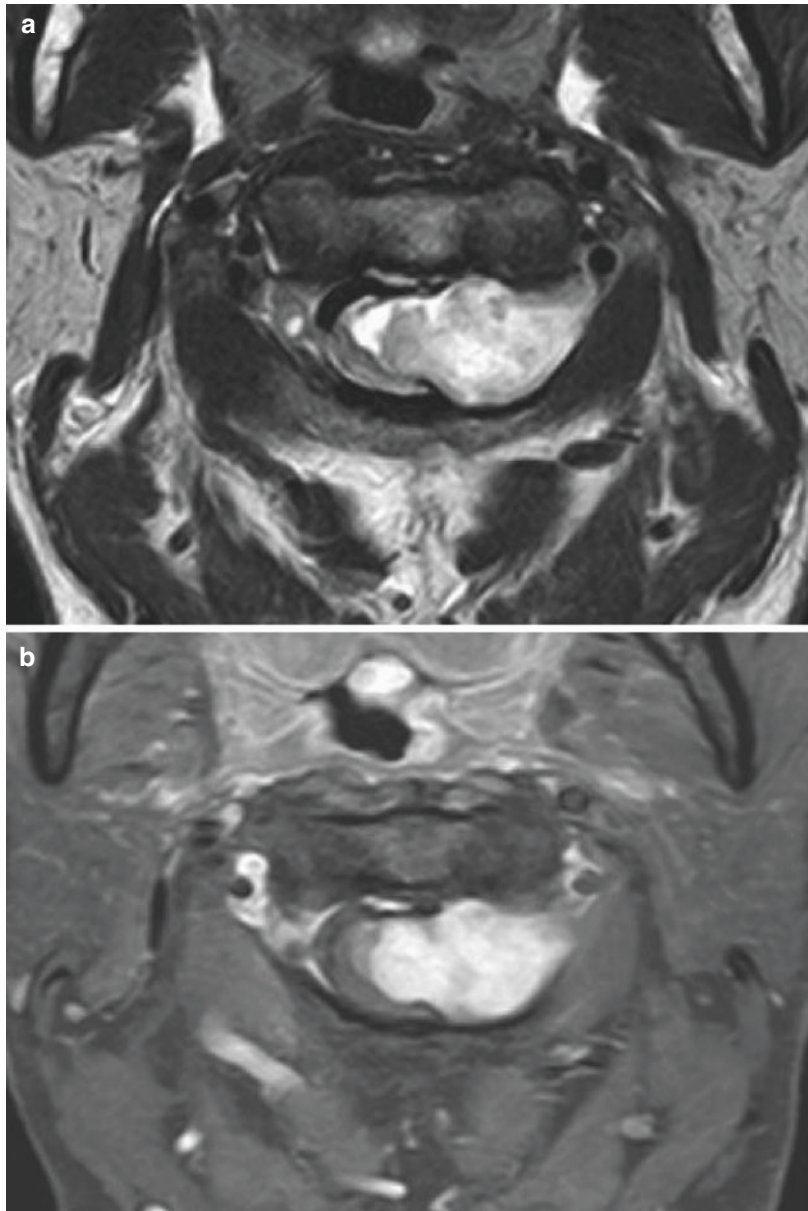


Fig. 4.9 Extradural schwannoma in a 53-year-old woman. T2-weighted axial MR image (a) shows a high-signal intensity left anterolateral extradural mass extending through the C1/C2 left neural foramen. Compression

and right-sided deviation of the spinal cord is noted. Contrast-enhanced T1-weighted axial MR image (b) shows heterogeneous enhancement



Fig. 4.10 Extradural schwannoma in a 65-year-old man. T2-weighted axial MR image (a) shows a high signal intensity right-sided extradural mass at L4/L5 level.

Contrast-enhanced T1-weighted axial MR image (b) shows peripheral enhancement (*white arrows*)

4.2.2 Neurofibroma

1. Epidemiology

- 30–60 years old
- M = F

2. Location

- Thoracic > lumbar, cervical

3. Characteristic imaging findings

- Peripheral high signal (myxoid material) + central low signal (nerve tissue) on T2-weighted images
- Fusiform shape in the neural foramen, swollen nerve rootlike shape

4. Spectrum of imaging findings

- Plexiform neurofibromas
 - Multiple neurofibromas in the brachial or lumbar plexus
- Neurofibromatosis type I

• Diffuse neurofibroma

- Ill-defined diffuse infiltration in the muscle and subcutaneous fat layer
- Neurofibromatosis type 1

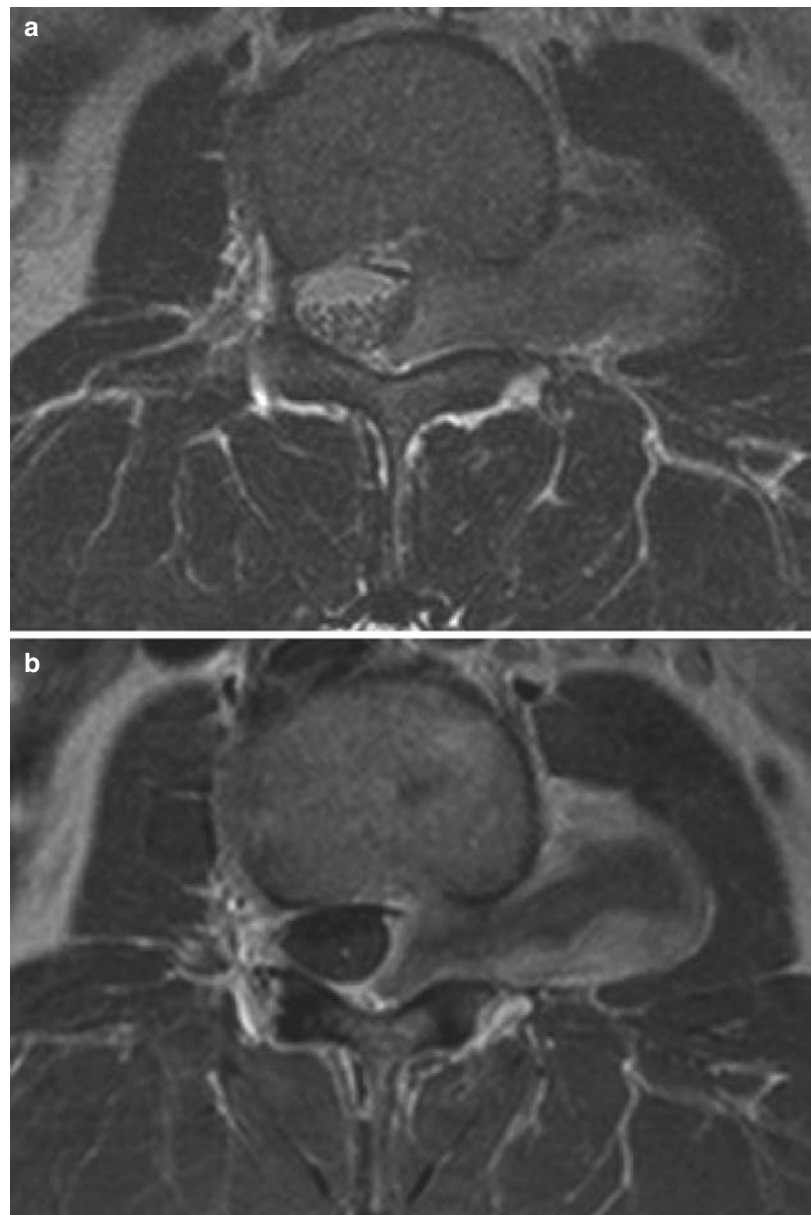
5. Differential diagnosis

- Schwannoma
 - Similar imaging findings
 - Rare target sign
- Malignant peripheral nerve sheath tumors (MPNST)
 - Large mass, more than 5 cm

4.2.2.1 Illustrations: Neurofibroma

Fig. 4.11 Extradural neurofibroma in a 33-year-old man.

T2-weighted axial MR image (**a**) shows a dumbbell-shaped heterogeneous high signal intensity extradural mass extending through the left L1/L2 neural foramen. Contrast-enhanced T1-weighted axial MR image (**b**) shows peripheral enhancement



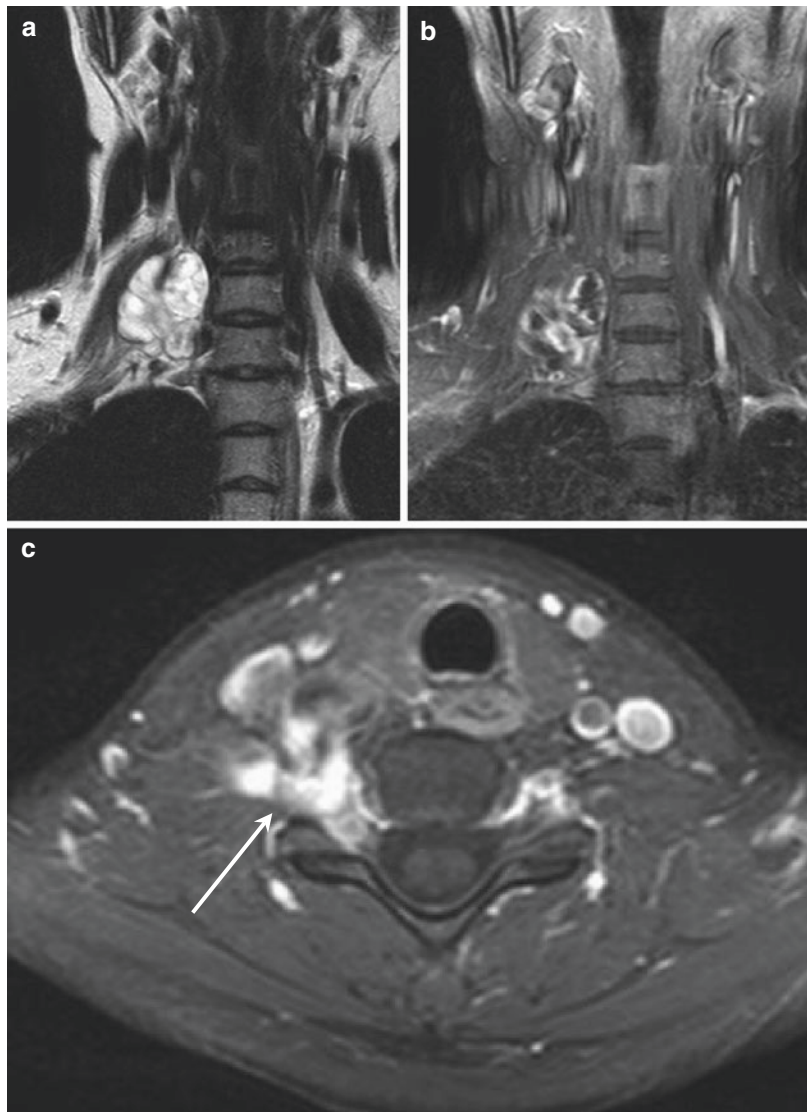


Fig. 4.12 Neurofibroma in a 35-year-old woman. T2-weighted coronal MR image (a) shows a high signal intensity lobulated paravertebral mass. Contrast-enhanced

T1-weighted coronal (b) and axial (c) MR images show a peripheral enhancing mass extending through the right C6/C7 neural foramen (*white arrow*)

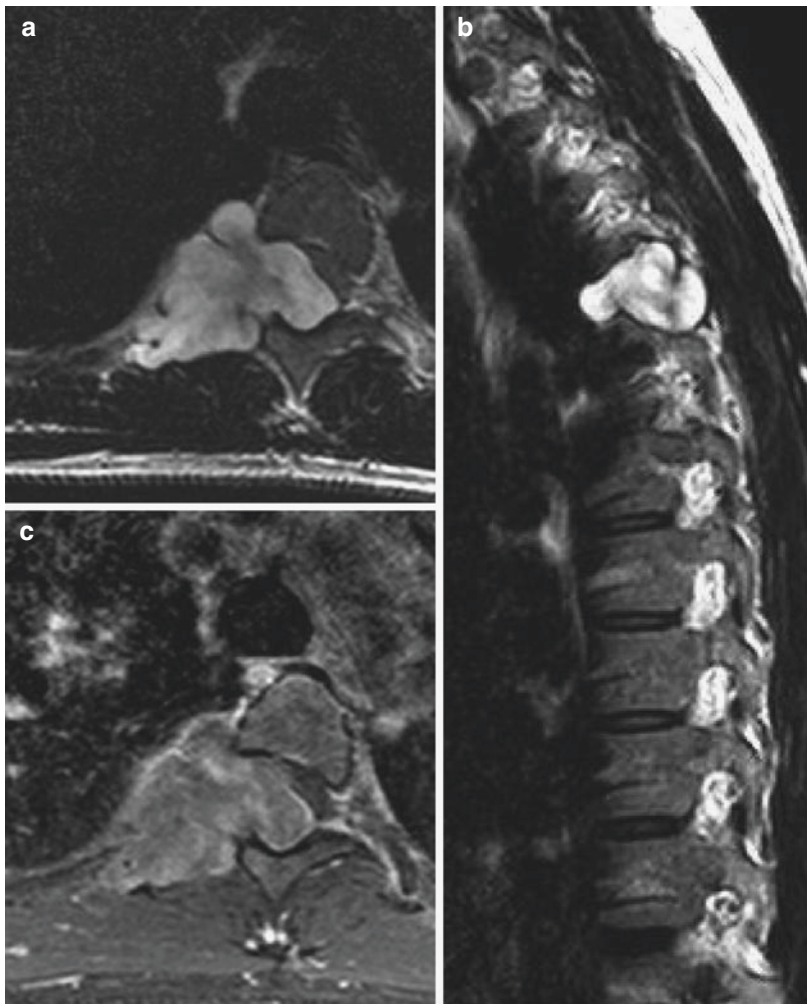


Fig. 4.13 Extradural neurofibroma in a 25-year-old woman. T2-weighted axial (**a**) and sagittal (**b**) MR images show a high signal intensity lobulated extradural mass extending through the enlarged right T4/T5 neural foramen.

Spinal cord compression and left-sided deviation is noted. Contrast-enhanced T1-weighted axial MR image (**c**) shows a peripheral enhancing mass

4.2.3 Herniated Intervertebral Disc (HIVD) (Sequestration)

1. Epidemiology

- All age
- M = F

2. Location

- Lumbar

3. Characteristic imaging findings

- Low signal on T2-weighted images
- No enhancement/peripheral enhancement with central T2-hypointensity

- Protrusion at the base of the adjacent intervertebral disc

4. Spectrum of imaging findings

- Rare intradural disc herniation
- Thick peripheral enhancement

5. Differential diagnosis

- Schwannomas
- Neurofibromas
- Abscess
- Hematoma

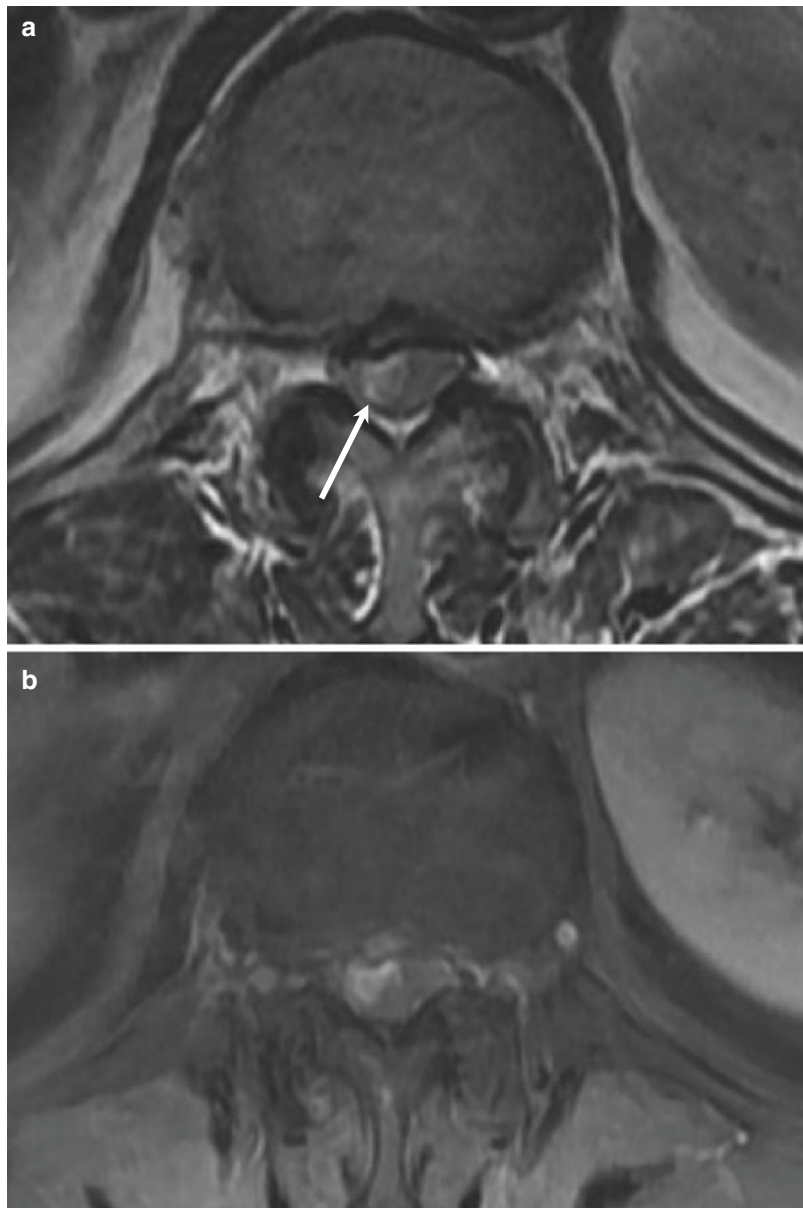
4.2.3.1 Illustrations: HIVD (Sequestration)

Fig. 4.14 Disc sequestration at T12/L1 level in a 65-year-old woman. T2-weighted axial MR image (a) shows a right epidural lesion with peripheral high signal intensity and inner low signal intensity area (*white arrow*). The

lesion causes cord compression and displacement to the left side. Contrast-enhanced T1-weighted axial MR image (b) shows peripheral enhancement

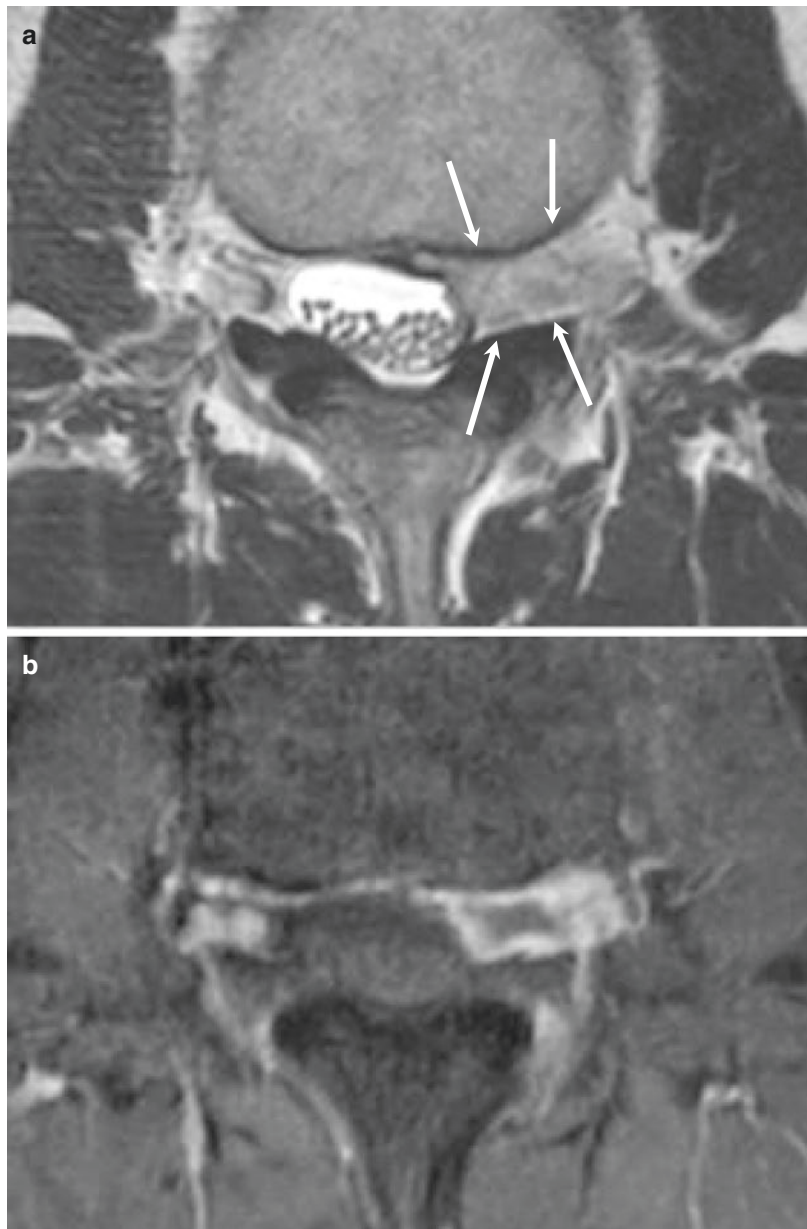


Fig. 4.15 Disc sequestration at L2/L3 level in a 57-year-old woman. T2-weighted axial MR image (a) shows a high signal intensity lesion extending from the ventral and

left lateral epidural space into the left neural foramen (white arrows). Contrast-enhanced T1-weighted axial MR image (b) shows peripheral enhancement

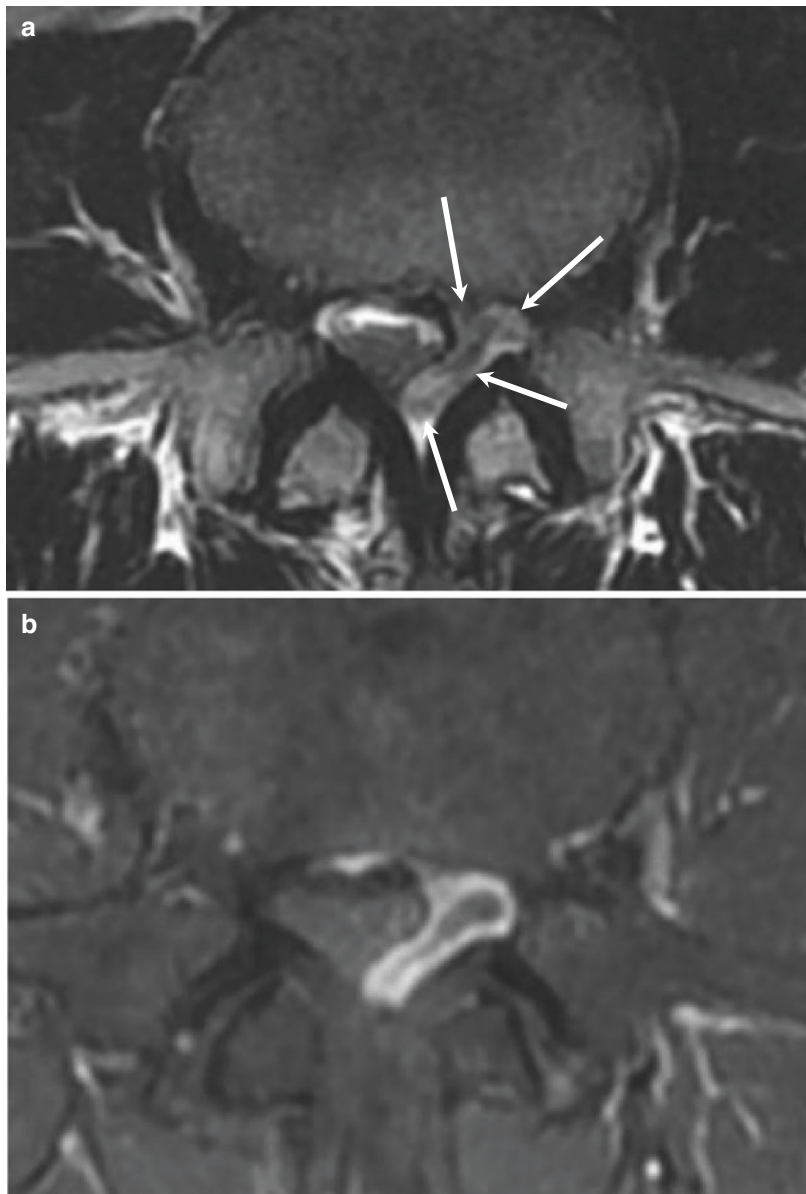


Fig. 4.16 Disc sequestration at L3/L4 level in a 61-year-old man. T2-weighted axial MR image (a) shows a high signal intensity lobulated left lateral and posterior epidural lesion (white arrows). The lesion causes left L4

nerve root compression and central canal compromise. Contrast-enhanced T1-weighted axial MR image (b) shows peripheral enhancement

4.3 Intradural Extramedullary (IDEM) Tumors

4.3.1 Schwannoma

1. Epidemiology

- 30–60 years old
- M = F

2. Location

- Thoracic = lumbar > cervical
- Eccentric

3. Characteristic imaging findings

- Well-defined intradural lobular, round, or ovoid mass
- Compressing spinal cord to the contralateral side
- High signal on T2-weighted image, avid enhancement

- Can extend and grow into the epidural space along nerve root (dumbbell shape)
- No calcification, no dural base

4. Spectrum of imaging findings

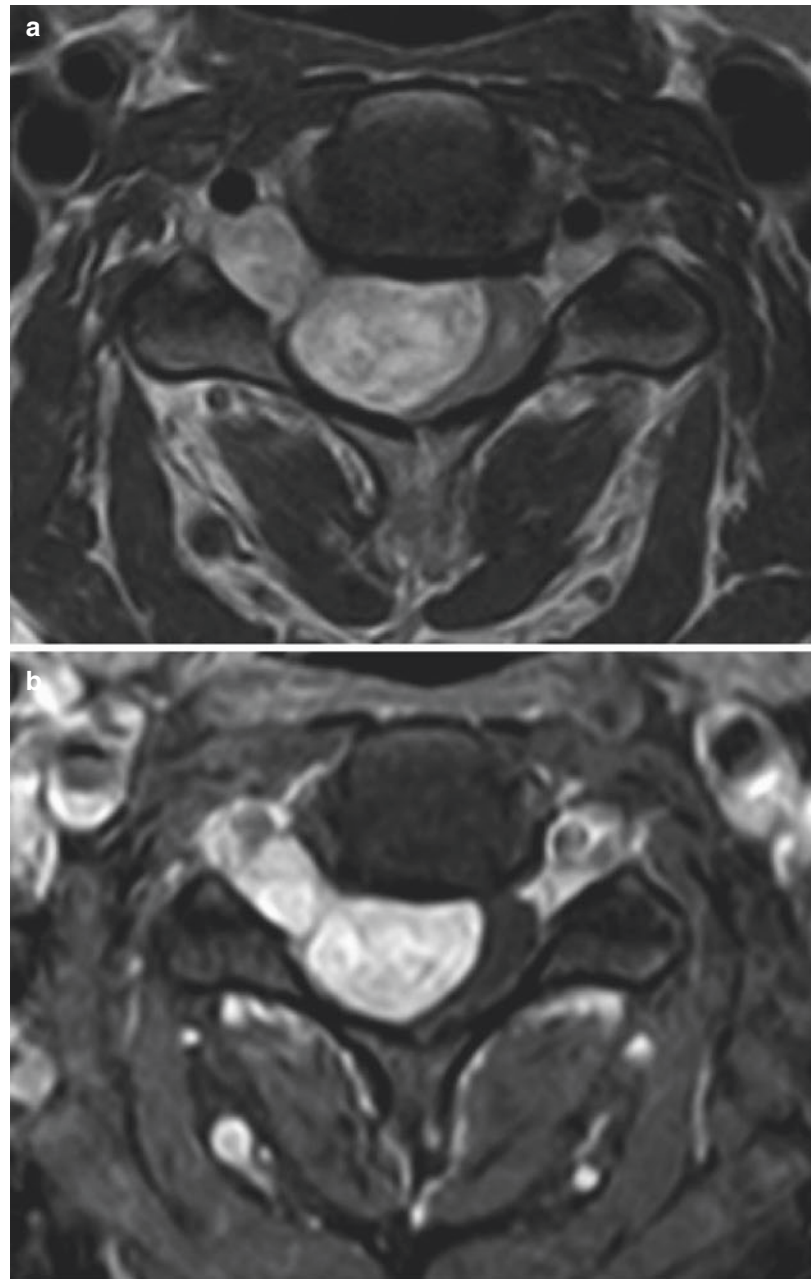
- Multiple schwannomas
- Intermediate signal intensity on T2-weighted image in cases of small nodules attaching to cauda equina

5. Differential diagnosis

- Meningioma
 - Intermediate signal intensity on T2-weighted images
 - Dural base
 - Thoracic
 - Calcification

4.3.1.1 Illustrations: Schwannoma

Fig. 4.17 Schwannoma at C3/C4 level in a 34-year-old woman. T2-weighted axial MR image (a) shows a well-defined intradural extramedullary mass with heterogeneous high signal intensity in the right side of the central canal at C3/C4 level with extension into the right C3/C4 neural foramen, compressing the spinal cord to the left. Contrast-enhanced T1-weighted axial MR image (b) shows avid enhancement



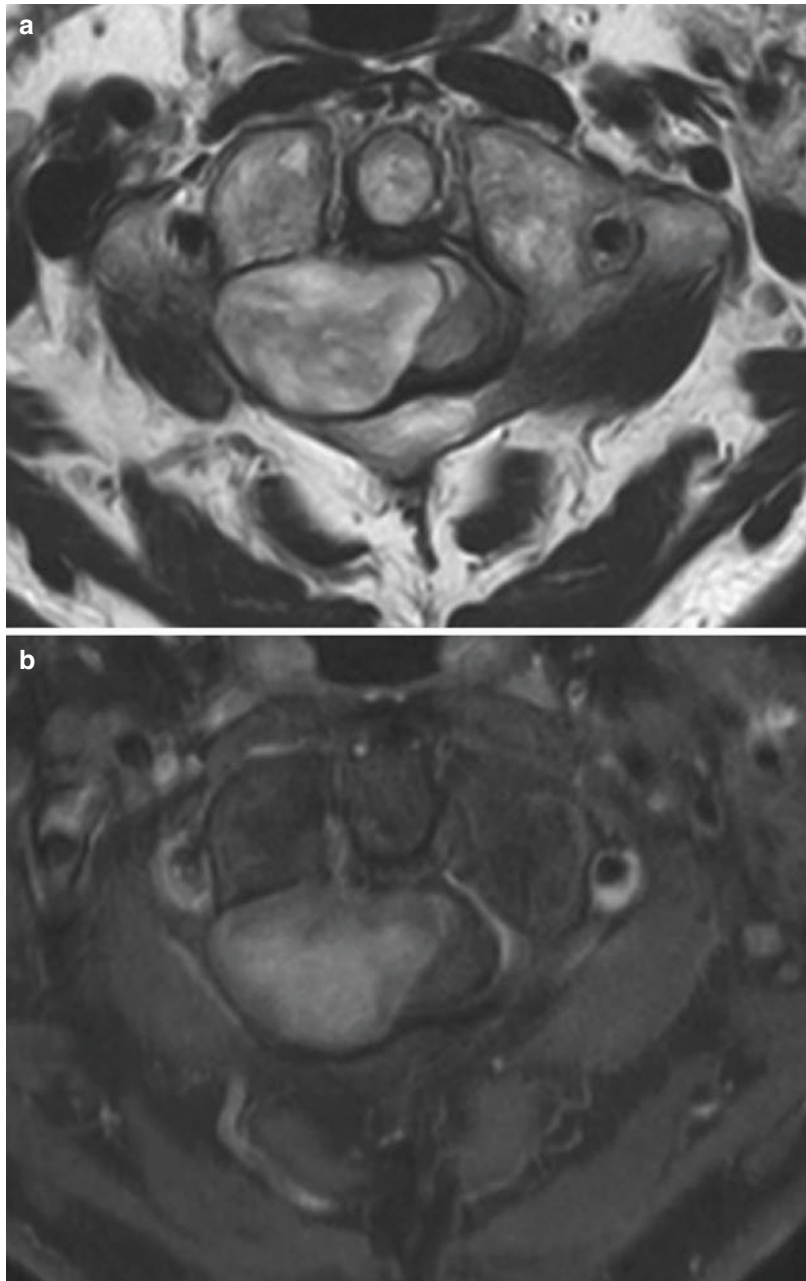
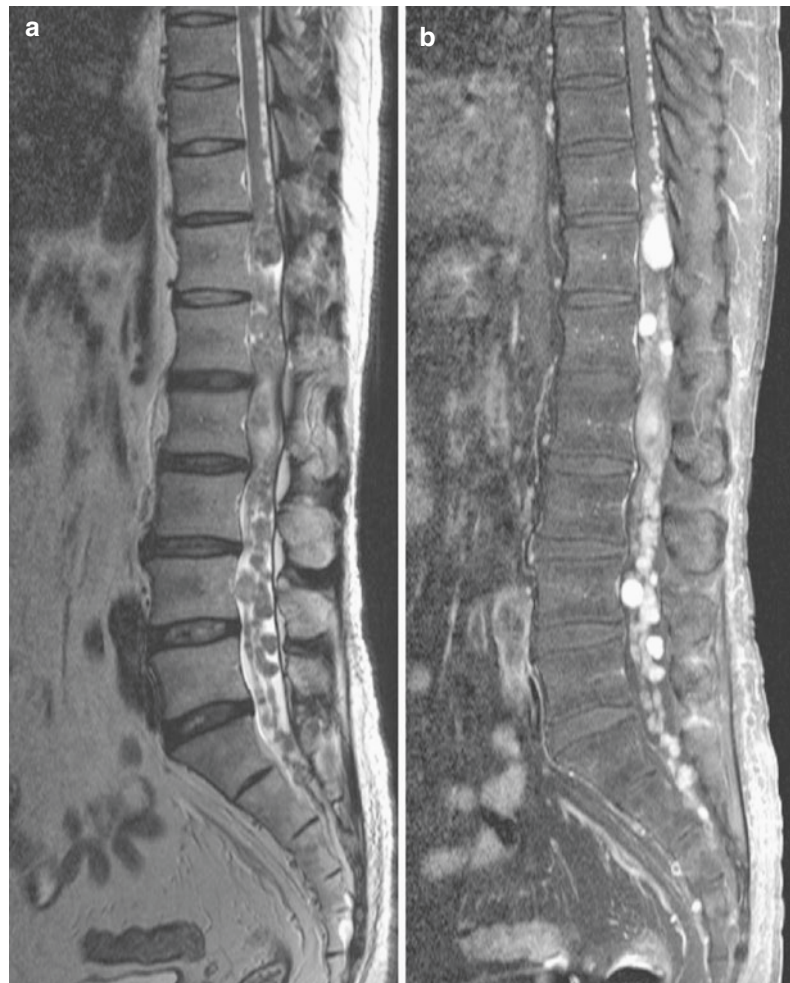


Fig. 4.18 Schwannoma at C1/C2 level in a 72-year-old woman. T2-weighted axial MR image (a) shows well-defined intradural extramedullary mass with heterogeneous high signal intensity in the right side of the central

canal at C1/C2 level with extension into the right C1/C2 neural foramen, compressing the spinal cord to the left. Contrast-enhanced T1-weighted axial MR image (b) shows enhancement

Fig. 4.19 Multiple schwannoma in a 45-year-old man. T2-weighted sagittal MR image (**a**) shows multiple well-defined small intradural extramedullary nodules attaching to the spinal cord and cauda equina with intermediate signal intensity at the thoracolumbar region. Contrast-enhanced T1-weighted sagittal MR image (**b**) shows avid enhancement



4.3.2 Meningioma

1. Epidemiology

- 40–50 years old
- F >> M

2. Location

- Thoracic spine

3. Characteristic imaging findings

- Dural-based mass with cord compression
- Intermediate signal intensity on T2-weighted images, avid enhancement
- Dural tail sign: dural enhancement near the mass
- Calcification

4. Spectrum of imaging findings

- En plaque meningioma
 - Plaque-like irregular mass attaching to dura

- WHO grade

- Meningioma (I)
- Atypical meningioma (II)
- Anaplastic meningioma (III)

5. Differential diagnosis

- Schwannoma

- High signal on T2-weighted image, avid enhancement
- Can grow to the epidural space along nerve root (dumbbell shape)
- No calcification, no dural base

4.3.2.1 Illustrations: Meningioma

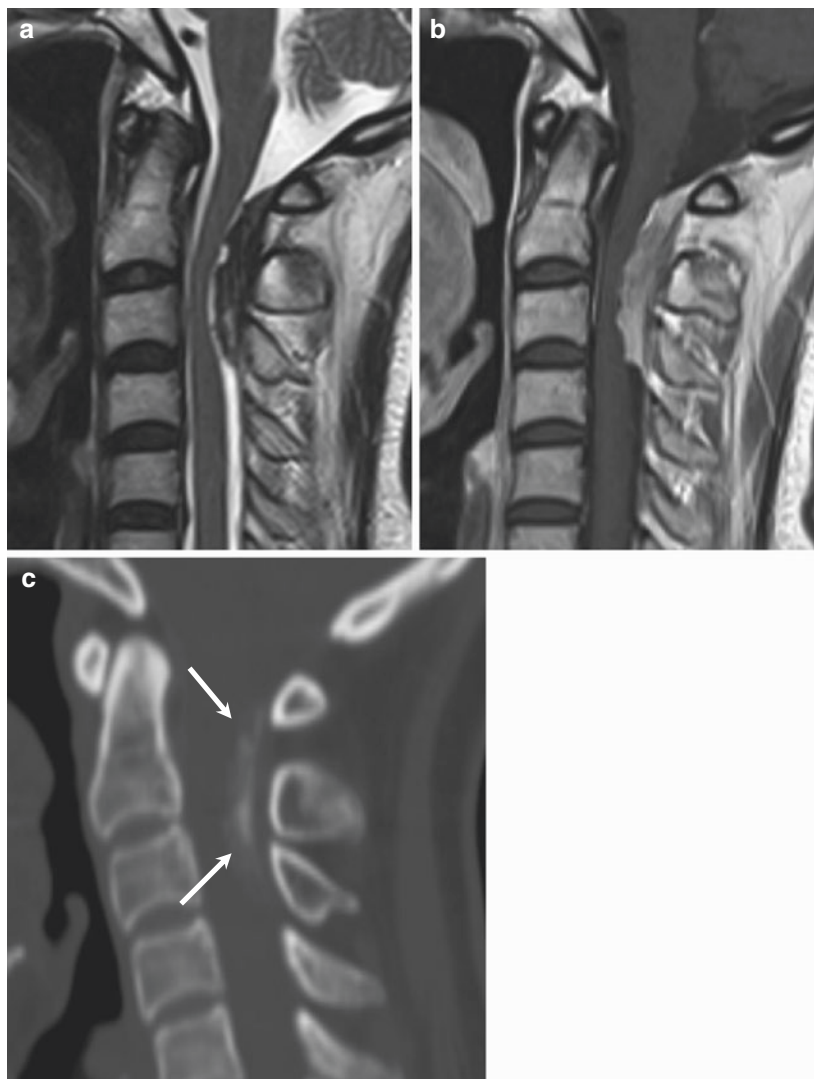


Fig. 4.20 Meningioma at C1 to C3 levels in a 44-year-old woman. T2-weighted sagittal MR image (a) shows a broad dural-based mass with low signal intensity in the posterior subarachnoid space with cord compression at C1

to C3 level. Contrast-enhanced T1-weighted sagittal MR image (b) shows avid enhancement with dural enhancement near the mass (dural tail sign). Sagittal CT scan of the cervical spine (c) shows calcification (white arrows)

Fig. 4.21 Meningioma at T8 to T9 levels in a 51-year-old woman. T2-weighted sagittal MR image (**a**) shows a broad dural-based mass with dark signal intensity in the posterior subarachnoid space at T8 to T9 levels with cord compression at T8/T9 level. Sagittal CT scan image (**b**) shows dense calcification within the mass



4.3.3 Myxopapillary Ependymoma

1. Epidemiology

- All ages
- M > F

2. Location

- Lumbar spine

3. Characteristic imaging findings

- Longitudinally large lobular mass, well-defined
- High signal on T2-weighted image before bleeding
- Low signal on T2-weighted image due to hemorrhage
- Avid enhancement
- Central location

4. Spectrum of imaging findings

- Leptomeningeal seeding
 - Multiple leptomeningeal enhancing nodules

- Superficial siderosis
 - Due to repeated bleeding
 - Dark signal on the surface of the spinal cord and cerebellum
- Intratumoral AV shunt
 - Prominent flow voids

5. Differential diagnosis

- Paraganglioma
 - Hypervascular mass with intratumoral AV shunt
- Schwannoma
 - Smaller intradural mass
 - Less hemorrhage
- Leptomeningeal metastases
 - Other site of metastatic mass
 - Irregular enhancement along the surface of the spinal cord

4.3.3.1 Illustrations: Myxopapillary Ependymoma

Fig. 4.22 Myxopapillary ependymoma from L5 to S2 levels in a 12-year-old boy. T2-weighted sagittal MR image (a) shows a well-defined, longitudinally large lobular intradural extramedullary mass of high signal intensity from L5 to S2 levels attached to the filum terminale. Contrast-enhanced T1-weighted sagittal MR image (b) shows avid enhancement



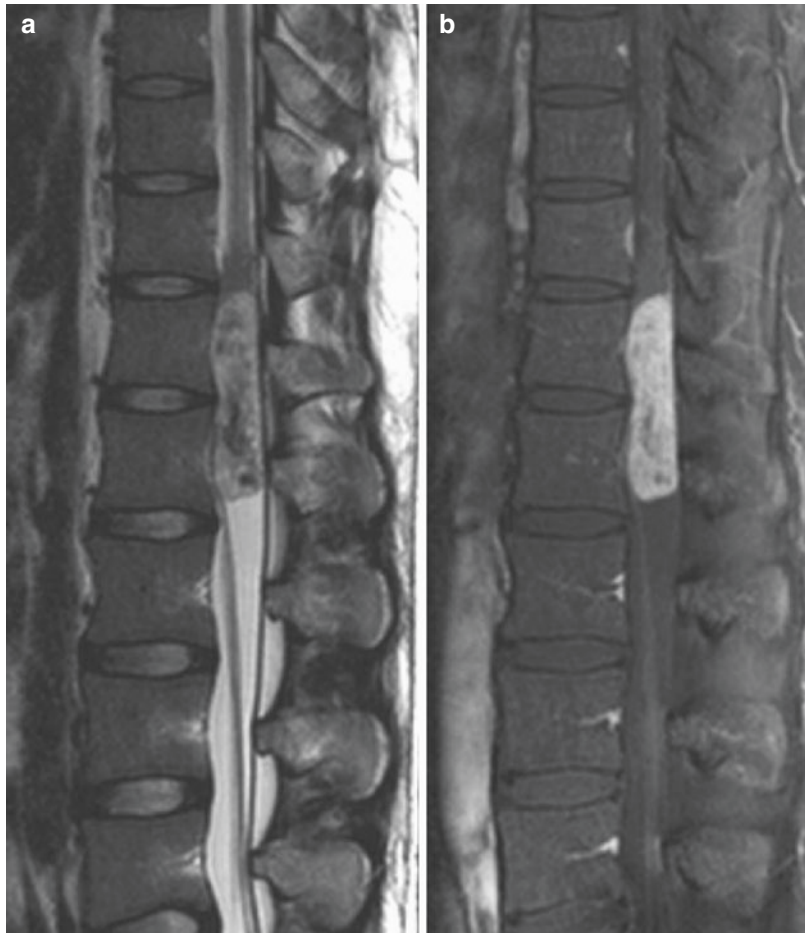


Fig. 4.23 Myxopapillary ependymoma at T12 to L1 levels in a 25-year-old man. T2-weighted sagittal MR image (a) shows a well-defined, longitudinally large lobular intradural extramedullary mass of heterogeneous signal

intensity posterior to the conus medullaris at T12 to L1 levels. Contrast-enhanced T1-weighted sagittal MR image (b) shows avid enhancement

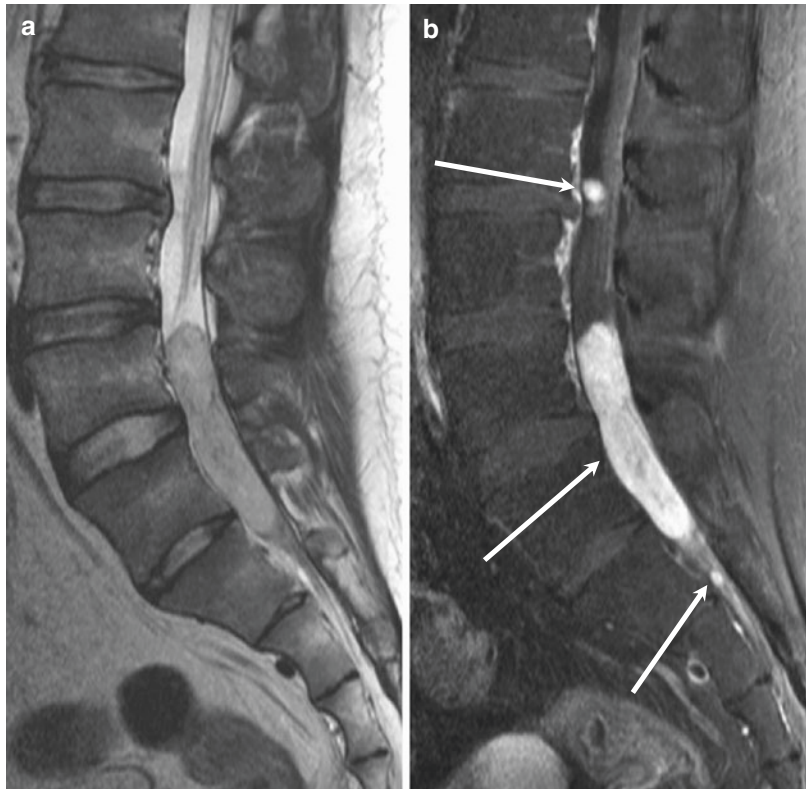


Fig. 4.24 Myxopapillary ependymoma with leptomeningeal seeding from L5 to S2 levels in a 23-year-old man. T2-weighted sagittal MR image (a) shows a well-defined, longitudinally large lobular intradural extramedullary

mass of high signal intensity from L5 to S2 levels, with smaller intradural nodules of subtle hyperintensity at L3/L4 and S2 levels. Contrast-enhanced T1-weighted sagittal MR image (b) shows avid enhancement (*white arrows*)

4.4 Intramedullary (IM) Tumors

4.4.1 Ependymoma

1. Epidemiology

- 35–45 years old
- Intramedullary type: M > F
- Intradural extramedullary type: F > M

2. Location

- Cervical > thoracic > conus medullaris

3. Characteristic imaging findings

- Typically 3–4 segments
- Well-circumscribed centrifugal growth and symmetric cord expansion
- High signal on T2-weighted images before bleeding
- Cap sign: low signal on T2-weighted images
 - Hemosiderin
- Avid enhancement

4. Spectrum of imaging findings

- Syrinx
 - CSF equivalent signal
- Tumoral cyst and polar cyst
 - Peripheral enhancement at tumoral cyst

- Four subtypes: cellular, papillary, clear cell, tanycytic
 - Hard to distinguish by imaging findings

- Minimal or non-enhancement: rare

- WHO grade

- Myxopapillary ependymoma (I)
- Subependymoma
- Ependymoma (II)
- Anaplastic ependymoma (III)

5. Differential diagnosis

- Astrocytoma
 - Eccentric, infiltrative
 - Hemorrhage uncommon
 - Tumor cyst or syrinx less common
- Hemangioblastoma
 - Cyst with highly enhancing nodule at posterior aspect of cord
 - Extensive surrounding edema
 - Vascular flow void
- Demyelinating disease
 - Ill defined
 - Faint nodular or patchy enhancement

4.4.1.1 Illustrations: Ependymoma

Fig. 4.25 Cellular ependymoma in a 65-year-old woman. T2-weighted sagittal image (a) shows an ovoid-shaped intramedullary mass with small cyst formation and hemosiderin deposition capping the superior margin of the

mass at C5–C6 level. Contrast-enhanced T1-weighted sagittal image (b) shows heterogeneous enhancement of the tumor along with the cranial and caudal non-enhancing cysts

Fig 4.26 Ependymoma in a 33-year-old woman. T2-weighted image

(a) shows an ovoid mass with intermediate signal intensity at C7 level and surrounding extensive peritumoral cysts.
Contrast-enhanced T1-weighted image
(b) shows strong and homogeneous enhancement of the mass



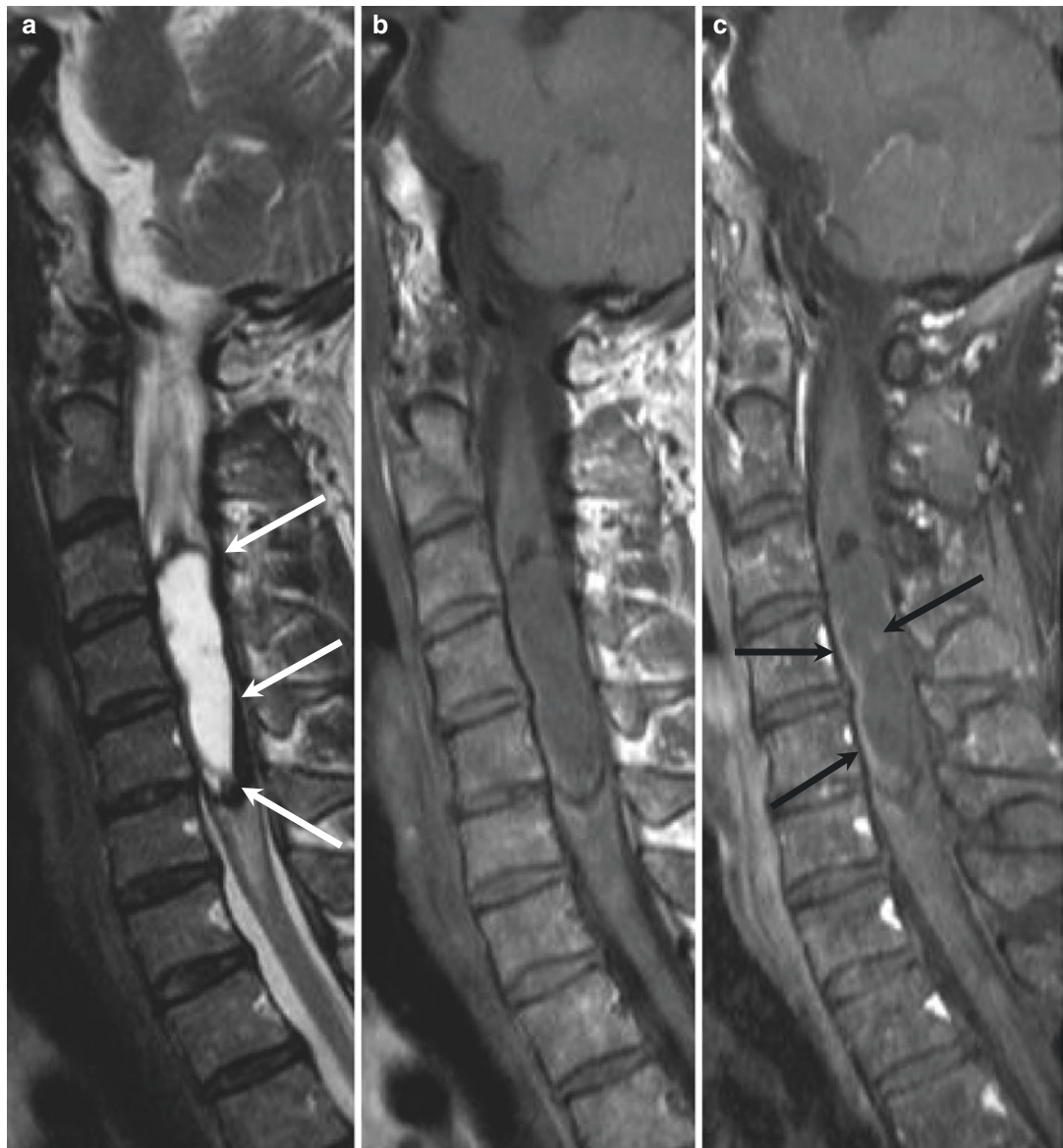


Fig 4.27 Ependymoma in a 55-year-old woman. T2-weighted sagittal image (a) and T1-weighted sagittal image (b) show cord expansion with a dominant cyst and hemosiderin deposition at both cranial and caudal aspects

of the cystic component (*white arrows*). Fat-saturated contrast-enhanced T1-weighted sagittal image (c) shows peripheral rim-like enhancement and focal enhancing solid portion within the lesion (*black arrows*)

4.4.2 Astrocytoma

1. Epidemiology

- Most common intramedullary tumor in child/young adults
- Second most common intramedullary tumor
- M > F
- NF 2 association

2. Location

- Cervical > thoracic

3. Characteristic imaging findings

- Fusiform expansion of spinal cord with variable enhancement
- Usually less than 4 segments
- Eccentric location with or without cyst or syrinx
- High signal on T2-weighted and PD image

4. Spectrum of imaging findings

- Multi-segmental or holocord
 - More common with pilocytic astrocytoma
- No enhancement
 - Up to 20–30%
- Scoliosis, expansion of canal

- Area of high signal on T1-weighted images
 - Methemoglobin

- WHO grade

- Pilocytic astrocytoma (I)
 - Fibrillary astrocytoma (II)
 - Pleomorphic xanthoastrocytoma (II)
 - Anaplastic astrocytoma (III)
 - Glioblastoma multiforme (IV)

5. Differential diagnosis

- Ependymoma
 - Older patient
 - Central > eccentric
 - Tumor cyst or syrinx and hemorrhage common
 - Intense enhancement
- Ganglioglioma
 - Mixed signal on T1-weighted image due to solid and cystic components
 - Homogenous high signal on T2-weighted image
 - Vascular flow void
- Lymphoma
 - Poorly defined enhancing mass
 - Slightly low signal on T2-weighted images

4.4.2.1 Illustrations: Astrocytoma

Fig. 4.28 Pilocystic astrocytoma in an 18-year-old boy. T2-weighted sagittal (a) and axial images (b) show an eccentrically located intramedullary tumor in the cervical cord. Note the intratumoral focal calcification or hemor-

rhage in the central portion of the tumor (white arrows). On pre- and postcontrast-enhanced T1-weighted sagittal images (c, d), this expansile tumor shows minimal enhancement



Fig. 4.29 Astrocytoma in a 43-year-old woman. T2-weighted sagittal image (a) shows a fusiform-shaped intramedullary hyperintense mass at T6–T8. Note eccentric

location of the lesion within the spinal cord. T1-weighted sagittal image (b) and contrast-enhanced T1-weighted sagittal image (c) shows poor enhancement of the mass



Fig. 4.30 Astrocytoma in a 23-year-old woman. T2-weighted sagittal image (**a**) demonstrates long-segment fusiform cord expansion involving almost the whole

thoracic cord. Contrast-enhanced T1-weighted sagittal (**b**) and axial (**c**) images show a focal eccentrically located enhancing nodule at T7 level (*white arrows*)

4.4.3 Hemangioblastoma

1. Epidemiology

- 30 years
- Earlier presentation in VHL
- M = F
- Third common intramedullary tumor

2. Location

- Thoracic > cervical > lumbar

3. Characteristic imaging findings

- Well-defined intense enhancing nodule at subpial and posterior aspect spinal cord
- Extensive peritumoral edema or syrinx
- Vascular flow voids: large lesion (>2.5 cm)
- Hemorrhage common

4. Spectrum of imaging findings

- Rarely anterior aspect of spinal cord
- Multiple hemangioblastomas in VHL (32%)

• AV shunting

- Methemoglobin

5. Differential diagnosis

- AVM
 - Focal enhancing nodule absent
 - Syrinx (-)
- Cavernous malformation
 - Hemosiderin rim
 - Minimal or non-enhancement
- Leptomeningeal metastases
 - Other sites of metastatic mass
 - Irregular enhancement along the surface of the spinal cord

4.4.3.1 Illustrations: Hemangioblastoma

Fig. 4.31 Cervical hemangioblastoma in a 33-year-old man. T2-weighted sagittal image (**a**) and contrast-enhanced T1-weighted sagittal image (**b**) exhibit a subpial enhancing mass with intramedullary cyst/syrinx and extensive peritumoral edema. There is a prominent serpentine vascular structure along the dorsal surface of the cord up to the medulla (white arrows)



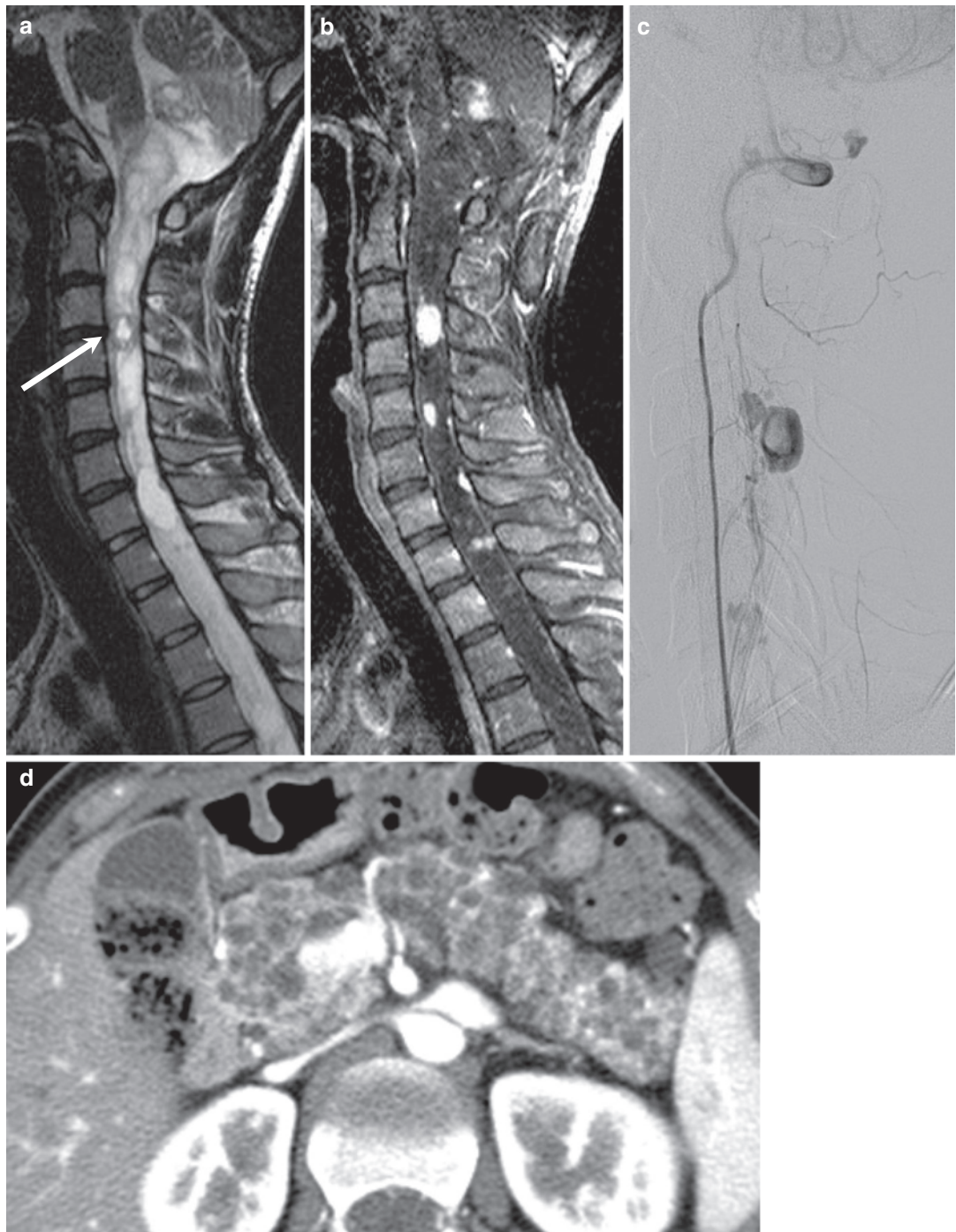


Fig 4.32 Hemangioblastomas in a 25-year-old woman with von Hippel-Lindau syndrome. T2-weighted sagittal image of the thoracic spine (**a**) shows several small subpial masses within extensive T2-hyperintensity in the cervical cord. Ring of hypointensity (white arrow) suggests susceptibility due to prior hemorrhage. Note the cerebellar

hemangioblastoma with cystic and solid portions. Post-contrast T1-weighted sagittal image (**b**) shows strong enhancement of the masses. Preoperative left vertebral angiography (**c**) reveals multiple hypervascular foci of tumor staining fed by an anterior spinal artery. Abdominal CT scan (**d**) shows numerous cysts in the pancreas

4.5 Multi-compartment Tumors

4.5.1 Lymphoma

1. Epidemiology

- 30–60 years old
- M > F

2. Location

- Multi-compartment (extradural > intradural > intramedullary)
 - Epidural: thoracic > lumbar > cervical
 - Osseous: long bone > spine
 - Intramedullary: cervical > thoracic > lumbar
 - Lymphomatous leptomeningitis

3. Characteristic imaging findings

- Epidural
 - Epidural mass with or without vertebral involvement
 - Homogenous intense enhancement
 - Extension through neural foramen
- Osseous
 - Low signal on T1-weighted image to normal bone marrow
 - Diffuse homogenous enhancement
 - Osteolytic or permeative bone destruction on CT
 - Epidural extension or soft tissue mass formation
- Intramedullary
 - Poorly defined enhancing mass
 - High signal on T2-weighted image with surrounding edema

- Leptomeningitis
 - Smooth, nodular pial enhancement
 - Thick nerve root enhancement with or without nodules

4. Spectrum of imaging findings

- Osseous
 - “Ivory” vertebra, vertebral plana
- ADC value
 - Tumor cellular density
- Dynamic contrast-enhancement MR
 - Decreased bone marrow enhancement after treatment

5. Differential diagnosis

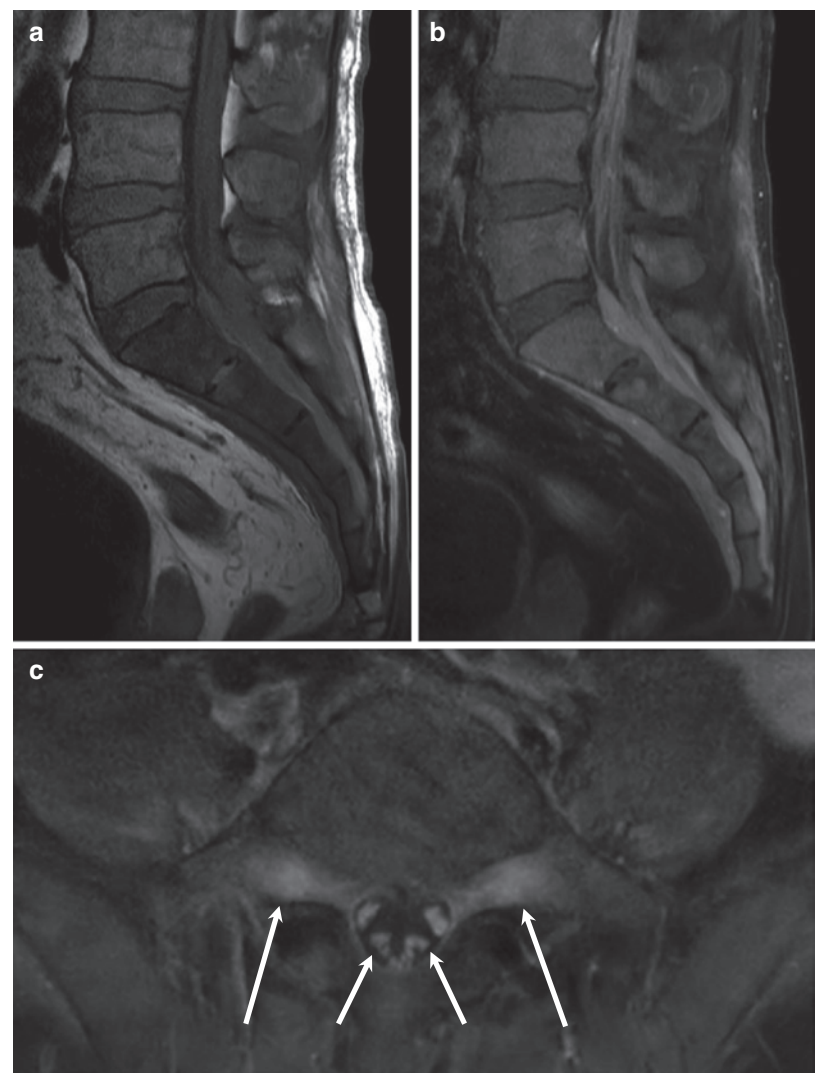
- Epidural
 - Hematoma
 - Heterogeneous signal
 - Abscess
 - Rim enhancement with central low signal
 - Metastasis
 - Extremely rare epidural metastasis only
- Osseous
 - Metastasis
 - LCH
 - Vertebral plana in young patients
- Intramedullary tumor
 - Ependymoma: hemorrhage, cyst common
 - Astrocytoma: multi-segmental, cyst common
 - Metastasis

4.5.1.1 Illustrations: Lymphoma

Fig. 4.33 Lymphoma involving the thoracic spine in a 49-year-old woman. T1-weighted sagittal MR image (**a**) shows diffuse low signal intensity of the T5 vertebral body, spinous process, and a soft tissue mass in the posterior epidural space (white arrows). Note the low signal intensity of the mass on T2-weighted image (**b**). Contrast-enhanced T1-weighted fat-suppressed axial MR image (**c**) shows lesions involving the T5 vertebra, right fifth rib, epidural space, bilateral neural foramen, and paravertebral muscles with homogenous contrast enhancement



Fig. 4.34 Lymphoma of the sacrum in a 69-year-old woman. T1-weighted sagittal MR image (**a**) shows diffuse low signal intensity of the sacrum and intermediate soft tissue signal intensity in the sacral canal. Contrast-enhanced T1-weighted fat-suppressed sagittal and axial MR image (**b, c**) shows homogenous enhancement of the soft tissue in the sacral canal and sacral bone marrow. Leptomeningeal enhancement of the cauda equina and both L5 nerve roots is seen (*white arrows*)



4.5.2 Leukemia

1. Epidemiology

- ALL: 2–10 years old
- AML: > 65 years old
- CML: > 40 years old
- CLL: 50–70 years old
- M > F

2. Location

- Multi-compartment
 - Child: multiple long bones and spine
 - Adults: axial skeleton (dominant)
 - Spinal granulocytic sarcoma
 - Multiple extramedullary masses with diffuse leukemic BM infiltration

3. Characteristic imaging findings

- Leukemic bone marrow infiltration
 - Diffuse low signal on T1-weighted image
 - Abnormal bone marrow enhancement
 - Diffuse, focal, leptomeninges
 - High signal on T2-weighted image

4. Spectrum of imaging findings

- Leukemic line (horizontal vertebral bands)
- Diffuse osteopenia with multiple compression fractures with or without lytic lesion

- Chloroma
 - Focal mass formation

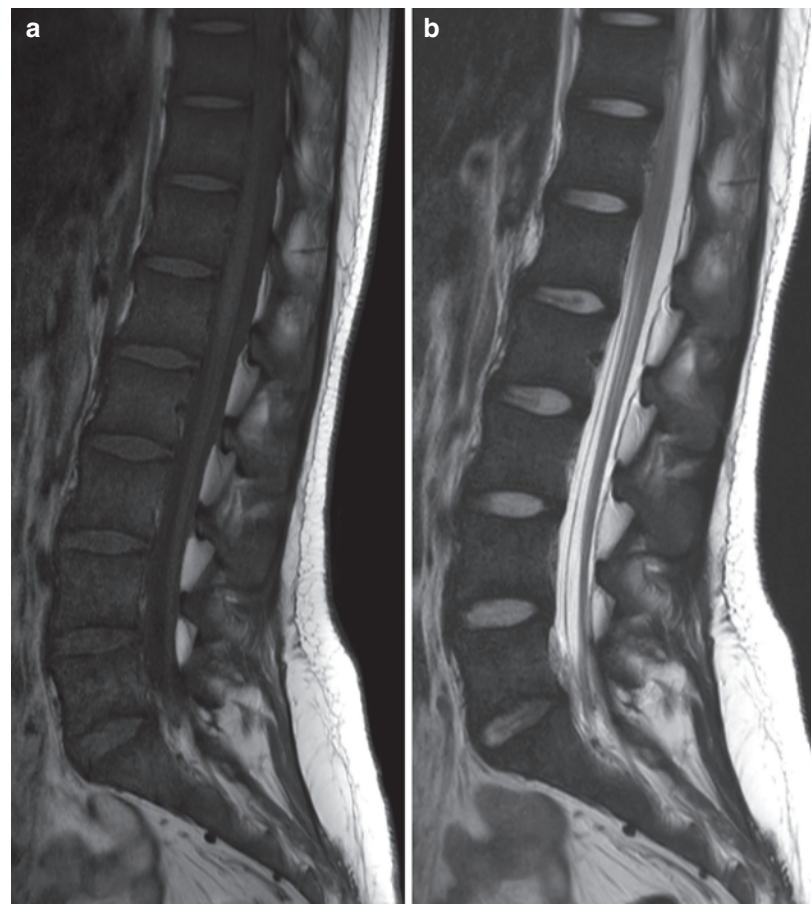
- Granulocytic sarcoma
 - Iso signal on T1-weighted image
 - Peripheral rim enhancement

5. Differential diagnosis

- Metastasis
 - Similar
 - Multifocal bone involvement
 - Metastatic neuroblastoma or rhabdomyosarcoma in child
 - Carcinoma in adults
- Langerhans cell histiocytosis
 - Lytic lesion with periosteal reaction and soft tissue mass
 - Vertebral plana in young patients
- Lymphoma
 - Older patient with large soft tissue mass
 - More multi-compartment involvement
- Ewing's sarcoma
 - Marked periosteal reaction with large soft tissue mass
 - No metaphyseal lucent line

4.5.2.1 Illustrations: Leukemia

Fig. 4.35 An 18-year-old patient with known acute myeloid leukemia. T1-weighted sagittal MR image and T2-weighted sagittal MR image (**a, b**) shows diffuse low signal intensity of the entire visible spine



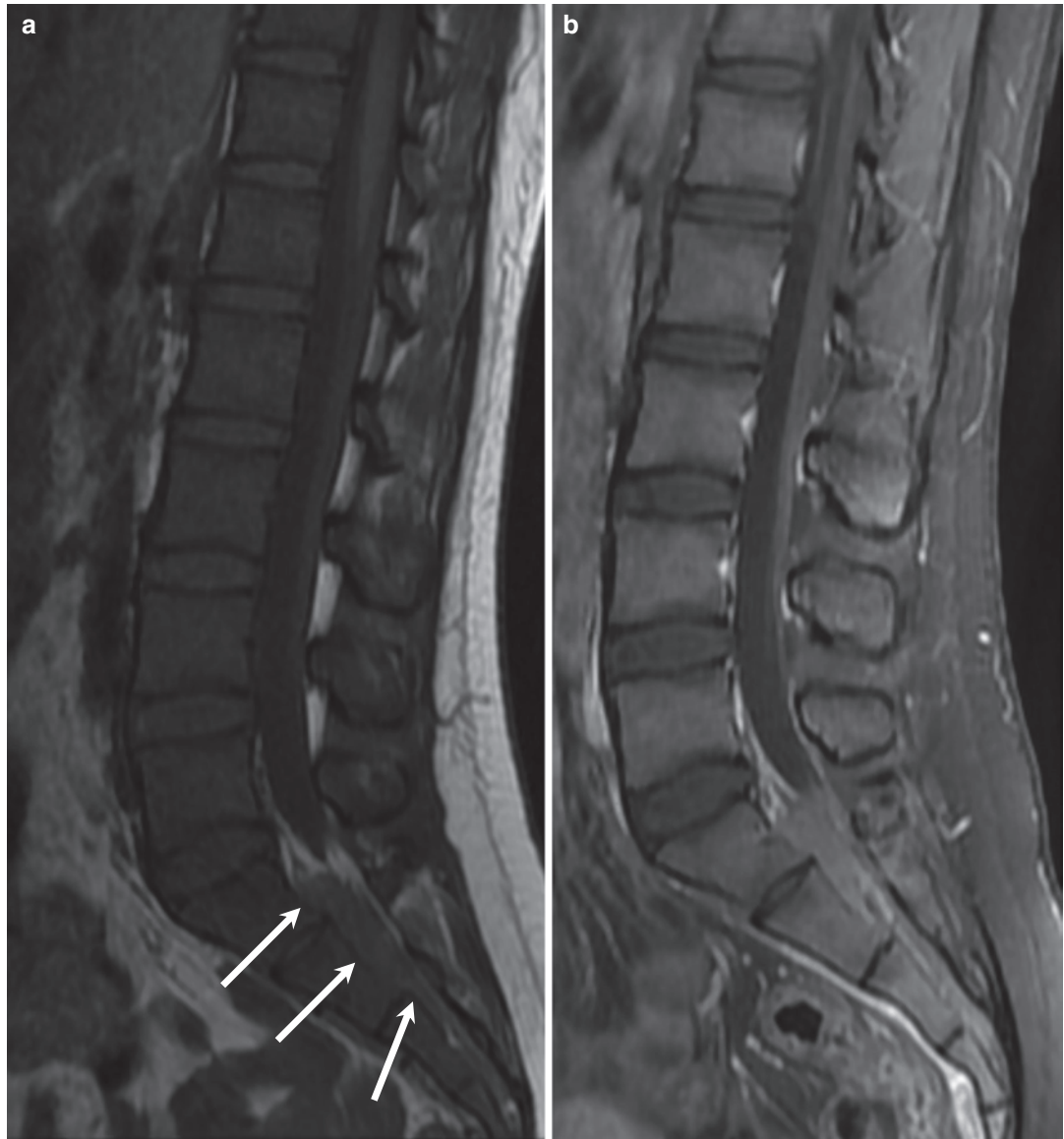


Fig. 4.36 Acute myeloid leukemia bone marrow involvement in a 20-year-old woman. T1-weighted sagittal MR image (a) shows diffuse low signal intensity of the entire visible bone marrow. Soft tissue with low signal intensity

in the sacral canal is seen (white arrows). T1-weighted sagittal image with contrast enhancement shows (b) homogenous enhancement of the bone marrow and soft tissue in the sacral canal

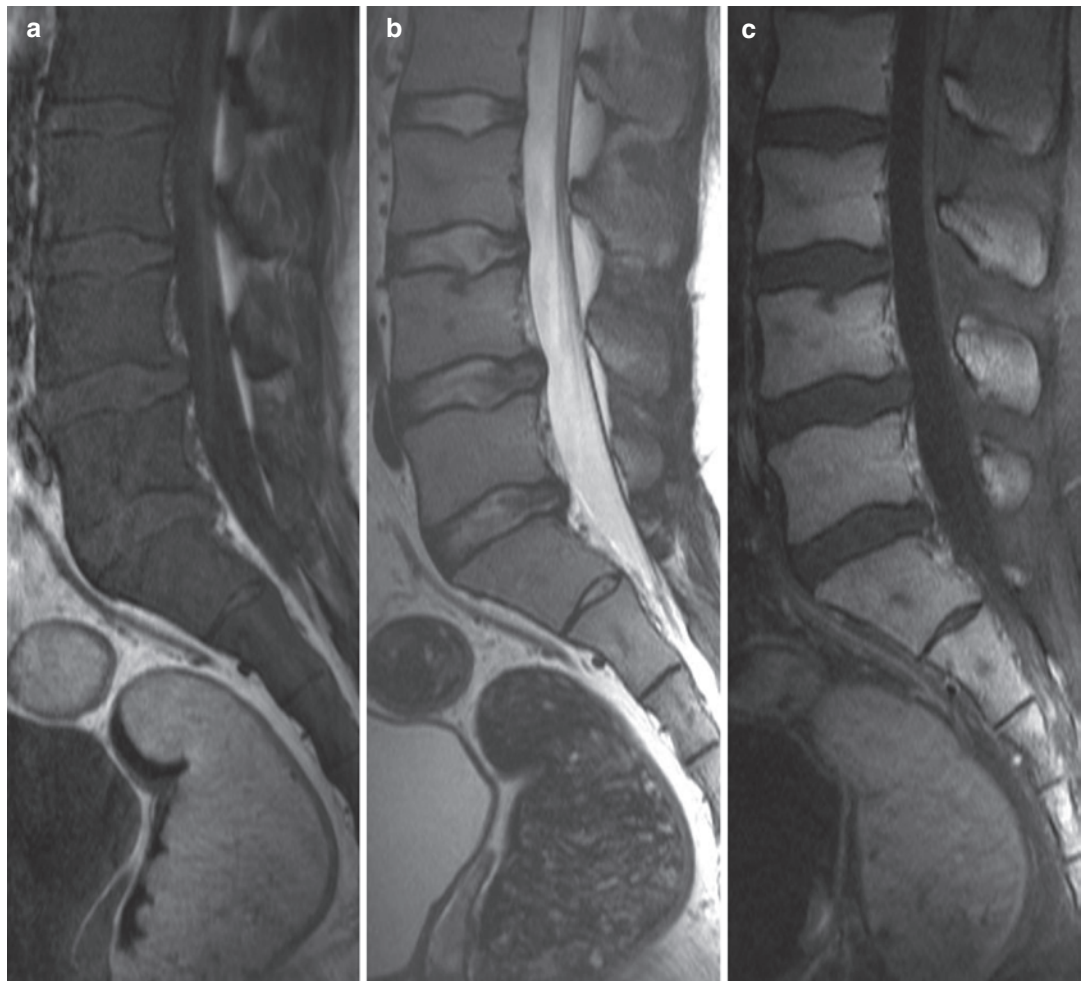


Fig. 4.37 Precursor B cell lymphoblastic leukemia bone marrow involvement in a 17-year-old boy. T1-weighted sagittal MR image (a) shows diffuse homogenous low signal intensity of the entire bone marrow. T2-weighted

sagittal MR image (b) shows diffuse homogenous high signal intensity of the entire visible bone marrow. T1-weighted sagittal image with contrast enhancement shows (c) homogenous enhancement of the bone marrow

4.5.3 Hemangioma

1. Epidemiology

- Peak incidence: 30–50 years old, tendency to increase in size with age
- Asymptomatic: M = F
- Symptomatic: M < F

2. Location

- Thoracic spine (60%) > lumbar spine (29%) > cervical spine (6%) > sacrum (5%)
- Vertebral body >> posterior element

3. Characteristic imaging findings

- Well-defined round or lobular intraosseous masses
- Thickened trabeculation on X-ray, CT, MR
- High signal on T1-weighted image and T2-weighted image
- Well enhancement

4. Spectrum of imaging findings

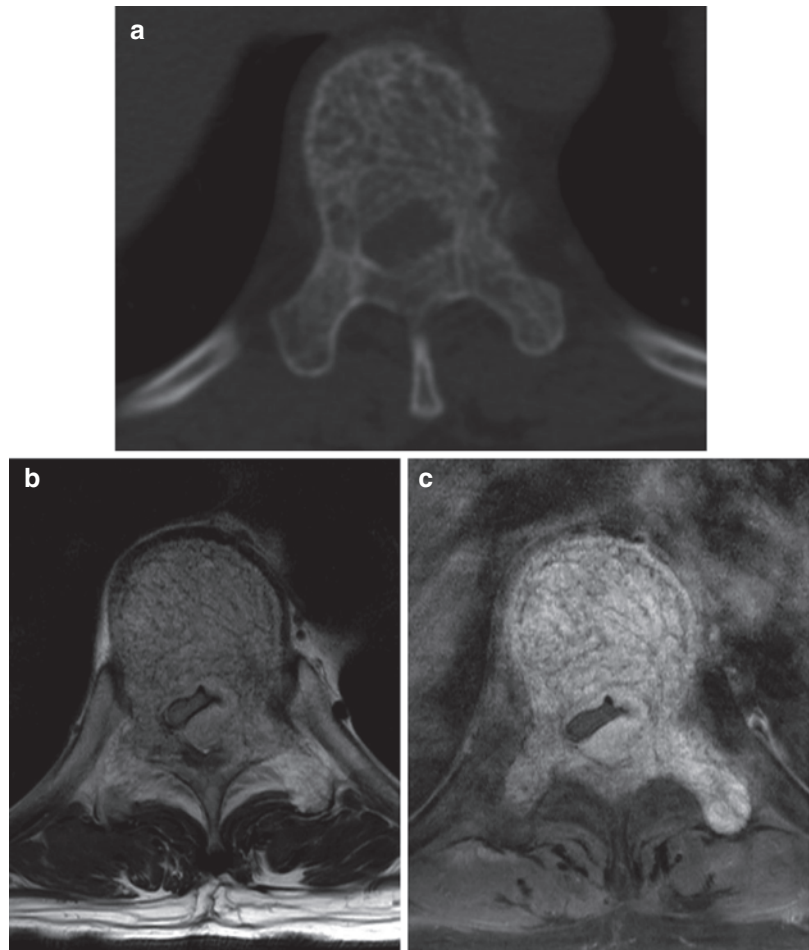
- Low signal on T1-weighted image in vascular (aggressive, symptomatic) hemangioma
- Poor enhancement in sclerosing hemangioma
- Both epidural and vertebral body involvement

5. Differential diagnosis

- Benign notochordal cell tumor
 - Sclerosis on CT
 - Low signal on T1-weighted images
 - No enhancement
- Metastasis
 - Cortical destruction
 - Low signal on T1-weighted image
- Focal fat
 - Irregular shape
 - No enhancement

4.5.3.1 Illustrations: Hemangioma

Fig. 4.38 A 57-year-old woman presented with a myelopathic gait. CT axial image (**a**) shows salt-and-pepper appearance of the T10 body extending into the left lamina. The left lamina shows cortical fraying. T2-weighted axial image (**b**) shows an intraosseous hemangioma with epidural extension compressing the dural sac. Contrast-enhanced T1-weighted axial image (**c**) shows strong enhancement of the lesion



4.6 Infant/Childhood Spinal Tumors

4.6.1 Sacrococcygeal Teratoma

1. Epidemiology

- 50–70% diagnosed in utero or during first day of life
- 80% by 6 month
- <10% beyond 2 years
- M < F

2. Location

- Sacrum/coccyx

3. Characteristic imaging findings

- Heterogeneous sacral mass
- Variable calcifications, mixed solid and cystic component, fat debris, bone, teeth or cartilage, hair
 - Calcification (<60%) on CT
 - Fat: high signal on T1- and T2-weighted image
 - Soft tissue: iso signal on T1- and T2-weighted image
 - Calcium: marked low signal on T1- and T2-weighted image
- Heterogeneous enhancement of solid portion

4. Spectrum of imaging findings

- Mature vs immature teratoma
- Exophytic (AAP types I and II) vs internal (AAP types III and IV)
- GRE
 - Calcification and hemorrhage

5. Differential diagnosis

- Anterior sacral meningocele
 - Cystic mass without solid portion
 - Enlarges with Valsalva maneuver
- Chordoma
 - Rare in child (40–50 years old)
 - High signal on T2-weighted image
 - Fuzzy calcification
- Dermoid tumor
 - Small and homogenous
 - High signal on T2-weighted/iso to high signal in T1-weighted image
- Exophytic rhabdomyosarcoma
 - Aggressive feature without calcification

4.6.1.1 Illustrations: Sacrococcygeal Teratoma

Fig. 4.39 Sacrococcygeal teratoma at the presacral area in a 10-day-old infant girl. Axial T2-weighted image (a) and T2-weighted fat-saturated image (b) at the level of the coccyx (C) show a well-defined heterogeneous presacral mass with predominantly fat components and focal cystic changes (white arrows). The rectum (R) was displaced anterolaterally

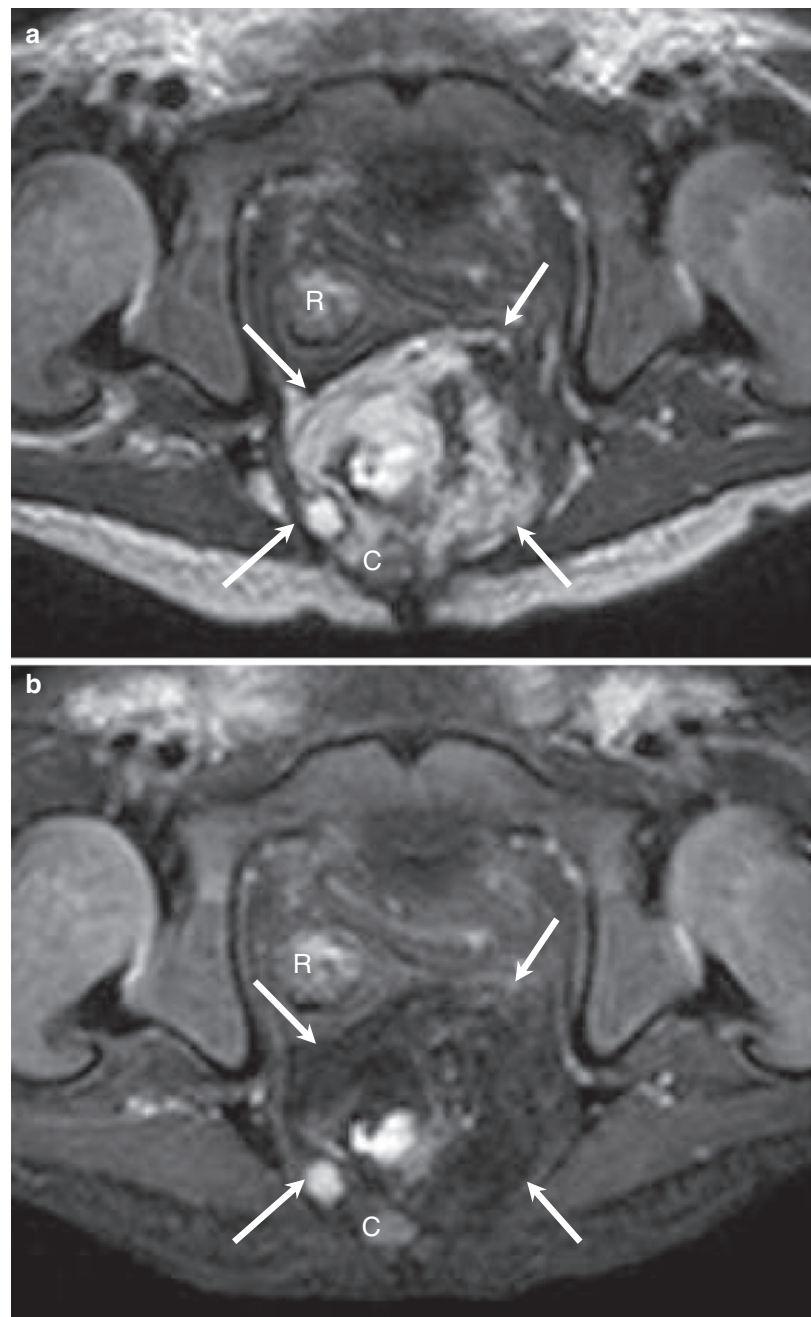
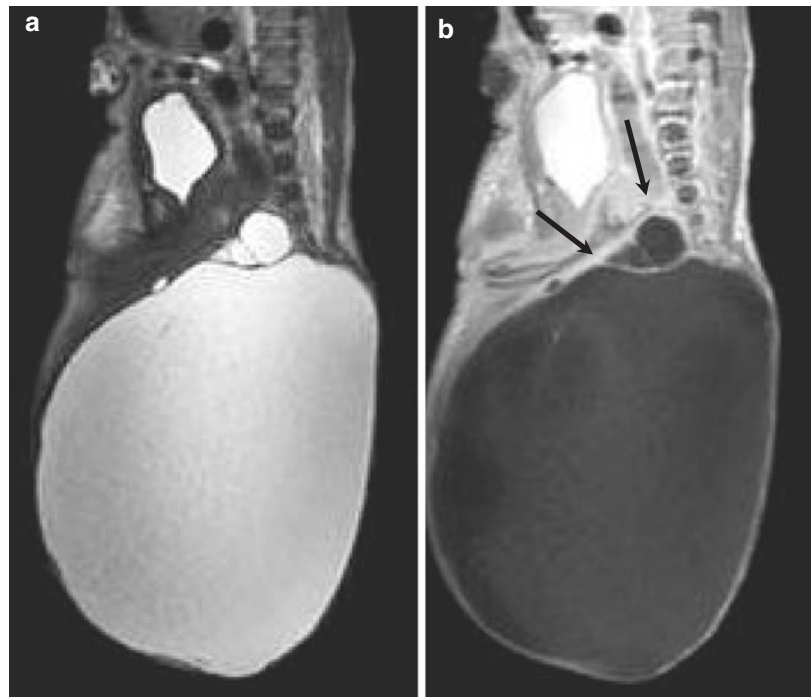


Fig. 4.40 Cystic sacrococcygeal teratoma in an infant girl. Sagittal T2-weighted MR image (**a**) and sagittal contrast-enhanced T1-weighted fat-saturated MR image (**b**) show a huge extrapelvic, septated, cystic mass with small presacral component (black arrows)



4.6.2 Langerhans Cell Histiocytosis

1. Epidemiology

- Predominantly children, adolescents, or young adults
- M > F

2. Location

- Calvarium > mandible > long bones > vertebrae
- Spine involvement: children > adult
 - Thoracic > lumbar > cervical

3. Characteristic imaging findings

- Vertebral plana without disc space or posterior element involvement
- Destructive lytic (non-sclerotic) lesion on CT
 - With or without pathologic fracture
- Homogenous enhancing soft tissue mass with paraspinal or epidural extension

- Low signal on T1-weighted image and high signal on T2-weighted image

4. Spectrum of imaging findings

- Scoliosis or kyphosis uncommon

5. Differential diagnosis

- Ewing's sarcoma
 - Permeative bone destruction
 - Large soft tissue mass formation
- Neuroblastoma
 - Abdominal or thoracic paraspinal mass with intraspinal extension
- Giant cell tumor
 - > 30 years old
 - Expansile lytic vertebral and soft tissue mass
- Metastasis/hematopoietic malignancy

4.6.2.1 Illustrations: Langerhans Cell Histiocytosis

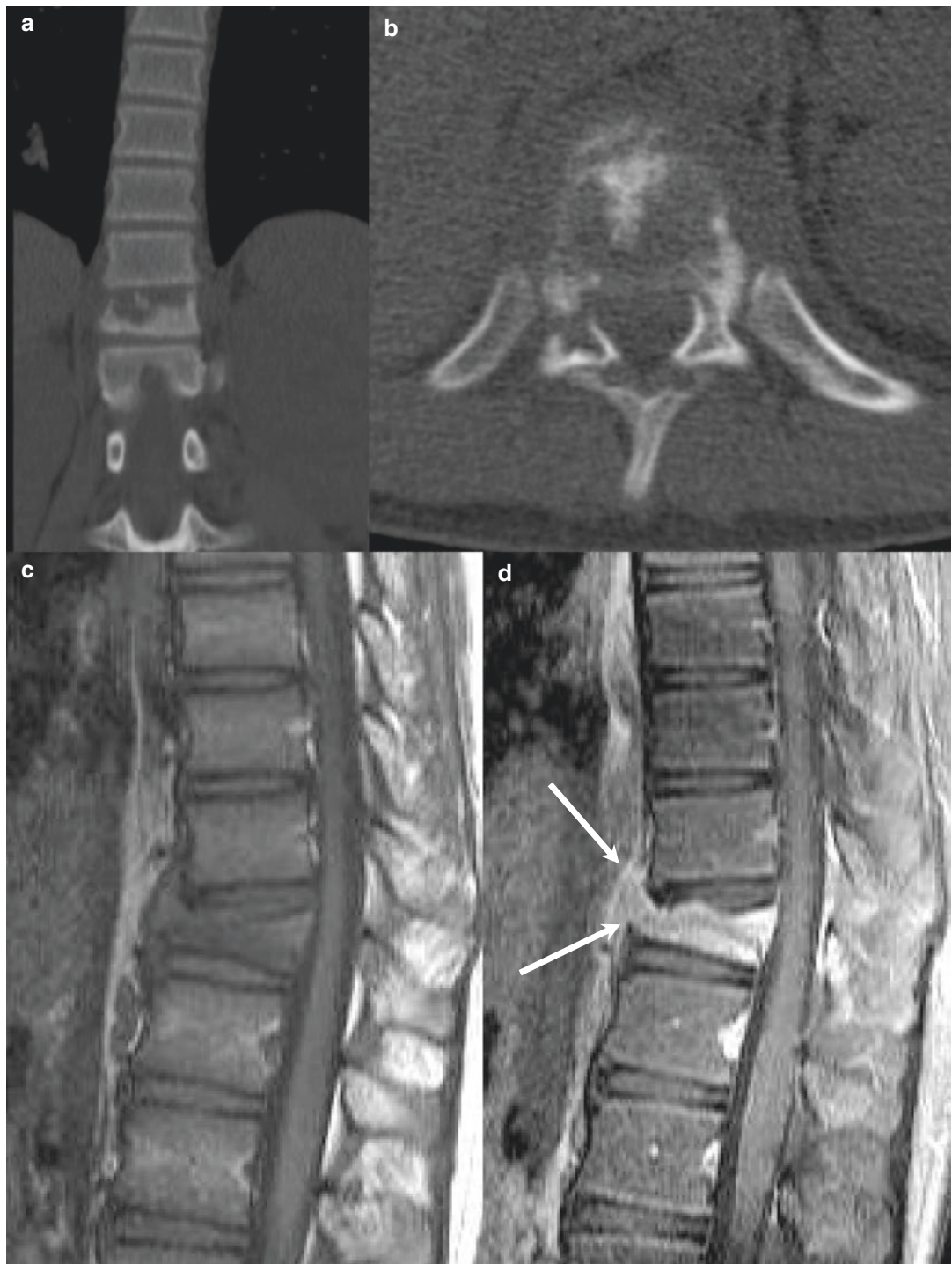


Fig. 4.41 Langerhans cell histiocytosis of the T11 body in a 13-year-old boy. Coronal and axial CT scan images (a, b) show a destructive osteolytic bone mass involving the T11 vertebral body and posterior elements. Sagittal T1-weighted MR image (c) shows collapse of the T11

body and of iso- to hypointense signal to the intervertebral disc. Sagittal contrast-enhanced T1-weighted fat-saturated MR image (d) shows homogeneous enhancement of the involved vertebra with prevertebral extension (*white arrows*). There is no compression of the spinal cord

Fig. 4.42 Langerhans cell histiocytosis of the C6 body in a 7-year-old boy. Sagittal T1-weighted MR image (**a**) shows severe collapse (vertebra plana) of the C6 body (*white arrows*). Sagittal contrast-enhanced T1-weighted fat-saturated MR image (**b**) shows enhancement of the C6 vertebra with involvement of its posterior elements (*black arrows*). There is no compression of the spinal cord

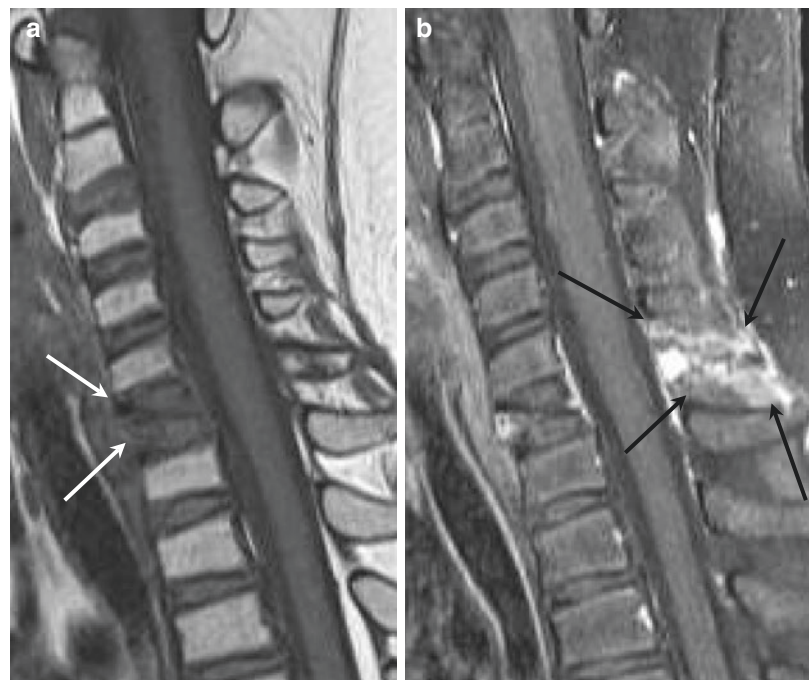




Fig. 4.43 Langerhans cell histiocytosis of the T9 body in an 8-year-old girl. Sagittal CT scan of thoracic spine (a) shows an osteolytic lesion with sclerotic margins and cortical destruction of the T9 body. Sagittal T1-weighted MR image (b) shows a mild collapse of the T9 body isointense

to slightly hypointense to the intervertebral disc. Sagittal contrast-enhanced T1-weighted fat-saturated MR image (c) shows intense enhancement of the involved vertebra with extension into its posterior elements (*white arrow*). There is no compression of the spinal cord

4.6.3 Ewing's Sarcoma

1. Epidemiology

- 1st peak: < 20 years old (90%)
- 2nd peak: 50 years old
- M > F

2. Location

- Spine: 5% of all Ewing's sarcoma
- Sacrum: m/c
- Vertebral body → neural arch
- Spreads along the peripheral nerve

3. Characteristic imaging findings

- Permeative lytic lesion of VB or sacrum with large soft tissue mass on CT
- Areas of central necrosis common
- “Percolates” through tiny perforations in cortex
 - “Smudged” appearance on MR
- Low signal on T1-weighted image and iso signal on T2-weighted image
- Heterogeneous contrast enhancement

4. Spectrum of imaging findings

- Rare sclerotic lesion (5%)
 - Reactive bone formation
 - No ossification at soft tissue component

• Tumor vs peritumoral edema

- Contrast enhancement at peritumoral edema with Gd

5. Differential diagnosis

- Primitive neuroectodermal tumor
 - Clinical/radiological identical to Ewing's sarcoma
- Langerhans cell histiocytosis
 - Discrete geographic lytic lesion
 - May identical radiologic appearance to Ewing's sarcoma
- Metastatic neuroblastoma
 - Adrenal or extra-adrenal primary
 - Children
- Osteosarcoma
 - Bone matrix on CT
 - Cortical destruction >> permeation
 - Vertebral body or neural arch involvement

4.6.3.1 Illustrations: Ewing's Sarcoma

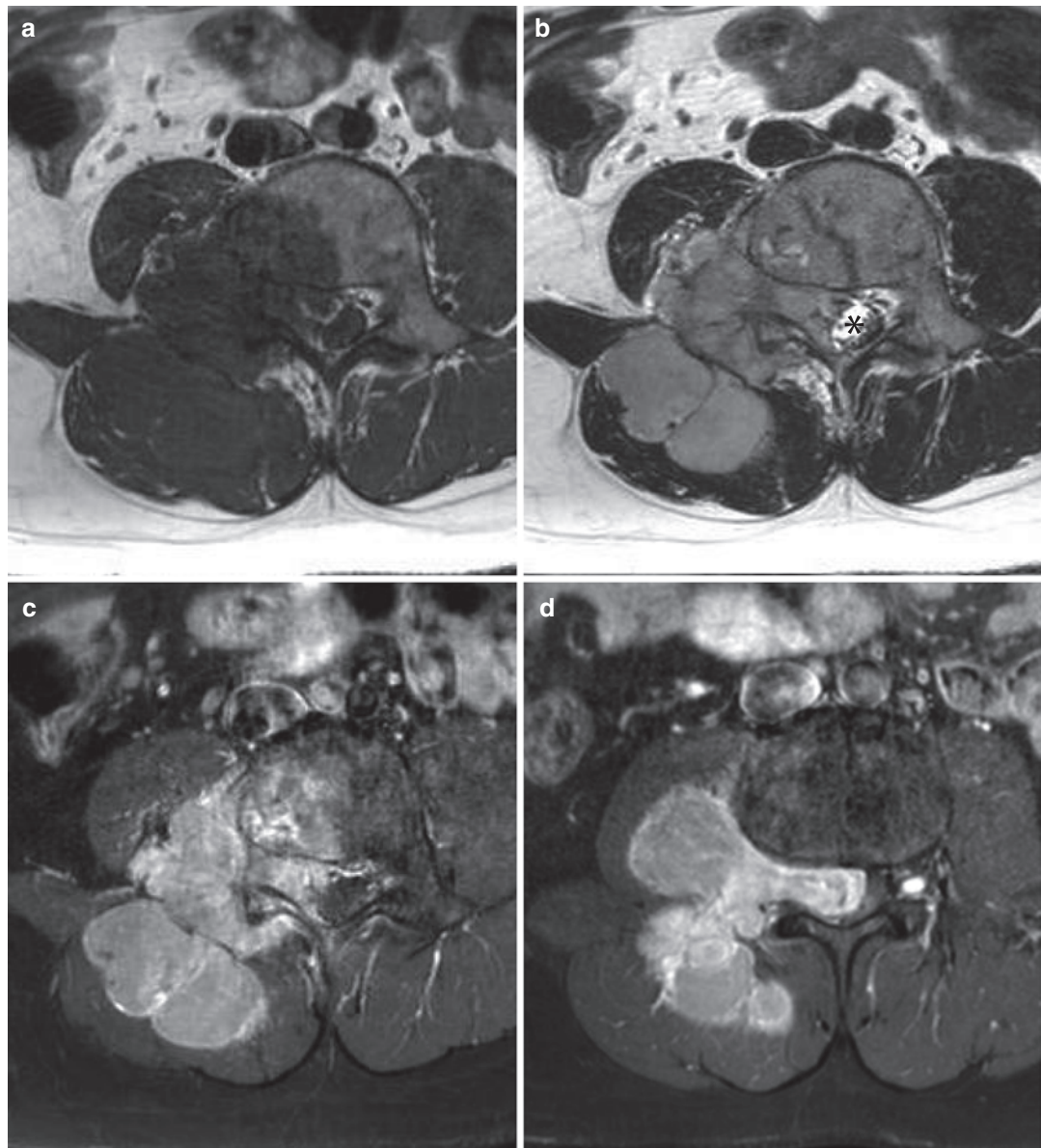


Fig. 4.44 Ewing's sarcoma involving the L4 vertebra in an 8-year-old boy. Axial T1-weighted (a), T2-weighted (b), and contrast-enhanced T1-weighted fat-saturated (c, d) MR images at the level of L4 vertebra show a lobulated

enhancing mass involving right side of the vertebral body and ipsilateral foraminal space with extension to the ipsilateral paraspinal muscles. Note the contralateral displacement of the thecal sac (asterisk in b)

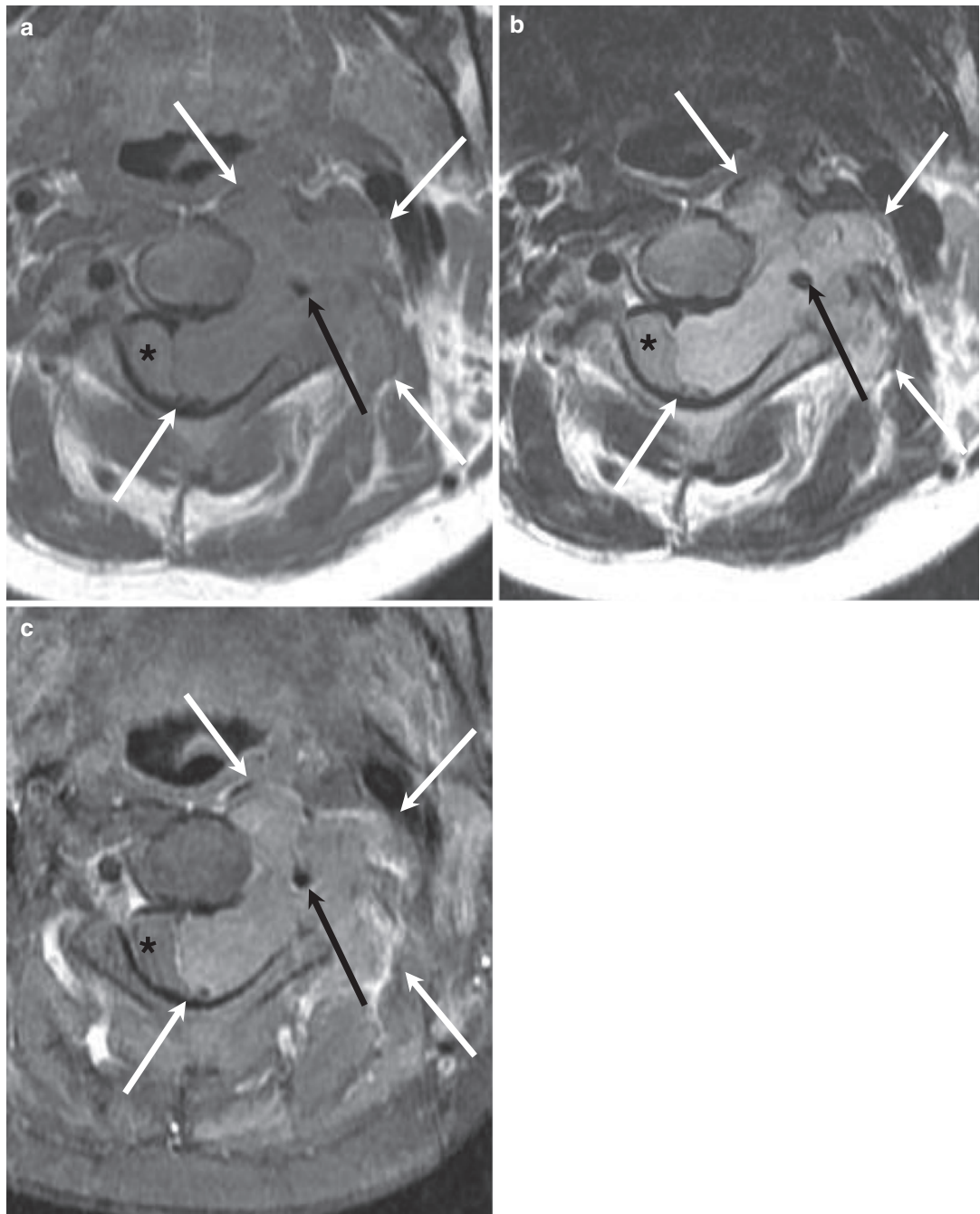
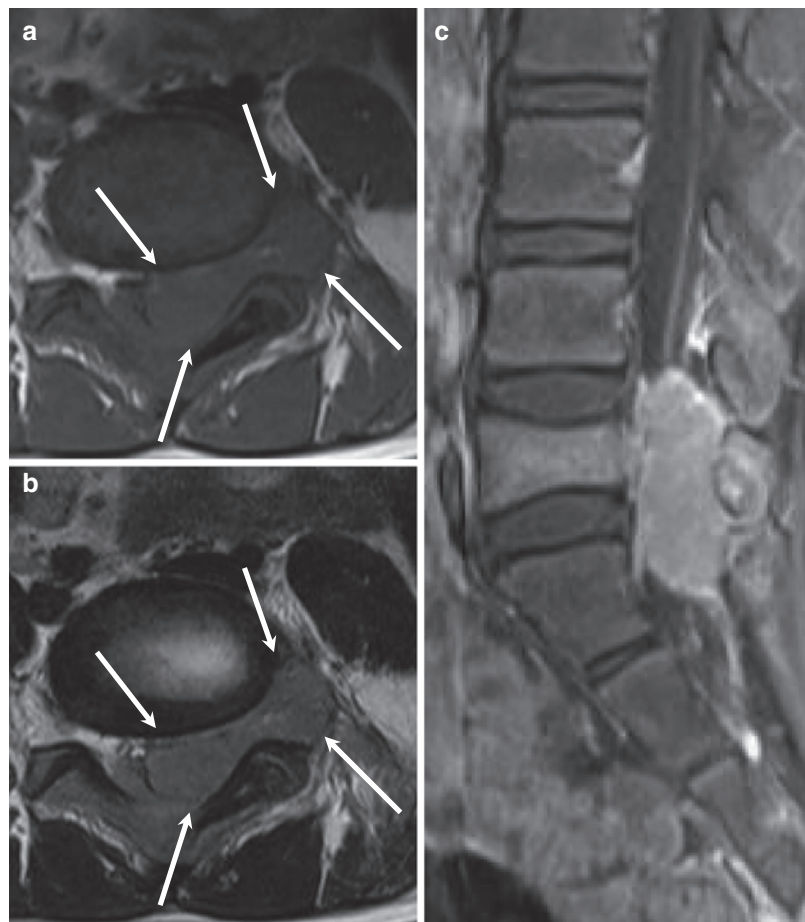


Fig. 4.45 Extraskeletal Ewing's sarcoma at the cervical paraspinal area in a 10-year-old girl. Axial T1-weighted (a), T2-weighted (b), and contrast-enhanced T1-weighted fat-saturated (c) MR images at the level of C3 vertebra show a lobulated enhancing mass (white arrows) in the left paraspinal area, isointense to muscle on T1-weighted

images (a) and hyperintense to muscle on T2-weighted images (c). The ipsilateral neural foraminal widening, encased ipsilateral vertebral artery (black arrow), and contralateral displacement of the spinal cord (asterisk) are observed. There is no intraosseous invasion

Fig. 4.46 Ewing's sarcoma involving the L5 vertebra in a 9-year-old boy. Axial T1-weighted (a) and T2-weighted (b) MR images at the level of the L5/S1 intervertebral disc show an epidural mass (white arrows) widening the left foraminal space. Contralateral displacement of the thecal sac is also observed. Sagittal contrast-enhanced T1-weighted fat-saturated MR image (c) shows diffuse enhancement with mild collapse of the L5 body



Bibliography

- Arima H, Hasegawa T, Togawa D, Yamato Y, Kobayashi S, Yasuda T, et al. Feasibility of a novel diagnostic chart of intramedullary spinal cord tumors in magnetic resonance imaging. *Spinal Cord.* 2014;52(10):769–73. doi:10.1038/sc.2014.127.
- Avni FE, Guibaud L, Robert Y, Segers V, Ziereisen F, Delaet MH, et al. MR imaging of fetal sacrococcygeal teratoma: diagnosis and assessment. *AJR Am J Roentgenol.* 2002;178(1):179–83. doi:10.2214/ajr.178.1.1780179.
- Bauerle T, Hillengass J, Fechtner K, Zechmann CM, Grenacher L, Moehler TM, et al. Multiple myeloma and monoclonal gammopathy of undetermined significance: importance of whole-body versus spinal MR imaging. *Radiology.* 2009;252(2):477–85. doi:10.1148/radiol.2522081756.
- Cramer GD, Darby SA. Clinical anatomy of the spine, spinal cord, and ANS. Philadelphia: Elsevier Health Sciences; 2013.
- Diehn FE, Rykken JB, Wald JT, Wood CP, Eckel LJ, Hunt CH, et al. Intramedullary spinal cord metastases: prognostic value of MRI and clinical features from a 13-year institutional case series. *AJNR Am J Neuroradiol.* 2015;36(3):587–93. doi:10.3174/ajnr.A4160.
- Do-Dai DD, Rovira MJ, Ho VB, Gomez RR. Childhood onset of myxopapillary ependymomatosis: MR features. *AJNR Am J Neuroradiol.* 1995;16(4 Suppl):835–9.
- Imagama S, Ito Z, Wakao N, Sakai Y, Kato F, Yukawa Y, et al. Differentiation of localization of spinal hemangioblastomas based on imaging and pathological findings. *Eur Spine J Off Publ Eur Spine Soc Eur Spinal Deformity Soc Eur Sect Cervical Spine Res Soc.* 2011;20(8):1377–84. doi:10.1007/s00586-011-1814-6.
- Kang HS, Lee JW, Kwon JW. Radiology illustrated: spine. Heidelberg: Springer Science & Business Media; 2014.
- Kim DH, Chang U-K, Kim S-H, Bilsky MH. Tumors of the spine. Philadelphia: Elsevier Health Sciences; 2008.
- Lecouvet FE, Whole-Body MR. Imaging: musculoskeletal applications. *Radiology.* 2016;279(2):345–65. doi:10.1148/radiol.2016142084.
- Lecouvet FE, Vande Berg BC, Maldague BE, Michaux L, Laterre E, Michaux JL, et al. Vertebral compression fractures in multiple myeloma. Part I. Distribution and appearance at MR imaging. *Radiology.* 1997;204(1):195–9. doi:10.1148/radiology.204.1.9205246.

- Lecouvet FE, Vande Berg BC, Michaux L, Malghem J, Maldague BE, Jamart J, et al. Stage III multiple myeloma: clinical and prognostic value of spinal bone marrow MR imaging. *Radiology*. 1998;209(3):653–60. doi:[10.1148/radiology.209.3.9844655](https://doi.org/10.1148/radiology.209.3.9844655).
- Lee JW, Cho EY, Hong SH, Chung HW, Kim JH, Chang KH, et al. Spinal epidural hemangiomas: various types of MR imaging features with histopathologic correlation. *AJNR Am J Neuroradiol*. 2007;28(7):1242–8. doi:[10.3174/ajnr.A0563](https://doi.org/10.3174/ajnr.A0563).
- Merhemic Z, Stosic-Opincal T, Thurnher MM. Neuroimaging of spinal tumors. *Magn Reson Imaging Clin N Am*. 2016;24(3):563–79. doi:[10.1016/j.mric.2016.04.007](https://doi.org/10.1016/j.mric.2016.04.007).
- Rodallec MH, Feydy A, Larousserie F, Anract P, Campagna R, Babinet A, et al. Diagnostic imaging of solitary tumors of the spine: what to do and say. *Radiographics Rev Publ Radiol Soc N Am Inc*. 2008;28(4):1019–41. doi:[10.1148/rг.284075156](https://doi.org/10.1148/rг.284075156).
- Ross JS, Moore KR. Diagnostic imaging: spine. Philadelphia: Elsevier Health Sciences; 2015.
- Scheinemann K, Bartels U, Huang A, Hawkins C, Kulkarni AV, Bouffet E, et al. Survival and functional outcome of childhood spinal cord low-grade gliomas. Clinical article. *J Neurosurg Pediatr*. 2009;4(3):254–61. doi:[10.3171/2009.4.PEDS08411](https://doi.org/10.3171/2009.4.PEDS08411).
- Vidal JA, Murphey MD. Primary tumors of the osseous spine. *Magn Reson Imaging Clin N Am*. 2007;15(2):239–55. vii doi:[10.1016/j.mric.2007.05.003](https://doi.org/10.1016/j.mric.2007.05.003).
- Yang C, Li G, Fang J, Wu L, Yang T, Deng X, et al. Intramedullary gangliogliomas: clinical features, surgical outcomes, and neuropathic scoliosis. *J Neurooncol*. 2014;116(1):135–43. doi:[10.1007/s11060-013-1267-3](https://doi.org/10.1007/s11060-013-1267-3).
- Young Poussaint T, Yousuf N, Barnes PD, Anthony DC, Zurakowski D, Scott RM, et al. Cervicomedullary astrocytomas of childhood: clinical and imaging follow-up. *Pediatr Radiol*. 1999;29(9):662–8. doi:[10.1007/s002470050671](https://doi.org/10.1007/s002470050671).

Common Spinal Tumors Outside the Top 3 Lists (in Alphabetical Order)

Contents

5.1	Aneurysmal Bone Cyst (ABC)	99
5.1.1	Illustrations: Aneurysmal Bone Cyst (ABC)	100
5.2	Benign Notochordal Cell Tumor (BNCT)	101
5.2.1	Illustrations: Benign Notochordal Cell Tumor (BNCT)	102
5.3	Bone Island	105
5.3.1	Illustrations: Bone Island	106
5.4	Cavernous Malformation (Intramedullary Cavernous Hemangioma, Cavernoma)	109
5.4.1	Illustrations: Cavernous Malformation	110
5.5	Chondrosarcoma	114
5.5.1	Illustrations: Chondrosarcoma	115
5.6	Chordoma	119
5.6.1	Illustrations: Chordoma	120
5.7	Giant Cell Tumor	123
5.7.1	Illustrations: Giant Cell Tumor	124
5.8	Lipoma	128
5.8.1	Illustrations: Lipoma	129
5.9	Osteoblastoma	132
5.9.1	Illustrations: Osteoblastoma	133
5.10	Osteochondroma	136
5.10.1	Illustrations: Osteochondroma	137
5.11	Osteoid Osteoma	140
5.11.1	Illustrations: Osteoid Osteoma	141
5.12	Osteosarcoma	144
5.12.1	Illustrations: Osteosarcoma	145
5.13	Plasmacytoma	147
5.13.1	Illustrations: Plasmacytoma	148
	Bibliography	151

5.1 Aneurysmal Bone Cyst (ABC)

1. Epidemiology
 - 10–20 years old
 - M < F
2. Location
 - Most common in thoracic spine
 - Intraosseous
 - Posterior arch > vertebral body
3. Characteristic imaging findings
 - Multiloculated cystic mass with fluid-fluid level on MRI due to hemorrhage
 - Ballooning appearance with cortical thinning
4. Spectrum of imaging findings
 - Solid enhancing portion suggestive of secondary aneurysmal bone cyst
 - Cause of secondary aneurysmal bone cyst
 - Giant cell tumor
 - Osteoblastoma
 - Chondroblastoma
5. Differential diagnosis
 - Giant cell tumor without aneurysmal bone cyst change
 - Solid portion
 - No fluid-fluid level
 - Sacrum
 - Telangiectatic osteosarcoma
 - Cortical destruction and paravertebral mass formation
 - Large solid enhancing portion

5.1.1 Illustrations: Aneurysmal Bone Cyst (ABC)

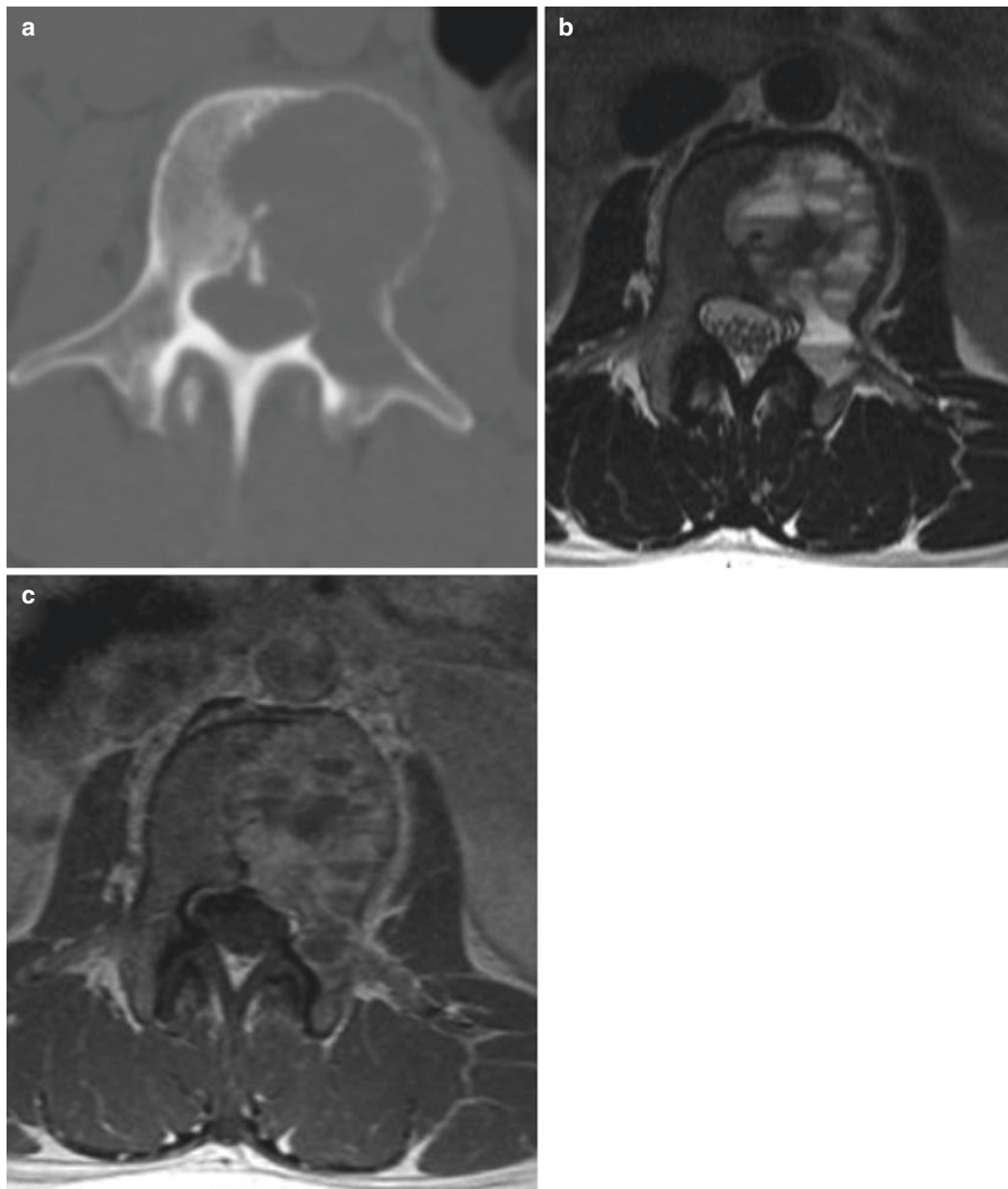


Fig. 5.1 Aneurysmal bone cyst of the L3 vertebrae in a 29-year-old woman. Axial CT scan of the lumbar spine (a) shows an expansile mass with cortical thinning of the L3 vertebral body and left side pedicle. T2-weighted axial

MR image (b) shows a multiloculated cystic mass with internal fluid-fluid levels due to hemorrhage. Contrast-enhanced T1-weighted axial MR image (c) shows internal septal wall enhancement

5.2 Benign Notochordal Cell Tumor (BNCT)

1. Epidemiology

- Mean: 40 years (10–60 years)
- M < F

2. Location

- Intraosseous
- Sacrococcygeal > skull base > cervical and lumbar vertebrae

3. Characteristic imaging findings

- CT: osteosclerosis in the vertebral body
- MR: low T1 SI, intermediate to high T2 SI, no contrast enhancement

4. Spectrum of imaging findings

- Can be extraosseous

5. Differential diagnosis

- Chordoma
 - Extraosseous components on CT
 - Contrast enhancement on CE T1WI
 - Bone destruction on CT
- Hemangioma
 - High signal on T1-weighted image
 - If low signal on T1-weighted image, enhancement due to vascular component (vascular hemangioma)
 - No osteosclerosis, thickening of vertical trabeculation

5.2.1 Illustrations: Benign Notochordal Cell Tumor (BNCT)

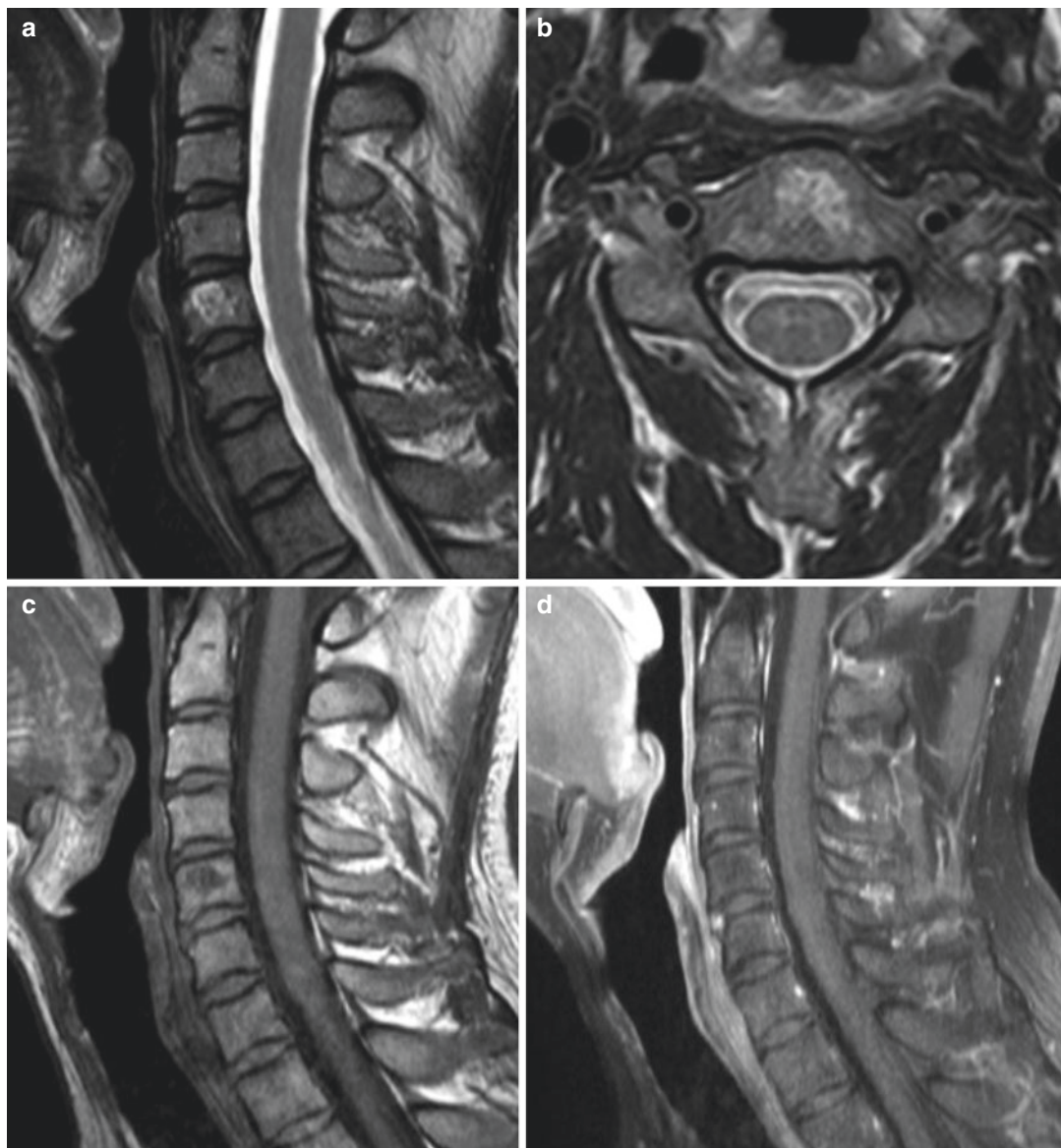


Fig. 5.2 Benign notochordal cell tumor of the C5 vertebrae in a 34-year-old man. T2-weighted sagittal and axial MR images (**a, b**) show a heterogeneous high signal intensity mass in the central portion of the C5 vertebral body.

The mass shows low signal intensity on T1-weighted sagittal MR image (**c**). Contrast-enhanced T1-weighted sagittal MR image (**d**) shows no enhancement of the mass

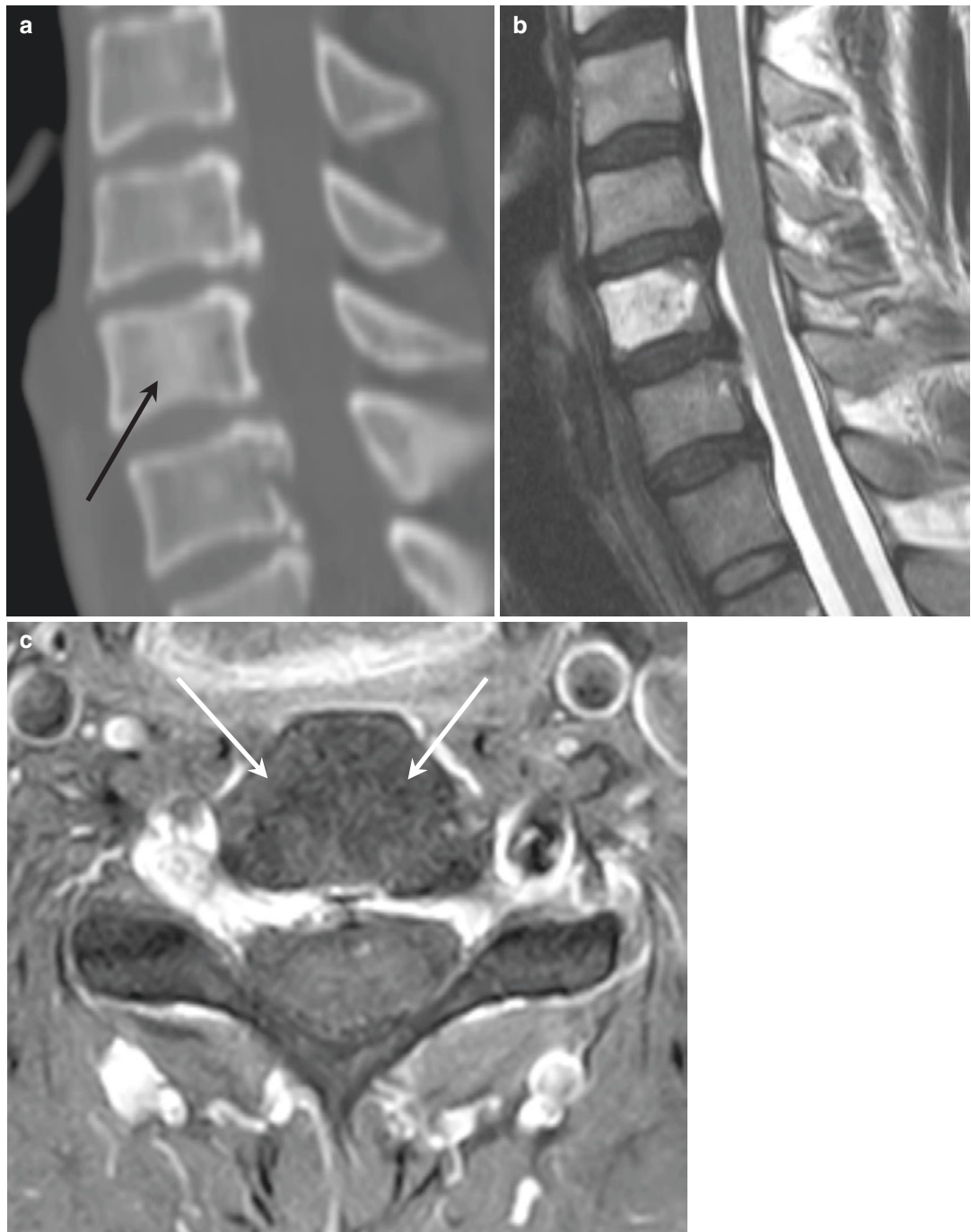


Fig. 5.3 Benign notochordal cell tumor of the C5 vertebrae in a 41-year-old man. C-spine CT sagittal image (a) shows ill-defined sclerosis in the central portion of the C5 vertebral body (*black arrow*). T2-weighted sagittal MR image (b) shows homogenous high signal intensity within the mass. Contrast-enhanced T1-weighted axial MR image (c) shows no enhancement of the mass (*white arrows*)

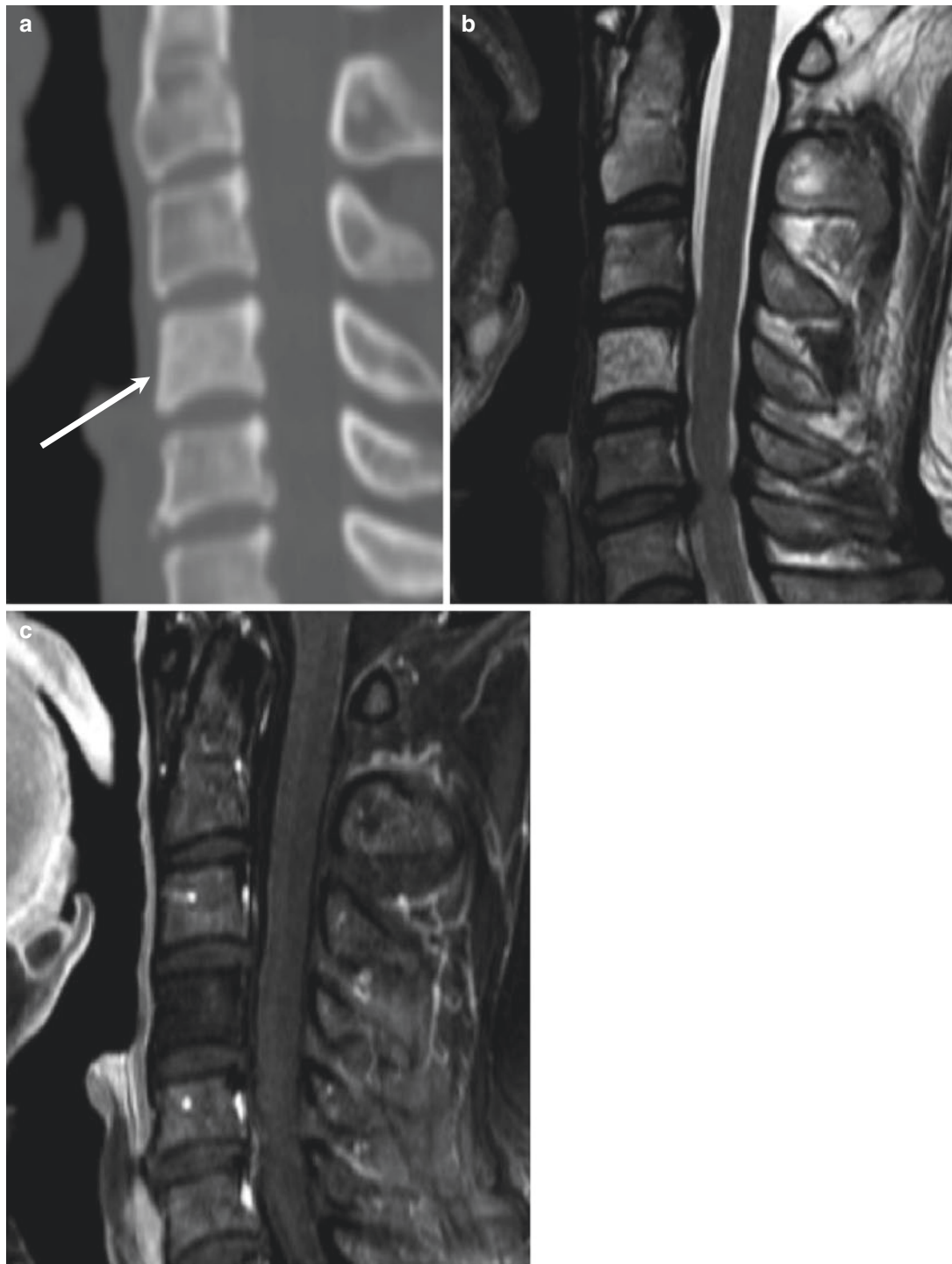


Fig. 5.4 Benign notochordal cell tumor of the C4 vertebrae in a 51-year-old woman. C-spine CT sagittal image (a) shows diffuse sclerosis involving the entire C4 vertebral body (white arrow). T2-weighted sagittal MR image

(b) shows homogenous high signal intensity of the C4 vertebral body. Contrast-enhanced T1-weighted sagittal MR image (c) shows low signal intensity with no enhancement

5.3 Bone Island

1. Epidemiology
2. Location
 - Anywhere in the spine
3. Characteristic imaging findings
 - Small round foci of dense bone within the medullary space on radiography and CT
 - Radiating spicules at the margins blending with surrounding trabeculae
 - “Thorny radiating” or “fingers”
 - Low signal intensity on all MR sequences
4. Spectrum of imaging findings
 - Giant bone island
 - More than 1 cm
 - Heterogeneous signal on MR
 - Increase in size over time

5. Differential diagnosis

- Osteoblastic metastasis
 - Enhancing area within or margin of the mass
 - Multiple
 - Osteolytic masses in the other site
- Osteosarcoma
 - Mixed areas of osteoblastic and osteolytic
 - Irregular margin
 - Extraskeletal component

5.3.1 Illustrations: Bone Island

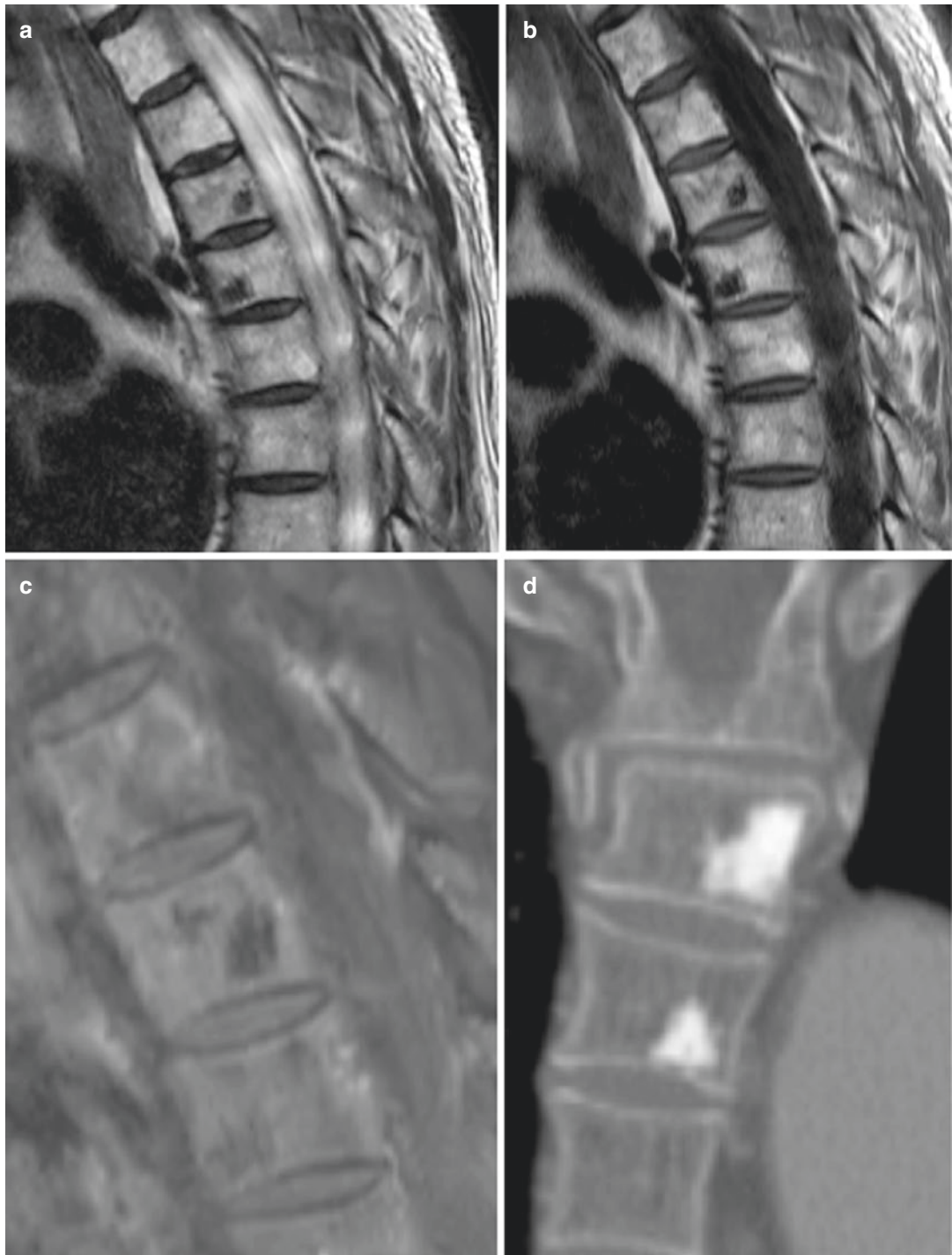


Fig. 5.5 Bone islands in a 75-year-old man. T2-weighted (a) and T1-weighted (b) sagittal MR images show dark signal foci in the T4 and T5 vertebral bodies. T1-weighted

sagittal image with contrast enhancement (c) shows no enhancement. Coronal image from the chest CT (d) shows sclerotic bone lesions in the same area

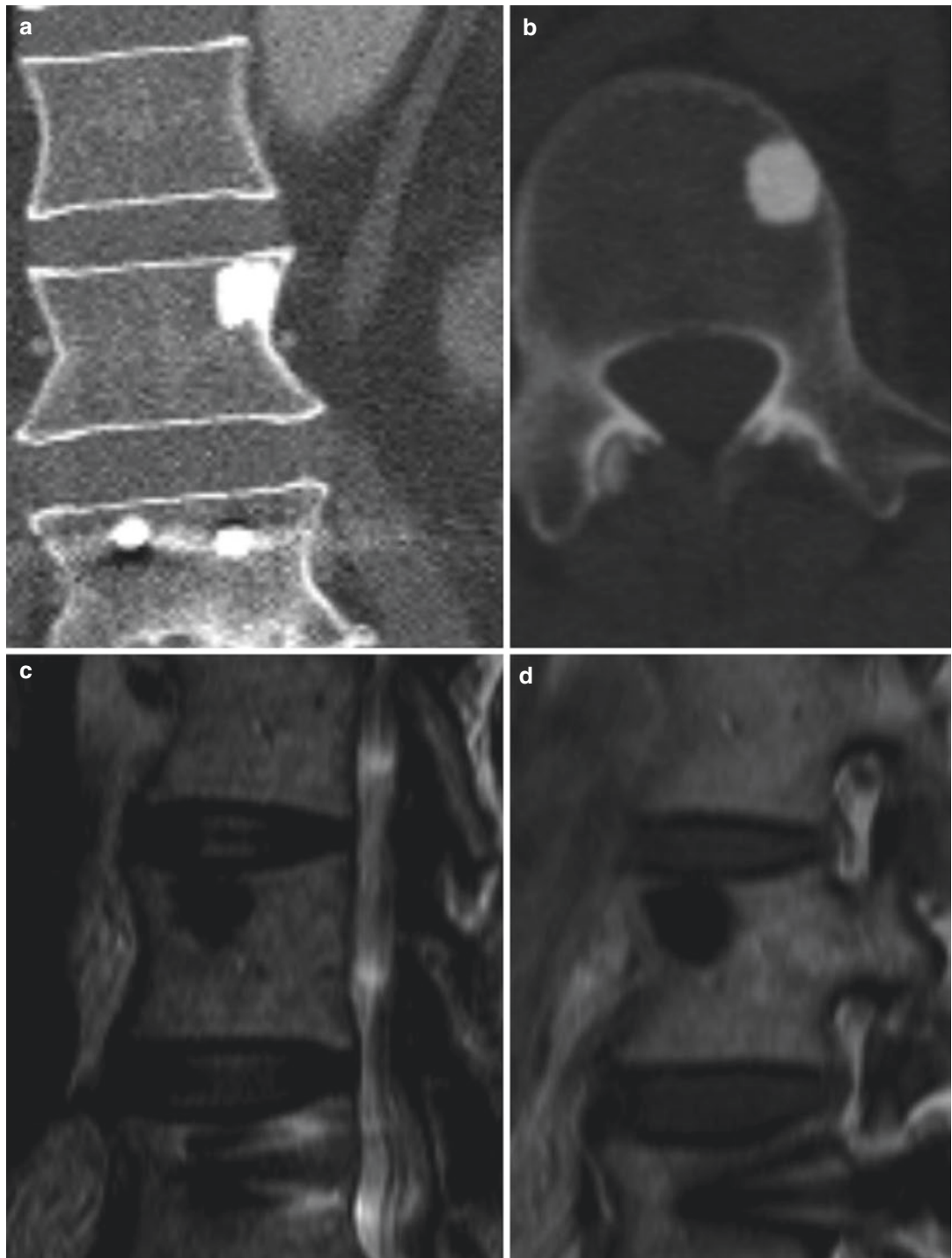


Fig. 5.6 Bone island in a 74-year-old man. Coronal and axial L-spine CT images (**a, b**) show well-defined dense sclerosis in the left superior aspect of the L1 vertebral body. T2-weighted sagittal MR image (**c**) shows dark signal intensity of the lesion. T1-weighted sagittal MR image with contrast enhancement (**d**) shows no enhancement

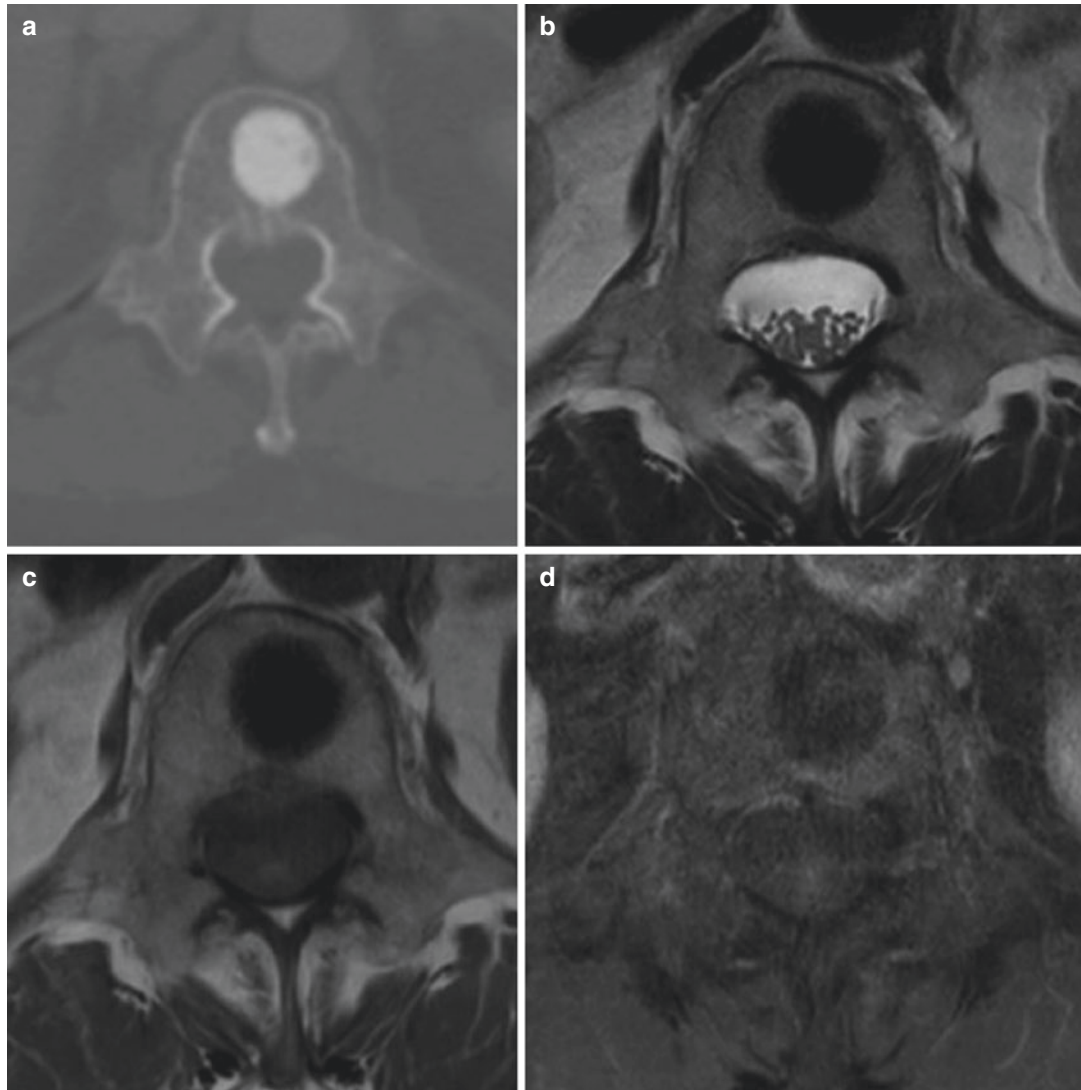


Fig. 5.7 Growing large bone island in a 66-year-old woman. CT axial image (a) shows a 1.9 cm dense sclerotic lesion in the L1 vertebral body. T2-weighted (b) and T1-weighted axial MR images (c) show dark signal

intensity of the lesion. T1-weighted axial MR image with contrast enhancement (d) shows no enhancement. Biopsy reveals histology results consistent with a bone island

5.4 Cavernous Malformation (Intramedullary Cavernous Hemangioma, Cavernoma)

1. Epidemiology

- F>M (2:1)
- 20–50 years

2. Location

3. Characteristic imaging findings

- Reticulate appearance with areas of mixed signal intensity on both T1WI and T2WI
 - Rim of low signal (T2WI) due to hemosiderin
 - No definite enhancement
- ### 4. Spectrum of imaging findings
- Acute hemorrhage
 - Foci of acute hemorrhage: low signal on T2-weighted image and high signal on T1-weighted image

- Spinal cord edema and swelling: area of T2-hyperintensity around the hemorrhagic foci

5. Differential diagnosis

- Spinal cord AVM
 - Abnormal vascular mass in the spinal cord
 - Engorged perimedullary veins
- Spinal cord metastasis
 - Enhancing mass with extensive cord edema
- Ependymoma
 - Enhancing mass
 - Syrinx

5.4.1 Illustrations: Cavernous Malformation

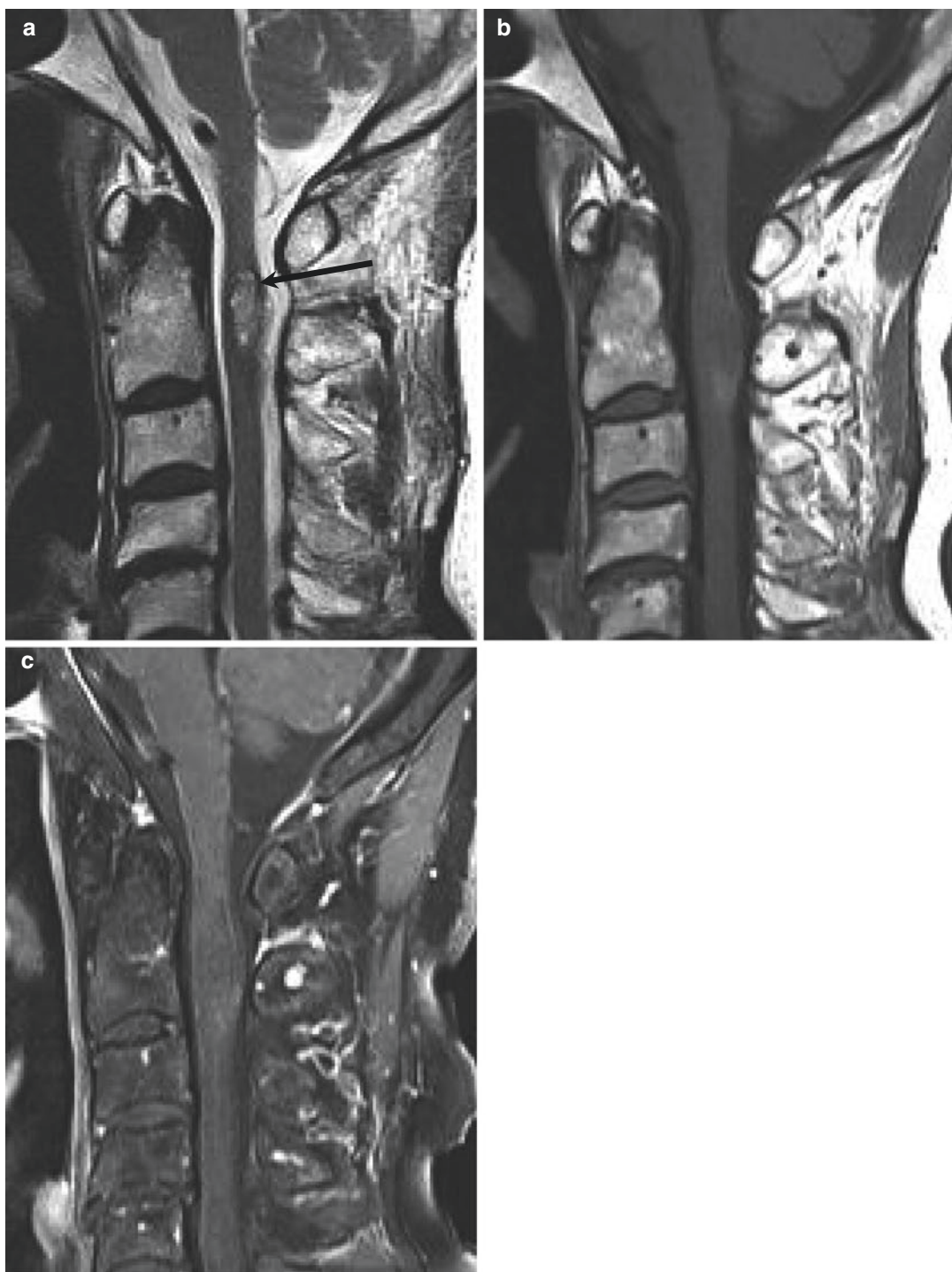


Fig. 5.8 Intramedullary cavernous malformation of the C2 vertebral body in a 71-year-old woman. T2-weighted sagittal MR image (a) shows a mixed hyperintense mass with hypointense hemosiderin rim in the posterior portion

of the spinal cord (black arrow). T1-weighted sagittal MR image (b) shows a peripheral high signal intensity area. Contrast-enhanced T1-weighted sagittal MR image (c) shows no definite enhancement

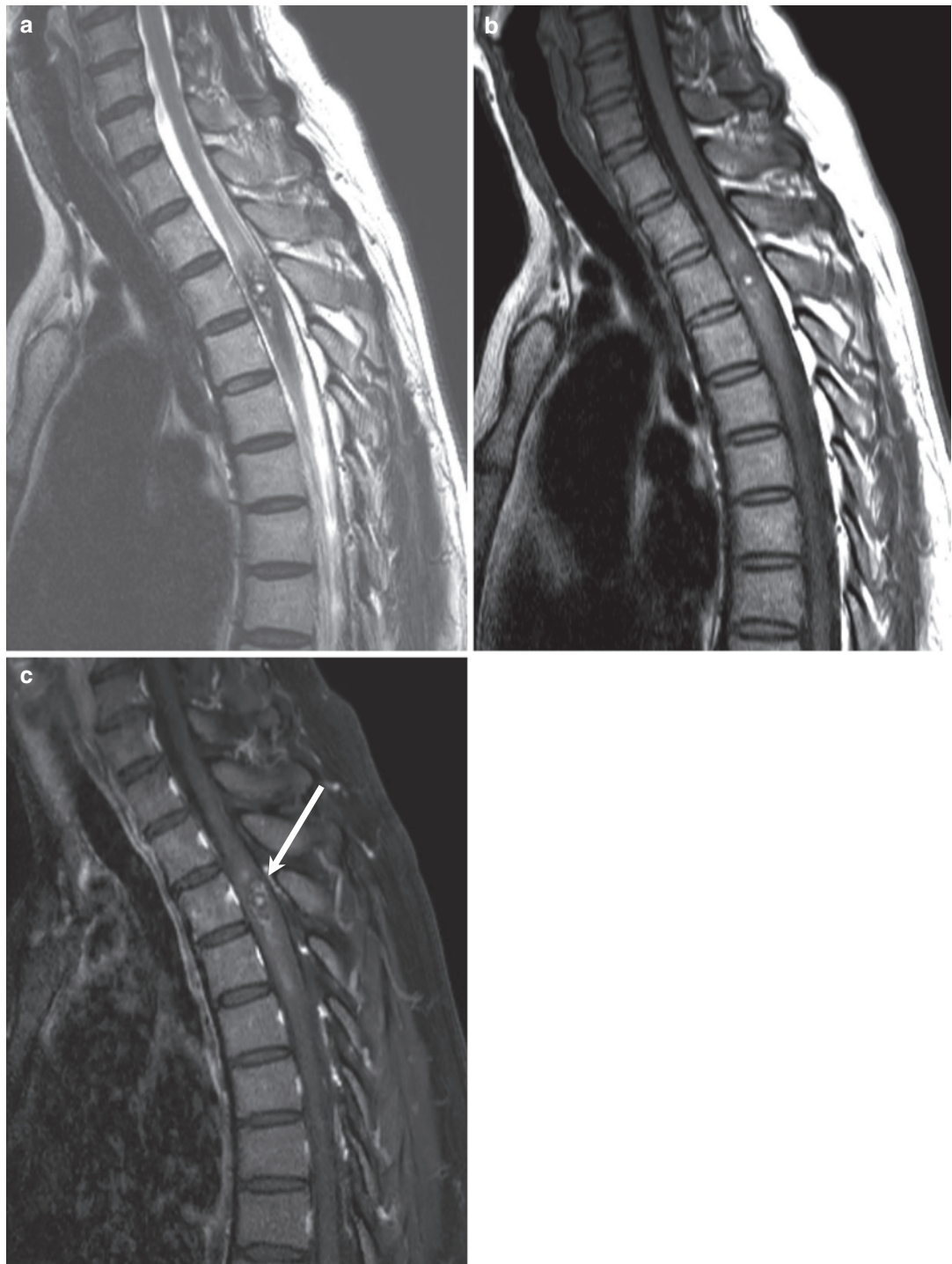


Fig. 5.9 Intramedullary cavernous malformation in a 47-year-old woman. T2-weighted (a) and T1-weighted (b) sagittal images show an ill-defined intramedullary heterogeneous signal intensity mass with extensive

hemorrhage and reactive edema/swelling involving the T1–T4 levels. T1-weighted sagittal MR image with contrast enhancement shows (c) mild enhancing portion of the lesion at the T2 vertebral body level



Fig. 5.10 Intramedullary cavernous malformation at T5/T6 level in a 67-year-old man. T2-weighted sagittal MR image (a) shows a small popcorn-like hyperintense intra-medullary mass with hypointense hemosiderin rim in the

spinal cord. T1-weighted sagittal MR image (b) shows similar signal intensity to the spinal cord. Contrast-enhanced T1-weighted sagittal MR image (c) shows a focal enhancing area



Fig. 5.11 Intramedullary cavernous malformation of the T9 vertebral body level in a 51-year-old woman. T2-weighted sagittal MR image (a) shows a small heterogeneous popcorn-like signal intensity intramedullary mass. Extensive

cord edema in the upper thoracic level is noted. T1-weighted sagittal MR image (b) shows a peripheral high signal intensity area. Contrast-enhanced T1-weighted sagittal MR image (c) shows no definite enhancement (*white arrow*)

5.5 Chondrosarcoma

1. Epidemiology

- 30 years (13–78 years)
- M = F

2. Location

- Thoracic spine > cervical, lumbar spine
- Vertebral body

3. Characteristic imaging findings

- “Rings and arcs,” punctate calcifications
- Osteolytic mass with paravertebral extension
- Mixed areas of high signal (non-mineralized chondroid matrix) and low signal (mineralized) on T2-weighted image
- Peripheral and lobulated rim enhancement

4. Spectrum of imaging findings

5. Differential diagnosis

- Osteosarcoma
 - Dense internal ossification
 - Lumbosacral
- Ewing’s sarcoma
 - Permeative transcortical extension
 - Younger patients
 - No internal calcifications
- Metastasis
 - No internal calcification
- Chordoma
 - Bright high signal on T2-weighted image
 - Multilobular appearance
 - Less internal calcifications
 - Sacrum, high cervical
 - Variable enhancement

5.5.1 Illustrations: Chondrosarcoma

Fig. 5.12 Chondrosarcoma involving a thoracic vertebral body and left rib. Axial CT scan of thoracic spine (**a**) shows a destructive vertebral mass containing fine, stippled calcifications. Left rib destruction is also noted.

T2-weighted axial MR image (**b**) shows a heterogeneous signal intensity mass extending into the epidural and left paravertebral spaces. Contrast-enhanced T1-weighted axial MR image (**c**) shows heterogeneous enhancement

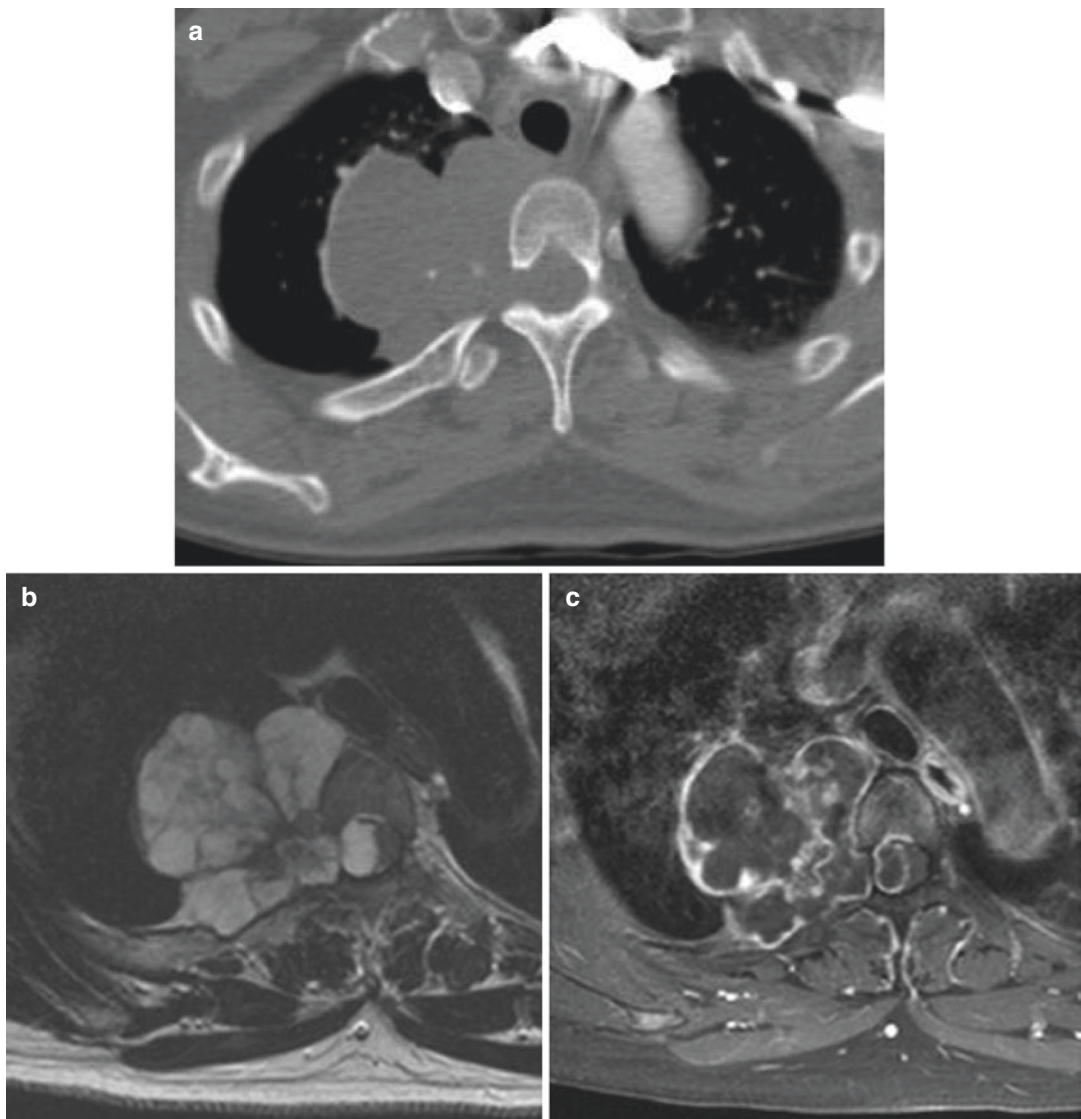


Fig. 5.13 Chondrosarcoma at the T3 paravertebral space in a 45-year-old woman. Axial CT scan of thoracic spine (a) shows a lobulated right paravertebral mass widening the right T3/4 neural foramen. A few fine, stippled calcifications within the mass are noted. T2-weighted axial MR

image (b) shows predominantly high signal intensity with internal hypointense septa-like structures. Epidural extension compressing the spinal cord to the left is noted. Contrast-enhanced T1-weighted axial MR image (c) shows enhancement of the peripheral rim and internal septa

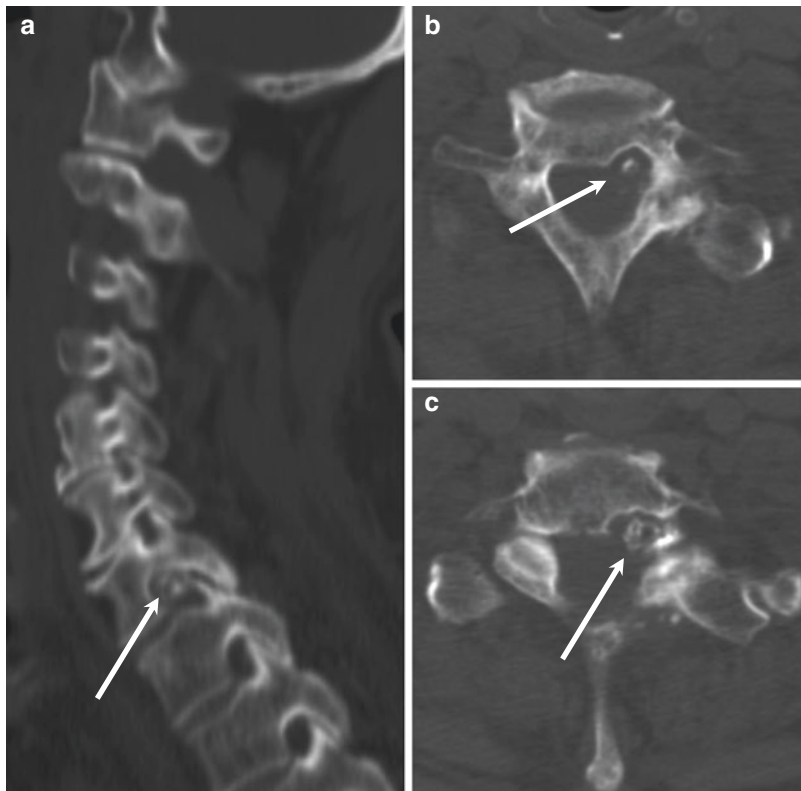


Fig. 5.14 Chondrosarcoma in a 75-year-old man. Sagittal and axial CT images (a–c) demonstrate calcifications in the left anterior epidural space and neural foramen (white arrows). Bony erosion with a sclerotic rim is seen at the posterior surface of the C7 body. Cervical spine MRI reveals an epidural mass with T2 hyperintensity and peripheral enhancement (d–g), encircling the dural sac

and causing cord compression at the level of C5-T1. Axial T1-weighted image (h) shows a nodular lesion with hyperintensity on both T1- and T2-weighted images in the left epidural space and neural foramen (black arrow), suggestive of calcification or ossification. Erosion of the posterior surface of the C7 body is also noted

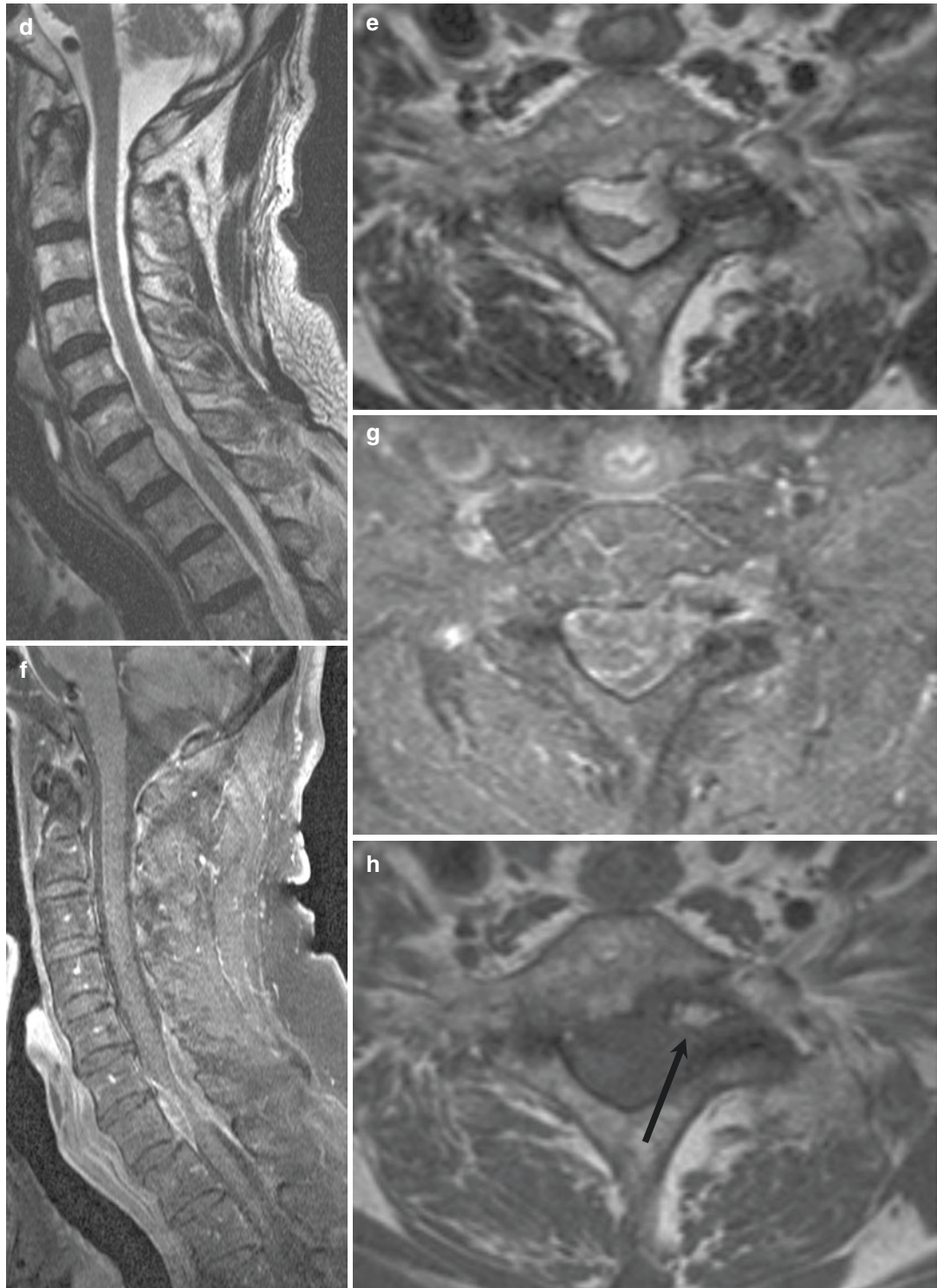


Fig. 5.14 (continued)

5.6 Chordoma

1. Epidemiology

- >40 years

2. Location

- Sacrococcygeal (50%) > sphenoo-occipital (35%) > mobile spine (15%)
- Vertebral body

3. Characteristic imaging findings

- Multi-lobulated mass with T2-hyperintensity, midline location, sacrococcygeal
- Osteolytic mass with large soft tissue mass (much larger than intraosseous component)
- Amorphous intratumoral calcification
- T2-hyperintensity with low signal septa
- Variable enhancement

4. Spectrum of imaging findings

- Paramedian location

5. Differential diagnosis

- Chondrosarcoma
 - Punctate calcification
 - Heterogeneous signal on T2-weighted image
 - Less lobular appearance
- Metastasis
 - Less bright on T2-weighted image
 - Less lobular appearance

5.6.1 Illustrations: Chordoma

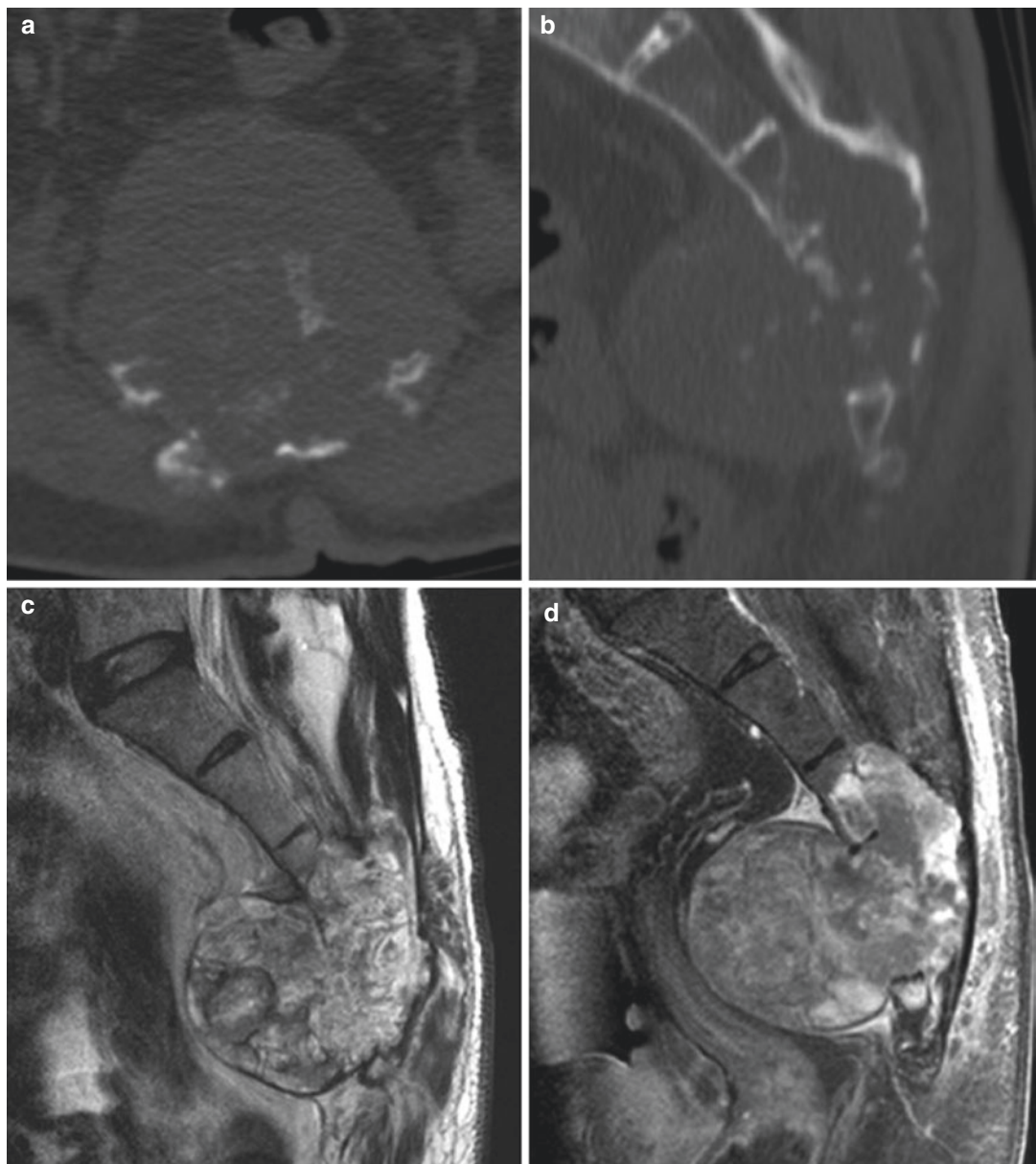


Fig. 5.15 Chordoma of the sacrum in a 63-year-old man. Axial and sagittal CT scans of the sacrum (**a, b**) show an osteolytic soft tissue mass with internal amorphous calcifications at S3-S4-S5. T2-weighted sagittal MR image (**c**) shows a multi-lobulated mass with hyperintensity and inter-

nal low signal intensity septa and calcifications. Contrast-enhanced T1-weighted sagittal MR image (**d**) shows heterogeneous enhancement with a focal non-enhancing necrotic portion

Fig. 5.16 Chordoma of the S2 to S5 vertebrae in a 57-year-old man. Axial CT scan of the sacrum (**a**) shows an osteolytic mass involving the posterior elements and both sacral ala with a large mass at the greater sciatic notch. T2-weighted axial MR image (**b**) shows a multi-lobulated mass of the posterior elements and both sacral ala with high signal intensity. There is also a large mass at the greater sciatic foramen with extrapelvic extension, involving the right piriformis muscle, bulging to the gluteal muscles, as well as extraosseous extension into the right paraspinal muscles. Contrast-enhanced T1-weighted axial MR image (**c**) shows heterogeneous enhancement

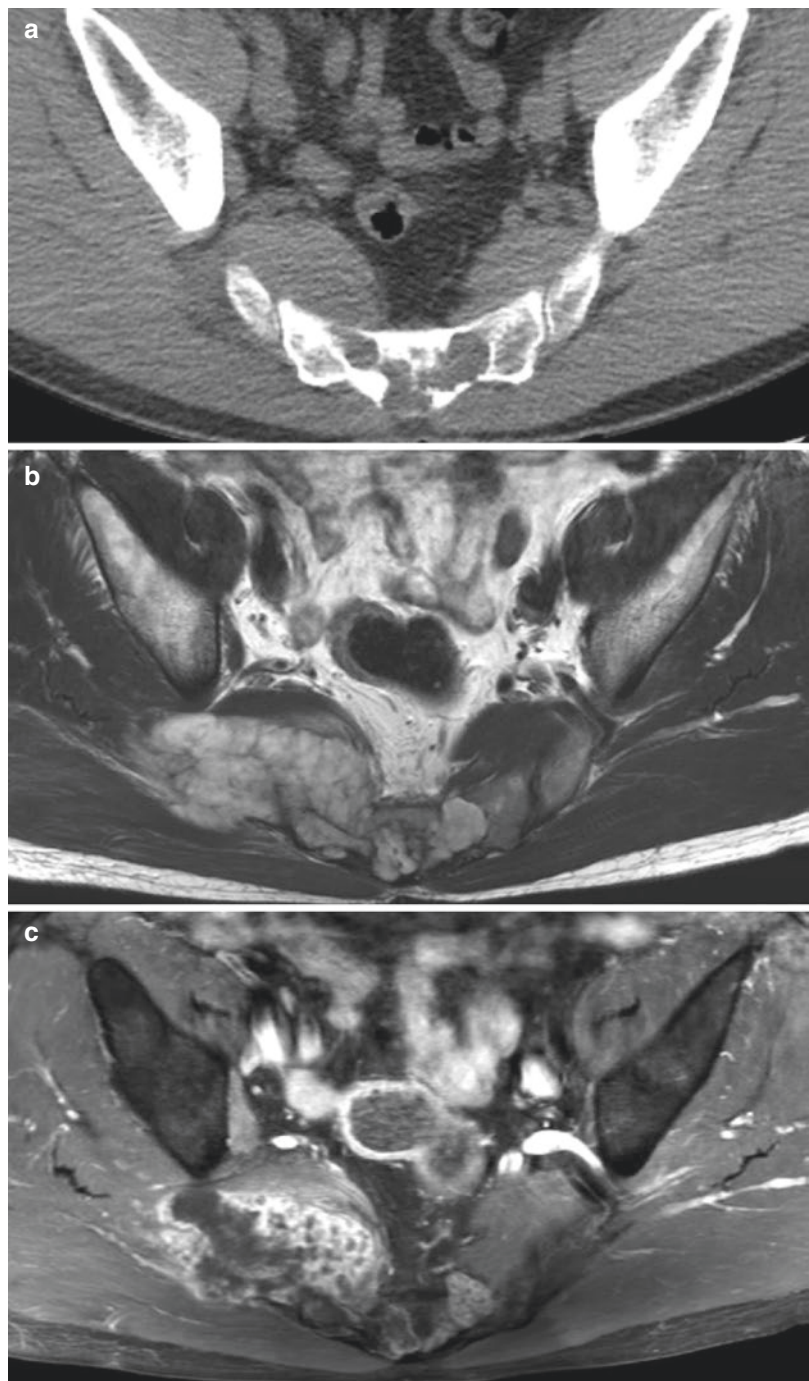
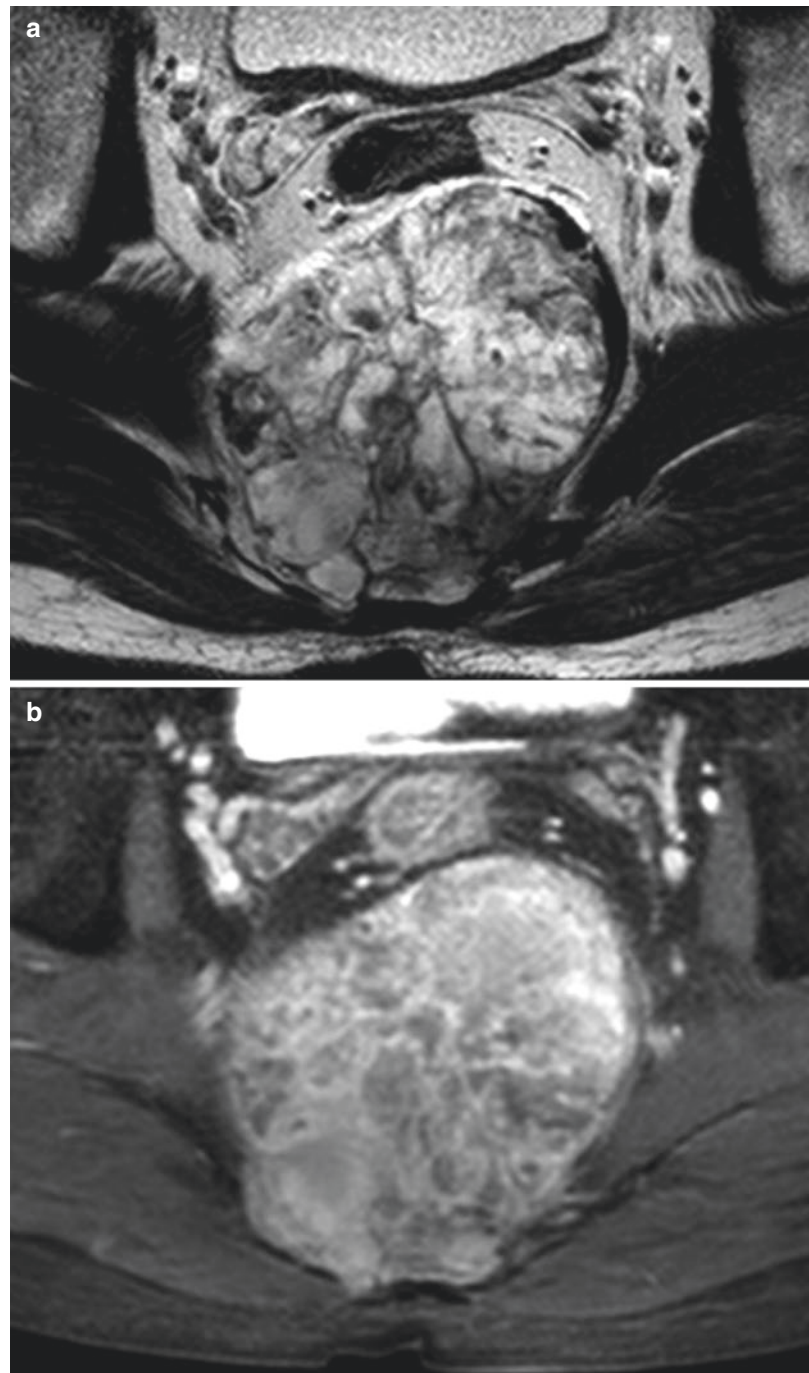


Fig. 5.17 Chordoma of the S4 to coccygeal vertebrae in a 45-year-old man. T2-weighted axial MR image (**a**) shows a lobulated mass at S4 to coccyx vertebrae with heterogeneous high signal intensity and internal multiple low signal intensity septa, along with exophytic anterior extension to the pelvic cavity. Contrast-enhanced T1-weighted axial MR image (**b**) shows prominent heterogeneous enhancement



5.7 Giant Cell Tumor

1. Epidemiology

- 80% in 3rd to 5th decades
- In spine, peak incidence: 2nd to 3rd decades
- Sex: F > M (2.5: 1)
- Sixth most common primary bone tumor

2. Location

- 3% of all giant cell tumor occur in spine
 - Centered in vertebral body
- 4% of all giant cell tumor occur in the sacrum
 - Multiple site involvement: rare

3. Characteristic imaging findings

- Lytic, expansile lesion of vertebral body or sacrum on CT (possible cortical breakage)
- No sclerotic rim, no internal mineral matrix
- Low to intermediate signal on T1-weighted image and intermediate to high signal on T2-weighted image
- Heterogeneous contrast enhancement

4. Spectrum of imaging findings

- Fluid-fluid level: associated secondary ABC change
- Thin curvilinear low signal lesion on all MR sequence: residual bone trabeculation or fibrous septa

5. Differential diagnosis

- Metastasis
 - Older, multiple
 - Neural arch involvement
- Aneurysmal bone cyst
 - Marked expansile
 - Arise in neural arch
- Plasmacytoma
 - Rare cortical breakage
- Chordoma
 - Midline location
 - Large soft tissue component
- Brown tumor of hyperparathyroidism
 - Identical to giant cell tumor

5.7.1 Illustrations: Giant Cell Tumor

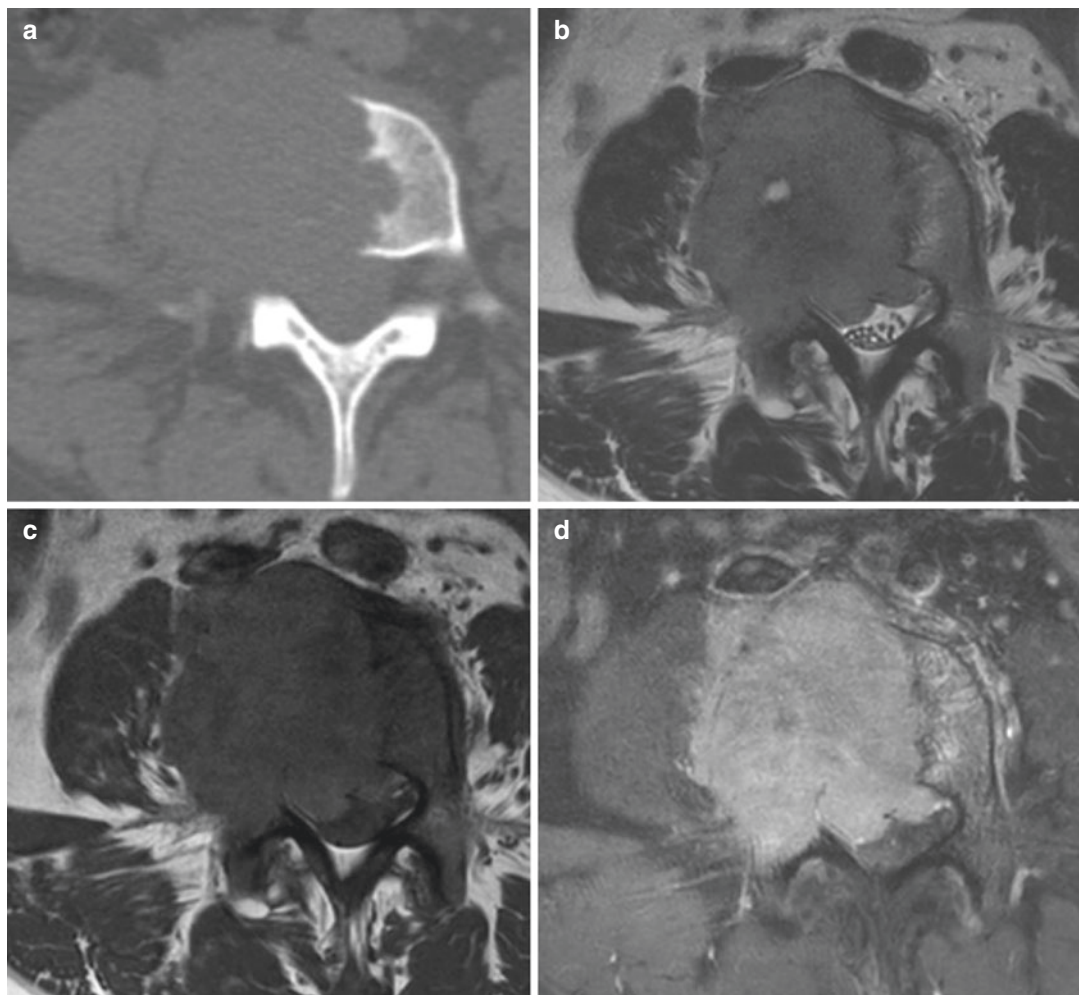
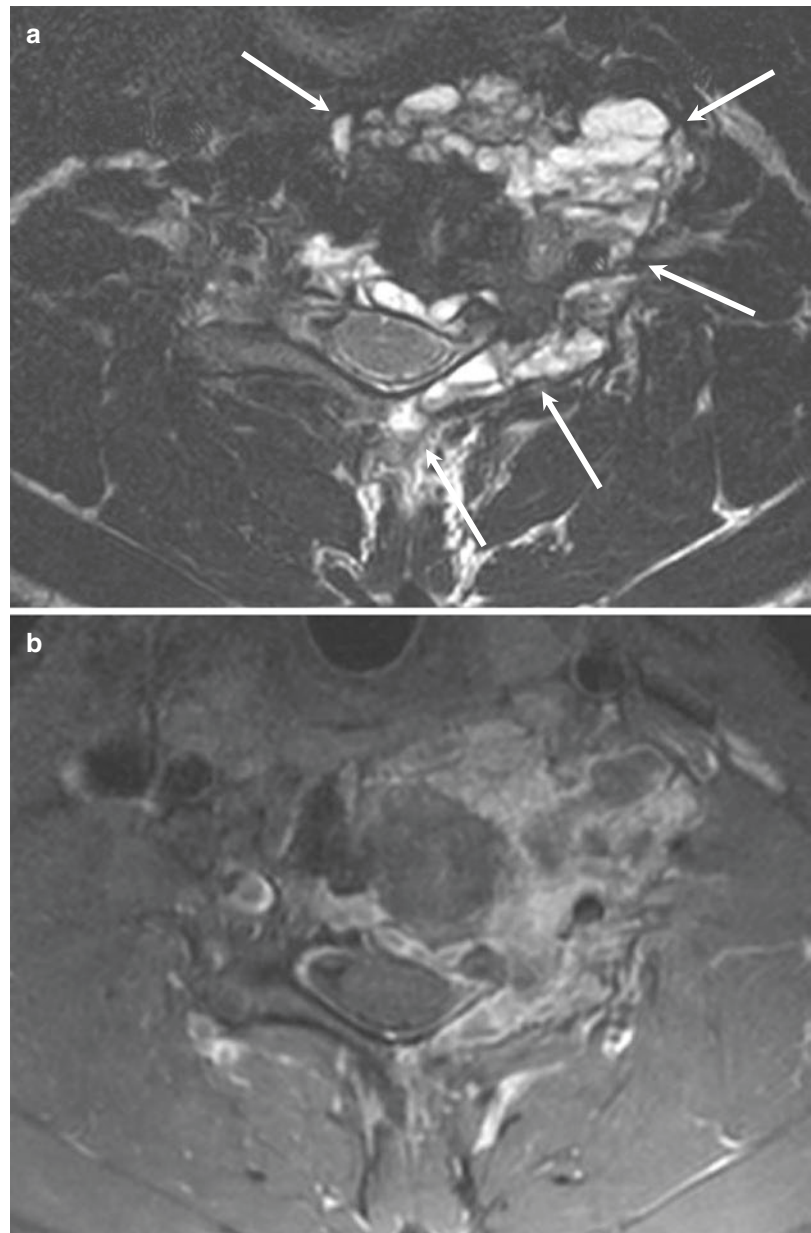


Fig. 5.18 Giant cell tumor of the L4 vertebrae in a 27-year-old woman. Axial CT scan of the lumbar spine (a) shows a lytic, expansile mass of the L4 vertebral body without sclerotic rim. T2-weighted axial MR image (b) shows an expansive mass with paravertebral and epidural

extension of intermediate signal intensity. T1-weighted axial MR image (c) shows low signal intensity of the lesion. Contrast-enhanced T1-weighted axial MR image (d) shows diffuse strong enhancement

Fig. 5.19 Giant cell tumor with secondary aneurysmal bone cyst (ABC) changes of the C6 vertebrae in a 21-year-old man. T2-weighted axial MR image (**a**) shows an expansile multi-lobulated mass with multiple fluid-fluid levels of the C6 vertebral body, left lamina, transverse process, and spinous process with paravertebral extension to the left anterior side (white arrows). Contrast-enhanced T1-weighted axial MR image (**b**) shows an enhancing solid portion



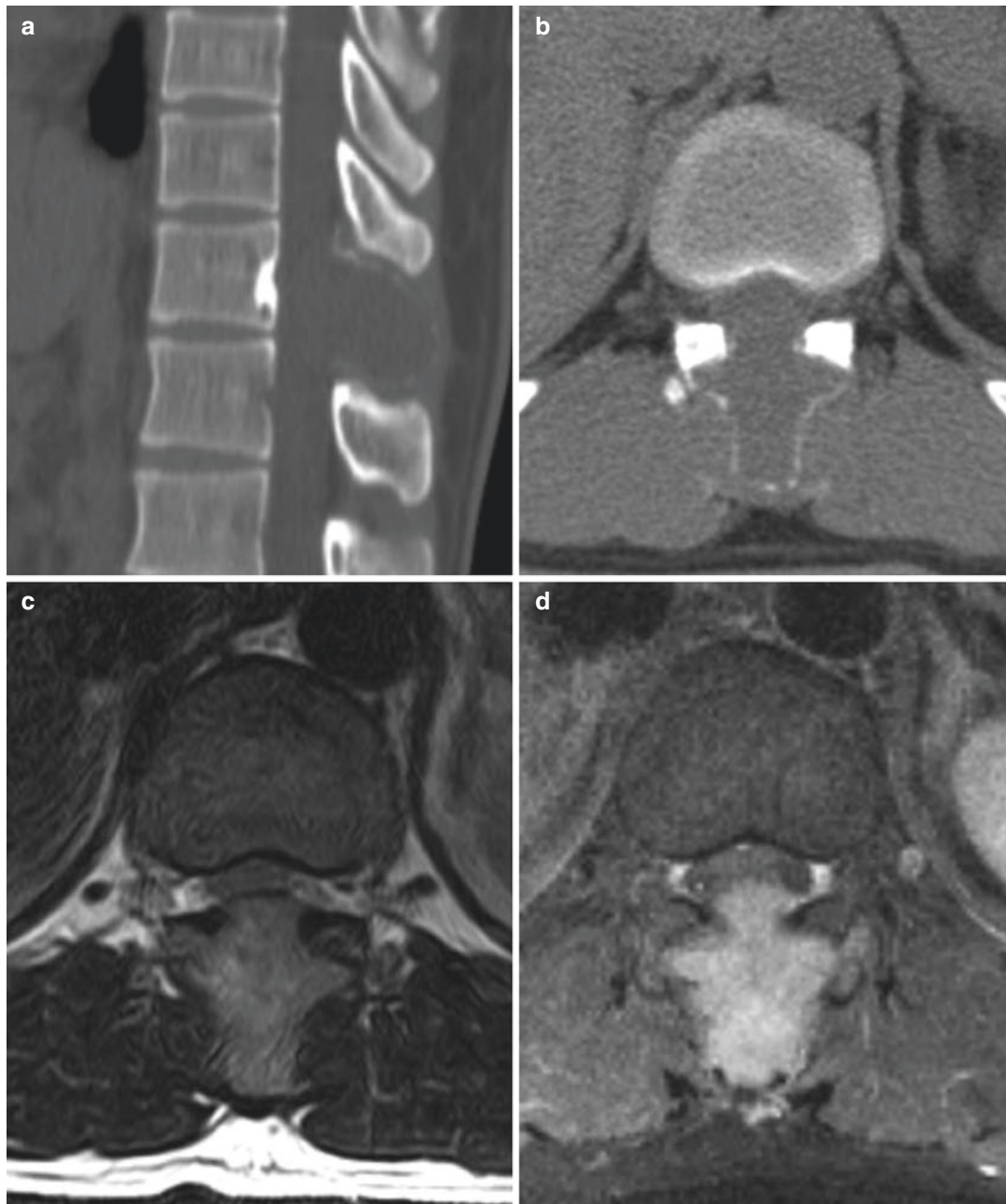


Fig. 5.20 Giant cell tumor of the T12 vertebrae in a 35-year-old man. Sagittal and axial CT scans of the thoracolumbar spine (**a, b**) show an expansile osteolytic bone mass without sclerotic rim of the T12 spinous process.

The mass shows intermediate to high signal intensity on T2-weighted image (**c**) with homogenous contrast enhancement (**d**). This expansile mass extends into the posterior epidural space with mild cord compression



Fig. 5.21 Sacral giant cell tumor with secondary ABC changes in a 15-year-old man. There is an expansile osteolytic soft tissue mass in the right sacral ala on lumbar spine CT scan (**a, b**). T2-weighted (**c**) and T1-weighted

(**d**) MR images show internal fluid-fluid levels with hemorrhagic components. On the contrast-enhanced T1-weighted image (**e**), the mass shows internal enhancing septa and solid portions

5.8 Lipoma

1. Epidemiology

- Peak incidence: three age peaks for presentation
 - Less than 5 years: 24%
 - 2nd to 3rd decades: 55%
 - 5th decade: 16%
- Intradural: M < or = F
- Terminal: M < F

2. Location

- Intradural lipoma: 4%
 - Thoracic (30%) > cervicothoracic (24%) > cervical (12%) > lumbosacral
- Lipomyelo(meningo)cele + terminal lipoma: 84%
- Filum lipoma: 12%

3. Characteristic imaging findings

- Intradural lipoma
 - Fat signal intensity (high signal on T1- and T2 weighted image) + fat suppression
 - No contrast enhancement

• Terminal lipoma

- Fat signal mass attached to distal cord/filum
- No contrast enhancement

4. Spectrum of imaging findings

- Intradural lipoma
 - Possible canal widening, local dysraphism
 - Spinal cord compression → cord high signal on T2-weighted image
- Terminal lipoma
 - Mass extends through lumbosacral dysraphism → subcutaneous fat
 - Cord tethering with or without syrinx

5. Differential diagnosis

- Lipomyelocele/lipomyelomeningocele
 - Closed neural placode-lipoma complex
 - Palpable mass with or without skin stigma
- Filum fibrolipoma
 - Common/asymptomatic
 - Symptomatic, if cord tethering
 - Fat signal mass with or without cord tethering and low-lying cord

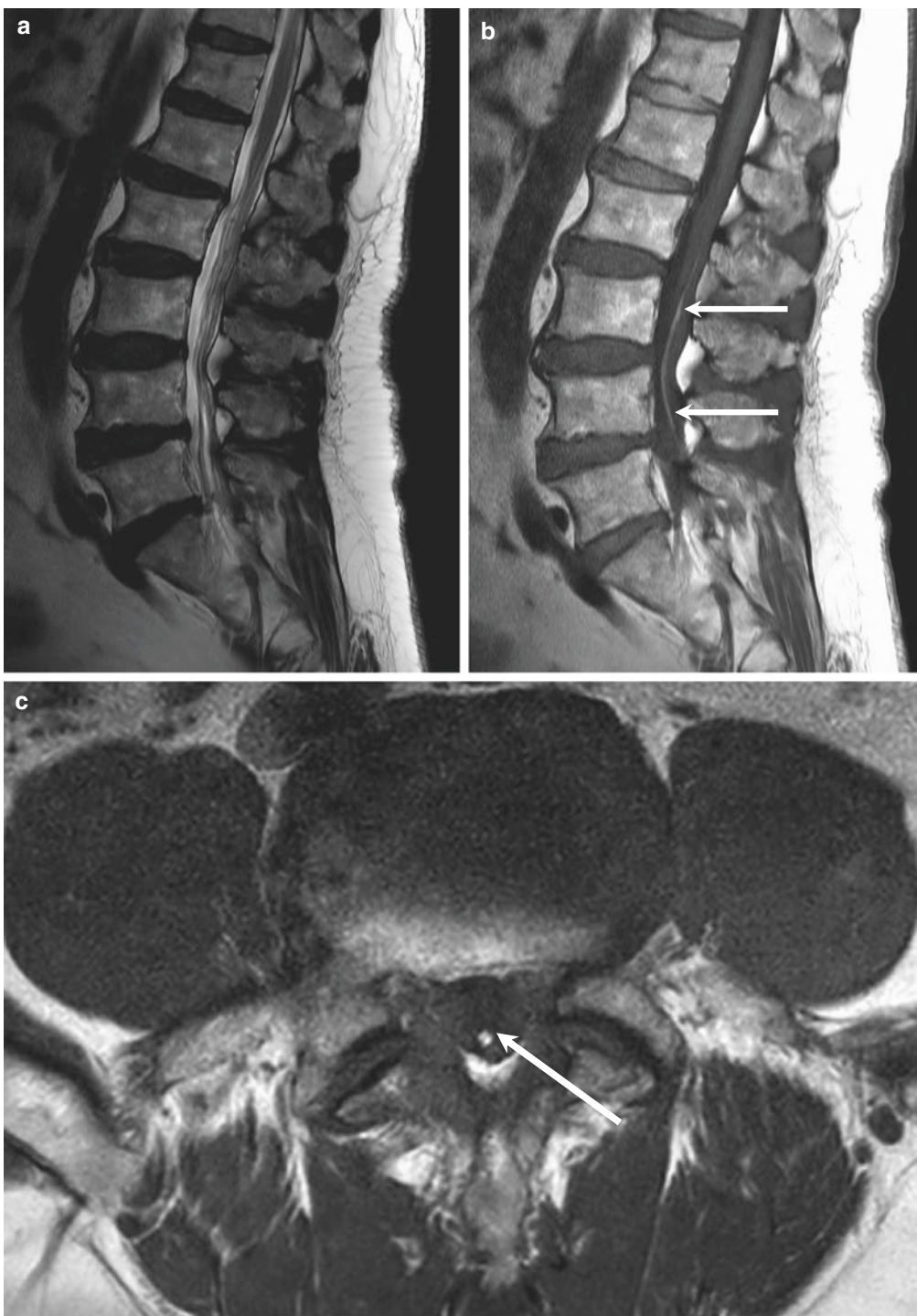
5.8.1 Illustrations: Lipoma

Fig. 5.22 Filum terminale fibrolipoma in a 77-year-old man. T2-weighted sagittal MR image (a) demonstrates normal-appearing filum terminale and conus terminating normally at L1 level. T1-weighted sagittal image of lum-

bar spine (b) shows a linear fat signal intensity lesion within the filum terminale (*white arrows*). T1-weighted axial image (c) shows fatty infiltration of the filum terminale dorsally located within the dural sac (*white arrow*)

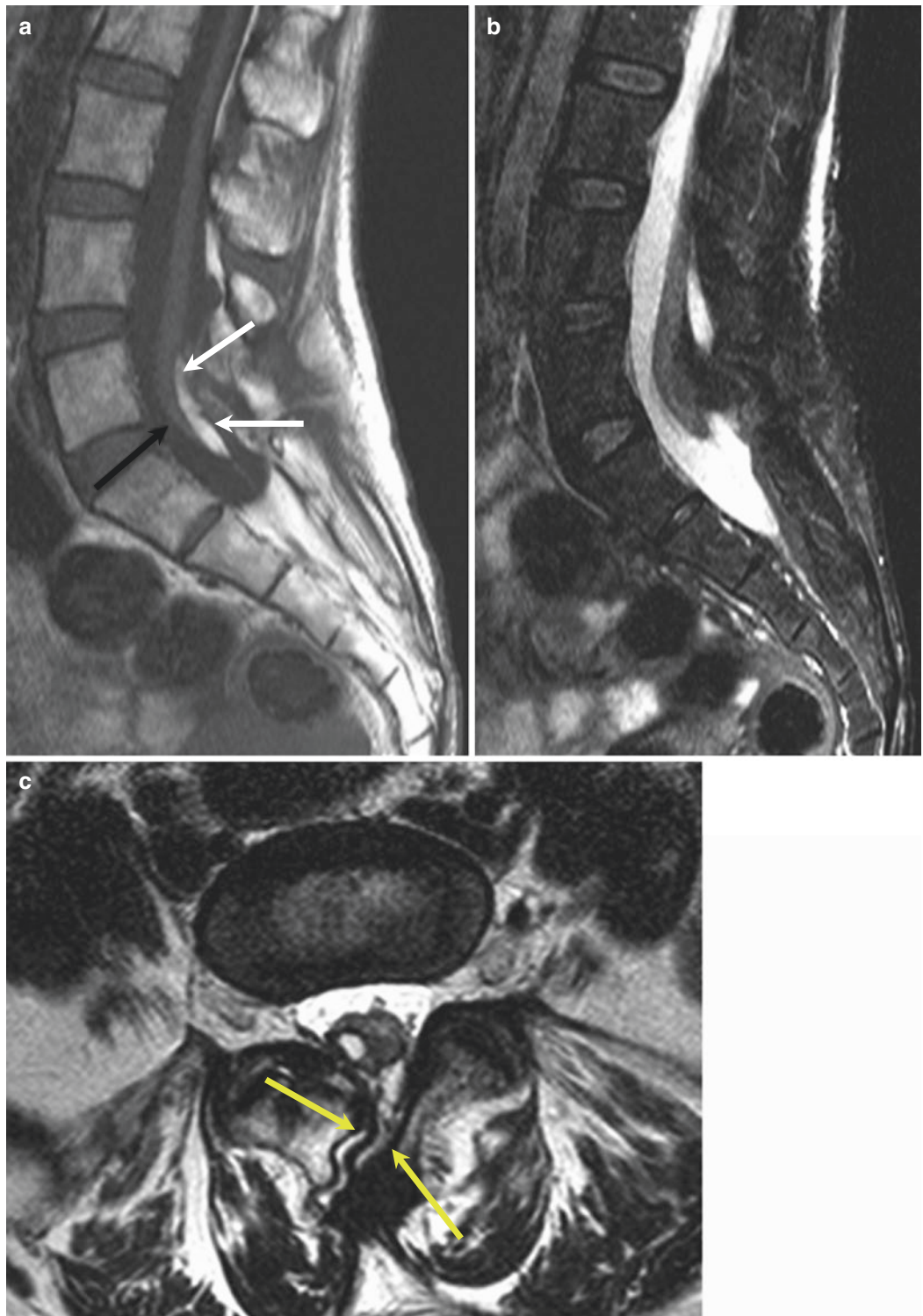


Fig. 5.23 Intramedullary lipoma with spinal cord tethering in a 58-year-old man. T1-weighted sagittal image (a) reveals an intramedullary juxtamедullary fatty mass (white arrows) attached to the conus dorsally with a low-lying conus

(black arrow). Fat-suppressed T2-weighted image (b) shows signal loss within the mass. T2-weighted axial image (c) shows associated spinal dysraphism at L5-S1 (yellow arrows)



Fig. 5.24 Intradural lipoma associated with spinal dysraphism and tethered cord in a 60-year-old man. Anteroposterior radiograph (a) shows spinal dysraphism of the lumbosacral spine. T2-weighted sagittal image (b)

and T1-weighted sagittal image (c) of the lumbar spine show a lobulated intradural fatty mass invaginating into the dorsal surface of the spinal cord. The conus tip is located at the L5/S1 level

5.9 Osteoblastoma

1. Epidemiology

- Peak incidence: 2nd to 3rd decades (90%)
 - But can occur up to 7th decade
- Sex: M > F (2–2.5: 1)

2. Location

- Spine: 40%
 - Cervical (40%) > lumbar (25%) > thoracic (20%) > sacrum (15–20%)
- Posterior element (neural arch origin)
 - Pedicle, lamina, transverse or spinous process, articular pillar, or pars interarticularis
- Size: > 1.5 cm

3. Characteristic imaging findings

- Expansile tumor in posterior elements
- Well-circumscribed expansile mass of neural arch on CT
 - Sclerotic rim/narrow transition zone
 - Variable degree mineralization (may small amount)
 - Widespread inflammatory response
 - Periosteal reaction of adjacent rib, pleural thickening with or without effusion
 - OLF
- Low to high signal on T2-weighted image
- Low to intermediate signal on T1-weighted image with variable enhancement of Gd

- Prominent peritumoral edema with enhancement (flare phenomenon)
 - Mimic malignancy

4. Spectrum of imaging findings

- Often associated with aneurysmal bone cyst (10–15%)
 - Fluid-fluid levels
- Vertebral body extension: often
- Aggressive osteoblastoma
 - Cortical breakage, wide transition zone
 - Mimic osteosarcoma

5. Differential diagnosis

- Osteoid osteoma
 - Size < 1.5 cm
 - Round nidus with surrounding sclerotic rim
 - Scoliosis
- Aneurysmal bone cyst
 - Absence matrix
 - Multiple blood-filled cavities with fluid-fluid levels
- Osteosarcoma
 - Bone matrix (+)
 - Rare in spine
 - Cortical breakage rather than expansion
- Infection
 - CT >> MR

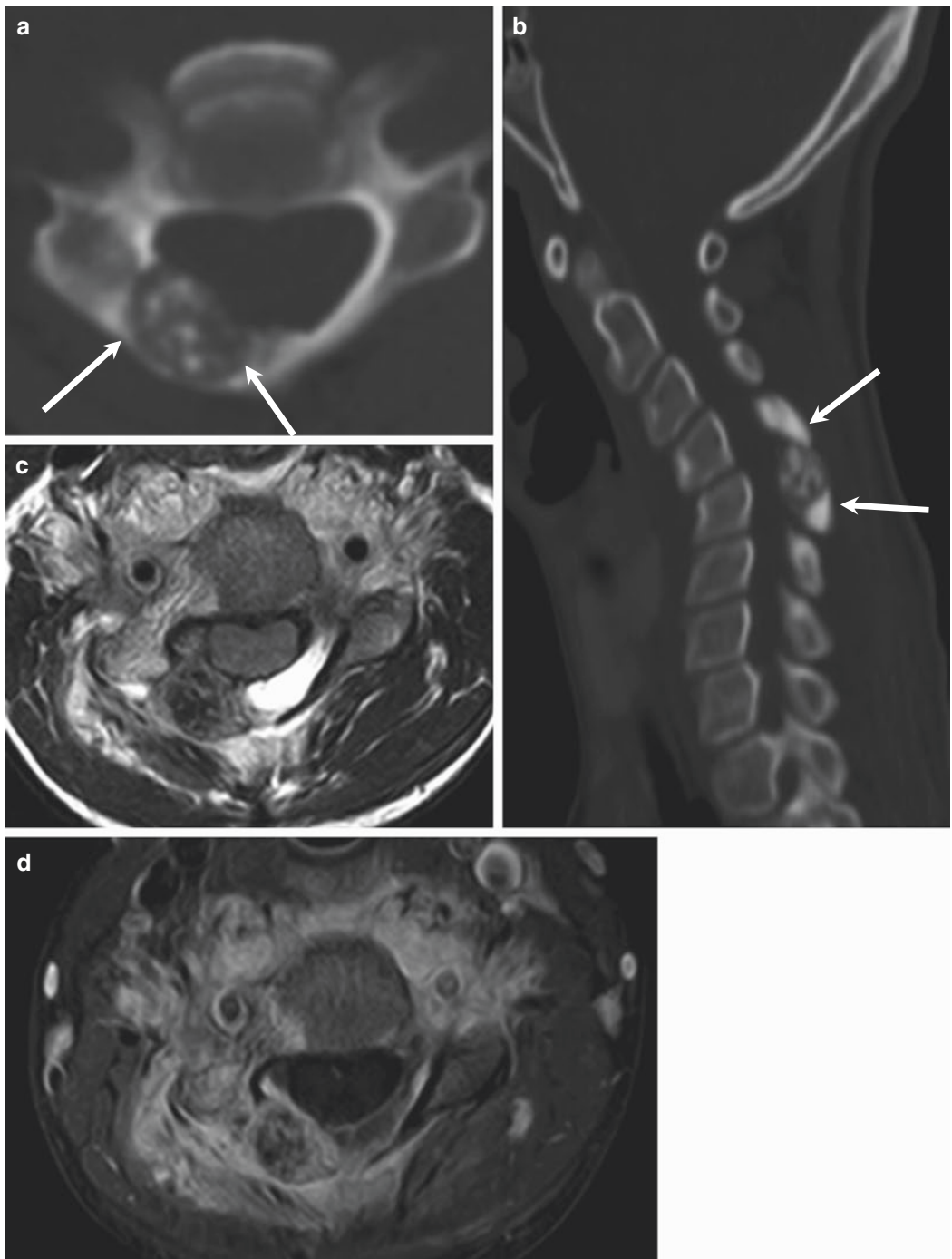
5.9.1 Illustrations: Osteoblastoma

Fig. 5.25 Cervical osteoblastoma in a 13-year-old girl. Axial (a) and sagittal CT (b) demonstrates an expansile osteolytic mass containing speckled calcifications with peritumoral sclerosis in the right lamina of the C5 vertebra (white arrows). T2-weighted axial MR image (c), con-

trast-enhanced T1-weighted axial MR image (d) show an expansile mass with heterogeneous, low to intermediate signal intensity and strong enhancement in the lamina. Note extensive edema and enhancement of the adjacent soft tissues

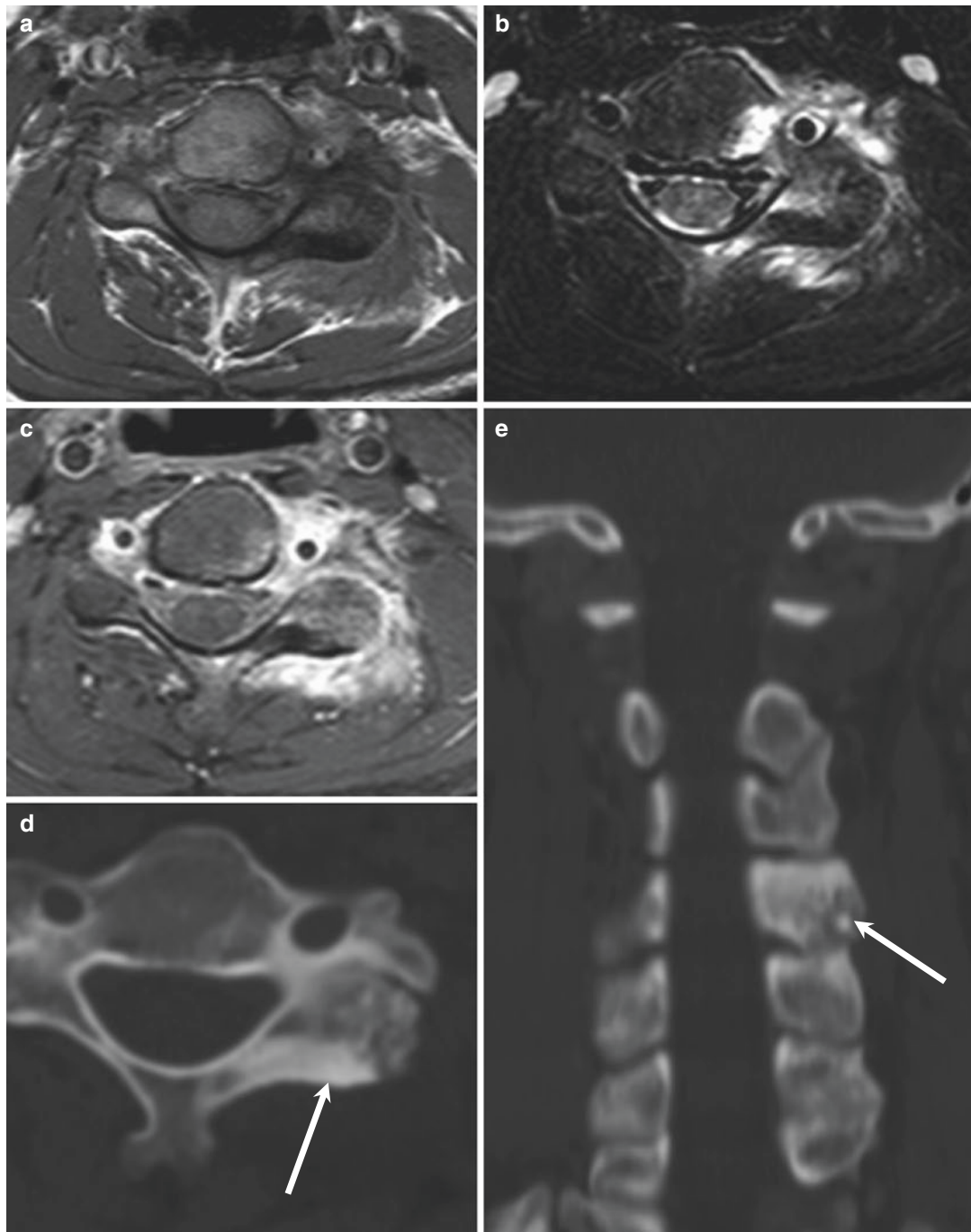
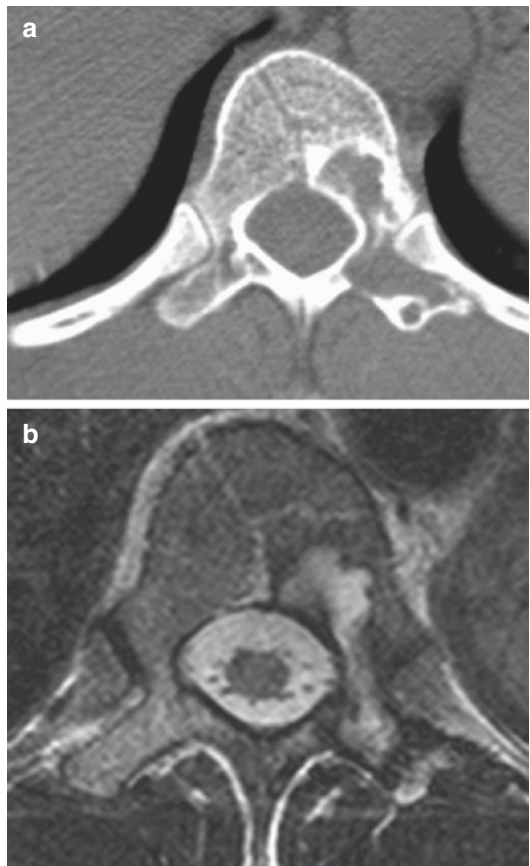


Fig. 5.26 Cervical osteoblastoma in a 16-year-old boy. T1-weighted axial image (a) and T2-weighted short-tau inversion recovery (STIR) image (b) show a low signal intensity, densely ossified mass expanding the left lamina. There is extensive reactive edema in the adjacent posterior elements and soft tissues. Fat-saturated contrast-enhanced

T1-weighted axial image (c) shows enhancement of the non-ossified portions of tumor as well as the adjacent soft tissue edema. Axial (d) and coronal reformatted CT (e) demonstrate the expansile mass containing irregular trabeculae and prominent peritumoral sclerosis (*white arrows*)

Fig. 5.27 Osteoblastoma with secondary aneurysmal bone cyst in a 46-year-old man. Axial bone CT (a) shows an expansile osteolytic mass with irregular ossifications involving the left posterior vertebral body, pedicle, and lamina of T11. T2-weighted axial MR image (b) shows secondary aneurysmal bone cyst with fluid signal within the mass



5.10 Osteochondroma

1. Epidemiology

- Peak incidence: 2nd~4th decade
 - Hereditary multiple exostoses: most patients diagnosed by 5 years
- Sex: M > F (3: 1)

2. Location

- Spine: < 5%
 - Cervical (50%, C2 predilection) > thoracic (T8 > T4 > others) > lumbar >> sacrum (2%)
- Spinous/transverse process > vertebral body

3. Characteristic imaging findings

- Sessile or pedunculated osseous protuberance with corticomедullary continuation with parent bone on CT
- Iso to high signal bone marrow with surrounding low signal cortex on T1- and T2-weighted image
- High signal hyaline cartilage cap on T2-weighted image

4. Spectrum of imaging findings

- Chondroid calcification in cartilage cap
- Peripheral, septal enhancement in cartilage cap
- Cartilage cap > 1.5 cm in adults
 - Possibility of malignant transformation

5. Differential diagnosis

- Chondrosarcoma
 - Lytic bone destruction with sclerotic margin
 - Soft tissue mass
 - Chondroid matrix (“ring and arc” pattern)
- Enthesophyte
 - DISH, ankylosing spondylitis, psoriatic arthropathy
- Tumoral calcinosis
 - Calcific periarticular mass
 - Spine involvement: uncommon

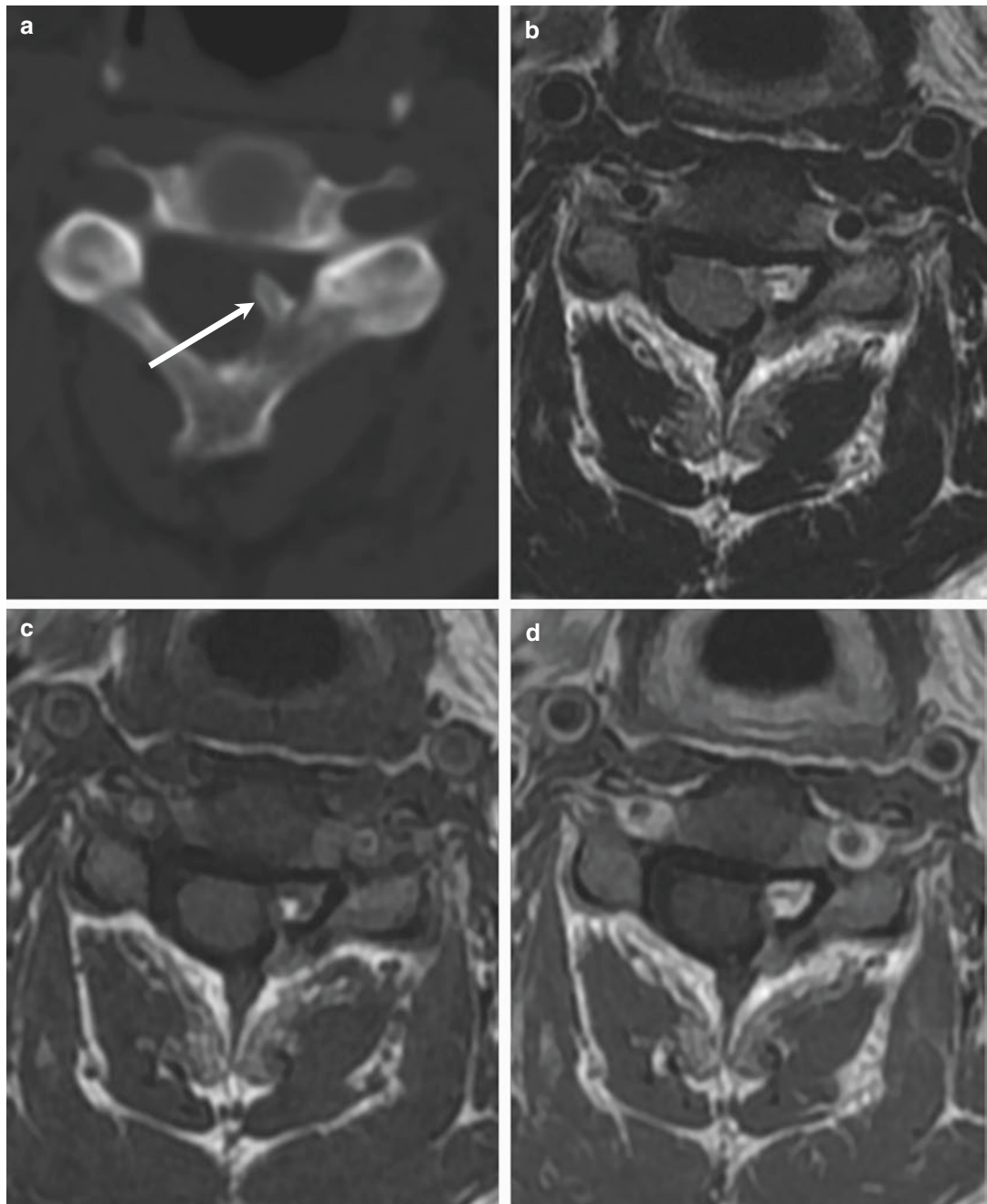
5.10.1 Illustrations: Osteochondroma

Fig. 5.28 Osteochondroma of the C4 vertebrae in a 37-year-old man. Axial CT scan of the cervical spine (a) shows a protruding mass arising from the left lamina of C4 (white arrow). T2-weighted axial (b) and T1-weighted

(c) MR images show a protruding mass with signal intensity similar to the bone marrow displacing the spinal cord to the right. Contrast-enhanced T1-weighted axial MR image (d) shows no definite enhancement

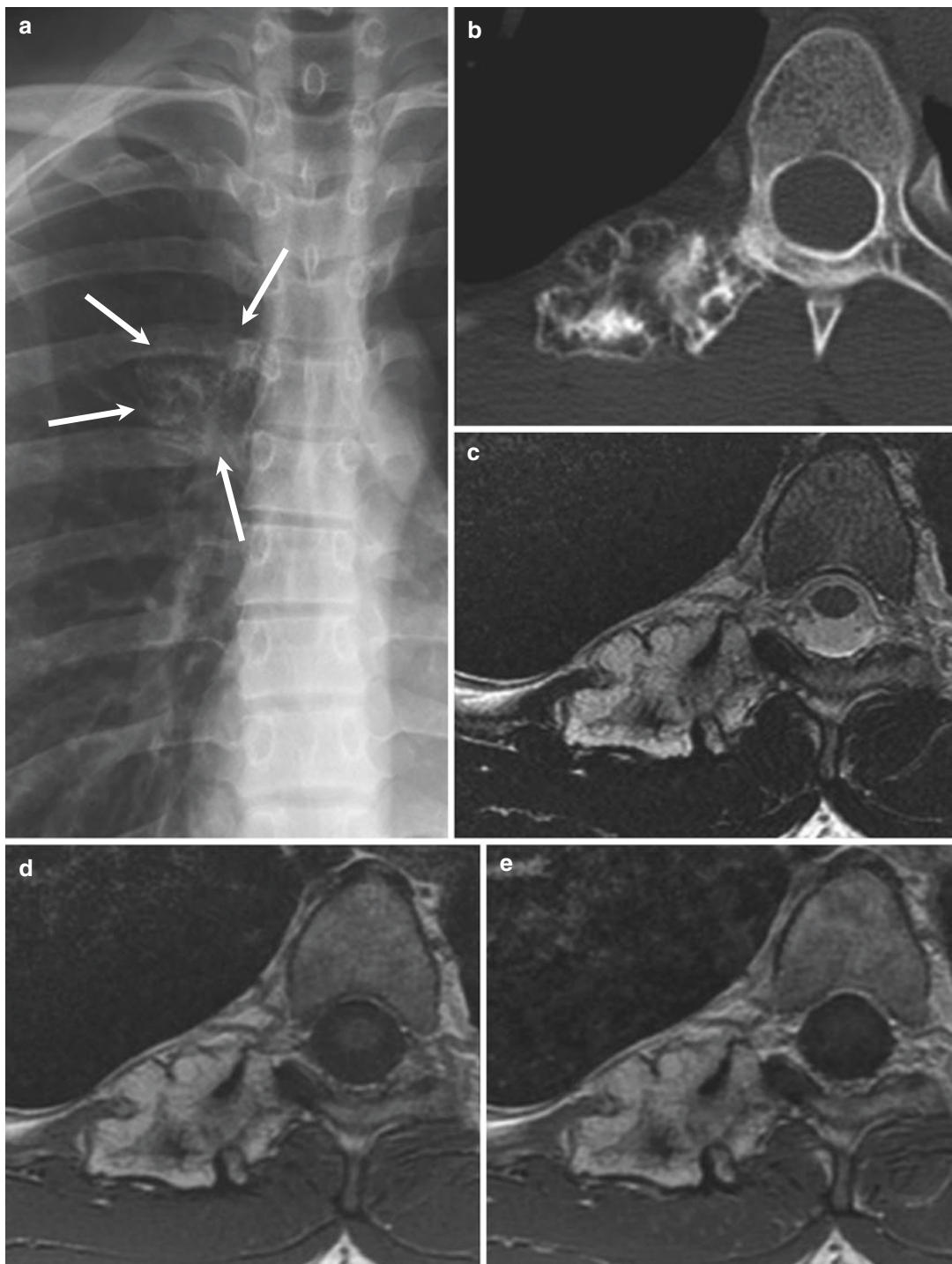


Fig. 5.29 Osteochondroma of the T5 vertebrae in a 20-year-old man. AP plain radiograph of thoracic spine (a) shows an exophytic mass at the right costovertebral junction (white arrows). Axial CT scan of the thoracic spine (b) shows a lobulated exophytic mass arising from

the right transverse process of T5. T2-weighted axial (c) and T1-weighted (d) MR images show a protruding mass with signal intensity similar to the bone marrow. Contrast-enhanced T1-weighted axial MR image (e) shows no definite enhancement

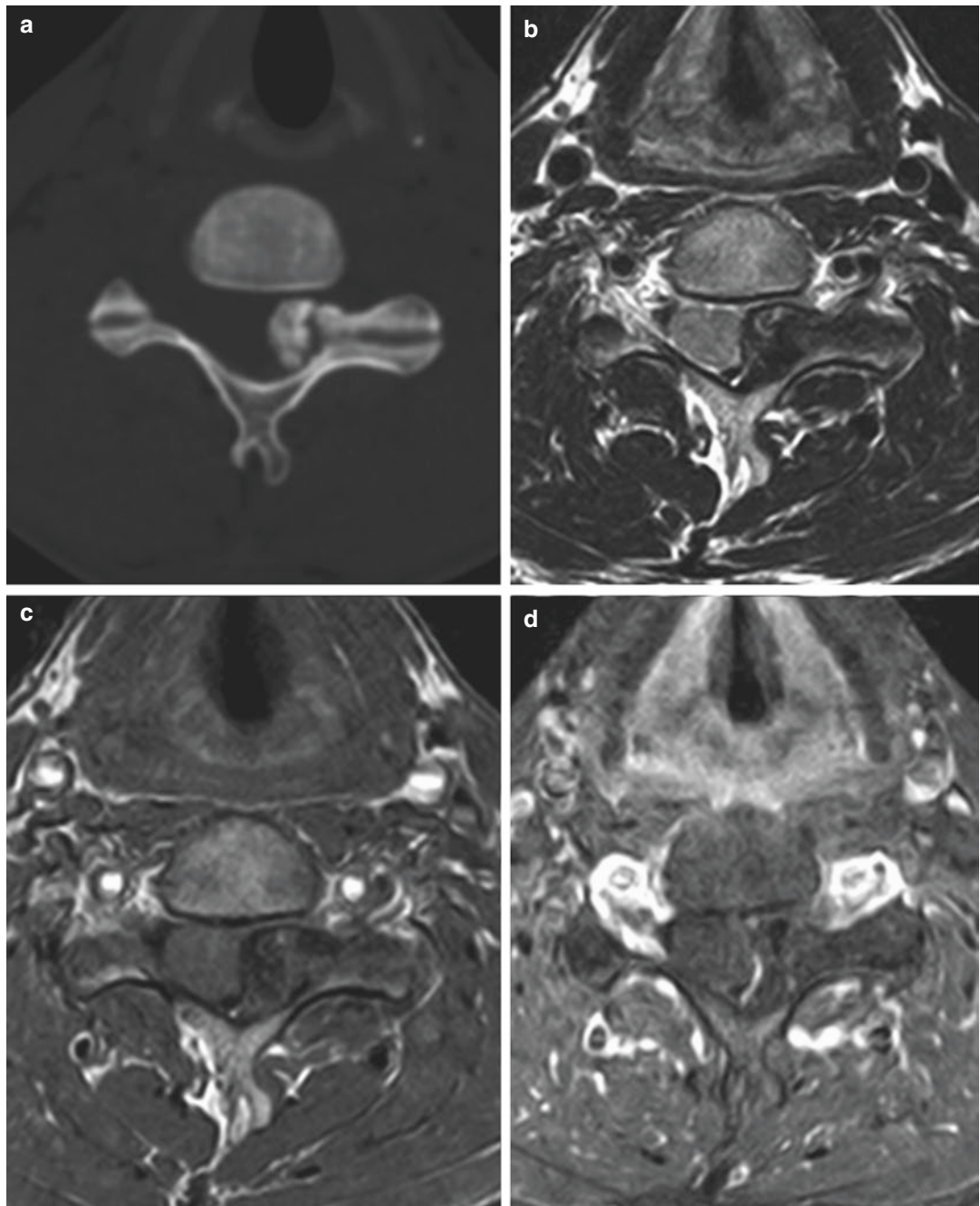


Fig. 5.30 Osteochondroma of the C4 vertebrae in a 39-year-old man. Axial CT scan of the cervical spine (a) shows an exophytic mass arising from the anteromedial aspect of the C4–C5 facet joint. T2-weighted axial (b)

T1-weighted (c) MR images show a protruding mass with signal intensity similar to the bone marrow, displacing the spinal cord to the right. Contrast-enhanced T1-weighted axial MR image (d) shows no definite enhancement

5.11 Osteoid Osteoma

1. Epidemiology

- Peak incidence: most in 2nd decade
 - But can occur up to 7th decade
- Sex: M > F (2–3: 1)

2. Location

- Spine: 10%
 - Lumbar (59%) > cervical (27%) > thoracic (12%) > sacrum (2%)
- Almost posterior element (neural arch origin)
 - Pedicle, lamina, transverse or spinous process, articular pillar, or pars interarticularis
- Size: nidus < 1.5 cm

3. Characteristic imaging findings

- Focal scoliosis concave on side of osteoid osteoma
- Central nidus (lucent > sclerotic) with surrounding sclerosis on CT
 - Variable periosteal reaction, common cortical thickening
 - Wide spread inflammatory response (soft tissue mass)
 - OLF
- Low signal central nidus on T1-weighted image
- High signal on T2-weighted image with enhancement of edema surrounding nidus
- Positive bone scan (all 3 phases of Tc-99 m MDP)

4. Spectrum of imaging findings

- Thoracic osteoid osteoma
 - Common pleural thickening, effusion, enhancement
- Adjacent vertebral body, rib and paraspinal soft tissue extension: often
- Small nidus
 - Misdiagnosis of malignancy or infection

5. Differential diagnosis

- Osteoblastoma
 - Size: > 1.5 cm
 - Expansile
- Sclerotic metastasis
 - Older patients
- Osteomyelitis
 - Sequestrum or focal abscess
 - Irregular shape (vs round nidus of osteoid osteoma)
 - Endplate destruction on CT

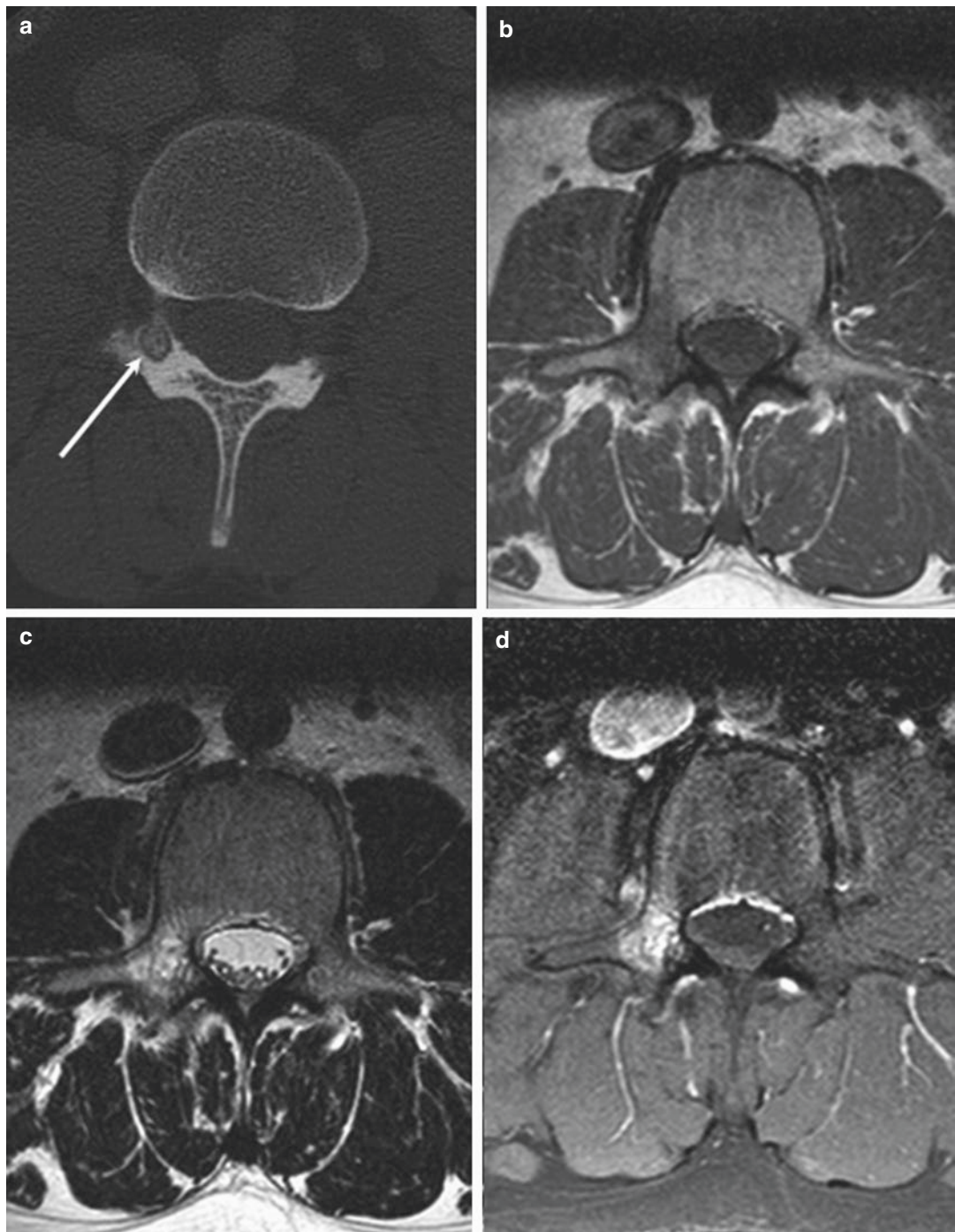
5.11.1 Illustrations: Osteoid Osteoma

Fig. 5.31 Osteoid osteoma of the L3 right pedicle in a 26-year-old woman. Axial CT scan of lumbar spine (a) shows a small osteolytic nidus in the inferior aspect of the right pedicle (white arrow). T1-weighted axial MR image (b) shows ill-defined hypointensity of the right pedicle of

L3. T2-weighted axial MR image (c) shows corresponding hyperintensity. Contrast-enhanced T1-weighted axial MR image (d) shows enhancement of the nidus and surrounding bone marrow

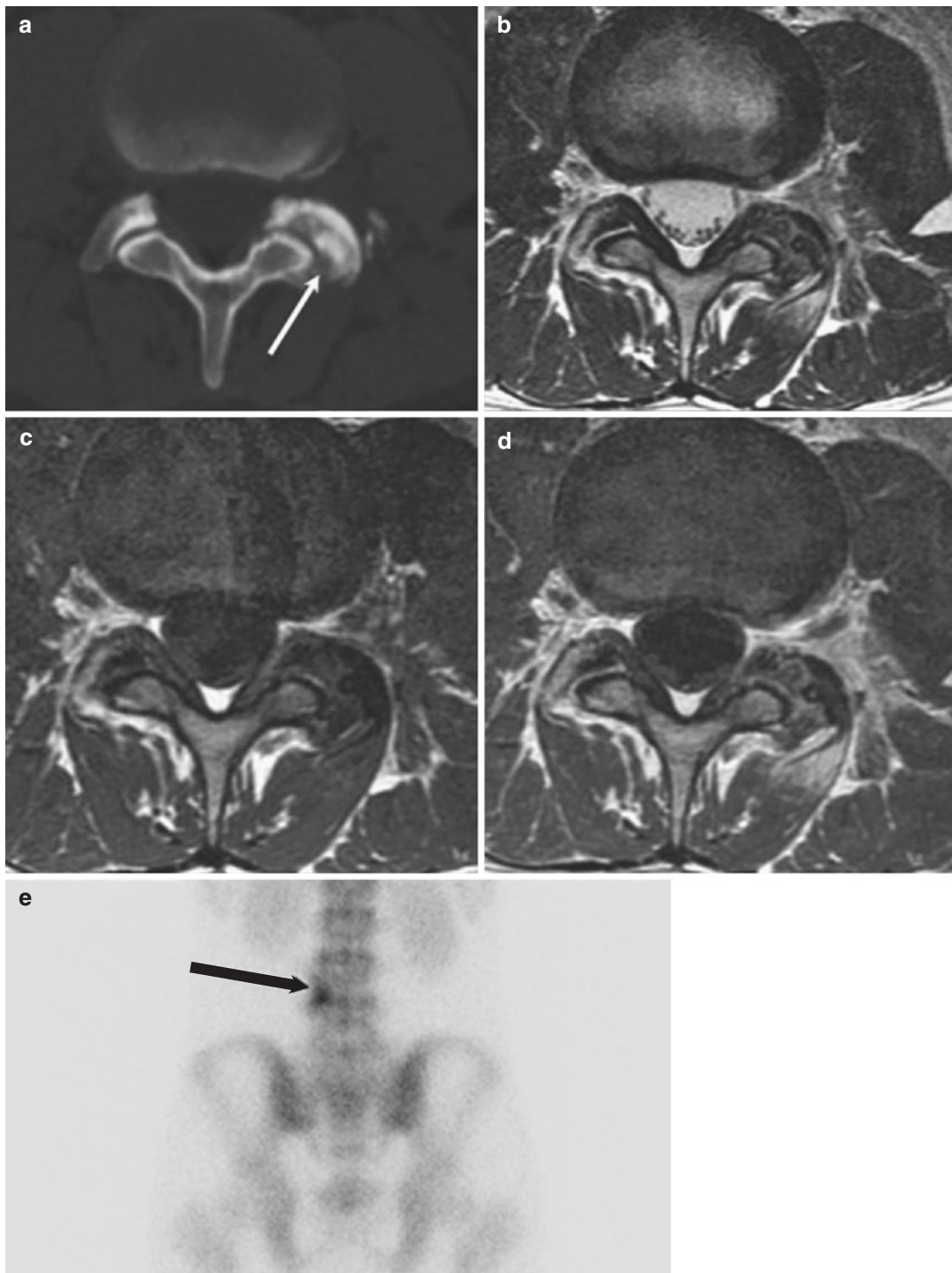


Fig. 5.32 Osteoid osteoma of the L4 vertebrae in a 20-year-old man. Axial CT scan of the cervical spine (a) shows central sclerotic nidus in the left superior facet of L4 (white arrow). T2-weighted axial MR image (b) shows a dark signal central nidus with increased signal intensity of the adjacent soft tissues. T1-weighted axial MR image

(c) also shows a dark signal central nidus. Contrast-enhanced T1-weighted axial MR image (d) shows extensive bone marrow and adjacent soft tissue enhancement. Bone scan (e) shows increased uptake of the left L3/4 facet joint (black arrow)

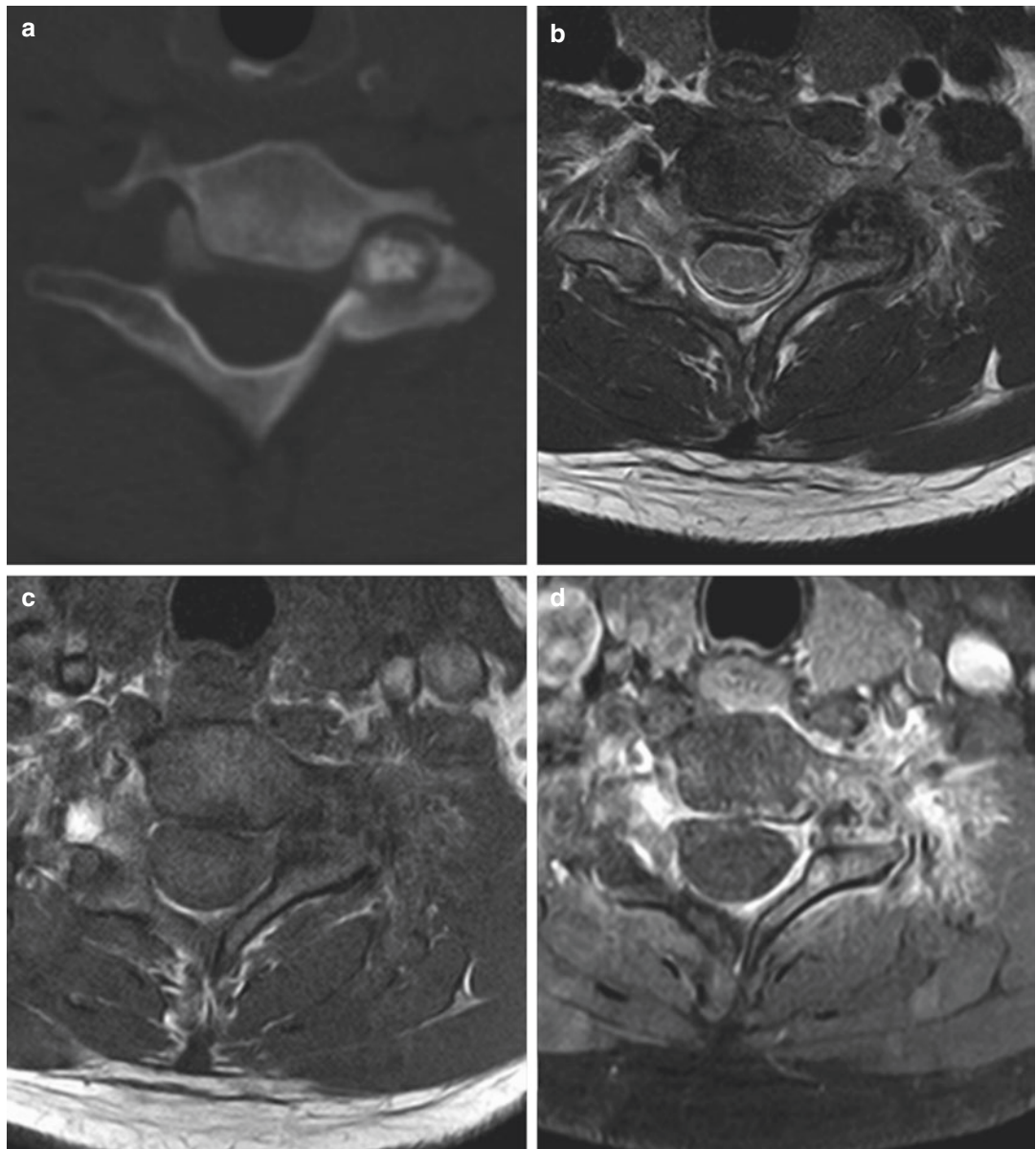


Fig. 5.33 Osteoid osteoma of the C7 vertebrae in a 26-year-old man. Axial CT scan of the cervical spine (a) shows a central sclerotic nidus with surrounding lucent rim in the left superior facet of C7. T2-weighted axial MR image (b) shows a dark signal central nidus with increased

signal intensity of the adjacent soft tissues. T1-weighted axial MR image (c) also shows a dark signal central nidus. Contrast-enhanced T1-weighted axial MR image (d) shows extensive bone marrow and adjacent soft tissue enhancement

5.12 Osteosarcoma

1. Epidemiology

- Peak incidence: 4th decade
 - Later than for appendicular osteosarcoma
- Sex: M=F
- Second most common primary bone malignancy (after multiple myeloma)

2. Location

- Primary osteosarcoma in the spine: 4% of all osteosarcoma
 - Posterior element arise: 79%
 - 17% involve adjacent 2 spinal levels
 - 84% invade spinal canal

3. Characteristic imaging findings

- Aggressive appearing lesion forming immature bone matrix
- Permeative or moth-eaten periosteal reaction with wide zone of transition
- Bony sclerosis due to immature bone formation
- Cortical breakage with soft tissue mass formation
- Heterogeneous signal intensity on T2-weighted image
 - Low signal on T1- and T2-weighted images of ossified portion

- Low signal on T1-weighted images and high signal on T2-weighted images of non-ossified tumor

4. Spectrum of imaging findings

- Telangiectatic osteosarcoma: fluid-fluid level
- Pure lytic mass without bone matrix: 20%

5. Differential diagnosis

- Sclerotic bone metastasis
 - Prostate, breast, gastrointestinal cancer
 - Multiple
 - Rarely extends beyond outer margin of the bone
- Osteoblastoma
 - Narrow zone of transition
- Aneurysmal bone cyst
 - Mimic telangiectatic osteosarcoma
 - Narrow zone of transition
 - Expansile lesion centered in posterior elements
- Malignant giant cell tumor
 - Rare
 - Lytic aggressive mass without bone matrix formation
- Giant bone island

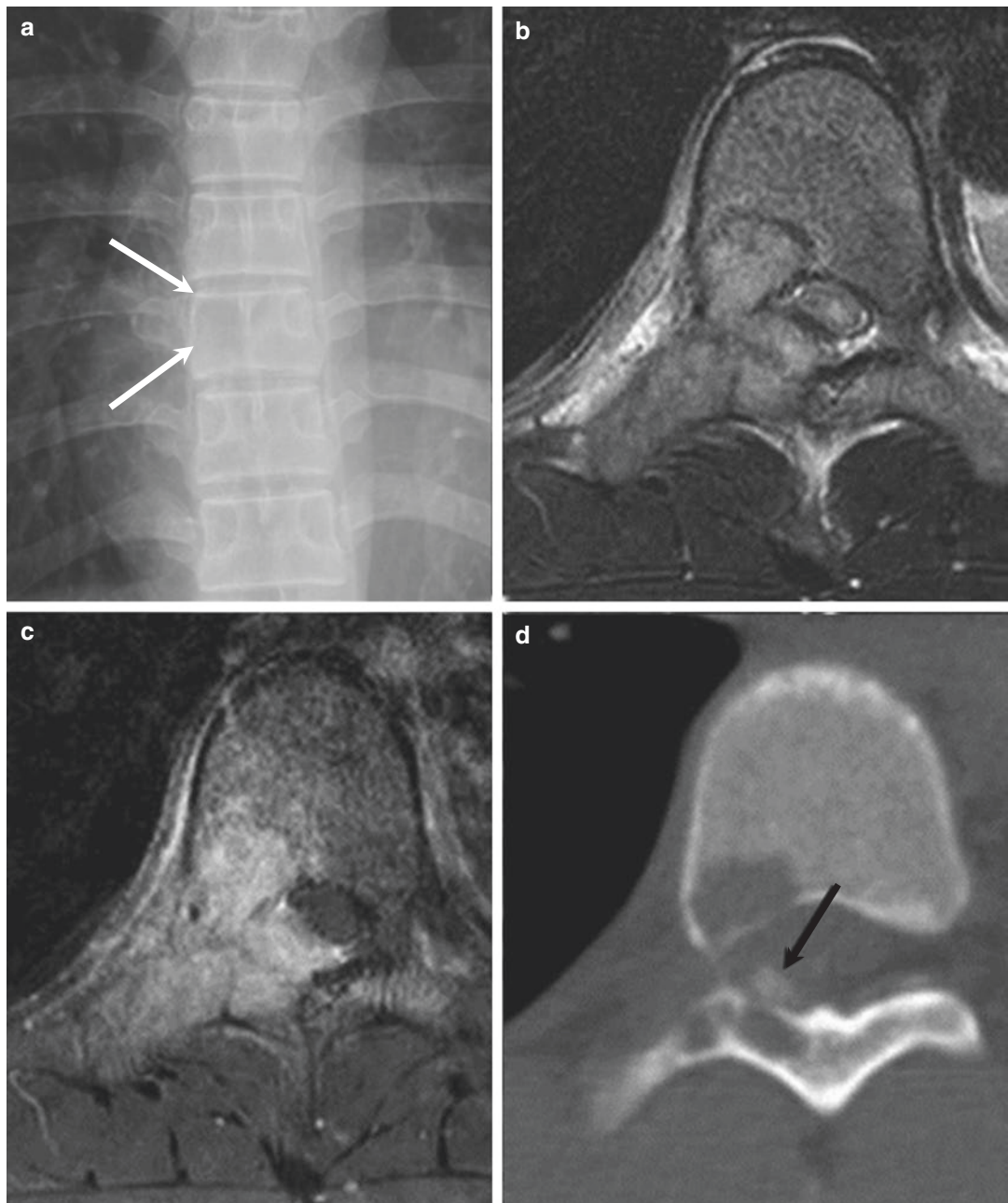
5.12.1 Illustrations: Osteosarcoma

Fig. 5.34 Primary vertebral osteosarcoma involving the T8 vertebra in a 14-year-old boy. Plain AP radiograph of the thoracic spine (a) shows an osteolytic bone lesion in the right side of the T8 vertebral body (*white arrows*). Note that the contour of the right pedicle of T8 has disappeared. Axial T2-weighted (b) and contrast-enhanced T1-weighted fat-saturated (c) MR images at the level of T8 vertebra show a T2 hyperintense mass with intense

enhancement involving the right posterior corner of the vertebral body, ipsilateral pedicle, transverse process, and lamina. The mass displaces the spinal cord with hyperintense signal alteration (*arrowheads*) suggesting compressive myelopathy. Axial CT image (d) just caudal to (b) and (c) shows a mainly osteolytic mass with a small focus of mineralization (*black arrow*)

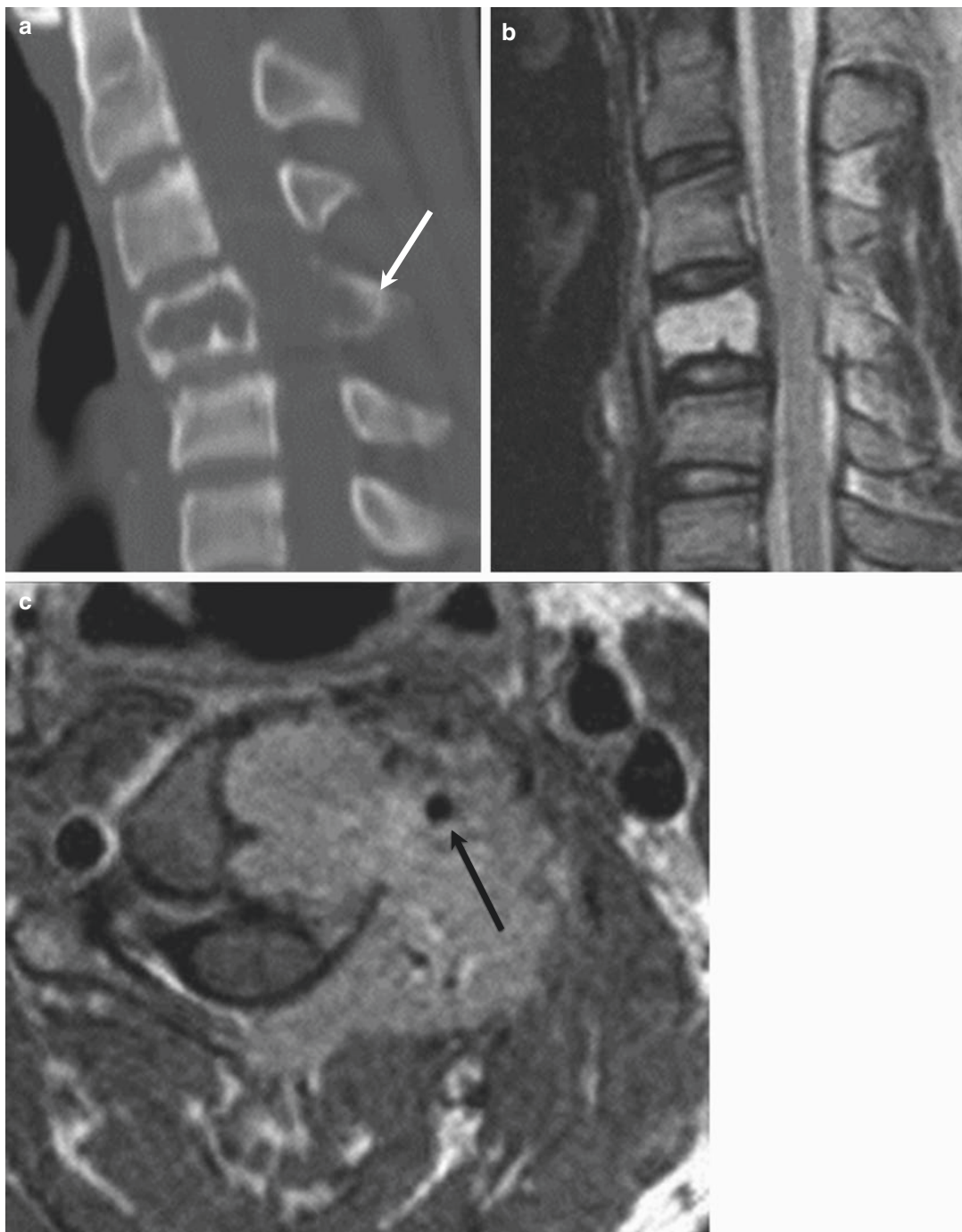


Fig. 5.35 Primary vertebral osteosarcoma of the C4 vertebra in an 18-year-old man. Sagittal CT scan (a) shows an osteolytic lesion involving the C4 body and spinous process (white arrow). There is no obvious matrix mineralization. Sagittal T2-weighted MR image (b) shows hyperintensity

of the mass. Axial contrast-enhanced T1-weighted MR image (c) shows an expansile, lobulated enhancing mass involving the left side of the vertebral body and posterior elements with extraosseous extension and encasement of the ipsilateral vertebral artery (black arrow)

5.13 Plasmacytoma

1. Epidemiology

- Mean age: 55 years (younger than patients with multiple myeloma)
- M > F (2: 1)

2. Location

- Axial skeleton: most common site of involvement (25–60%), followed by extremities
- Vertebral body: most common site of solitary bone plasmacytoma
- Thoracic > lumbar > cervical

3. Characteristic imaging findings

- T1 low signal bone marrow with curvilinear low signal areas
- “Mini brain” appearance due to thick cortical struts in the expanded vertebral body
- Lytic bone mass with cortical thinning on CT

4. Spectrum of imaging findings

- Variable degree of contrast enhancement (possible peripheral enhancement)
- Heterogeneous T2 signal intensity with internal curvilinear signal voids
- Variable degree of compression
- Rare involvement of disc or adjacent vertebrae
- Rare osteosclerosis (3%)

5. Differential diagnosis

- Aggressive vertebral hemangioma
 - Similar to plasmacytoma
 - Intense enhancement
- Multiple myeloma
 - Second lesion found in 33% of cases with presumed spine solitary bone plasmacytoma
- Metastasis
 - No involvement of disc or adjacent vertebrae

5.13.1 Illustrations: Plasmacytoma

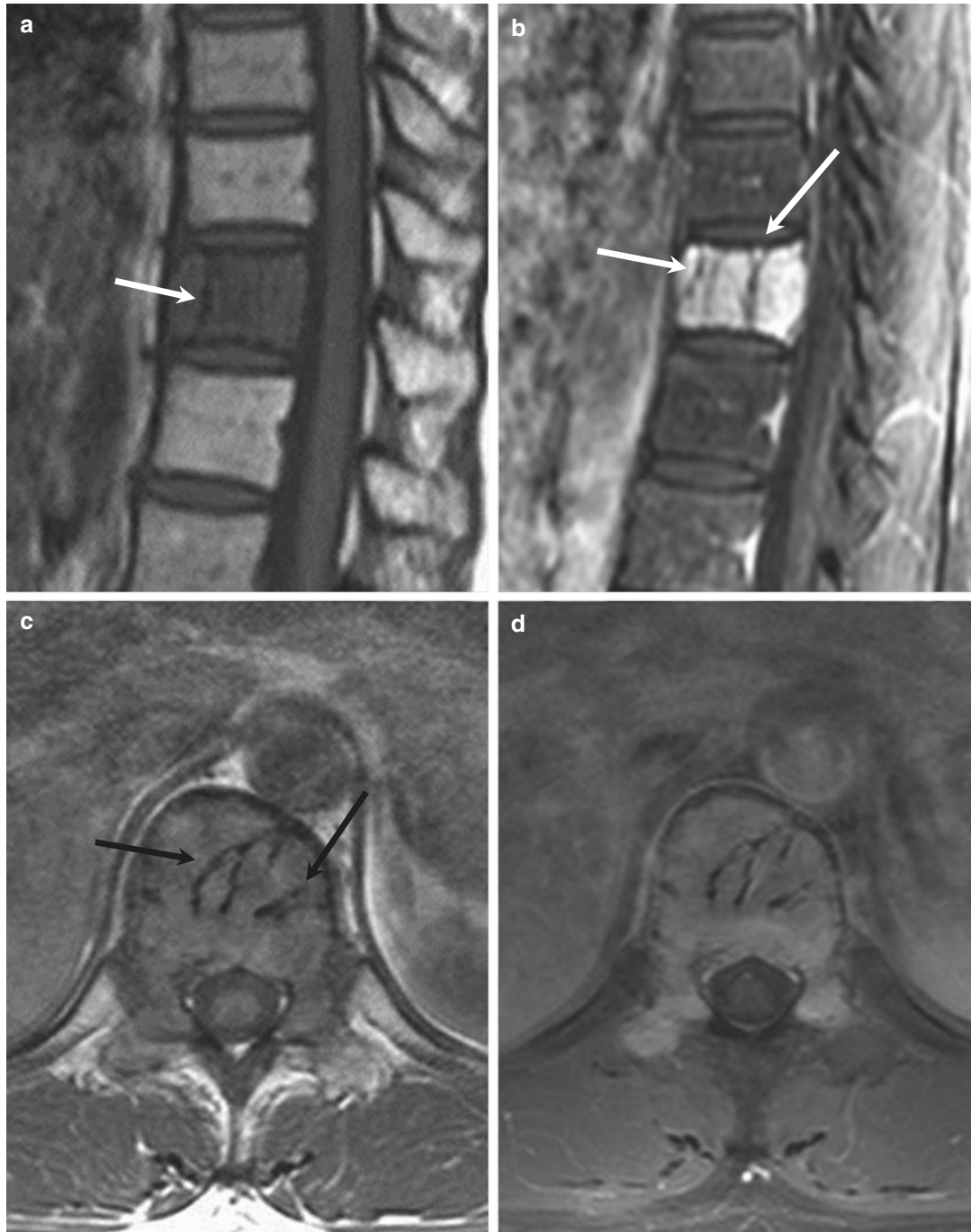
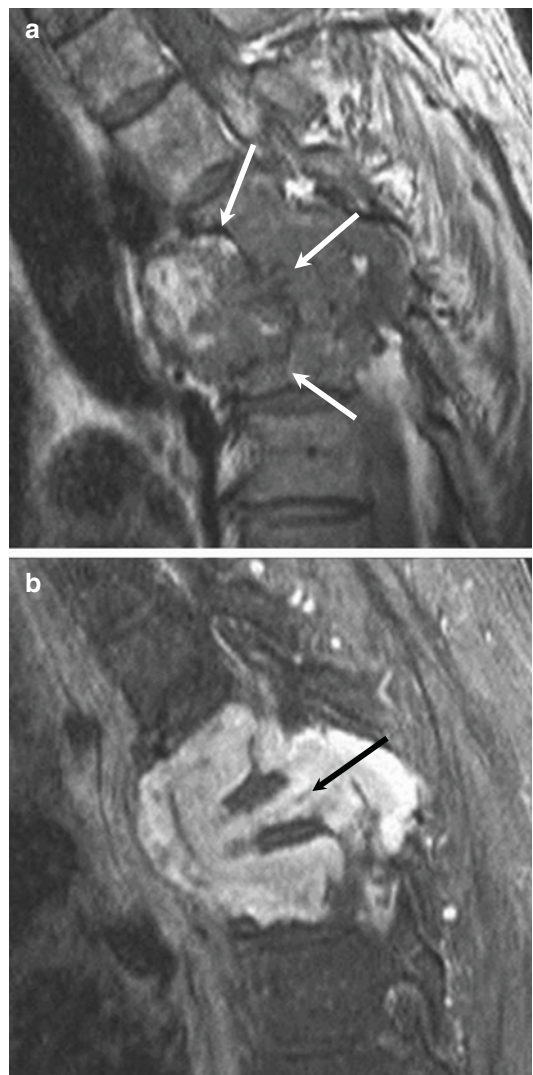


Fig. 5.36 Plasmacytoma of the T11 body in a 39-year-old woman. Sagittal pre- and post-contrast T1-weighted MR images (**a, b**) show a mildly expansile mass of hypointense signal relative to disc and linear low signal intensities that

represent cortical thickening (*white arrows*). Strong contrast enhancement is also noted. Axial pre- and post-contrast T1-weighted MR image (**c, d**) shows curvilinear low signal intensities resembling sulci of the brain (*black arrows*)

Fig. 5.37 Plasmacytoma involving the T3, T4, and T5 vertebral bodies in a 40-year-old man. Sagittal T1-weighted MR image (**a**) shows an expansile mass isointense relative to muscle and curvilinear low signal intensity struts (*white arrows*). Sagittal contrast-enhanced fat-saturated T1-weighted MR image (**b**) at a different level shows intense enhancement of the mass with collapse of the T4 body (*black arrow*) and relative preservation of the intervertebral disc spaces



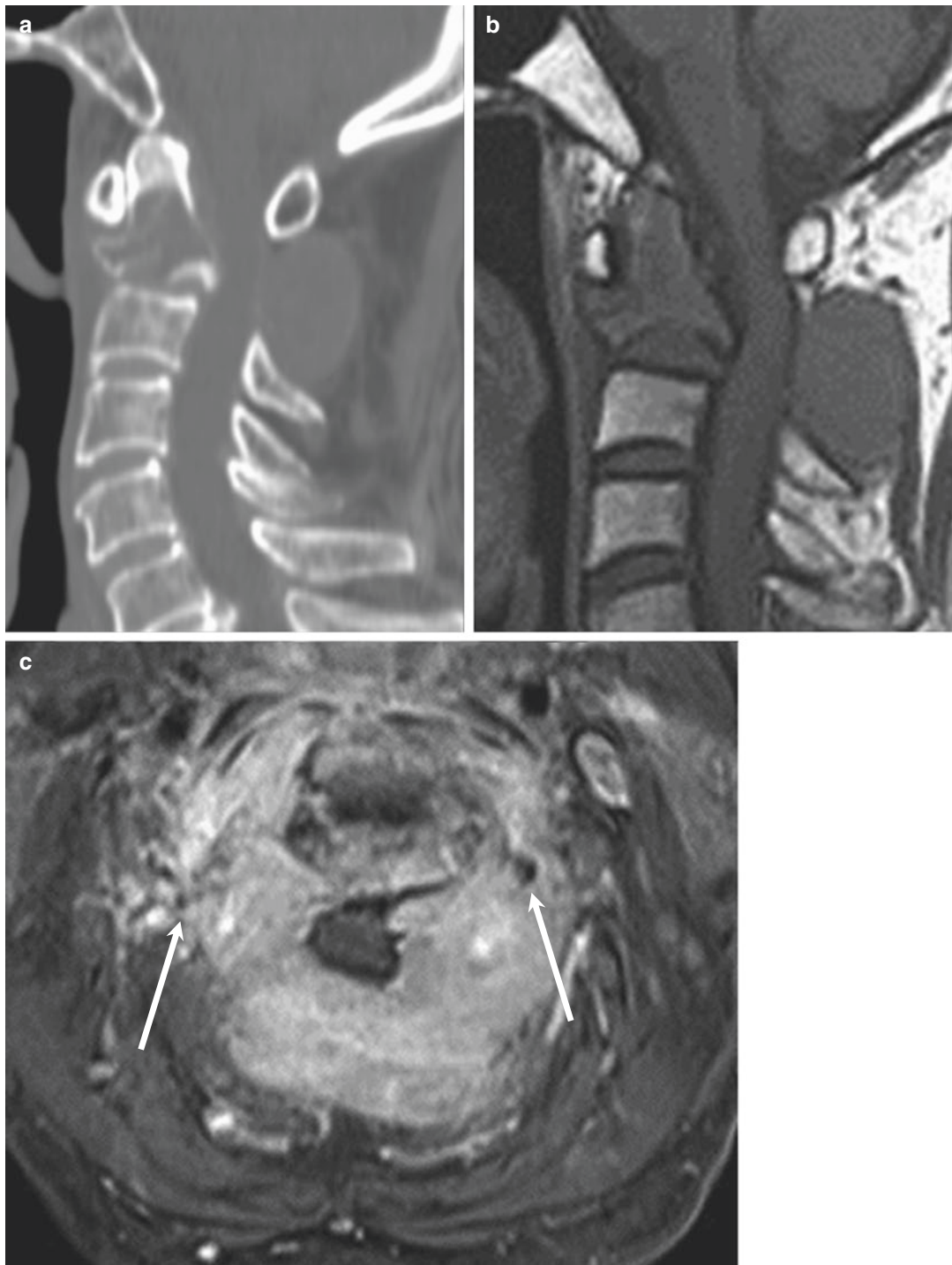


Fig. 5.38 Plasmacytoma involving the C2 vertebra in a 72-year-old man. Sagittal CT scan of the cervical spine (a) shows an expansile osteolytic mass involving C2 with cortical destruction and thinning. Sagittal T1-weighted MR image (b) also shows an expansile, cortical destructive mass of isointense signal relative to muscle involving

the C2 body and posterior elements. Axial contrast-enhanced T1-weighted fat-saturated MR image (c) at the level of the C2/C3 intervertebral space shows intense enhancement of the mass and epidural extension with encasement of thecal sac and bilateral vertebral arteries (white arrows)

Bibliography

- Boriani S, Bandiera S, Casadei R, Boriani L, Donthineni R, Gasbarrini A, et al. Giant cell tumor of the mobile spine: a review of 49 cases. *Spine*. 2012;37(1):E37–45. doi:[10.1097/BRS.0b013e3182233cccd](https://doi.org/10.1097/BRS.0b013e3182233cccd).
- Cerase A, Priolo F. Skeletal benign bone-forming lesions. *Eur J Radiol*. 1998;27(Suppl 1):S91–7.
- Cramer GD, Darby SA. Clinical anatomy of the spine, spinal cord, and ANS. Philadelphia: Elsevier Health Sciences; 2013.
- Kang HS, Lee JW, Kwon JW. Radiology illustrated: spine. Heidelberg: Springer Science & Business Media; 2014.
- Kim DH, Chang U-K, Kim S-H, Bilsky MH. Tumors of the spine. Philadelphia: Elsevier Health Sciences; 2008.
- Krandsdorf MJ, Sweet DE. Aneurysmal bone cyst: concept, controversy, clinical presentation, and imaging. *AJR Am J Roentgenol*. 1995;164(3):573–80. doi:[10.2214/ajr.164.3.7863874](https://doi.org/10.2214/ajr.164.3.7863874).
- Kroon HM, Schurmans J. Osteoblastoma: clinical and radiologic findings in 98 new cases. *Radiology*. 1990;175(3):783–90. doi:[10.1148/radiology.175.3.2343130](https://doi.org/10.1148/radiology.175.3.2343130).
- Kwon JW, Chung HW, Cho EY, Hong SH, Choi SH, Yoon YC, et al. MRI findings of giant cell tumors of the spine. *AJR Am J Roentgenol*. 2007;189(1):246–50. doi:[10.2214/AJR.06.1472](https://doi.org/10.2214/AJR.06.1472).
- Merhemic Z, Stosic-Opincal T, Thurnher MM. Neuroimaging of Spinal Tumors. *Magn Reson Imaging Clin N Am*. 2016;24(3):563–79. doi:[10.1016/j.mric.2016.04.007](https://doi.org/10.1016/j.mric.2016.04.007).
- Murphy MD, Andrews CL, Flemming DJ, Temple HT, Smith WS, Smirniotopoulos JG. From the archives of the AFIP. Primary tumors of the spine: radiologic pathologic correlation. *Radiographics Rev Publ Radiol Soc N Am Inc*. 1996;16(5):1131–58. doi:[10.1148/radiographics.16.5.8888395](https://doi.org/10.1148/radiographics.16.5.8888395).
- Nishiguchi T, Mochizuki K, Ohsawa M, Inoue T, Kageyama K, Suzuki A, et al. Differentiating benign notochordal cell tumors from chordomas: radiographic features on MRI, CT, and tomography. *AJR Am J Roentgenol*. 2011;196(3):644–50. doi:[10.2214/AJR.10.4460](https://doi.org/10.2214/AJR.10.4460).
- Orguc S, Arkun R. Primary tumors of the spine. *Semin Musculoskelet Radiol*. 2014;18(3):280–99. doi:[10.1055/s-0034-1375570](https://doi.org/10.1055/s-0034-1375570).
- Rodallec MH, Feydy A, Larousserie F, Anract P, Campagna R, Babinet A, et al. Diagnostic imaging of solitary tumors of the spine: what to do and say. *Radiographics Rev Publ Radiol Soc N Am Inc*. 2008;28(4):1019–41. doi:[10.1148/radiographics.284075156](https://doi.org/10.1148/radiographics.284075156).
- Ross JS, Moore KR. Diagnostic imaging: spine. Philadelphia: Elsevier Health Sciences; 2015.
- Si MJ, Wang CG, Wang CS, Du LJ, Ding XY, Zhang WB, et al. Giant cell tumours of the mobile spine: characteristic imaging features and differential diagnosis. *Radiol Med*. 2014;119(9):681–93. doi:[10.1007/s11547-013-0352-1](https://doi.org/10.1007/s11547-013-0352-1).

Rare But Interesting Spinal Tumors (in Alphabetical Order)

6

Contents

6.1	Angiolipoma	153
6.1.1	Illustrations: Angiolipoma	154
6.2	Atypical Teratoid/Rhabdoid Tumor (ATRT)	155
6.2.1	Illustrations: Atypical Teratoid/Rhabdoid Tumor (ATRT)	156
6.3	Chondroblastoma	157
6.3.1	Illustrations: Chondroblastoma	158
6.4	Epidural Hemangioma	159
6.4.1	Illustrations: Epidural Hemangioma	160
6.5	Epithelioid Angiosarcoma	163
6.5.1	Illustrations: Epithelioid Angiosarcoma	164
6.6	Epithelioid Hemangioendothelioma	166
6.6.1	Illustrations: Epithelioid Hemangioendothelioma	167
6.7	Ganglioglioma	168
6.7.1	Illustrations: Ganglioglioma	169
6.8	Ganglioneuroma	170
6.8.1	Illustrations: Ganglioneuroma	171
6.9	Undifferentiated Pleomorphic Sarcoma	172
6.9.1	Illustrations: Undifferentiated Pleomorphic Sarcoma	173
6.10	Malignant Peripheral Nerve Sheath Tumor	175
6.10.1	Illustrations: Malignant Peripheral Nerve Sheath Tumor	176
6.11	Oligodendroglioma	177
6.11.1	Illustrations: Oligodendroglioma	178
6.12	Paraganglioma	179
6.12.1	Illustrations: Paraganglioma	180
6.13	Primitive Neuroectodermal Tumor (PNET)	181
6.13.1	Illustrations: Primitive Neuroectodermal Tumor (PNET)	182
6.14	Solitary Fibrous Tumor (Hemangiopericytoma)	183
6.14.1	Illustrations: Solitary Fibrous Tumor (Hemangiopericytoma)	184
6.15	Teratoma	186
6.15.1	Illustrations: Teratoma	187
	Bibliography	188

6.1 Angiolipoma

1. Epidemiology
 - 40–50 years
 - F>M
2. Location
 - Thoracic spine
 - Dorsal epidural space
3. Characteristic imaging findings
 - Well-defined lobular mass
 - Both fatty and vascular component
 - High signal on T1-weighted image, low density on CT due to fatty component
 - Strong enhancement on contrast enhancement with fat suppression due to vascular component
4. Spectrum of imaging findings
 - Infiltrating angiolipoma
 - Can infiltrate into adjacent structure

5. Differential diagnosis

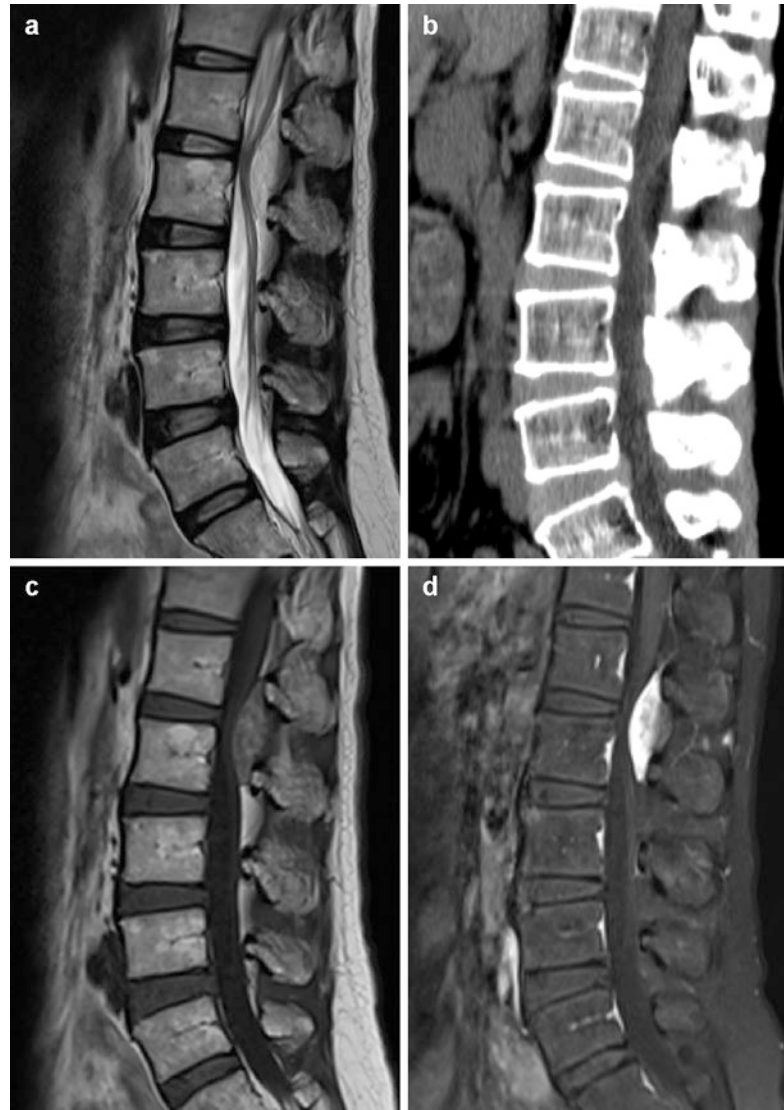
- Epidural hemangioma
 - No fatty component
- Epidural lipomatosis
 - No vascular component

• Hematoma

- No enhancement
- No fat suppression
- High density on CT

6.1.1 Illustrations: Angiolipoma

Fig. 6.1 Epidural angiolipoma in a 53-year-old woman. T2-weighted sagittal and axial images of the lumbar spine (a) show a 4 cm well-defined mass in the posterior epidural space at L1–2 level. Sagittal CT scan (b) shows internal fatty component. T1-weighted sagittal MR image (c) shows heterogeneous signal intensity of the lesion indicating mixed fatty and vascular components. Contrast-enhanced T1-weighted image (d) shows strong enhancement with some areas of fat signal suppression



6.2 Atypical Teratoid/Rhabdoid Tumor (ATRT)

1. Epidemiology

- Young children and infant, 7 months~17 years
(more common in less than 3 years)

2. Location

- Most commonly in the brain, very rare in the spine
- Intradural extramedullary, intramedullary
- Cervical, thoracic, lumbar spine

3. Characteristic imaging findings

- Large heterogeneous mass
- Internal hemorrhage
- Diffuse contrast enhancement
- CSF seeding

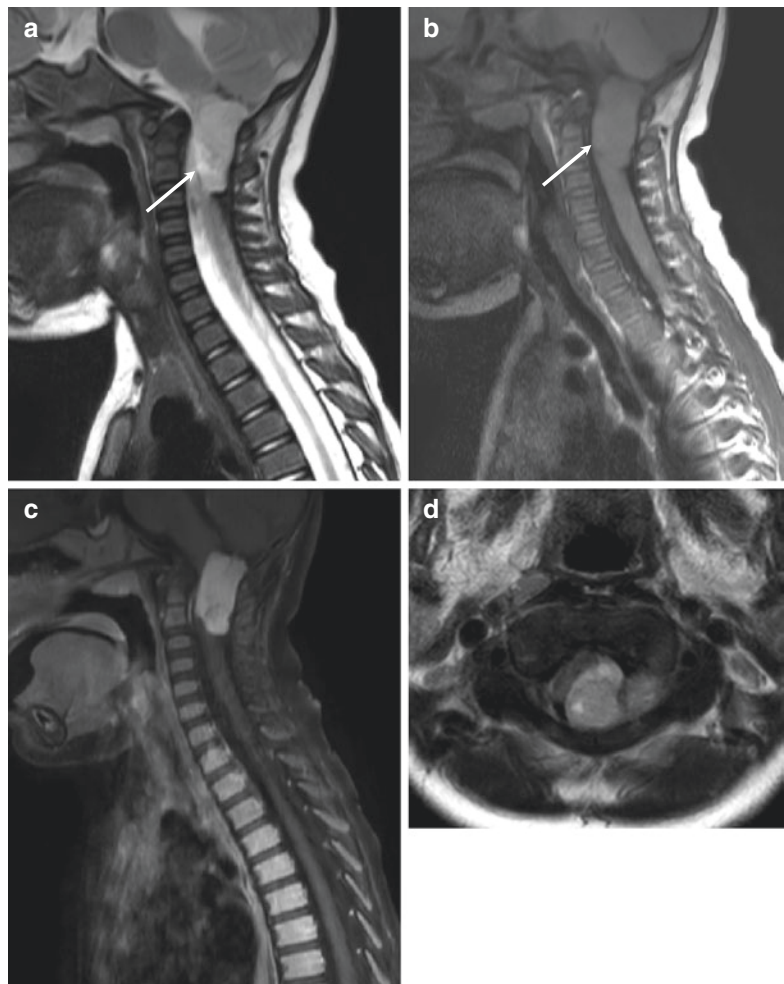
4. Spectrum of imaging findings

5. Differential diagnosis

- Myxopapillary ependymoma and malignant peripheral nerve sheath tumor in extramedullary location
- PNET, ependymoma, metastasis in intramedullary location

6.2.1 Illustrations: Atypical Teratoid/Rhabdoid Tumor (ATRT)

Fig. 6.2 Atypical teratoid/rhabdoid tumor (ATRT) in a 2-year-old child. Sagittal T2- and T1-weighted images (**a–c**) show a large heterogeneous mass at C1-C2-C3 levels with strong contrast enhancement. There is a focal cystic portion with suspected area of hemorrhage in the anteroinferior aspect of the tumor (*white arrows*). T2-weighted axial MR image (**d**) shows intradural extramedullary location of the tumor with cord compression and extradural extension into the left C1/C2 neural foramen



6.3 Chondroblastoma

1. Epidemiology

- 20 years (9–62 years)
- M > F

2. Location

- Very rare in spine, anywhere in the spine
(most common in the thoracic spine)
- Vertebral body and posterior elements

3. Characteristic imaging findings

- Expansive
- Aggressive morphologic features with bony destruction and soft tissue mass
- Calcification within the mass

4. Spectrum of imaging findings

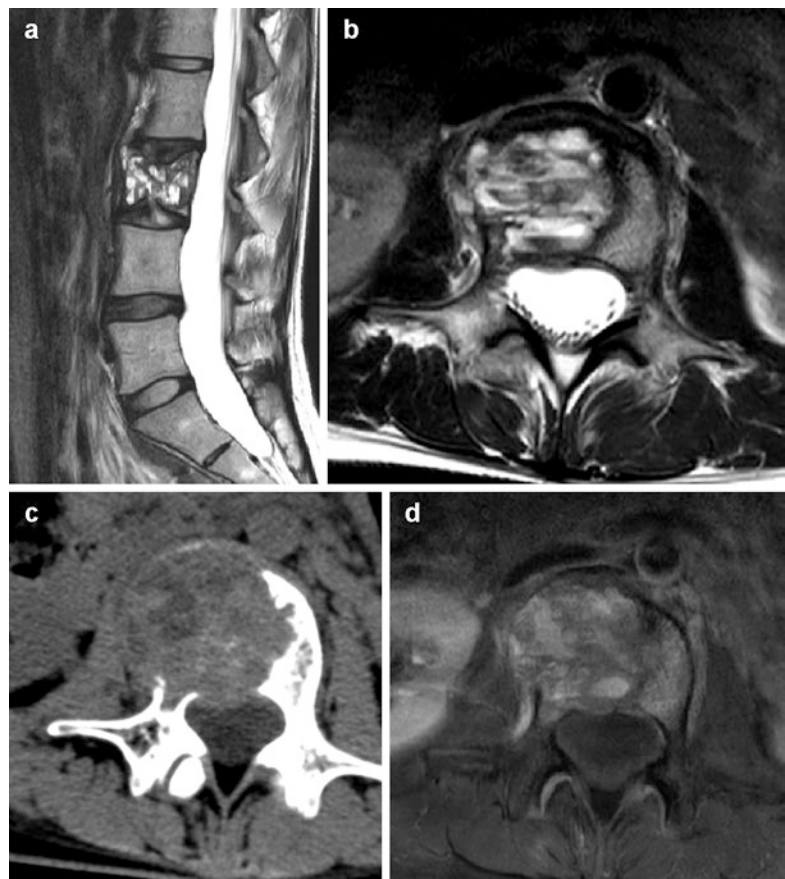
- Secondary aneurysmal bone cyst
- Bone marrow edema

5. Differential diagnosis

- Chondrosarcoma
 - Indistinguishable
 - Older ages (45–55 years)

6.3.1 Illustrations: Chondroblastoma

Fig. 6.3 Chondroblastoma of the L3 vertebrae in a 25-year-old woman. T2-weighted sagittal and axial MR images (**a, b**) show pathologic compression fracture of the L3 vertebral body with multiple hemorrhagic fluid-fluid levels within the mass. Axial CT scan (**c**) shows internal fuzzy calcifications with cortical destruction at the right anterior aspect and paravertebral extension. The mass shows enhancing solid portions with adjacent bone marrow edema (**d**)



6.4 Epidural Hemangioma

1. Epidemiology

- Any age (mean age, 38 years; age range, 2–62 years)
- M = F

2. Location

- Cavernous hemangioma: dorsal epidural space
- Venous hemangioma: ventral epidural space, lumbar spine

3. Characteristic imaging findings

- Cavernous hemangioma: lobular contour, solid intense enhancement

4. Spectrum of imaging findings

- Manifested as epidural hematoma
- Venous hemangioma: small cystic mass, T1-hyperintensity, ventral location

5. Differential diagnosis

- HIVD
 - T1-hypointensity, T2-hypointensity
 - Peripheral enhancement
- Hematoma
 - No solid enhancement in acute stage
- Schwannoma
 - Peripheral enhancement, less intense enhancement
 - Solid component

6.4.1 Illustrations: Epidural Hemangioma

Fig. 6.4 Epidural hemangioma in a 28-year-old woman. T2-weighted sagittal and axial MR images (**a, b**) show an extradural mass of high signal intensity at the left side of the T1 vertebra. T1-weighted MR image (**c**) shows intralesional high signal intensity suggesting internal hemorrhagic areas. T1-weighted axial MR image (**d**) shows mild enhancement

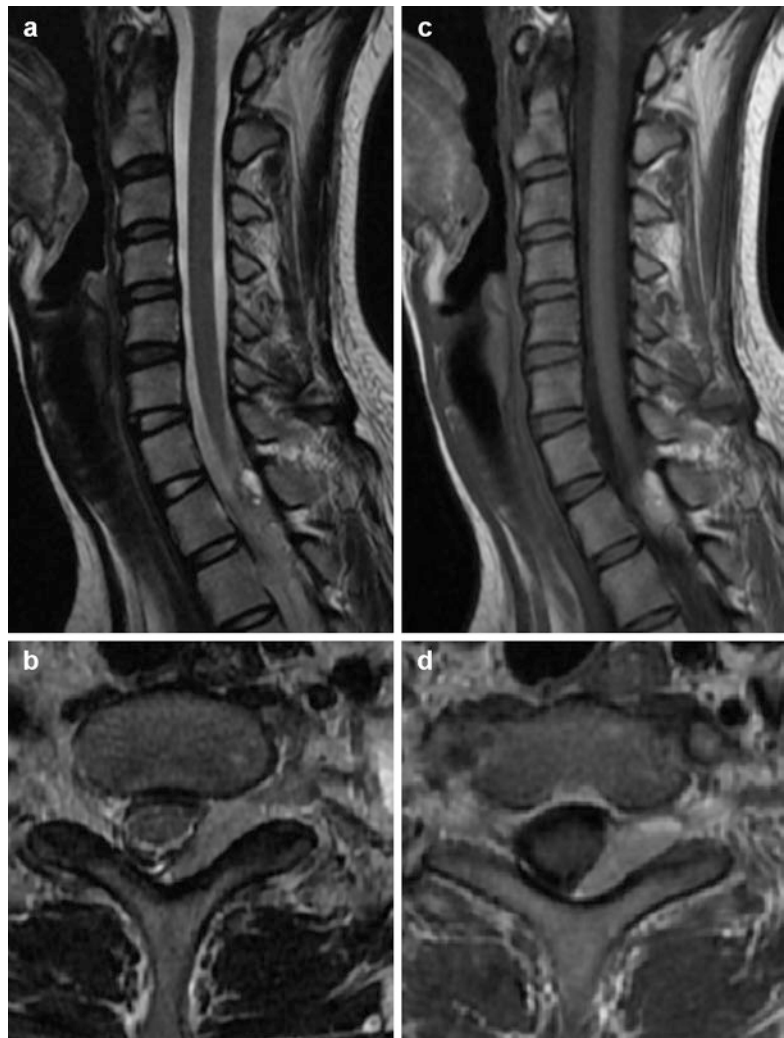


Fig. 6.5 Epidural hemangioma in a 30-year-old man. Lumbar spine MR images demonstrate a T2 hyperintense lesion with rim enhancement in the right anterior epidural space at the level of the upper body of L4 (a, b)

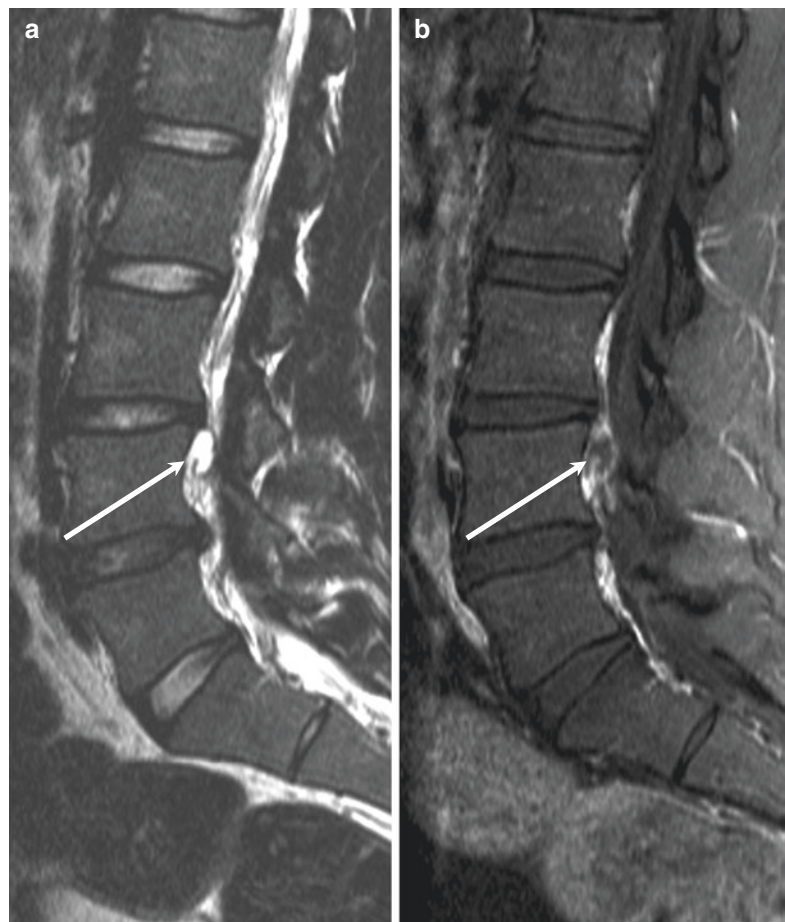


Fig. 6.6 Spontaneous epidural hematoma without any tumor in a 36-year-old woman.

Cervical spine MR images show an anterior epidural mass-like lesion extending from the levels of C7 to T4 of iso signal intensity on T1-weighted (a) and intermediate to high signal intensity on T2-weighted images (b). Nodular enhancement is seen centrally in the anterior spinal epidural lesion (c, d) indicating extravasation of contrast material by leaking vessels. Hyperacute to acute hematoma was diagnosed



6.5 Epithelioid Angiosarcoma

1. Epidemiology

- An extremely rare subtype of angiosarcoma, which is characterized by large cells with an epithelioid morphology
- Middle aged and older
- M = F

2. Location

- Rare in the spine

3. Characteristic imaging findings

- Feature of aggressive, high-grade bone tumor: destructive osteolytic mass with

paravertebral extension, central necrosis, peripheral enhancement due to hyperperfusion

4. Spectrum of imaging findings

- Multicentricity (20–50%): multiple masses in a single bone

5. Differential diagnosis

- Epithelioid hemangioendothelioma
 - Difficult to differentiate
 - Less aggressive
- Metastasis
 - Difficult to differentiate
 - Less hypervascular

6.5.1 Illustrations: Epithelioid Angiosarcoma

Fig. 6.7 Epithelioid angiosarcoma in a 73-year-old man. T2 SPAIR and T1-weighted sagittal MR images (**a, b**) show a heterogeneous signal mass in the L1 vertebral body with extensive bone marrow edema. T2-weighted axial MR images (**c, d**) show internal tortuous low signal flow voids (*white arrows*). Pre-surgical angiography for tumor embolization (**e**) shows marked hypervascularity within and around the tumor



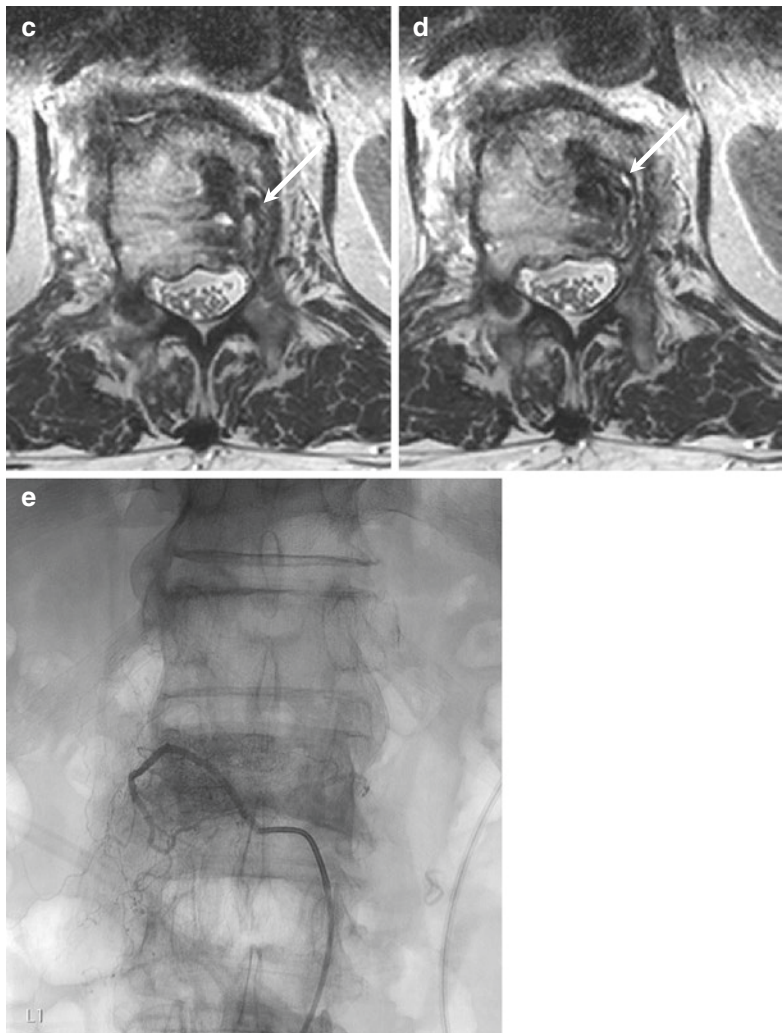


Fig. 6.7 (continued)

6.6 Epithelioid Hemangioendothelioma

1. Epidemiology

- Vascular tumor, intermediate between hemangiomas and conventional angiosarcomas
- Very rare in the spine
- Middle aged and older
- M = F

2. Location

- Cervical, lumbar

3. Characteristic imaging findings

- Nonspecific vascular tumor
- Osteolytic mass, hypervascularity, single or multiple

4. Spectrum of imaging findings

- Distant metastasis (20–30%)

5. Differential diagnosis

- Hemangioma
 - Less aggressive
 - Can be cystic
 - Epidural hematoma
- Angiosarcoma
 - More aggressive
 - More bony destruction and paravertebral extension
- Metastasis
 - Less hypervascular

6.6.1 Illustrations: Epithelioid Hemangioendothelioma

Fig. 6.8 Epithelioid hemangioendothelioma in a 55-year-old man.
T2-weighted sagittal MR image (**a**) shows a 2 cm intramedullary mass of high signal intensity at the level of T10 vertebra. Extensive spinal cord edema is combined.
Contrast-enhanced T1-weighted axial MR image (**b**) shows an exophytic intramedullary mass in the left side with intense homogenous enhancement.
Contrast-enhanced T1-weighted sagittal MR image (**c**) shows a vascular pedicle in the inferior aspect of the tumor (*white arrow*).
Hypervasculat tumor staining from the left T10 spinal artery (*black arrow*) is demonstrated on angiography (**d, e**)



6.7 Ganglioglioma

1. Epidemiology

- Children, young adult
- M = F

2. Location

- Intramedullary location
- Cervical spinal cord > thoracic spinal cord

3. Characteristic imaging findings

- Long segments of spinal cord
- Eccentric location
- Mixed signal intensity on T1-weighted images
- No surrounding edema
- Patchy enhancement
- Calcification

4. Spectrum of imaging findings

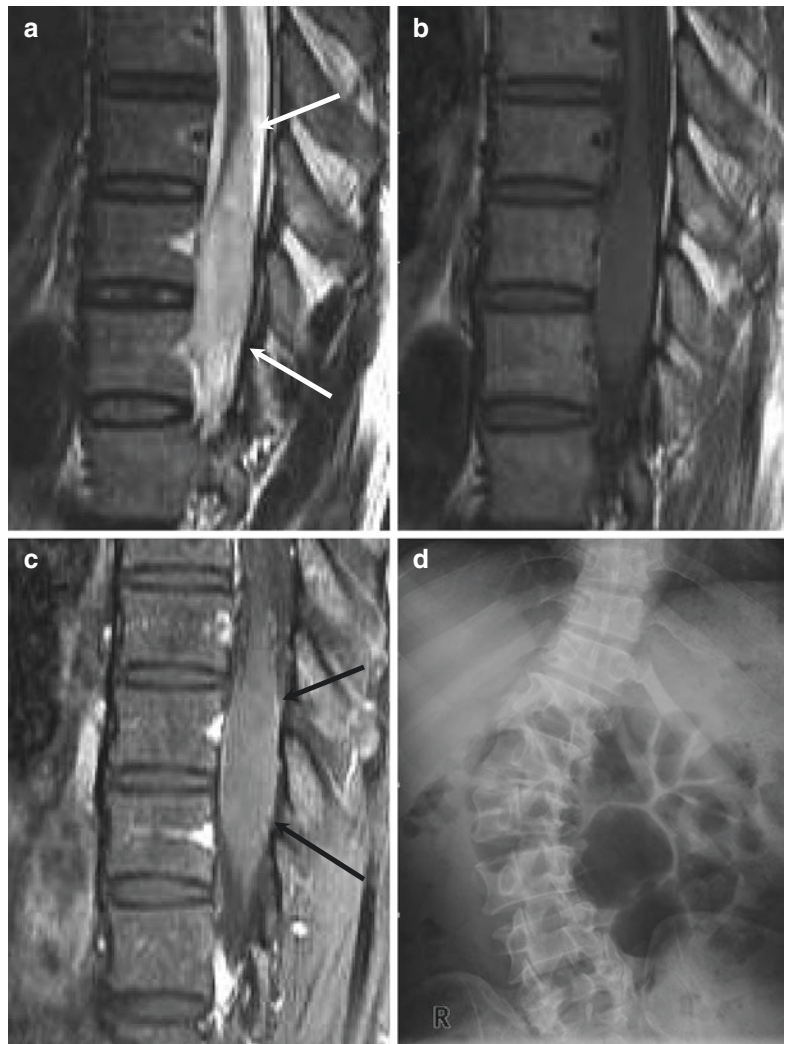
- Tumoral cysts
- No enhancement

5. Differential diagnosis

- Spinal astrocytoma
 - Large cystic component in children (pilocytic astrocytoma)
 - More areas of enhancement
 - Less longitudinal involvement
- Spinal ependymoma
 - Less longitudinal involvement
 - Central location with syrinx
 - Hemosiderin cap

6.7.1 Illustrations: Ganglioglioma

Fig. 6.9 Ganglioglioma in a 43-year-old man. T2-weighted (**a**) and T1-weighted (**b**) sagittal MR images show an intramedullary bulging mass of T2 high signal intensity from T10 to the conus medullaris (white arrows). The tumor shows eccentric location at the level of T10. There is no adjacent cord edema. Contrast-enhanced T1-weighted sagittal MR image (**c**) shows mild homogenous enhancement. Plain AP radiograph of the thoracolumbar spine (**d**) shows thoracolumbar scoliosis



6.8 Ganglioneuroma

1. Epidemiology

- Children, young adult
- M = F

2. Location

- Extradural paravertebral location
- Most common in posterior paraspinal mediastinum

3. Characteristic imaging findings

- Well-defined large solid masses in posterior paraspinal mediastinum in children
- Heterogeneous intermediate signal on both T1- and T2-weighted images
- Variable contrast enhancement

4. Spectrum of imaging findings

- Calcification may be present.

5. Differential diagnosis

- Neuroblastoma
 - Metastases
 - Calcification
- Benign nerve sheath tumor (schwannoma and neurofibroma)
 - Middle-aged adults

6.8.1 Illustrations: Ganglioneuroma

Fig. 6.10 Ganglioneuroma in a 12-year-old girl. T2-weighted (**a**) and T1-weighted (**b**) sagittal MR images show a well-defined heterogeneous large solid mass in the right extradural, paravertebral space extending into the neural foramen of T3/T4 and T4/T5 with widening. Contrast-enhanced T1-weighted axial MR image (**c**) shows a mass located in the posterior paravertebral mediastinum with patchy enhancement



6.9 Undifferentiated Pleomorphic Sarcoma

1. Epidemiology

- Extremely rare
- Peak incidence: 5th decade
- Sex: M > F

2. Location

- Thoracic > lumbar > sacrum > cervical

3. Characteristic imaging findings

- Intermediate to low signal intensity on T1-weighted image
- Inhomogeneous high signal intensity on T2-weighted image

4. Spectrum of imaging findings

- Calcification: 5–20%
- High-grade myxoid lesions
 - Cystic appearance
 - Nodular non-myxomatous elements on contrast enhancement

5. Differential diagnosis

- Metastasis
- Other high-grade sarcoma such as osteosarcoma

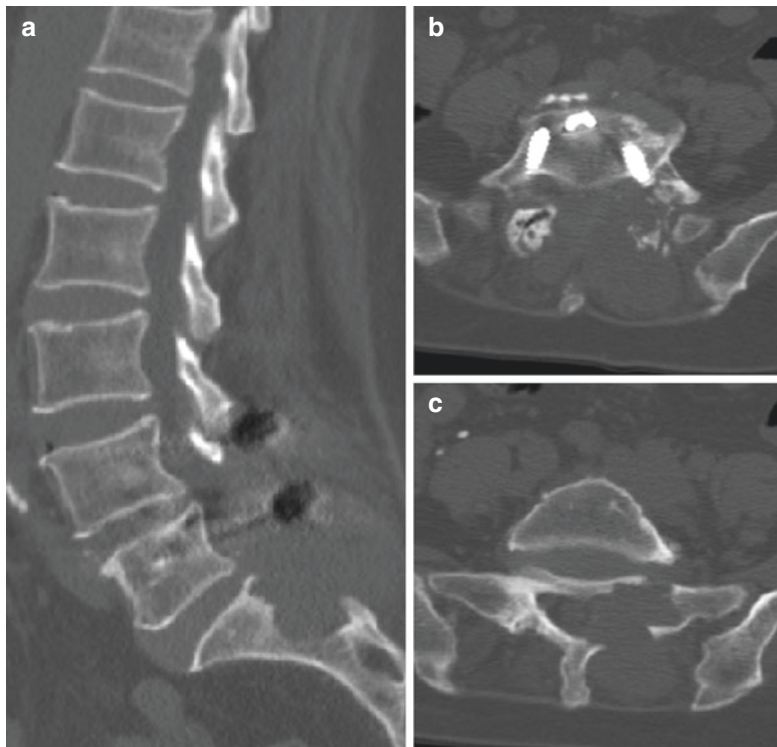
6.9.1 Illustrations: Undifferentiated Pleomorphic Sarcoma

Fig. 6.11 Undifferentiated pleomorphic sarcoma in a 64-year-old woman. She underwent previous spinal operation with interbody fusion and posterior screw fixation at L4–L5 10 years ago. Sagittal (a) and axial (b, c) CT scan shows an osteolytic soft tissue mass involving L5 and the left side of S1, mainly affecting the posterior elements with extrasosseous extension but without definite internal

calcification. The mass shows a lobulated contour with T2 intermediate (d) and T1 low (e) signal intensities as well as multiple internal cystic portions (*white arrows*). Contrast-enhanced T1-weighted sagittal and axial images (f, g) show homogenous enhancement, except for the cystic area

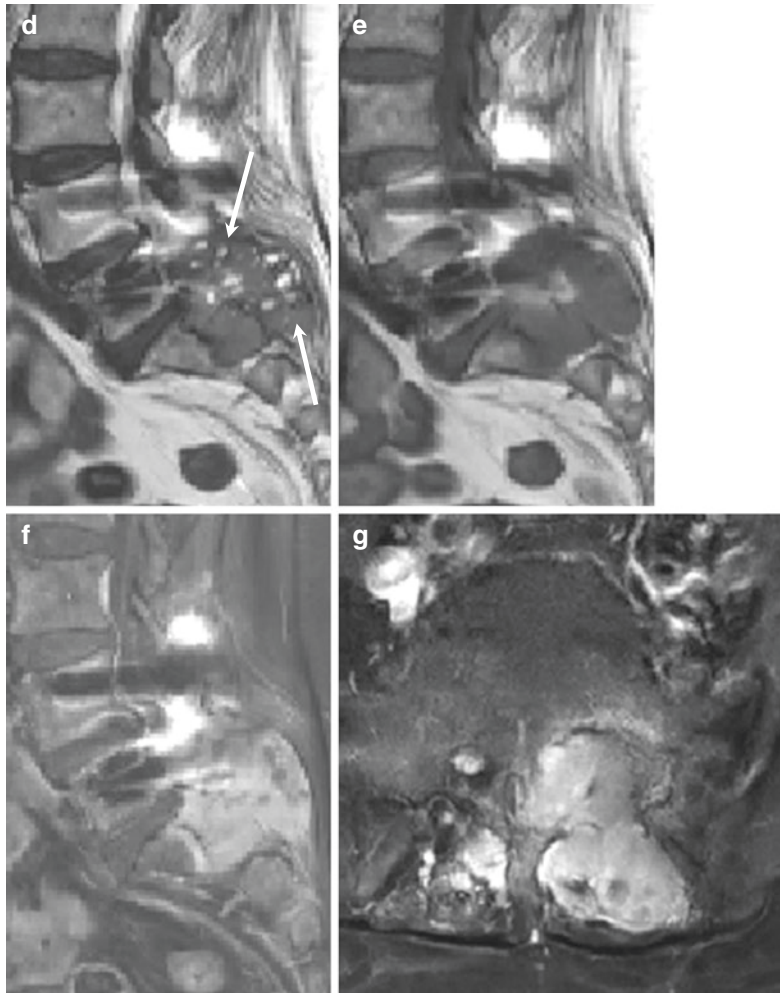


Fig. 6.11 (continued)

6.10 Malignant Peripheral Nerve Sheath Tumor

1. Epidemiology

- Presents in 4th decade (mean age: 39.7 years)
- If associated with NF 1: 26–42 years (mean age: 28.7 years)
- Sex: M = F (if NF 1, M > F)

2. Location

- Paravertebral >> intraspinal (rare)
 - Posterior mediastinum
 - Retroperitoneum
- Proximal portion of extremities along neurovascular bundle
 - Especially brachial plexus and sciatic nerve

3. Characteristic imaging findings

- Size > 5 cm
- Large infiltrative heterogeneous soft tissue mass on T2-weighted image, often hemor-

rhagic, calcification, cystic degeneration, and necrosis

- Marked contrast enhancement with infiltration to adjacent tissue planes

4. Spectrum of imaging findings

- Loss of homogeneity, loss of “target sign” within plexiform neurofibroma

5. Differential diagnosis

- Benign peripheral nerve sheath tumor
 - No invasion to surrounding structures
 - Well circumscribed
 - Variable enhancement
 - Sudden, painful enlargement of preexisting neurofibroma in NF 1: suspicious malignant transformation
- Other soft tissue sarcoma
 - Not related to adjacent neurovascular bundle
- Hematoma
 - No enhancing solid portion

6.10.1 Illustrations: Malignant Peripheral Nerve Sheath Tumor

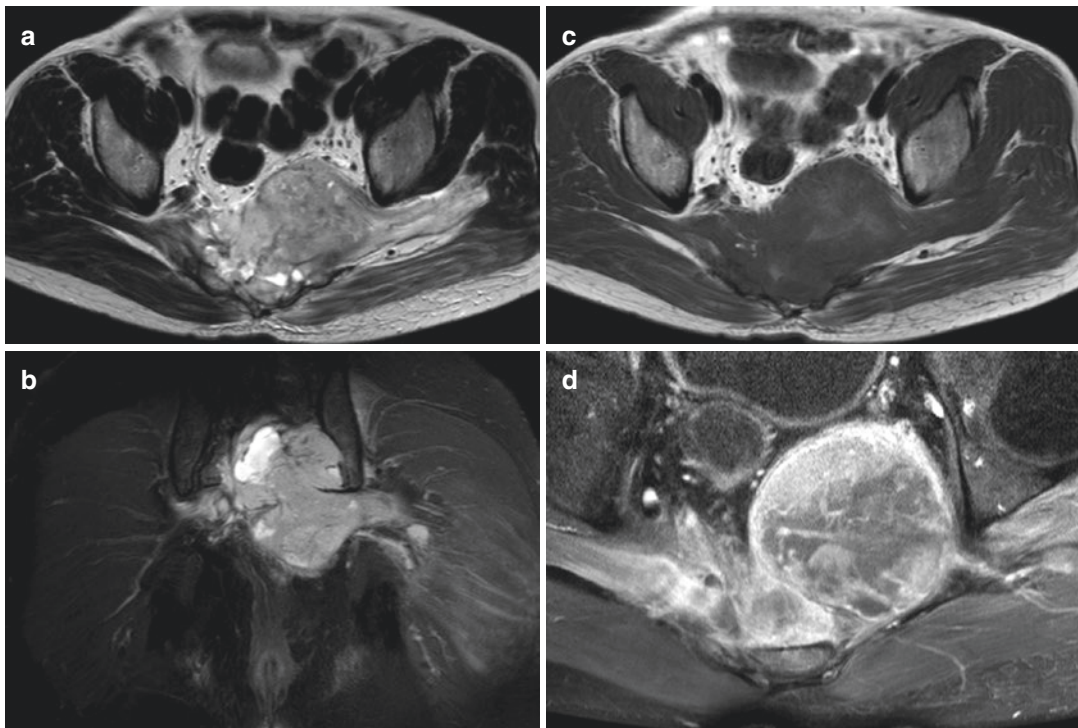


Fig. 6.12 Malignant peripheral nerve sheath tumor (MPNST) in a 37-year-old man. Axial T2-weight MR image (**a**) and coronal fat-suppressed T2-weighted image (**b**) show a large bony destructive mass of the sacrum with involvement of the bilateral sacral nerve roots. The mass

extends toward the greater sciatic foramen, left piriformis muscle, and sciatic nerve. Axial T1-weighted MR image (**c**) and contrast-enhanced T1-weighted MR image (**d**) show heterogeneous enhancement with intratumoral hemorrhage and necrosis

6.11 Oligodendroglioma

1. Epidemiology

- Extremely rare
 - Only 2% of all spinal cord tumors
- Mean age: 28.4 years
- Sex: M = F (M > F in intracranial oligodendro glioma)

2. Location

- Most common in the thoracic
 - Thoracic > cervical > thoracocervical junction > lumbar > thoracolumbar level

3. Characteristic imaging findings

- Heterogeneous hypo or iso signal intense lesions on T1-weighted image
- Hyper-signal intense lesions on T2-weighted image
- Mild to moderate heterogeneous spotty enhancement
- Calcification: 28–40%

4. Spectrum of imaging findings

- Cystic component or cystic necrosis possible
 - High-grade spinal oligodendro glioma
- CT: combined skeletal deformity

5. Differential diagnosis

- Astrocytoma
- Ganglioglioma

6.11.1 Illustrations: Oligodendrolioma

Fig. 6.13 Oligodendrolioma in a 24-year-old man. T2-weighted sagittal MR image (**a**) shows a bulky heterogeneous intramedullary mass in the thoracic spinal cord. The mass shows slightly high signal intensity with syrinx formation at its cranial aspect. Contrast-enhanced T1-weighted sagittal image (**b**) shows mild spotty enhancement. Sagittal and coronal CT scan (**c, d**) shows multifocal stippled intratumoral calcifications



6.12 Paraganglioma

1. Epidemiology

- Peak incidence: 45–50 years (range: 13–70 years)
- Sex: M = F

2. Location

- Spine: rare
 - Most common: filum terminale
 - Osteolytic bone metastases by malignant paraganglioma
 - Case reports: primary intraosseous or extradural paragangliomas

3. Characteristic imaging findings

- Well-defined intradural extramedullary hypervascular enhancing mass at the cauda equina
- Iso to low signal on T1-weighted image
- Heterogeneous high signal on T2-weighted image
- Intense contrast enhancement
- Hypervascular mass with large draining veins

4. Spectrum of imaging findings

- Possible cystic portion
- Hemosiderin
- Prominent flow voids due to prominent draining veins

5. Differential diagnosis

- Myxopapillary ependymoma
 - Similar to paraganglioma (central location)
 - More common
- Schwannoma
 - Rare hemorrhage
 - Paracentral location
 - No vascular flow voids
 - Much more common
- Drop metastasis
- Hemangioblastoma in the filum terminale
 - Rare location
 - Hypervascular, enlarged vessels

6.12.1 Illustrations: Paraganglioma

Fig. 6.14 Paraganglioma in a 58-year-old woman. T2-weighted (**a**) and T1-weighted (**b**) sagittal MR images show a 2 cm well-defined intradural extramedullary mass at L3-L3/L4 level. The mass shows heterogeneous high signal intensity on T2-weighted images and iso signal intensity on T1-weighted images with intense contrast enhancement (**c**)



6.13 Primitive Neuroectodermal Tumor (PNET)

1. Epidemiology

- 1st peak: < 20 years old (90%)
- 2nd peak: 50 years old
- M > F

2. Location

- Spine: 5% of all Ewing's sarcoma
- Sacrum: m/c
- Vertebral body → neural arch
- Spreads along the peripheral nerve

3. Characteristic imaging findings

- Permeative lytic lesion of VB or sacrum with large soft tissue mass on CT
- Areas of central necrosis common
- "Percolates" through tiny perforations in cortex
 - "Smudged" appearance on MR
- Low signal on T1-weighted image and iso signal on T2-weighted image
- Heterogeneous contrast enhancement

4. Spectrum of imaging findings

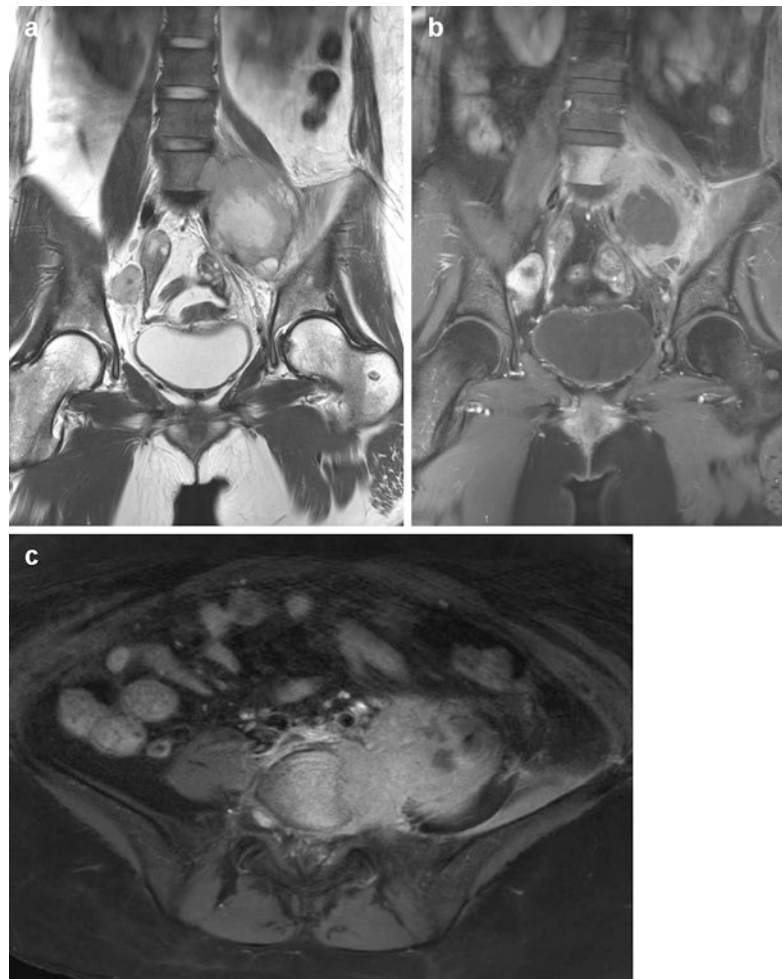
- Rare sclerotic lesion (5%)
 - Reactive bone formation
 - No ossification at soft tissue component
- Tumor vs peritumoral edema
 - Contrast enhancement at peritumoral edema with Gd

5. Differential diagnosis

- Primitive neuroectodermal tumor
 - Clinical/radiological identical to Ewing's sarcoma
- Langerhans cell histiocytosis
 - Discrete geographic lytic lesion
 - May have identical radiologic appearance to Ewing's sarcoma
- Metastatic neuroblastoma
 - Adrenal or extra-adrenal primary
 - Children
- Osteosarcoma
 - Bone matrix on CT
 - Cortical destruction >> permeation
 - Vertebral body or neural arch involvement

6.13.1 Illustrations: Primitive Neuroectodermal Tumor (PNET)

Fig. 6.15 Primitive neuroectodermal tumor (PNET) in a 36-year-old woman. T2-weighted coronal MR image (**a**), contrast-enhanced T1-weighted coronal (**b**) and axial (**c**) MR images show a large heterogeneous enhancing mass with internal necrosis of the left iliopsoas muscle. Direct invasion into the L5 vertebral body with epidural extension and encasement of the neurovascular bundle along the left iliac chain is noted



6.14 Solitary Fibrous Tumor (Hemangiopericytoma)

1. Epidemiology

- 20–70 years of age (median: 40 years)
- No gender prediction
- Rare

2. Location

- Dural based, epidural, paraspinal: most often
- Intradural/pial, intramedullary: possible
- Osseous metastasis from extraspinal hemangiopericytoma

3. Characteristic imaging findings

- Vividly enhancing lesion expanding/eroding adjacent osseous structures, with large soft tissue component
- Low signal on T1-weighted images and mild to moderate high signal on T2-weighted images
- Vivid homogenous enhancement

4. Spectrum of imaging findings

- No phlebolith or calcific component on CT
- Marked hypervascularity in arterial phase with abnormal irregular vessels on angiography

5. Differential diagnosis

- Meningioma
 - Well circumscribed, no bony erosion
 - Calcification
- Schwannoma
 - Avidly enhancing mass in the spinal canal or neural foramen
 - High signal on T2-weighted image
 - Bony remodeling, foraminal expansion or vertebral scalloping
- Vascular metastasis (renal or thyroid carcinoma)
 - Centered in the bone, posterior vertebral body
- Angiosarcoma
 - Extremely rare location

6.14.1 Illustrations: Solitary Fibrous Tumor (Hemangiopericytoma)

Fig. 6.16 Intramedullary solitary fibrous tumor (hemangiopericytoma) in a 36-year-old woman. T2-weighted (**a**) and T1-weighted (**b**) sagittal MR images show a 1.5 cm well-defined intramedullary mass at the C4/5 intervertebral disc level. The mass shows low signal intensity on T2-weighted images and heterogeneous iso signal intensity on T1-weighted images with prominent surrounding cord edema and swelling. Contrast-enhanced T1-weighted sagittal (**c**) and axial (**d**) MR images show strong contrast enhancement



Fig. 6.17 Intradural extramedullary solitary fibrous tumor (hemangiopericytoma) in a 22-year-old woman. T2-weighted sagittal (**a**) and axial (**b**) MR images show a well-defined IDEM tumor in the left ventral aspect of C1/C2 causing severe spinal cord compression. The mass shows heterogeneous slight high signal intensity with internal dark signal void-like structures (white arrows). Strong contrast enhancement (**c**) with hypervascularity on angiography (**d**) is also noted



6.15 Teratoma

1. Epidemiology

- Extremely rare (0.1% of all spinal tumors)
- Mean age: 38.7 years
- No gender prediction

2. Location

- Intramedullary
 - Predominantly lower thoracic and conus medullaris >> cervical
- Extramedullary

3. Characteristic imaging findings

- Intradural: oval or lobulated heterogeneous mass
- CT: calcification
- Fat component: high signal on both T1- and T2-weighted images

4. Spectrum of imaging findings

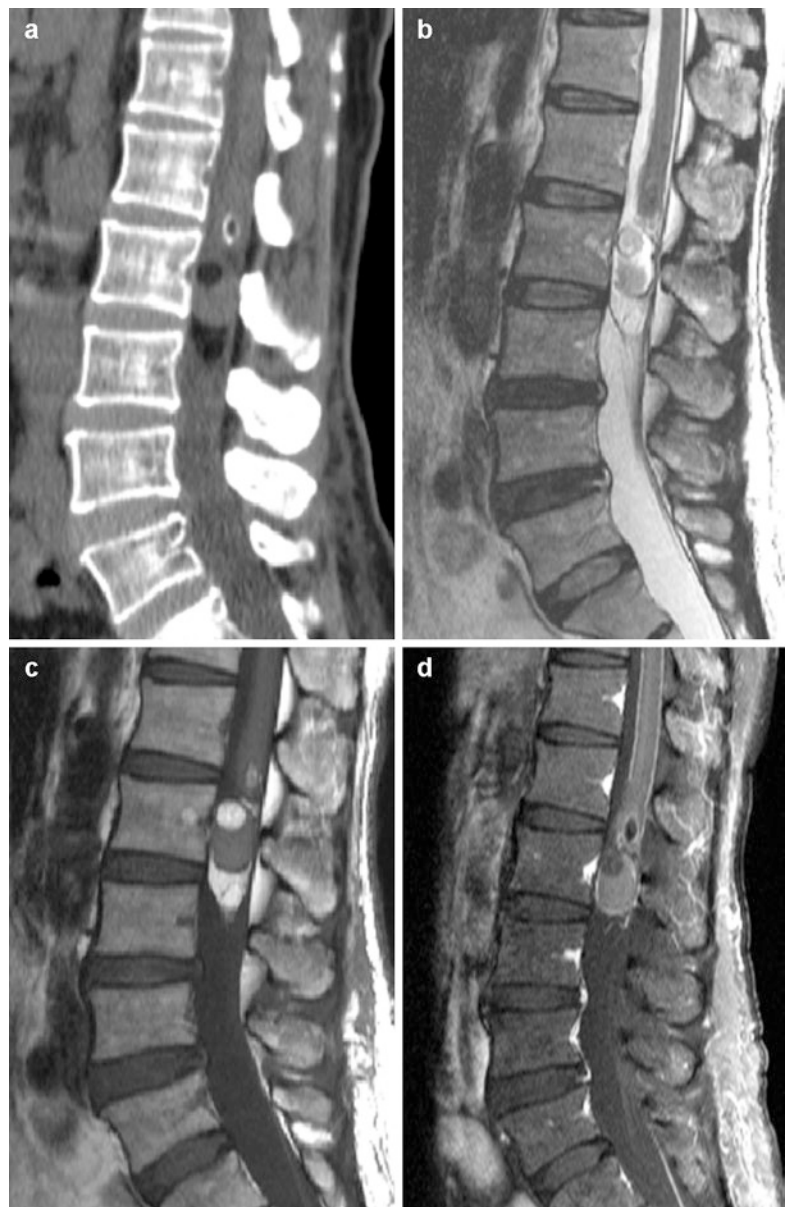
- Enhancing solid portion
- Extradural: dumbbell-shaped mass accompanied with vertebral body malformation

5. Differential diagnosis

- Lipoma

6.15.1 Illustrations: Teratoma

Fig. 6.18 Intradural teratoma in a 52-year-old woman. Sagittal spine CT scan (**a**) shows a fat-containing mass with focal calcifications at L1-L2-L3 level. T2-weighted (**b**) and T1-weighted (**c**) sagittal MR images also demonstrate intratumoral fatty and cystic components. The calcifications are observed to abut upon the conus medullaris. The fatty component shows definite signal loss on fat suppression (**d**)



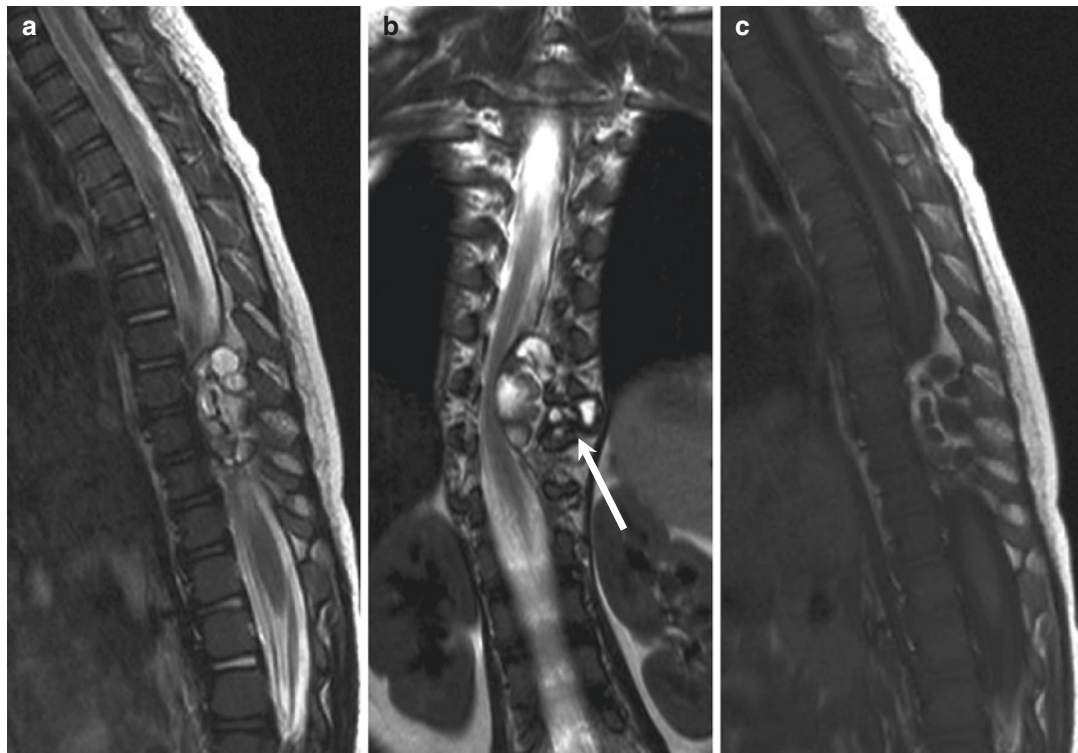


Fig. 6.19 Epidural teratoma in a 34-year-old woman. MRI demonstrates a well-demarcated multiloculated epidural mass at the level of T9–T11 extending into the left paravertebral region through the left neural foramen of T9–T10 (white arrow). This lesion is hyperintense on

T2-weighted MR image (a, b), with hypointense areas surrounded by a hyperintense rim on T1-weighted image (c). This mass compresses the spinal cord. Scoliosis of the thoracolumbar spine is observed

Bibliography

Armao DM, Stone J, Castillo M, Mitchell KM, Bouldin TW, Suzuki K. Diffuse leptomeningeal oligodendroglomatosis: radiologic/pathologic correlation. AJNR Am J Neuroradiol. 2000;21(6):1122–6.

Bloomer CW, Ackerman A, Bhatia RG. Imaging for spine tumors and new applications. Top Magn Reson Imaging TMRI. 2006;17(2):69–87. doi:[10.1097/RMR.0b013e31802bb38f](https://doi.org/10.1097/RMR.0b013e31802bb38f).

Boriani S, Bandiera S, Casadei R, Boriani L, Donthineni R, Gasbarrini A, et al. Giant cell tumor of the mobile spine: a review of 49 cases. Spine. 2012;37(1):E37–45. doi:[10.1097/BRS.0b013e3182233ccd](https://doi.org/10.1097/BRS.0b013e3182233ccd).

Cerase A, Priolo F. Skeletal benign bone-forming lesions. Eur J Radiol. 1998;27(Suppl 1):S91–7.

Cramer GD, Darby SA. Clinical anatomy of the spine, spinal cord, and ANS. Philadelphia: Elsevier Health Sciences; 2013.

Hu S, Hu CH, Hu XY, Wang XM, Dai H, Fang XM, et al. MRI features of spinal epidural angioplipomas.

Korean J Radiol. 2013;14(5):810–7. doi:[10.3348/kjr.2013.14.5.810](https://doi.org/10.3348/kjr.2013.14.5.810).

Kang HS, Lee JW, Kwon JW. Radiology illustrated: spine. Heidelberg: Springer Science & Business Media; 2014.

Kim DH, Chang U-K, Kim S-H, Bilsky MH. Tumors of the spine. Philadelphia: Elsevier Health Sciences; 2008.

Krandsdorf MJ, Sweet DE. Aneurysmal bone cyst: concept, controversy, clinical presentation, and imaging. AJR Am J Roentgenol. 1995;164(3):573–80. doi:[10.2214/ajr.164.3.7863874](https://doi.org/10.2214/ajr.164.3.7863874).

Kroon HM, Schurmanns J. Osteoblastoma: clinical and radiologic findings in 98 new cases. Radiology. 1990;175(3):783–90. doi:[10.1148/radiology.175.3.2343130](https://doi.org/10.1148/radiology.175.3.2343130).

Kwon JW, Chung HW, Cho EY, Hong SH, Choi SH, Yoon YC, et al. MRI findings of giant cell tumors of the spine. AJR Am J Roentgenol. 2007;189(1):246–50. doi:[10.2214/AJR.06.1472](https://doi.org/10.2214/AJR.06.1472).

Lee JW, Cho EY, Hong SH, Chung HW, Kim JH, Chang KH, et al. Spinal epidural hemangiomas: various types of MR

- imaging features with histopathologic correlation. AJNR Am J Neuroradiol. 2007;28(7):1242–8. doi:[10.3174/ajnr.A0563](https://doi.org/10.3174/ajnr.A0563).
- Lu YH, Wang HH, Lirng JF, Guo WY, Wong TT, Teng MM, et al. Unusual giant intraspinal teratoma in an infant. J Chin Med Assoc JCMA. 2013;76(7):411–4. doi:[10.1016/j.jcma.2013.03.006](https://doi.org/10.1016/j.jcma.2013.03.006).
- Maira G, Amante P, Denaro L, Mangiola A, Colosimo C. Surgical treatment of cervical intramedullary spinal cord tumors. Neurol Res. 2001;23(8):835–42. doi:[10.1179/016164101101199432](https://doi.org/10.1179/016164101101199432).
- Marthya A, Patinharayil G, Puthezeth K, Sreedharan S, Kumar A, Kumaran CM. Multicentric epithelioid angiosarcoma of the spine: a case report of a rare bone tumor. Spine J Off J N Am Spine Soc. 2007;7(6):716–9. doi:[10.1016/j.spinee.2006.08.013](https://doi.org/10.1016/j.spinee.2006.08.013).
- Merhemic Z, Stosic-Opinca T, Thurnher MM. Neuroimaging of spinal tumors. Magn Reson Imaging Clin N Am. 2016;24(3):563–79. doi:[10.1016/j.mric.2016.04.007](https://doi.org/10.1016/j.mric.2016.04.007).
- Meyers SP, Khademian ZP, Biegel JA, Chuang SH, Korones DN, Zimmerman RA. Primary intracranial atypical teratoid/rhabdoid tumors of infancy and childhood: MRI features and patient outcomes. AJNR Am J Neuroradiol. 2006;27(5):962–71.
- Monajati A, Spitzer RM, Wiley JL, Heggeness L. MR imaging of a spinal teratoma. J Comput Assist Tomogr. 1986;10(2):307–10.
- Moscovici S, Ramirez-DeNoriega F, Fellig Y, Rosenthal G, Cohen JE, Itshayek E. Intradural extramedullary hemangiopericytoma of the thoracic spine infiltrating a nerve root: a case report and literature review. Spine. 2011;36(23):E1534–9. doi:[10.1097/BRS.0b013e31822dddf4](https://doi.org/10.1097/BRS.0b013e31822dddf4).
- Murphy MD, Andrews CL, Flemming DJ, Temple HT, Smith WS, Smirniotopoulos JG. From the archives of the AFIP. Primary tumors of the spine: radiologic pathologic correlation. Radiographics Rev Publ Radiol Soc N Am Inc. 1996;16(5):1131–58. doi:[10.1148/radiographics.16.5.8888395](https://doi.org/10.1148/radiographics.16.5.8888395).
- Murphy MD, Fairbairn KJ, Parman LM, Baxter KG, Parsa MB, Smith WS. From the archives of the AFIP. Musculoskeletal angiomatous lesions: radiologic-pathologic correlation. Radiographics Rev Publ Radiol Soc N Am Inc. 1995;15(4):893–917. doi:[10.1148/radiographics.15.4.7569134](https://doi.org/10.1148/radiographics.15.4.7569134).
- Nishiguchi T, Mochizuki K, Ohsawa M, Inoue T, Kageyama K, Suzuki A, et al. Differentiating benign notochordal cell tumors from chordomas: radiographic features on MRI, CT, and tomography. AJR Am J Roentgenol. 2011;196(3):644–50. doi:[10.2214/AJR.10.4460](https://doi.org/10.2214/AJR.10.4460).
- Orguc S, Arkun R. Primary tumors of the spine. Semin Musculoskelet Radiol. 2014;18(3):280–99. doi:[10.1055/s-0034-1375570](https://doi.org/10.1055/s-0034-1375570).
- Rodallec MH, Feydy A, Larousserie F, Anract P, Campagna R, Babinet A, et al. Diagnostic imaging of solitary tumors of the spine: what to do and say. Radiographics Rev Publ Radiol Soc N Am Inc. 2008;28(4):1019–41. doi:[10.1148/rg.284075156](https://doi.org/10.1148/rg.284075156).
- Ross JS, Moore KR. Diagnostic imaging: spine. Philadelphia: Elsevier Health Sciences; 2015.
- Sardaro A, Bardoscia L, Petruzzelli MF, Portaluri M. Epithelioid hemangioendothelioma: an overview and update on a rare vascular tumor. Oncol Rev. 2014;8(2):259. doi:[10.4081/oncol.2014.259](https://doi.org/10.4081/oncol.2014.259).
- Shin JY, Lee SM, Hwang MY, Sohn CH, Suh SJ. MR findings of the spinal paraganglioma: report of three cases. J Korean Med Sci. 2001;16(4):522–6. doi:[10.3346/jkms.2001.16.4.522](https://doi.org/10.3346/jkms.2001.16.4.522).
- Si MJ, Wang CG, Wang CS, Du LJ, Ding XY, Zhang WB, et al. Giant cell tumours of the mobile spine: characteristic imaging features and differential diagnosis. La Radiologia Medica. 2014;119(9):681–93. doi:[10.1007/s11547-013-0352-1](https://doi.org/10.1007/s11547-013-0352-1).
- Vialle R, Feydy A, Rillardon L, Tohme-Noun C, Anract P, Colombari M, et al. Chondroblastoma of the lumbar spine. Report of two cases and review of the literature. J Neurosurg Spine. 2005;2(5):596–600. doi:[10.3171/spi.2005.2.5.0596](https://doi.org/10.3171/spi.2005.2.5.0596).
- Walker EA, Salesky JS, Fenton ME, Murphy MD. Magnetic resonance imaging of malignant soft tissue neoplasms in the adult. Radiol Clin N Am. 2011;49(6):1219–34, vi. doi:[10.1016/j.rcl.2011.07.006](https://doi.org/10.1016/j.rcl.2011.07.006).
- Wu L, Deng X, Yang C, Xu Y. Spinal intradural malignant peripheral nerve sheath tumor in a child with neurofibromatosis type 2: the first reported case and literature review. Turkish Neurosurg. 2014;24(1):135–9. doi:[10.5137/1019-5149.JTN.8104-13.0](https://doi.org/10.5137/1019-5149.JTN.8104-13.0).

Contents

7.1	Epidural Abscess	191	7.13	Retro-odontoid (Periodontoid) Pseudotumor	218
7.1.1	Illustrations: Epidural Abscess	193	7.13.1	Illustrations: Retro-odontoid (Periodontoid) Pseudotumor	219
7.2	Arachnoid Cyst	195	7.14	Facet Synovial Cyst	220
7.2.1	Illustrations: Arachnoid Cyst	196	7.14.1	Illustrations: Facet Synovial Cyst	221
7.3	Arachnoiditis	198	7.15	Tuberculosis	223
7.3.1	Illustrations: Arachnoiditis	199	7.15.1	Illustrations: Tuberculosis	224
7.4	Cysticercosis	200	7.16	Ventriculus Terminalis	225
7.4.1	Illustrations: Cysticercosis	201	7.16.1	Illustrations: Ventriculus Terminalis	226
7.5	Discal Cyst	202		Bibliography	227
7.5.1	Illustrations: Discal Cyst	203			
7.6	Echinococcosis	204			
7.7	Extramedullary Hematopoiesis	204			
7.7.1	Illustrations: Extramedullary Hematopoiesis	205			
7.8	(Vertebral Tophaceous) Gout	207			
7.8.1	Illustrations: (Vertebral Tophaceous) Gout	208			
7.9	Idiopathic Hypertrophic Pachymeningitis	209			
7.9.1	Illustrations: Idiopathic Hypertrophic Pachymeningitis	210			
7.10	Perineural (Root Sleeve) Cyst	212			
7.10.1	Illustrations: Perineural (Root Sleeve) Cyst	213			
7.11	Pigmented Villonodular Synovitis (PVNS)	214			
7.11.1	Illustrations: Pigmented Villonodular Synovitis (PVNS)	215			
7.12	(Focal) Red Marrow (Hematopoietic Marrow)	216			
7.12.1	Illustrations: (Focal) Red Marrow (Hematopoietic Marrow)	217			

7.1 Epidural Abscess

1. Epidemiology

- All age groups (peak incidence: 6th~7th decade)
- M > F: 1: 0.56
- 0.2–2.8 cases per 10,000

2. Location

- Posterior (80%) and anterior (20%) epidural space
- Lower thoracic and lumbar > upper thoracic and cervical

3. Characteristic imaging findings

- Peripherally enhancing fluid collection
- Findings of spondylodiscitis with homogeneous or heterogeneous enhancing phlegmon
- Diffusion restriction (high signal on DWI, low signal on ADC map)

4. Spectrum of imaging findings

- Diffuse dural enhancement in extensive spinal epidural abscess
 - Spinal cord signal change due to compression, ischemia, or direct extension of infection
 - Enhancing prominent anterior epidural or basivertebral venous plexus adjacent to abscess
- Iso to low signal on T2-weighted image
 - Intact vertebral endplate
- Epidural hematoma
 - Heterogeneous high signal on T2-weighted image
 - Iso signal (acute stage) and high signal (subacute to chronic stage) on T1-weighted image.

5. Differential diagnosis

- Herniated intervertebral disc (extruded or sequestered)
 - Adjacent parent disc degeneration or combined Herniated intervertebral disc

7.1.1 Illustrations: Epidural Abscess

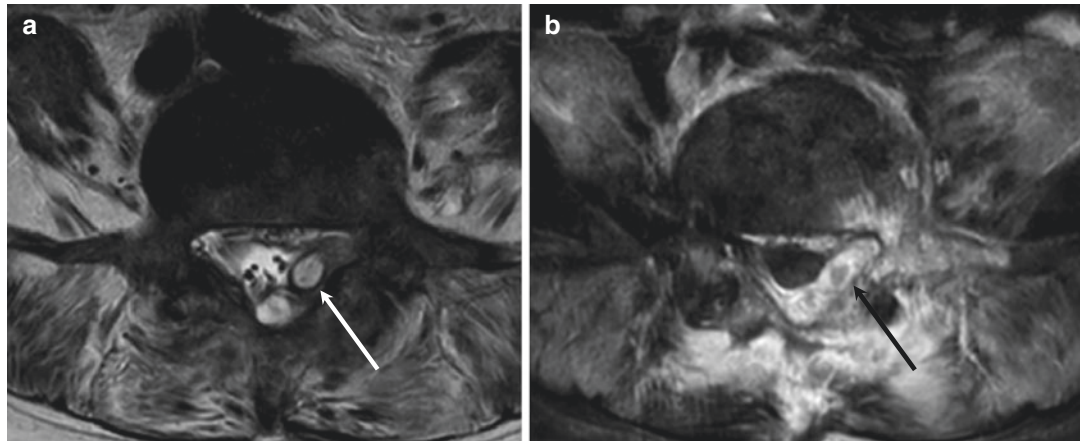
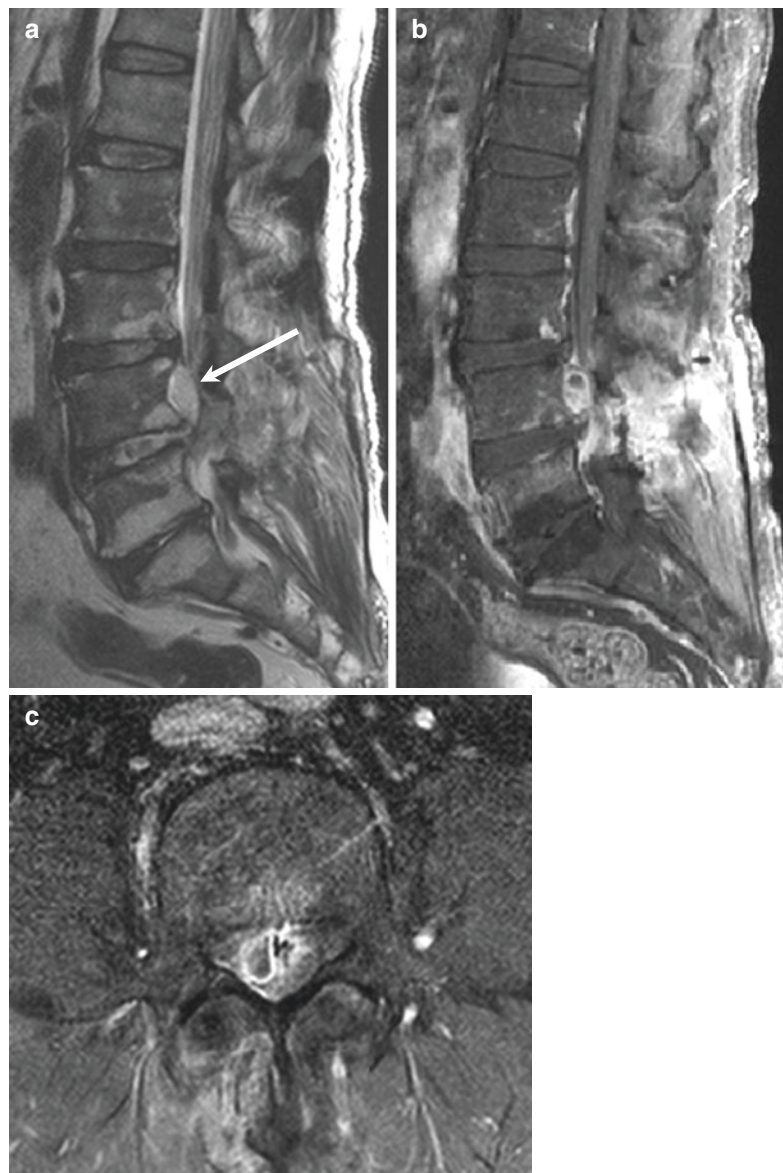


Fig. 7.1 Epidural abscess in a 71-year-old woman. T2-weighted axial MR image (**a**) shows a well-defined cystic mass-like lesion in the left posterior epidural space (white arrow). This lesion shows strong peripheral contrast enhancement with adjacent phlegmon formation

(black arrow) on contrast-enhanced T1-weighted MR image (**b**). Additional diffuse signal change and enhancement of the bone marrow; paravertebral and bilateral psoas muscles are also noted

Fig. 7.2 Epidural abscess in a 74-year-old man. Postoperative lumbar spine MRI (a) reveals a right anterior epidural lesion with T2-hyperintensity (white arrow) at the level of L4 vertebral body. Peripheral enhancement was noted on sagittal and axial fat-saturated contrast-enhanced T1-weighted MR images (b, c)



7.2 Arachnoid Cyst

1. Epidemiology

- Any age

2. Location

- Extradural: posterior or posterolateral lower thoracic spine
- Intradural: dorsal mid-thoracic spine
- Anterior: uncommon

3. Characteristic imaging findings

- Well circumscribed, oval, elongated
- Dumbbell shape: extension to neural foramen, bony canal expansion
- CSF signal on T1- and T2-weighted image
- No enhancement

4. Spectrum of imaging findings

- Cyst wall can be seen on extradural arachnoid cyst.

- Low signal flow artifact on T2-weighted image.

- Syringohydromyelia: may result from partial obstruction of CSF by arachnoid cyst.

5. Differential diagnosis

- Idiopathic spinal cord herniation
 - Upper to mid-thoracic level
 - Focal cord atrophy and ventral deviation to dural defect
- Schwannoma
 - Heterogeneous T2 signal intensity with enhancing peripheral wall
- Pseudomeningocele
- Dural ectasia
 - Diffuse dilatation of thecal sac without cord distortion

7.2.1 Illustrations: Arachnoid Cyst

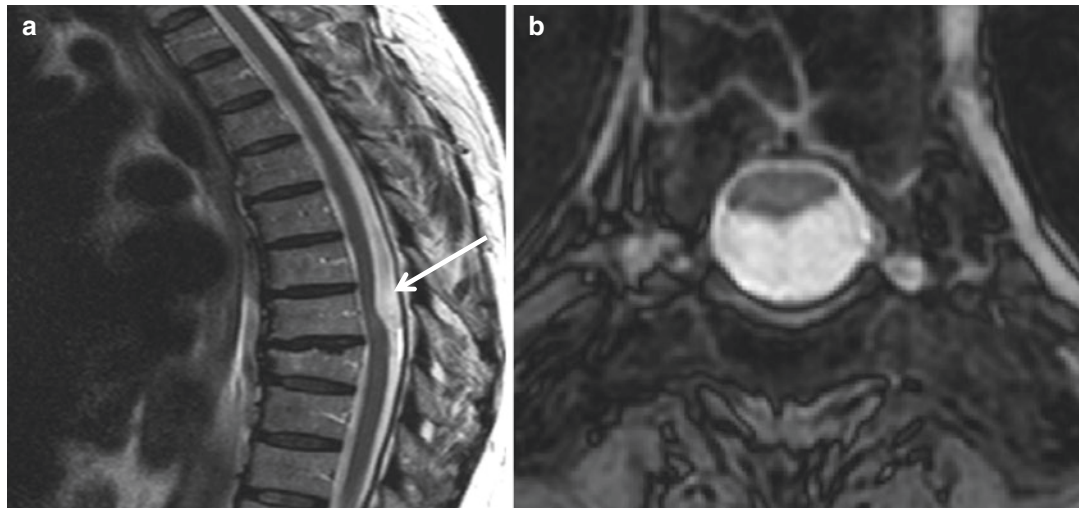


Fig. 7.3 Dorsal intradural arachnoid cyst in a 65-year-old woman. T2-weighted sagittal MR image (**a**) shows a focal cystic mass-like lesion with cord compression at T2 vertebral body level (white arrow). The lesion shows

similar signal to CSF. On the axial scan (**b**), there is no evidence of herniated spinal cord outside the dura nor rotation of the spinal cord. Absence of CSF flow artifact is also noted

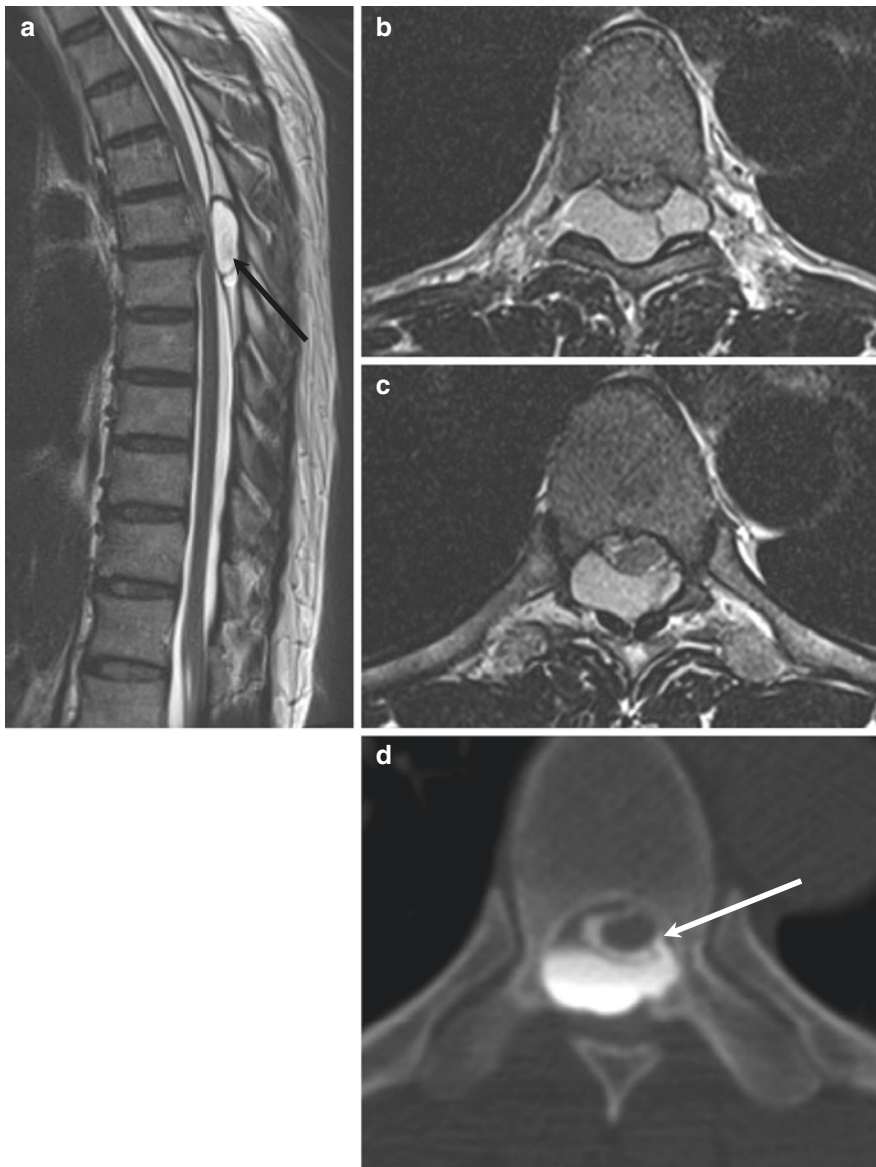


Fig. 7.4 Dorsal extradural arachnoid cyst in a 50-year-old man. T2-weighted sagittal (a) and axial (b, c) MR images show a well-defined cystic mass in the dorsal epidural space with dural sac and spinal cord compression. CSF flow artifact is noted (black arrow) inside the cystic

mass. There is no definite solid portion with a relatively thick wall. CT myelography (d) clearly shows a dorsal dural defect at the left side (white arrow) with contrast media communicating between the subarachnoid space and cystic mass

7.3 Arachnoiditis

1. Epidemiology

- No gender prediction
- Uncommon
- 6–16% of postoperative patients

2. Location

- Lumbar spine (especially cauda equina)

3. Characteristic imaging findings

- Intrathecal clumping of nerve roots causing enlarged cord
- “Empty sac” appearance with peripheral nerve roots clumping to dura
- Pseudomass filling the central portion of the thecal sac
- Minimal to mild pial and dural enhancement

4. Spectrum of imaging findings

- Type 1: central nerve root clumping with only 2–3 nerve roots
- Type 2: peripheral nerve root clumping, central CSF without nerve root (empty thecal sac sign)
- Type 3: soft tissue mass filling most of the thecal sac, obliteration of subarachnoid space

5. Differential diagnosis

- Cauda equine neoplasms
 - Large nerve sheath tumor
 - Myxopapillary ependymoma
 - Paraganglioma
- Carcinomatous meningitis
- Intradural metastasis

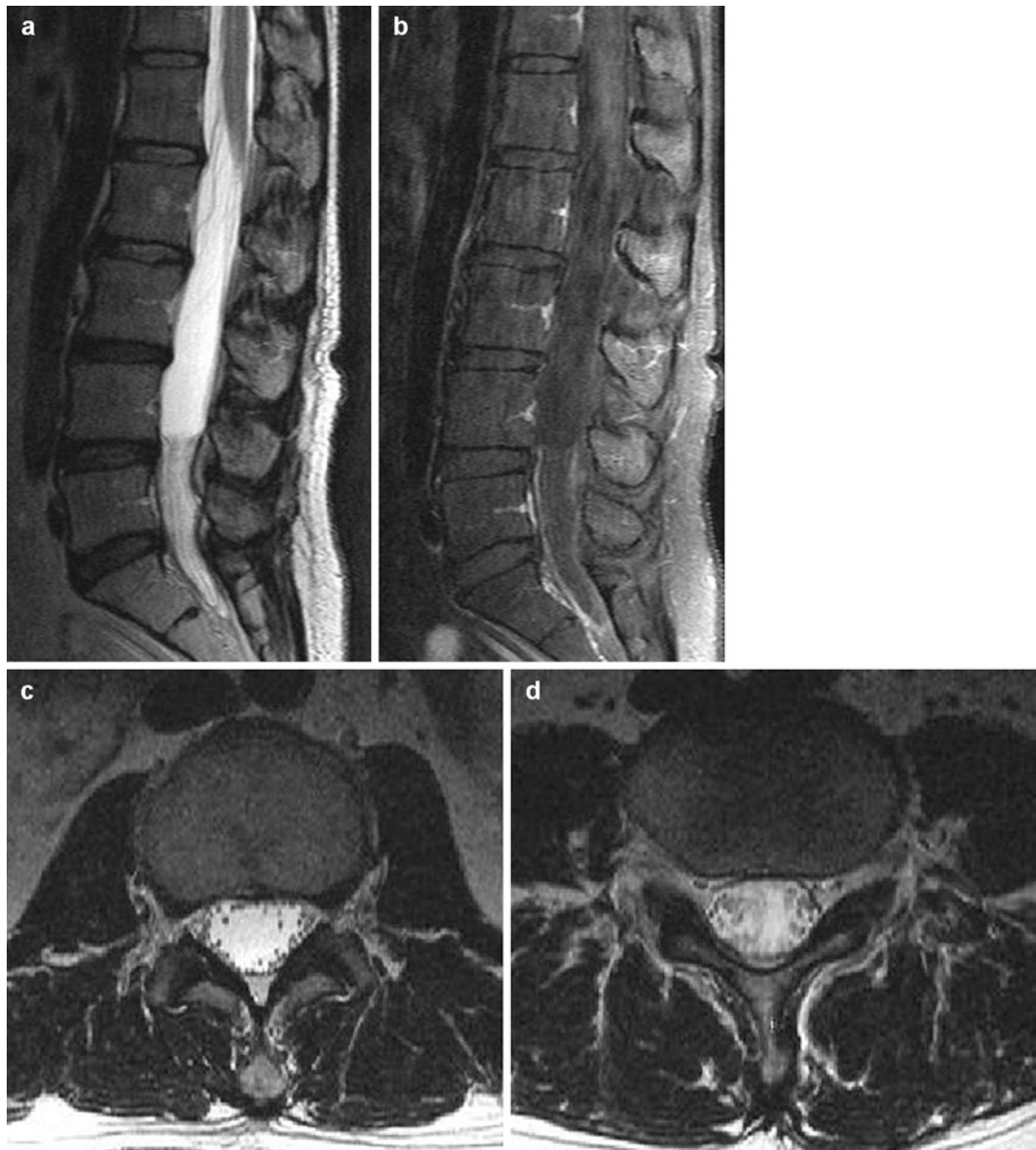
7.3.1 Illustrations: Arachnoiditis

Fig. 7.5 Adhesive arachnoiditis in a 52-year-old woman. The patient has a history of endometrial cancer and underwent hysterectomy and CCRT. T2-weighted sagittal MR image (a) shows a large pseudomass filling the thecal sac in the lumbar spine. On the contrast-enhanced T1-weighted

sagittal MR image (b), there is no definite enhancement of the central cystic portion. T2-weighted axial MR images show peripheral nerve root clumping (c) with central CSF flow artifact (d)

7.4 Cysticercosis

1. Epidemiology

- Most common worldwide parasitic infection

2. Location

- Parenchymal, leptomeningeal, intraventricular, and spinal
- Rare spinal cysticercosis

3. Characteristic imaging findings

- Intradural cyst with evidence of similar lesion in the brain
 - Cyst with “dot” appearance
- Subarachnoid
 - CSF signal cystic lesion, variable mass effect to cord and cauda equina
 - Peripheral cyst enhancement
- Intramedullary
 - Focal cystic lesion with diffuse cord edema with or without syrinx
 - Peripheral cyst enhancement
 - May show only nonspecific sheet-like enhancement of subarachnoid space, cord pial surface

4. Spectrum of imaging findings

- Vesicular stage
 - CSF signal intensity.
 - Scolex appears as a high intensity nodule within the cyst: “hole-with-dot” pattern.
- Colloidal stage
 - Thick, hypointense cyst walls, varied perilesional edema
- Granular nodular stage
 - Areas of signal void on both T1- and T2-weighted images surrounded by edema or gliosis
- Final involution stage
 - Calcified cysticerci: small hypointense area

5. Differential diagnosis

- Pyogenic abscess
- Arachnoid cyst
- Echinococcosis
- Granulomatous osteomyelitis
 - Tuberculosis
 - Sarcoidosis

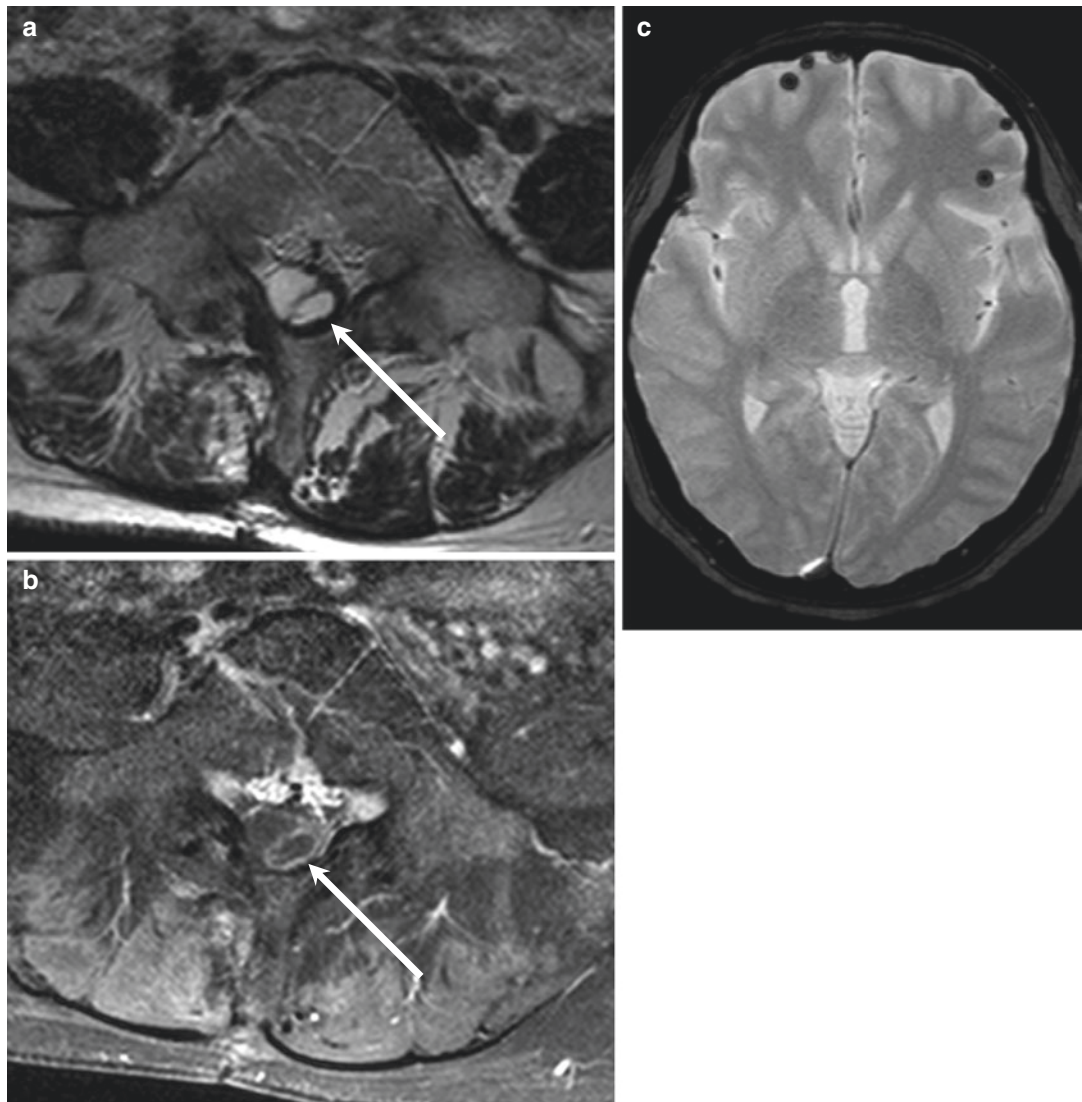
7.4.1 Illustrations: Cysticercosis

Fig. 7.6 Cysticercosis in a 47-year-old woman. T2-weighted (a) and contrast-enhanced T1-weighted (b) MR images show an intradural cystic mass with mild peripheral enhancement at L5 vertebral level (white

arrows). There are multiple small calcifications in the CSF space at both frontal convexities on the gradient echo brain MR image (c) suggesting calcified cysticerci

7.5 Discal Cyst

1. Epidemiology

- Extremely rare
- M >> F

2. Location

- L4/L5: most common

3. Characteristic imaging findings

- Minimal degeneration of the involved disc
- Ventrolateral extradural cyst attached to a lumbar disc
- Cyst containing bloody-to-clear serous fluid
- Low signal on T1, high signal on T2 with cyst wall enhancement

4. Spectrum of imaging findings

- Occasional extension into the lateral recess

5. Differential diagnosis

- Ganglion or synovial cyst
- Perineural cyst
- Epidural abscess
- Extradural arachnoid cyst
- Peripheral nerve sheath tumor with cystic degeneration

7.5.1 Illustrations: Discal Cyst

Fig. 7.7 Discal cyst in a 29-year-old man. T2-weighted (a) and T1-weighted (b) sagittal MR image shows a 12 mm cystic lesion with a thin peripheral rim at L4 vertebral body level. T2-weighted axial MR image (c) shows that the cystic lesion is located in the anterior epidural

space (right subarticular zone) with right L4 nerve root compression. On the contrast enhancement T1-weighted images (d, e), the cystic lesion shows peripheral enhancement without a definite solid portion

7.6 Echinococcosis

1. Epidemiology

- Any age
- M = F (no gender predilection)
 - Disease caused by cyst stage of infestation by tapeworm *Echinococcus* spp.

2. Location

- Liver, lung involvement most common
 - Bone: 0.5–4%
 - Spine involvement in 50% of cases
- Thoracic (50%), cervical (10%), lumbar (20%), sacrum (20%)
 - Extradural
 - Intradural extramedullary: rare
 - Intramedullary: extremely rare

3. Characteristic imaging findings

- Multiloculated multi-septated, T2 high signal intensity mass in vertebral body/posterior elements
 - Epidural extension with cord compression
- Minimal or no contrast enhancement
- Multiloculated osteolytic mass on CT

4. Spectrum of imaging findings

- Degenerated cyst
 - Iso signal to muscle on T1-weighted image
 - Low signal relative to CSF on T2-weighted image

5. Differential diagnosis

- Cystic metastasis (renal cell or thyroid carcinoma)
- Cysticercosis
- Primary bone tumor
 - Osteosarcoma
 - Chondrosarcoma
 - Aneurysmal bone cyst
 - Giant cell tumor
 - Chordoma

7.7 Extramedullary Hematopoiesis

1. Epidemiology

- More common in adults (3rd~4th decade)
- Hemoglobinopathy
 - Sickle cell disease: African-Americans
 - Thalassemia: Eastern Mediterranean population
 - Myeloproliferative disease

2. Location

- Mid-thoracic > cervical, lumbar
- Epidural, paravertebral
- Multi-segmental

3. Characteristic imaging findings

- Minimally enhancing isointense thoracic intra- or paraspinal masses with associated diffuse marrow hypointensity
- Well-circumscribed, homogenous, and lobular soft tissue mass
- Iso signal (to spinal cord) on T1-weighted image
- Iso to high signal (to spinal cord) on T2-weighted image
- Diffuse vertebral marrow low signal on T1-weighted image

4. Spectrum of imaging findings

- Low signal on T2-weighted image due to increased iron content in hematopoietic tissue
- Variable contrast enhancement
- Variable spinal cord or nerve root compression

5. Differential diagnosis

- Spinal epidural lymphoma
 - Intense homogenous enhancement on Gd
 - Adjacent vertebral involvement
- Epidural or paraspinal metastasis
 - Extension from adjacent vertebral lesions
- Epidural hematoma
- Peripheral nerve sheath tumor
 - Often single level
 - Widening of intervertebral foramen
 - Multiple neurofibromas with neurofibromatosis type 1

7.7.1 Illustrations: Extramedullary Hematopoiesis

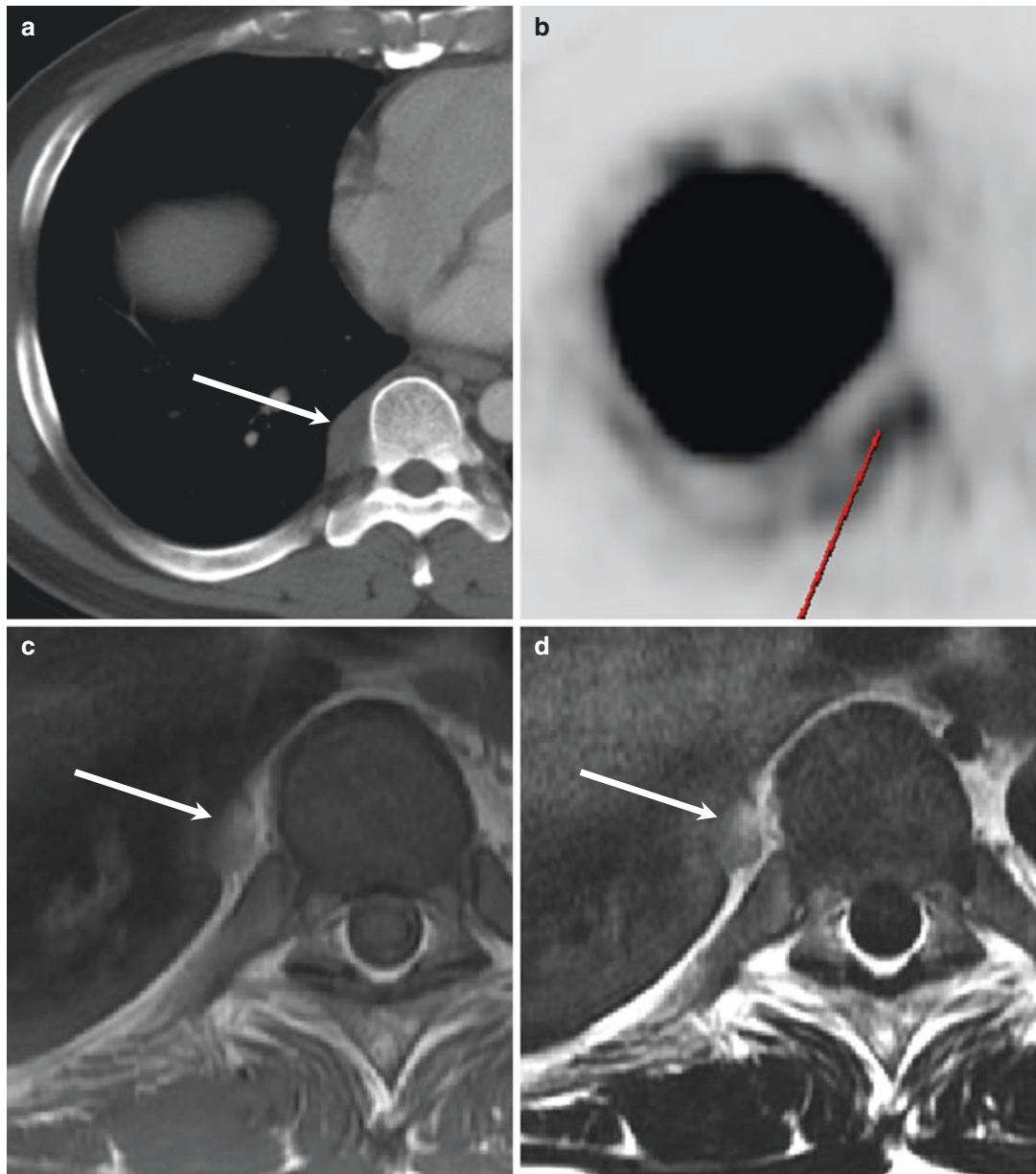


Fig. 7.8 Extramedullary hematopoiesis in a 48-year-old man (known hereditary spherocytosis). Chest CT scan (a) shows a well-defined soft tissue mass in the right paravertebral space at T8 vertebral level (*white arrow*) with increased uptake on PET CT scan (b). This lesion shows

T1-hyperintensity with mild inhomogeneous enhancement (c, d). T1-weight sagittal MR images (e, f) show diffuse bone marrow signal decrease in the axial skeleton without definite enhancement indicating an underlying bone marrow replacement disease



Fig. 7.8 (continued)

7.8 (Vertebral Tophaceous) Gout

1. Epidemiology

- The middle aged and elderly
- M >> F: 20: 1

2. Location

- Rare spine involvement
- Lumbar spine (m/c)

3. Characteristic imaging findings

- Endplate and facet erosion (“punched out”)
- Prevertebral soft tissue mass on CT
- Intermediate to low signal on T1-weighted image

4. Spectrum of imaging findings

- High protein content or water content of the tophi: variable T2 signal
- Calcification found within gouty tophi
- Differences in the relative amounts of vascular fibrous tissue found within the tophus: variable enhancement pattern with Gd

5. Differential diagnosis

- Osteomyelitis
- Hemodialysis arthropathy
- Calcium pyrophosphate deposition (CPPD) disease
 - More extensive calcifications, linear
- Neurotrophic arthropathy
 - Extensive bone destruction
- RA
 - Calcification (-)
- Seronegative spondyloarthropathy

7.8.1 Illustrations: (Vertebral Tophaceous) Gout

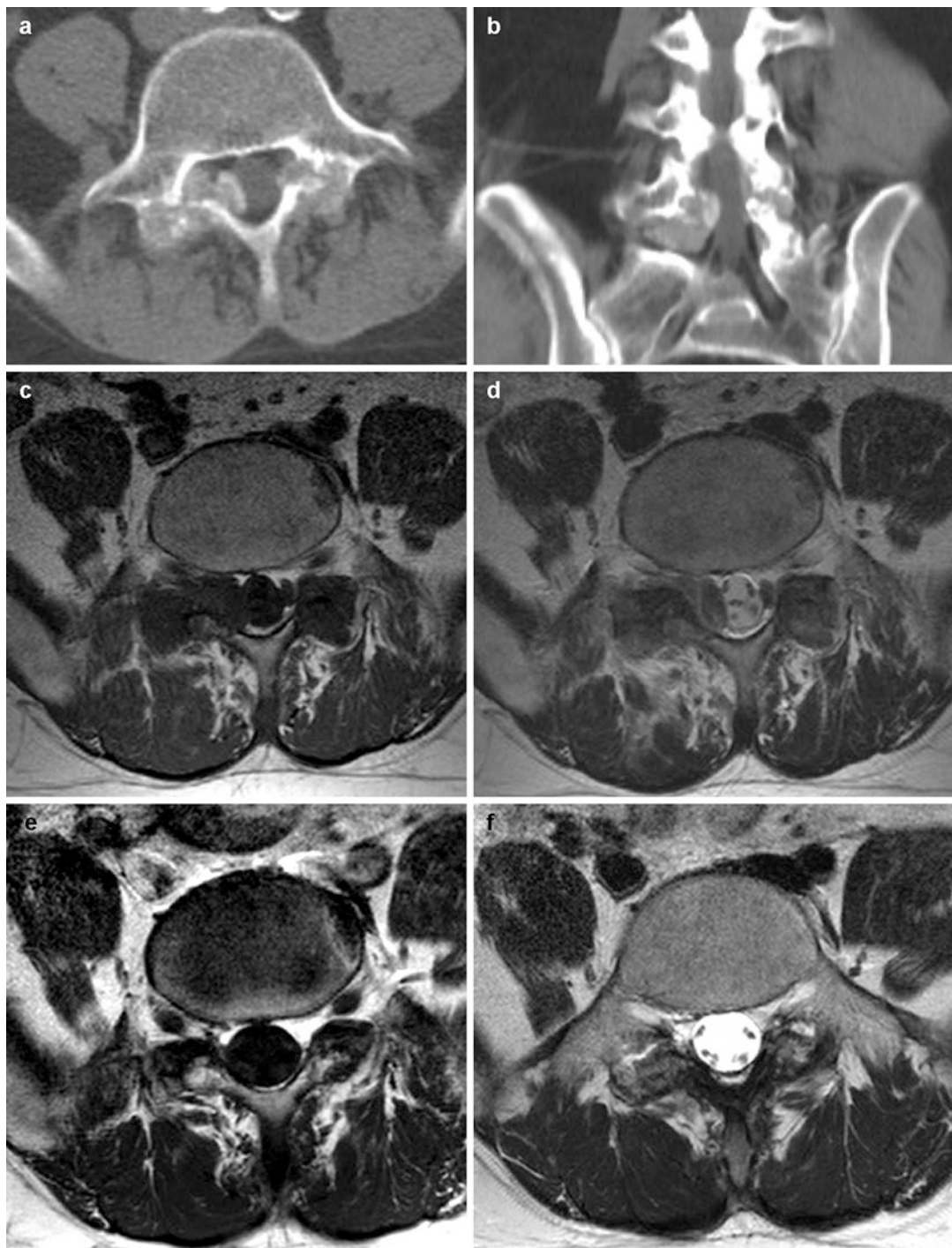


Fig. 7.9 Vertebral tophaceous gout in a 44-year-old man. Bone-destructive high attenuated mass-like lesion around the bilateral L5/S1 facet joints with calcifications on CT scan (**a, b**). The lesion shows low signal intensity on T1-weighted image (**c**) with central canal and right neural foraminal compromise (**d**). After 4-year follow-up, there

is dramatic improvement of the spinal canal compromise with markedly decreased extent of the lesion (**e, f**), presumably related to improvement of the gouty arthritis involving the bilateral facet joints and tophi extending into the central canal. Eroded facet joints due to previous gouty attacks are also noted

7.9 Idiopathic Hypertrophic Pachymeningitis

1. Epidemiology

- Peak incidence: 6th decade
- M > F (3.5: 1)

2. Location

- Any meningeal location, including skull base and spine

3. Characteristic imaging findings

- Diffuse smooth dural thickening with low signal intensity on T2-weighted image
 - No direct involvement of spinal cord
- Linear low signal mass involving dura with variable mass effect to the spinal cord
- Homogenous or marked peripheral enhancing thickened dural mass

4. Spectrum of imaging findings

- Peripheral enhancement related to peripheral zone of active inflammation with chronic central fibrosis

5. Differential diagnosis

- Meningioma
 - Focal dural-based lesion with homogeneous enhancement
- Lymphoma
 - Homogenous enhancement
 - Iso to low signal on T2-weighted image with diffusion restriction
- Tuberculosis
 - Multifocal lesion with possible parenchymal involvement
- Sarcoidosis
- Dural metastasis

7.9.1 Illustrations: Idiopathic Hypertrophic Pachymeningitis



Fig. 7.10 Idiopathic hypertrophic pachymeningitis in a 59-year-old woman. T2-weighted (a) and T1-weighted (b) MR images show a smooth marginated low signal mass-like lesion along the posterior dura at C6-C7-T1 level. On the contrast-enhanced MR images (c), the lesion

shows strong contrast enhancement with central canal compromise and neural foraminal extension to the right side (*black arrows*). On the axial scan (d), there is an internal linear poorly enhancing portion suggesting chronic central fibrosis (*white arrows*)

Fig. 7.11 Idiopathic hypertrophic pachymeningitis in a 55-year-old woman. C-spine MRI demonstrates a flowing mass with lobulated contour posterior to the vertebral bodies of C6-T6, of T2 low and T1 intermediate signal intensities (**a, b**) with strong contrast enhancement (**c**). The spinal cord is compressed by this mass. Faint enhancement is suspected of the posterior dura at the levels of C6 to T6 (**c, d**)



7.10 Perineural (Root Sleeve) Cyst

1. Epidemiology

- 30–40 years old
- M = F
- Common
 - Incidental, usually asymptomatic
 - 4.6–9% of adults

2. Location

- Anywhere along whole spinal axis
 - Common in lower lumbar and sacrum
 - S2 and S3 nerve root most commonly involved

3. Characteristic imaging findings

- Thin-walled CSF intensity mass-like lesion extending into or through neural foramen
- No contrast enhancement
- Neural foraminal widening, pedicle thinning reflecting bone remodeling

4. Spectrum of imaging findings

- None

5. Differential diagnosis

- Facet joint synovial cyst
- Nerve sheath tumor
- Spinal nerve root avulsion
- Meningocele

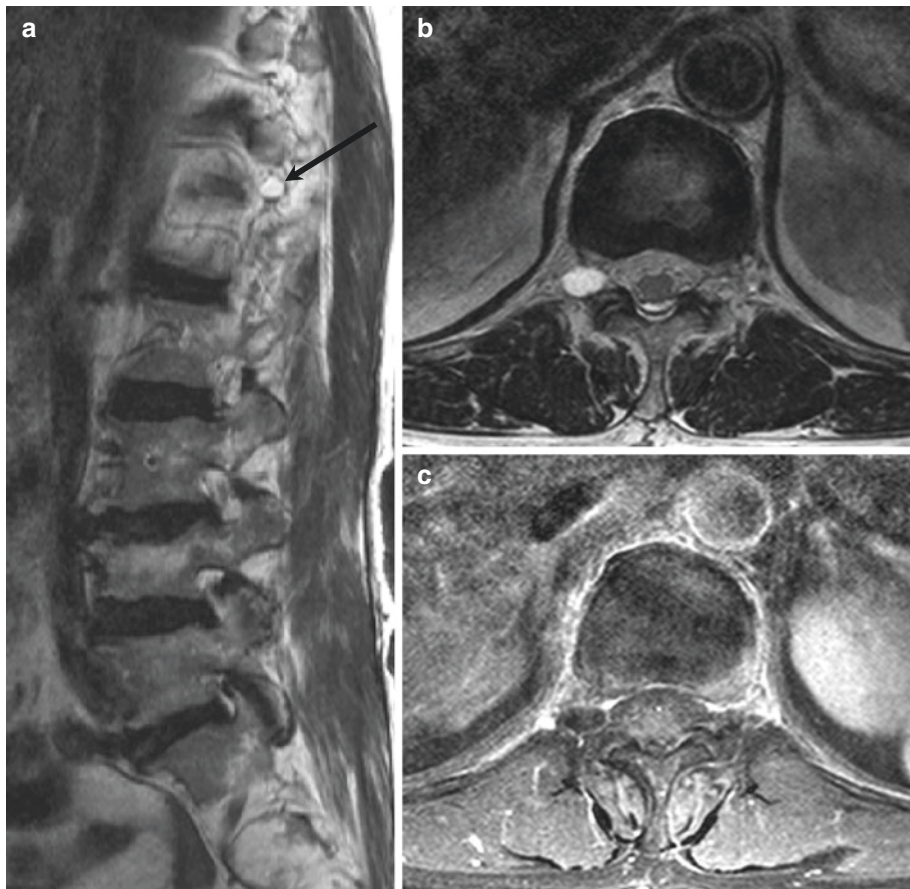
7.10.1 Illustrations: Perineural (Root Sleeve) Cyst

Fig. 7.12 Perineural (root sleeve) cyst in a 72-year-old woman. T2-weighted sagittal MR image (a) shows a small cystic lesion at the right extraforaminal space at T12/L1 level. T2-weighted axial MR image (b)

that the cystic mass-like lesion is located in the foraminal to extraforaminal space of T12/L1 along the right T12 nerve root. On the contrast-enhanced T1-weighted image (c), there is no definite enhancement observed

7.11 Pigmented Villonodular Synovitis (PVNS)

1. Epidemiology

- Extremely rare
- 3rd and 4th decades (11–84 years)
- F (64%) > M
 - No sexual predilection in general PVNS except spine

2. Location

- Cervical (50–73%) > thoracic (7–25%) > lumbosacral (20–25%)
- Posterior elements, facet joint (93%), and paraspinal soft tissue (93%)
- Neural foramen (73%), pedicle (63%), lamina (67%)
- Uncommon: vertebral body (27%), spinous process (7%)

3. Characteristic imaging findings

- Heterogeneous low to intermediate signal intensity on both T1- and T2-weighted images
- “Blooming artifact” on GRE sequence
- Diffuse, moderate to marked contrast enhancement
- Lytic soft tissue mass without internal calcification on CT

4. Spectrum of imaging findings

- Frequent epidural space extension (70%)
- Reported foramen transversarium and vertebral artery involvement

5. Differential diagnosis

- Metastasis
- Multiple myeloma
- Giant cell tumor
- Gout

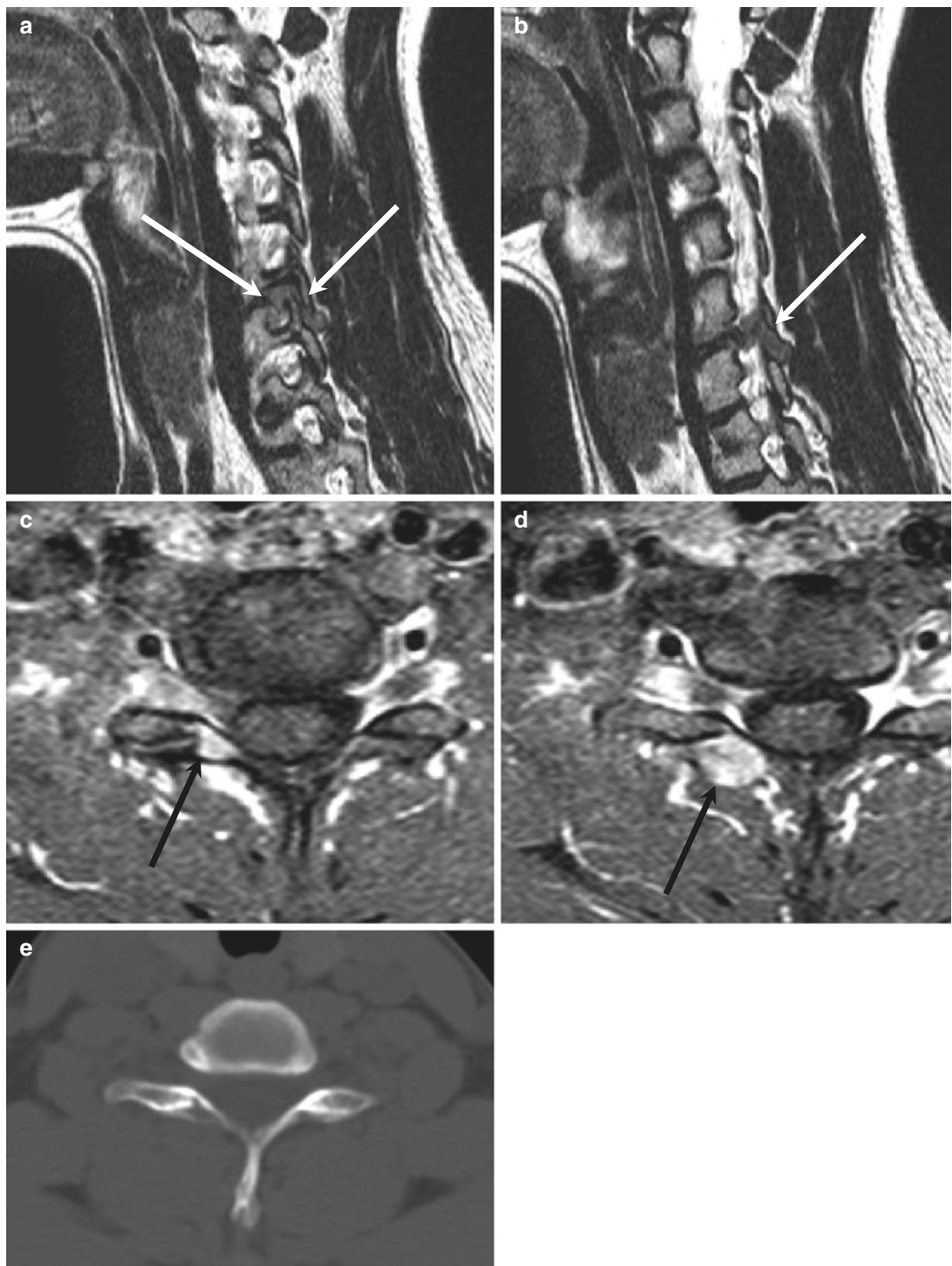
7.11.1 Illustrations: Pigmented Villonodular Synovitis (PVNS)

Fig. 7.13 Cervical pigmented villonodular synovitis (PVNS) in 29-year-old woman. T2-weighted sagittal MR images (**a, b**) show a low signal mass-like lesion involving the right facet joint of C6–C7 with extension into the neu-

ral foramen and lamina (*white arrows*). Strong enhancement (*black arrows*) is also noted on contrast-enhanced T1-weighted axial images (**c, d**). There is no definite calcification nor ossification on the CT scan (**e**)

7.12 (Focal) Red Marrow (Hematopoietic Marrow)

1. Epidemiology

- Reconversion from fatty to erythropoietic marrow
- Smoking, anemia, obesity, high athletic activity, bone marrow transplantation, erythropoietic-stimulating agents related

2. Location

- Vertebral body

3. Characteristic imaging findings

- Iso to low signal on T1-weighted image
 - But relatively high than intervertebral T1 signal intensity
- Intermediate signal on T2-weighted image (similar to muscle)
- Slight contrast enhancement
- Normal trabeculation preserved on CT

4. Spectrum of imaging findings

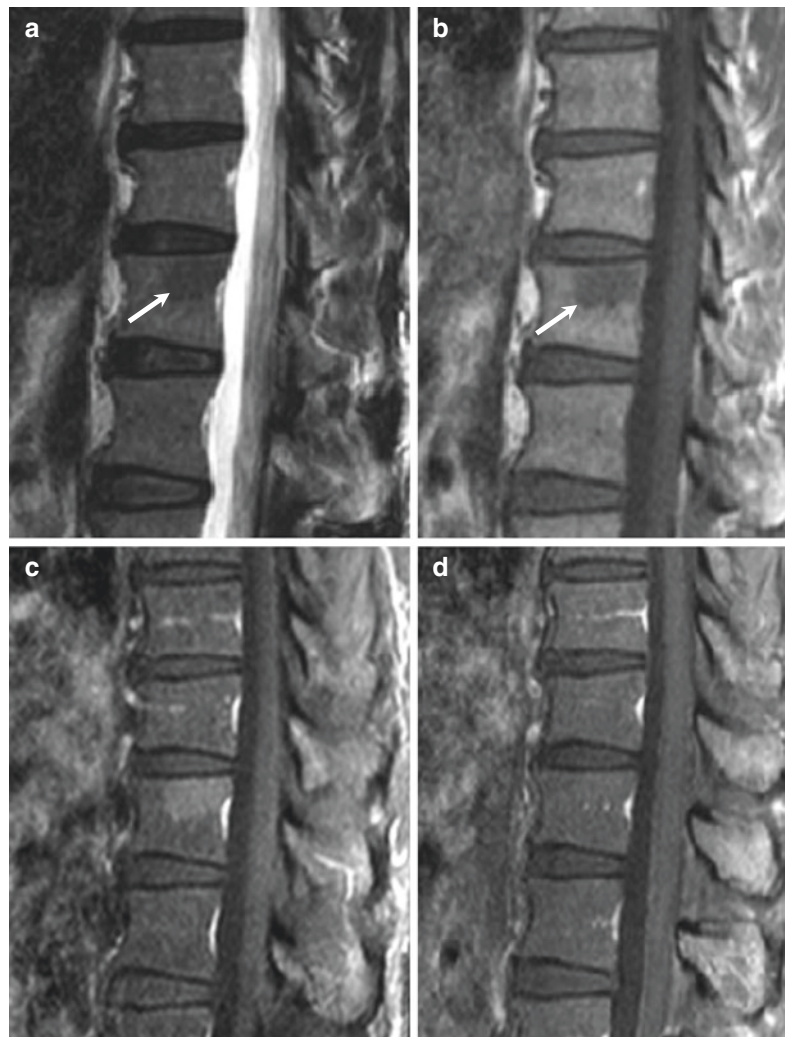
- May show peripheral enhancement
- Variable cystic or erosive change of the adjacent vertebra

5. Differential diagnosis

- Metastasis
 - Lower signal on T1-weighted image than intervertebral disc
- Hemangioma
 - Usually containing fat portion
- Leukemia/multiple myeloma
 - Early: similar to red marrow
 - Late: lower signal on T1-weighted image than intervertebral disc
 - CT: focal trabecular destruction

7.12.1 Illustrations: (Focal) Red Marrow (Hematopoietic Marrow)

Fig. 7.14 Focal red marrow of the T1 vertebral body in a 60-year-old woman with a history of ovarian cancer. T2-weighted (**a**) and T1-weighted sagittal MR images show a slightly low signal lesion at the posterosuperior aspect of the T9 vertebral body (*white arrows*). The T1-weighted image (**b**) shows lesion of relatively higher signal than the intervertebral disc signal. Mild contrast enhancement is also noted on contrast-enhanced T1-weighted sagittal image (**c**). After 4-year follow-up MR (**d**), the observed contrast enhancement disappeared



7.13 Retro-odontoid (Periodontoid) Pseudotumor

1. Epidemiology

- More than 60 years (7% of adults by age 70)
- F > M

2. Location

- Retro-odontoid soft tissue and transverse ligament

3. Characteristic imaging findings

- Iso to low signal retro-odontoid mass on T1-weighted image
- Low signal on T2-weighted image
- Curvilinear, stippled, or mixed pattern of calcification posterior to odontoid

4. Spectrum of imaging findings

- May show peripheral enhancement
- Variable cystic or erosive change of the adjacent vertebra

5. Differential diagnosis

- CPPD
- Rheumatoid arthritis
- Osteoarthritis
- Os odontoideum

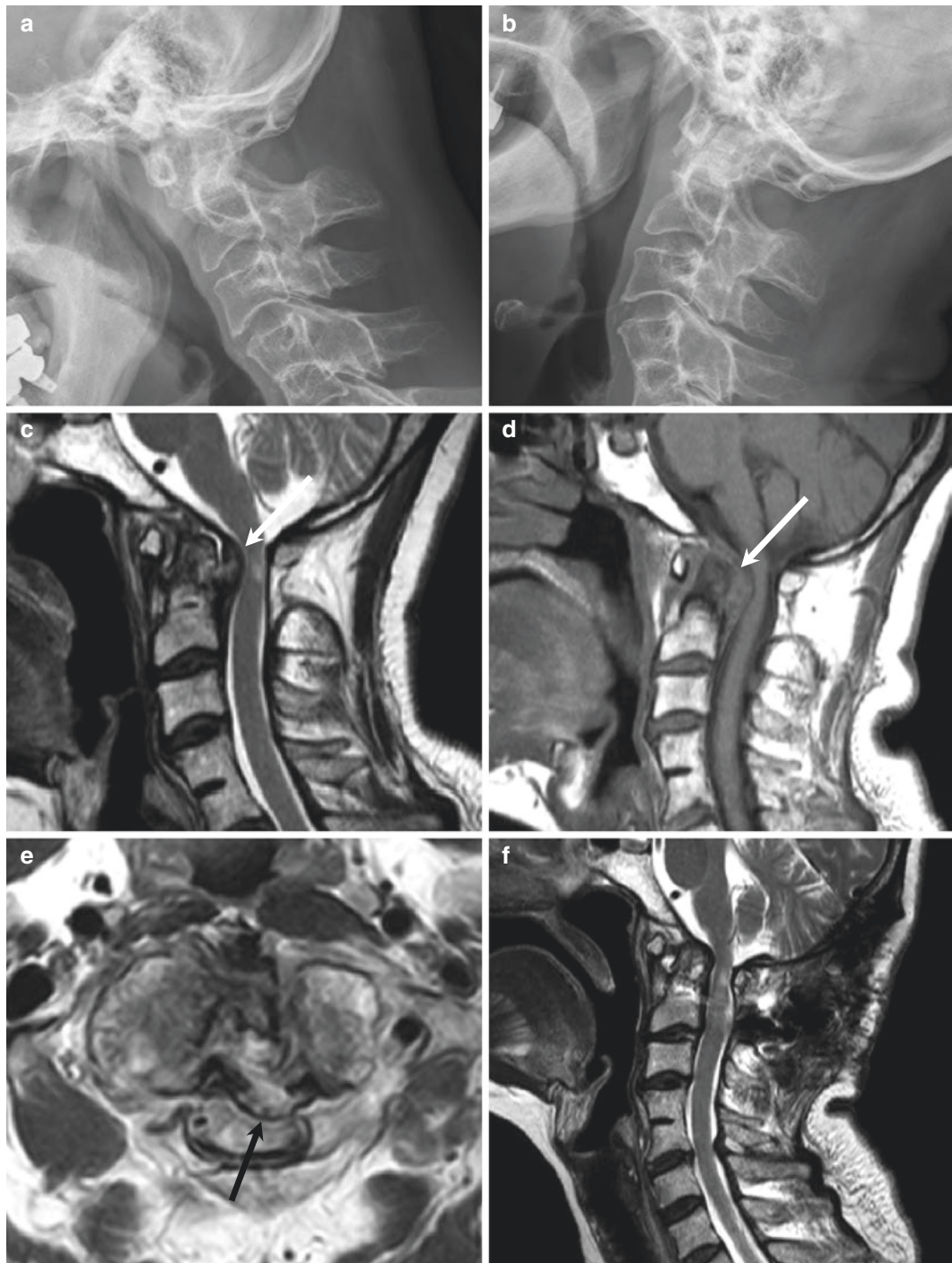
7.13.1 Illustrations: Retro-odontoid (Periodontoid) Pseudotumor

Fig. 7.15 Retro-odontoid pseudotumor in a 54-year-old woman with atlanto-occipital assimilation. Flexion-extension cervical spine lateral radiographs (**a, b**) show C1/C2 instability. T2-weighted sagittal MR image (**c**) shows heterogeneous low signal soft tissue mass of the retro-odontoid space with cord compression and cord sig-

nal change suggesting compressive myelopathy. On the T1-weighted image (**d**), the mass is of iso signal intensity. T2-weighted axial MR image (**e**) shows the soft tissue mass involvement of the transverse ligament (*black arrow*). After surgical fixation of C1/C2, the mass shows markedly decreased size (**f**)

7.14 Facet Synovial Cyst

1. Epidemiology

- More than 60 years
- F > M

2. Location

- Posterolateral to the thecal sac
- Adjacent to the facet joint
- Lumbar spine: 90%
 - L4/L5: 70–80%
- Uncommon
 - Cervical and thoracic spine
 - Foraminal or extraforaminal
 - Bilateral

3. Characteristic imaging findings

- Posterolateral extradural cystic mass communication with facet joint
- Similar to CSF signal on T1- and T2-weighted images
- Well-circumscribed enhancing wall
- Associated ligamentum flavum hypertrophy and facet joint arthropathy

4. Spectrum of imaging findings

- High signal on T1-weighted image due to hemorrhage or proteinaceous content
- Mural calcification

5. Differential diagnosis

- Sequestered disc fragment
 - Uncommon posterolateral location (anterior epidural location)
 - No connection to facet joint
 - Relatively low signal on T2-weighted image
- Ganglion cyst
 - Likely from ligamentum flavum
 - Contains myxoid material lined by fibrous connective tissue capsule
 - Difficult to distinguish using MR
- Cystic nerve sheath tumor
- Epidural abscess

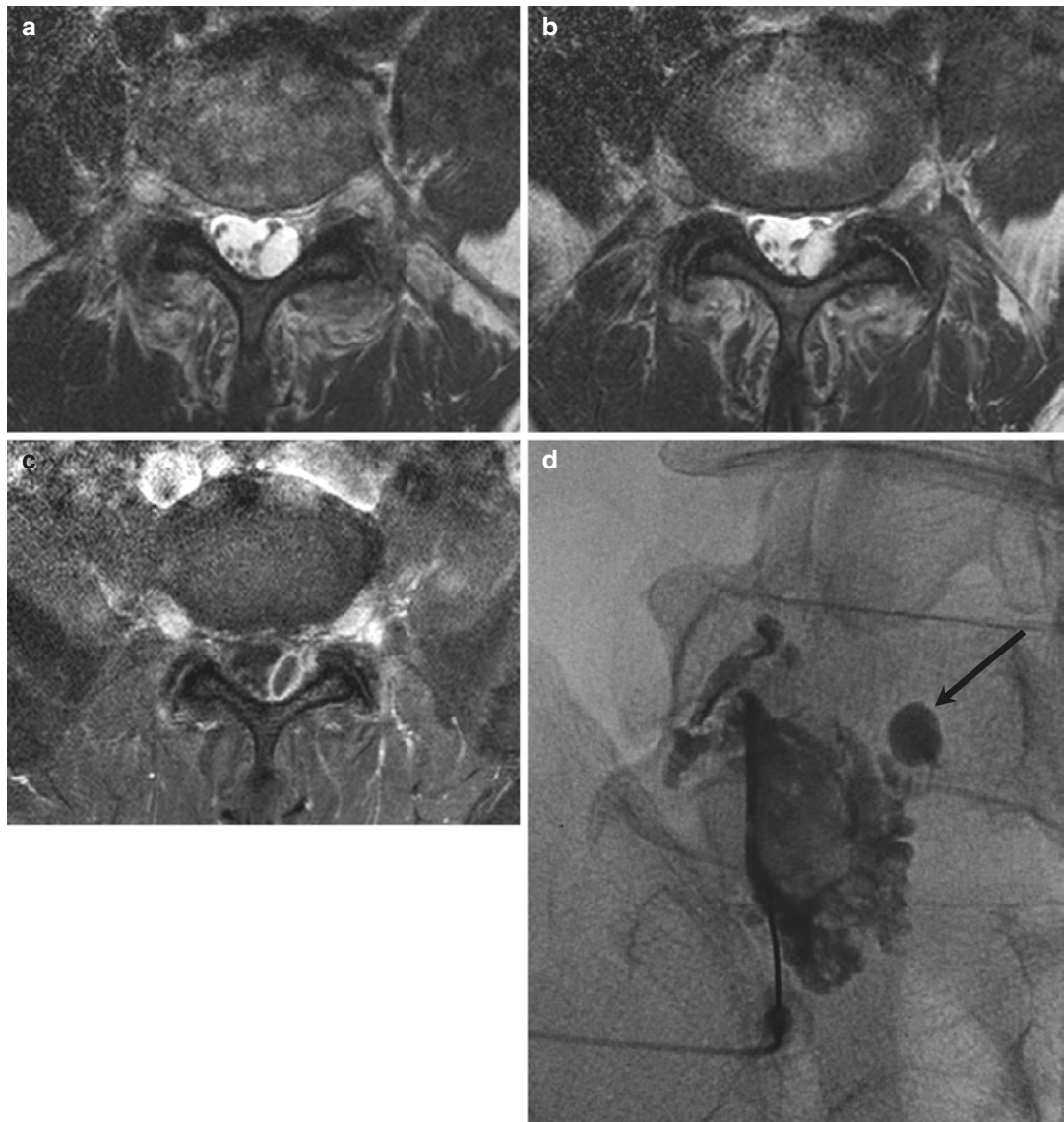
7.14.1 Illustrations: Facet Synovial Cyst

Fig. 7.16 Left facet joint synovial cyst of L5/S1 in a 66-year-old man. T2-weighted axial MR images (**a**, **b**) show a 1.2 cm cystic lesion at the ventral aspect of the left L5/S1 facet joint with mild dural sac compression.

Contrast-enhanced T1-weighted axial image (**c**) shows mild peripheral enhancement. During facet joint injection (**d**), contrast filling into the cyst is well visualized (*black arrow*)

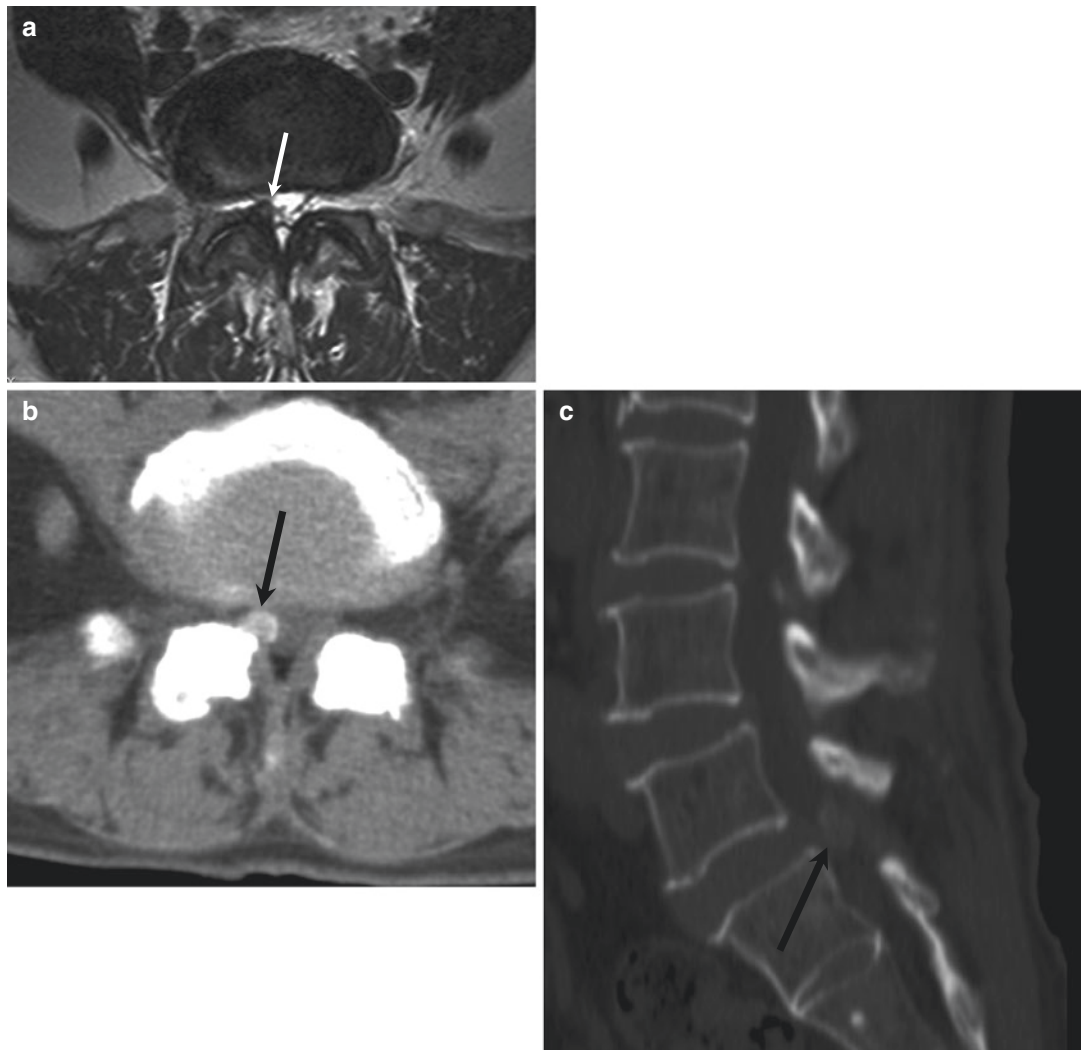


Fig. 7.17 Calcified right facet joint synovial cyst of L5/S1 in a 74-year-old man. Axial T2-weighted MR image at the level of the L5-S1 disc (a) shows a nodular lesion in the right posterolateral epidural space causing compression of the dural sac (*white arrow*). The lesion arises from

right facet joint. A T2 hypointense rim around this nodular lesion was observed. Axial and sagittal CT scan image (b, c) shows the nodular lesion with a calcified rim adjacent to right facet joint of L5-S1 in the right posterolateral epidural space (*black arrows*)

7.15 Tuberculosis

1. Epidemiology

- Most common: 5th decade
- M=F

2. Location

- Thoracolumbar spine: 80%
- Isolated tuberculosis of the sacrum: rare (5%)

3. Characteristic imaging findings

- Diffuse bone marrow edema
- Erosive and osteolytic changes in the bones on CT
- Can mimic neoplastic conditions

4. Spectrum of imaging findings

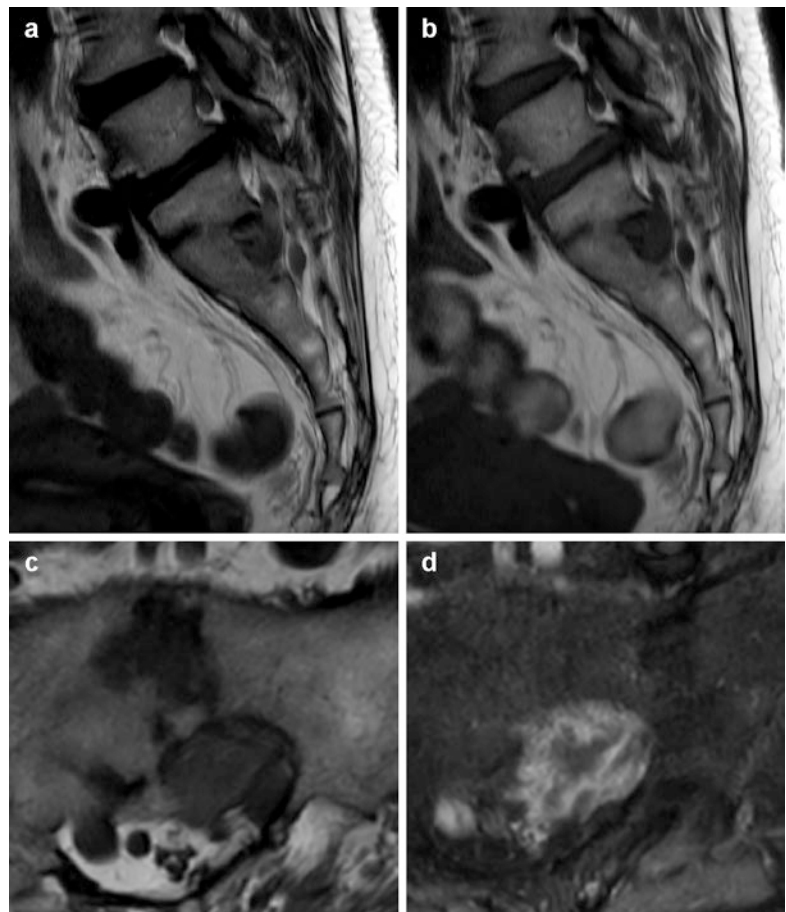
- T1 hypointense and T2 hyperintense signal
- Phlegmon with peripheral enhancing soft tissue
- Calcified chronic paravertebral abscess/endplate fusion

5. Differential diagnosis

- Metastasis

7.15.1 Illustrations: Tuberculosis

Fig. 7.18 Sacral tuberculosis in a 52-year-old woman. (a) T2- and (b) T1-weighted sagittal MR images show a low signal mass-like lesion involving the posterior aspect of the sacrum. Interestingly union of L5 vertebral body and S1 is also noted. On the axial images (c, d), the mass involves the left posterior vertebral body and epidural space with irregular peripheral enhancement. There is no significant bone marrow edema



7.16 Ventriculus Terminalis

1. Epidemiology

- 2.6% in < 5 years old
- Isolated form of ventriculus terminalis in adults: extremely rare

2. Location

- Conus medullaris

3. Characteristic imaging findings

- Well-circumscribed cystic cavity localized inside the conus medullaris

- Identical to CSF signal on T1- and T2-weighted images

- No enhancement

4. Spectrum of imaging findings

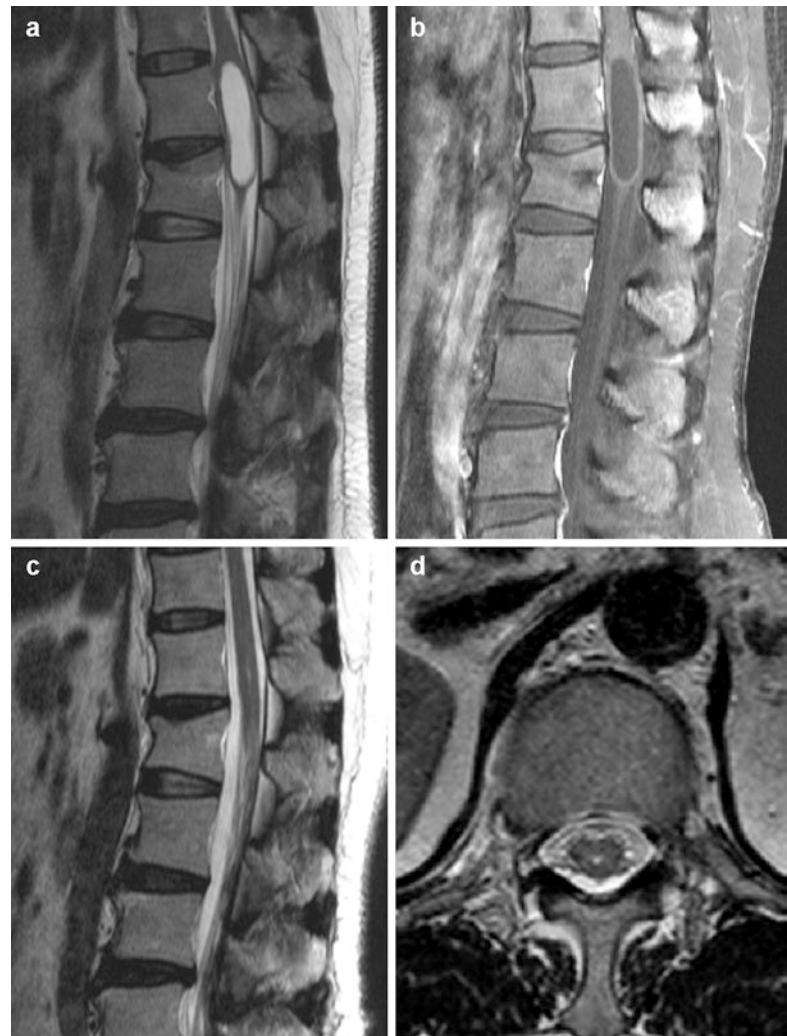
- May be associated with malformations of the CNS (Arnold-Chiari syndrome, syringohydromyelia, tethered cord, spina bifida, myelomeningocele, etc.)

5. Differential diagnosis

- Syringohydromyelia

7.16.1 Illustrations: Ventriculus Terminalis

Fig. 7.19 Incidentally detected ventriculus terminalis in a 49-year-old woman. T2-weighted sagittal MR image (a) shows a well-defined cystic mass-like lesion of the lower thoracic spinal cord extending to the conus medullaris without a definite enhancing portion (b). T2 signal of the internal fluid content appears similar to CSF. After 4-year follow-up, spontaneous regression of the lesion is observed (c, d)



Bibliography

- Alyas F, Saifuddin A, Connell D. MR imaging evaluation of the bone marrow and marrow infiltrative disorders of the lumbar spine. *Magn Reson Imaging Clin N Am.* 2007;15(2):199–219, vi. doi:[10.1016/j.mric.2007.03.002](https://doi.org/10.1016/j.mric.2007.03.002).
- Apostolaki E, Davies AM, Evans N, Cassar-Pullincino VN. MR imaging of lumbar facet joint synovial cysts. *Eur Radiol.* 2000;10(4):615–23. doi:[10.1007/s003300050973](https://doi.org/10.1007/s003300050973).
- Armao DM, Stone J, Castillo M, Mitchell KM, Bouldin TW, Suzuki K. Diffuse leptomeningeal oligodendrogliomatosis: radiologic/pathologic correlation. *AJR Am J Neuroradiol.* 2000;21(6):1122–6.
- Bloomer CW, Ackerman A, Bhatia RG. Imaging for spine tumors and new applications. *Top Magn Reson Imaging TMRI.* 2006;17(2):69–87. doi:[10.1097/RMR.0b013e31802bb38f](https://doi.org/10.1097/RMR.0b013e31802bb38f).
- Boriani S, Bandiera S, Casadei R, Boriani L, Donthineni R, Gasbarrini A, et al. Giant cell tumor of the mobile spine: a review of 49 cases. *Spine.* 2012;37(1):E37–45. doi:[10.1097/BRS.0b013e3182233cccd](https://doi.org/10.1097/BRS.0b013e3182233cccd).
- Caldemeyer KS, Smith RR, Harris A, Williams T, Huang Y, Eckert GJ, et al. Hematopoietic bone marrow hyperplasia: correlation of spinal MR findings, hematologic parameters, and bone mineral density in endurance athletes. *Radiology.* 1996;198(2):503–8. doi:[10.1148/radiology.198.2.8596857](https://doi.org/10.1148/radiology.198.2.8596857).
- Cerase A, Priolo F. Skeletal benign bone-forming lesions. *Eur J Radiol.* 1998;27(Suppl 1):S91–7.
- Chikuda H, Seichi A, Takeshita K, Shoda N, Ono T, Matsudaira K, et al. Radiographic analysis of the cervical spine in patients with retro-odontoid pseudotumors. *Spine.* 2009;34(3):E110–4. doi:[10.1097/BRS.0b013e31818acd27](https://doi.org/10.1097/BRS.0b013e31818acd27).
- Chourmouzi D, Pistevou-Gompaki K, Plataniotis G, Skaragas G, Papadopoulos L, Drevelegas A. MRI findings of extramedullary haemopoiesis. *Eur Radiol.* 2001;11(9):1803–6. doi:[10.1007/s003300000802](https://doi.org/10.1007/s003300000802).
- Coffin CM, Weill A, Miaux Y, Srour A, Cognard C, Dubard T, et al. Posttraumatic spinal subarachnoid cyst. *Eur Radiol.* 1996;6(4):523–5.
- Conner C, Paydar A. Intradural extramedullary arachnoid cyst presenting as arteriovenous malformation in the thoracic spinal cord. *Radiol Case Rep.* 2009;4(2):263. doi:[10.2484/rctr.v4i2.263](https://doi.org/10.2484/rctr.v4i2.263).
- Cramer GD, Darby SA. Clinical anatomy of the spine, spinal cord, and ANS. Philadelphia: Elsevier Health Sciences; 2013.
- Hsu CY, Shih TT, Huang KM, Chen PQ, Sheu JJ, Li YW. Tophaceous gout of the spine: MR imaging features. *Clin Radiol.* 2002;57(10):919–25.
- Hu S, Hu CH, Hu XY, Wang XM, Dai H, Fang XM, et al. MRI features of spinal epidural angiomyomas. *Korean J Radiol.* 2013;14(5):810–7. doi:[10.3348/kjr.2013.14.5.810](https://doi.org/10.3348/kjr.2013.14.5.810).
- Kang HS, Lee JW, Kwon JW. Radiology illustrated: spine. Heidelberg: Springer Science & Business Media; 2014.
- Kim DH, Chang U-K, Kim S-H, Bilsky MH. Tumors of the spine. Philadelphia: Elsevier Health Sciences; 2008.
- Kim JH, Park YM, Chin DK. Idiopathic hypertrophic spinal pachymeningitis : report of two cases and review of the literature. *J Korean Neurosurg Soc.* 2011;50(4):392–5. doi:[10.3340/jkns.2011.50.4.392](https://doi.org/10.3340/jkns.2011.50.4.392).
- Kim K, Chun SW, Chung SG. A case of symptomatic cervical perineural (Tarlov) cyst: clinical manifestation and management. *Skelet Radiol.* 2012;41(1):97–101. doi:[10.1007/s00256-011-1243-y](https://doi.org/10.1007/s00256-011-1243-y).
- Krandsorf MJ, Sweet DE. Aneurysmal bone cyst: concept, controversy, clinical presentation, and imaging. *AJR Am J Roentgenol.* 1995;164(3):573–80. doi:[10.2214/ajr.164.3.7863874](https://doi.org/10.2214/ajr.164.3.7863874).
- Kroon HM, Schurmans J. Osteoblastoma: clinical and radiologic findings in 98 new cases. *Radiology.* 1990;175(3):783–90. doi:[10.1148/radiology.175.3.2343130](https://doi.org/10.1148/radiology.175.3.2343130).
- Kwon JW, Chung HW, Cho EY, Hong SH, Choi SH, Yoon YC, et al. MRI findings of giant cell tumors of the spine. *AJR Am J Roentgenol.* 2007;189(1):246–50. doi:[10.2214/AJR.06.1472](https://doi.org/10.2214/AJR.06.1472).
- Lang N, Yuan HS. Computed tomography and magnetic resonance manifestations of spinal pigmented villonodular synovitis. *J Comput Assist Tomogr.* 2015;39(4):601–6. doi:[10.1097/RCT.0000000000000244](https://doi.org/10.1097/RCT.0000000000000244).
- Lee HK, Lee DH, Choi CG, Kim SJ, Suh DC, Kahng SK, et al. Discal cyst of the lumbar spine: MR imaging features. *Clin Imaging.* 2006;30(5):326–30. doi:[10.1016/j.clinimag.2006.05.026](https://doi.org/10.1016/j.clinimag.2006.05.026).
- Lee JW, Cho EY, Hong SH, Chung HW, Kim JH, Chang KH, et al. Spinal epidural hemangiomas: various types of MR imaging features with histopathologic correlation. *AJR Am J Neuroradiol.* 2007;28(7):1242–8. doi:[10.3174/ajnr.A0563](https://doi.org/10.3174/ajnr.A0563).
- Lu YH, Wang HH, Linng JF, Guo WY, Wong TT, Teng MM, et al. Unusual giant intraspinal teratoma in an infant. *J Chin Med Assoc JCMA.* 2013;76(7):411–4. doi:[10.1016/j.jcma.2013.03.006](https://doi.org/10.1016/j.jcma.2013.03.006).
- Maira G, Amante P, Denaro L, Mangiola A, Colosimo C. Surgical treatment of cervical intramedullary spinal cord tumors. *Neurol Res.* 2001;23(8):835–42. doi:[10.1179/016164101101199432](https://doi.org/10.1179/016164101101199432).
- Marthya A, Patinharayil G, Puthezeth K, Sreedharan S, Kumar A, Kumaran CM. Multicentric epithelioid angiosarcoma of the spine: a case report of a rare bone tumor. *Spine J Off J N Am Spine Soc.* 2007;7(6):716–9. doi:[10.1016/j.spinee.2006.08.013](https://doi.org/10.1016/j.spinee.2006.08.013).
- Merhemic Z, Stosic-Opincal T, Thurnher MM. Neuroimaging of spinal tumors. *Magn Reson Imaging Clin N Am.* 2016;24(3):563–79. doi:[10.1016/j.mric.2016.04.007](https://doi.org/10.1016/j.mric.2016.04.007).
- Meyers SP, Khademian ZP, Biegel JA, Chuang SH, Korones DN, Zimmerman RA. Primary intracranial atypical teratoid/rhabdoid tumors of infancy and childhood: MRI features and patient outcomes. *AJR Am J Neuroradiol.* 2006;27(5):962–71.
- Monajati A, Spitzer RM, Wiley JL, Heggeness L. MR imaging of a spinal teratoma. *J Comput Assist Tomogr.* 1986;10(2):307–10.

- Moscovici S, Ramirez-DeNoriega F, Fellig Y, Rosenthal G, Cohen JE, Itshayek E. Intradural extramedullary hemangiopericytoma of the thoracic spine infiltrating a nerve root: a case report and literature review. *Spine*. 2011;36(23):E1534–9. doi:[10.1097/BRS.0b013e31822ddd4](https://doi.org/10.1097/BRS.0b013e31822ddd4).
- Murphy MD, Andrews CL, Flemming DJ, Temple HT, Smith WS, Smirniotopoulos JG. From the archives of the AFIP. Primary tumors of the spine: radiologic-pathologic correlation. *Radiographics Rev Publ Radiol Soc N Am Inc.* 1996;16(5):1131–58. doi:[10.1148/radiographics.16.5.8888395](https://doi.org/10.1148/radiographics.16.5.8888395).
- Murphy MD, Fairbairn KJ, Parman LM, Baxter KG, Parsa MB, Smith WS. From the archives of the AFIP. Musculoskeletal angiomatous lesions: radiologic-pathologic correlation. *Radiographics Rev Publ Radiol Soc N Am Inc.* 1995;15(4):893–917. doi:[10.1148/radiographics.15.4.7569134](https://doi.org/10.1148/radiographics.15.4.7569134).
- Nishiguchi T, Mochizuki K, Ohsawa M, Inoue T, Kageyama K, Suzuki A, et al. Differentiating benign notochordal cell tumors from chordomas: radiographic features on MRI, CT, and tomography. *AJR Am J Roentgenol.* 2011;196(3):644–50. doi:[10.2214/AJR.10.4460](https://doi.org/10.2214/AJR.10.4460).
- Orguc S, Arkun R. Primary tumors of the spine. *Semin Musculoskelet Radiol.* 2014;18(3):280–99. doi:[10.1055/s-0034-1375570](https://doi.org/10.1055/s-0034-1375570).
- Papakonstantinou O, Athanassopoulou A, Passomenos D, Kalogeropoulos I, Balanika A, Baltas C, et al. Recurrent vertebral hydatid disease: spectrum of MR imaging features. *Singap Med J.* 2011;52(6):440–5.
- Parmar H, Shah J, Patwardhan V, Patankar T, Patkar D, Muzumdar D, et al. MR imaging in intramedullary cysticercosis. *Neuroradiology.* 2001;43(11):961–7.
- Rodallec MH, Feydy A, Larousserie F, Anract P, Campagna R, Babinet A, et al. Diagnostic imaging of solitary tumors of the spine: what to do and say. *Radiographics Rev Publ Radiol Soc N Am Inc.* 2008;28(4):1019–41. doi:[10.1148/radiographics.2841019](https://doi.org/10.1148/radiographics.2841019).
- Ross JS, Moore KR. Diagnostic imaging: spine. Philadelphia: Elsevier Health Sciences; 2015.
- Sardaro A, Bardoscia L, Petruzzelli MF, Portaluri M. Epithelioid hemangioendothelioma: an overview and update on a rare vascular tumor. *Oncol Rev.* 2014;8(2):259. doi:[10.4081/oncol.2014.259](https://doi.org/10.4081/oncol.2014.259).
- Shin JY, Lee SM, Hwang MY, Sohn CH, Suh SJ. MR findings of the spinal paraganglioma : report of three cases. *J Korean Med Sci.* 2001;16(4):522–6. doi:[10.3346/jkms.2001.16.4.522](https://doi.org/10.3346/jkms.2001.16.4.522).
- Si MJ, Wang CG, Wang CS, Du LJ, Ding XY, Zhang WB, et al. Giant cell tumours of the mobile spine: characteristic imaging features and differential diagnosis. *La Radiologia Medica.* 2014;119(9):681–93. doi:[10.1007/s11547-013-0352-1](https://doi.org/10.1007/s11547-013-0352-1).
- Sivalingam J, Kumar A. Spinal tuberculosis resembling neoplastic lesions on MRI. *J Clin Diagn Res JCDR.* 2015;9(11):TC01–3. doi:[10.7860/JCDR/2015/14030.6719](https://doi.org/10.7860/JCDR/2015/14030.6719).
- Stabler A, Reiser MF. Imaging of spinal infection. *Radiol Clin N Am.* 2001;39(1):115–35.
- Thakar S, Hegde AS. Symmetric paraspinal lesions in a young adult. *Radiographics Rev Publ Radiol Soc N Am Inc.* 2013;13(9):1165–6. doi:[10.1016/j.spinee.2013.05.049](https://doi.org/10.1016/j.spinee.2013.05.049).
- Vialle R, Feydy A, Rillardon L, Tohme-Noun C, Anract P, Colombari M, et al. Chondroblastoma of the lumbar spine. Report of two cases and review of the literature. *J Neurosurg Spine.* 2005;2(5):596–600. doi:[10.3171/spi.2005.2.5.0596](https://doi.org/10.3171/spi.2005.2.5.0596).
- Walker EA, Salesky JS, Fenton ME, Murphy MD. Magnetic resonance imaging of malignant soft tissue neoplasms in the adult. *Radiol Clin N Am.* 2011;49(6):1219–34, vi. doi:[10.1016/j.rcl.2011.07.006](https://doi.org/10.1016/j.rcl.2011.07.006).
- Wallace ZS, Carruthers MN, Khosroshahi A, Carruthers R, Shinagare S, Stemmer-Rachamimov A, et al. IgG4-related disease and hypertrophic pachymeningitis. *Medicine.* 2013;92(4):206–16. doi:[10.1097/MD.0b013e31829cce35](https://doi.org/10.1097/MD.0b013e31829cce35).
- Wu L, Deng X, Yang C, Xu Y. Spinal intradural malignant peripheral nerve sheath tumor in a child with neurofibromatosis type 2: the first reported case and literature review. *Turk Neurosurg.* 2014;24(1):135–9. doi:[10.5137/1019-5149.JTN.8104-13.0](https://doi.org/10.5137/1019-5149.JTN.8104-13.0).
- Yen PS, Lin JF, Chen SY, Lin SZ. Tophaceous gout of the lumbar spine mimicking infectious spondylodiscitis and epidural abscess: MR imaging findings. *J Clin Neurosci Off J Neurosurgical Soc Australasia.* 2005;12(1):44–6. doi:[10.1016/j.jocn.2004.03.020](https://doi.org/10.1016/j.jocn.2004.03.020).
- Yoo M, Lee CH, Kim KJ, Kim HJ. A case of intradural-extramedullary form of primary spinal cysticercosis misdiagnosed as an arachnoid cyst. *J Korean Neurosurg Soc.* 2014;55(4):226–9. doi:[10.3340/jkns.2014.55.4.226](https://doi.org/10.3340/jkns.2014.55.4.226).

Part III

Final Steps: Differential Diagnosis

Practical Tips for Differential Diagnosis

8

Contents

8.1	Focal Red Marrow Versus Metastasis	232	8.9	Intramedullary Metastasis Versus Ependymoma	240
8.2	Hemangioma Versus Benign Notochordal Cell Tumor (BNCT)	233	8.10	Hemangioblastoma Versus Vascular Malformation	241
8.3	Aggressive Hemangioma Versus Metastasis	234	8.11	Schwannoma Versus Meningioma	242
8.4	Hemangioma Versus Focal Fat Deposition	235	8.12	Herniated Intervertebral Disc (Sequestration) Versus Schwannoma	243
8.5	Metastasis Versus Schmorl's Node	236	8.13	Sacral Tumors: Chordoma Versus Giant Cell Tumor	244
8.6	Osteoblastic Metastasis Versus Bone Island	237	8.14	Spinal Cord Tumor Versus Non-tumorous Myelopathy	245
8.7	Ependymoma Versus Astrocytoma	238	8.15	Osteoblastoma Versus Osteosarcoma	246
8.8	Multiple Myeloma Versus Lymphoma	239	8.16	Chondrosarcoma Versus Osteosarcoma	247
			8.17	Primary Versus Secondary Aneurysmal Bone Cyst (ABC)	248

8.1 Focal Red Marrow Versus Metastasis

	Focal red marrow (Fig. 8.1a, b)	Metastasis (Fig. 8.1c, d)
Similarities	Focal nodule Lower signal on T1-weighted image than that of surrounding fatty marrow Enhancement	
Differences	Isointense or slightly hyperintense to the intervertebral disc on T1-weighted images Bright central area on T1-weighted images Patchy enhancement	Hypointense to the intervertebral disc on T1-weighted images No central fatty area Strong enhancement

Fig. 8.1



8.2 Hemangioma Versus Benign Notochordal Cell Tumor (BNCT)

	Hemangioma (Fig. 8.2a–c)	BNCT (Fig. 8.2d–f)
Similarities	Well-defined round mass in the vertebral body Preserved vertical trabeculation T2-hyperintensity	
Differences	T1-hyperintensity Well enhancement No sclerosis on CT	T1-hypointensity No enhancement Sclerosis on CT



Fig. 8.2

8.3 Aggressive Hemangioma Versus Metastasis

	Aggressive hemangioma (Fig. 8.3a–c)	Metastasis (Fig. 8.3d–f)
Similarities	Osteolytic mass in the vertebral body Contrast enhancement on MRI	
Differences	Thickened but preserved bony trabeculation Portion of T1-hyperintensity Round, Well-defined	Destructive bony trabeculation No area of T1-hyperintensity Poorly-defined



Fig. 8.3

8.4 Hemangioma Versus Focal Fat Deposition

	Hemangioma (Fig. 8.4a, b)	Focal fat deposition (Fig. 8.4c, d)
Similarities	Focal lesion with T1-hyperintensity in the vertebral body	
Differences	Round or ovoid Well-defined enhancement	Irregular shape Poorly-defined No enhancement

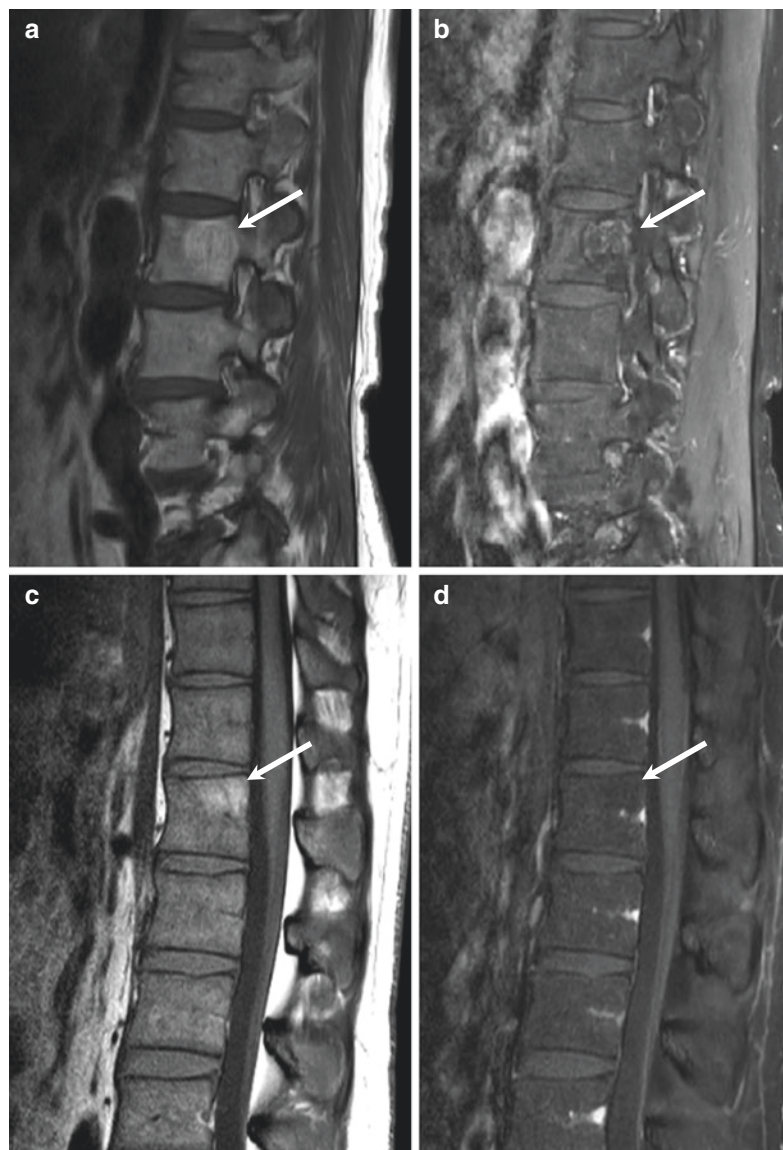


Fig. 8.4

8.5 Metastasis Versus Schmorl's Node

	Metastasis (Fig. 8.5a, b)	Schmorl's node (Fig. 8.5c, d)
Similarities	Focal nodular bony destruction in the vertebral body adjacent endplate Can be enhanced	
Differences	Peripheral rim-like edema Stronger enhancement No continuity with intervertebral disc	Endplate disruption Continuity with intervertebral disc

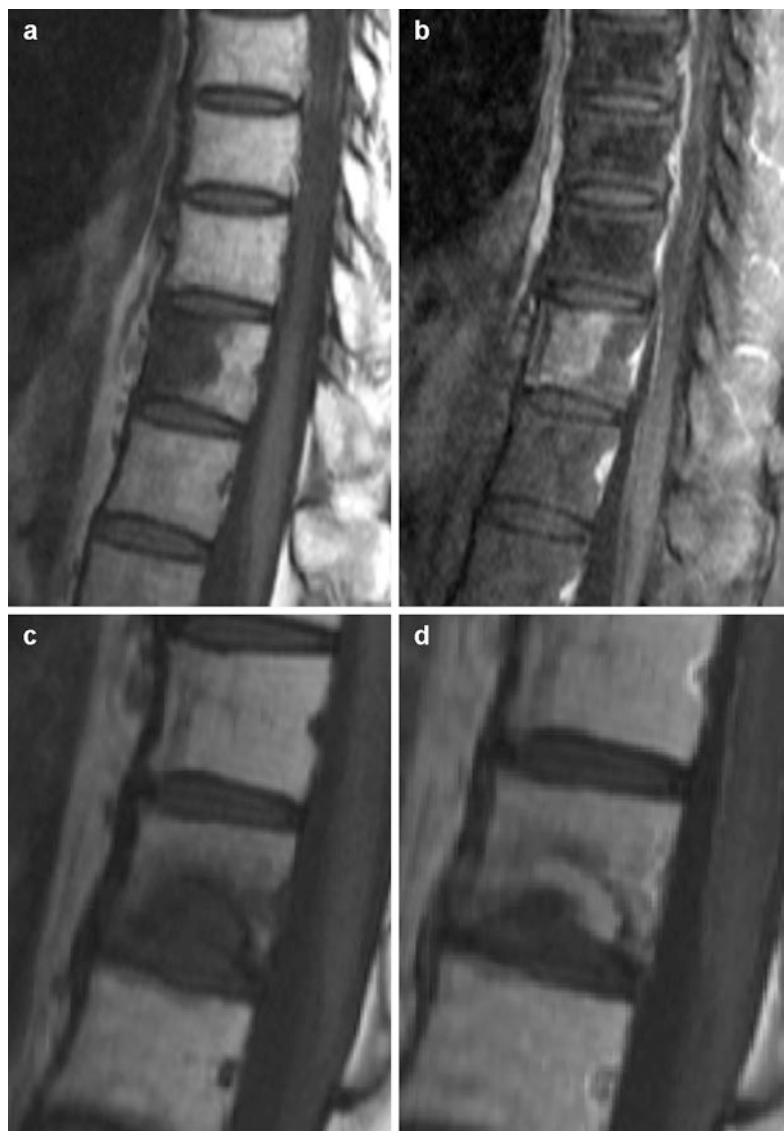


Fig. 8.5

8.6 Osteoblastic Metastasis Versus Bone Island

	Osteoblastic Metastasis (Fig. 8.6a–c)	Bone island (Fig. 8.6d–f)
Similarities	Osteoblastic mass in the vertebral body	
Differences	Multiple Peripheral enhancement Underling malignancy	Single No enhancement

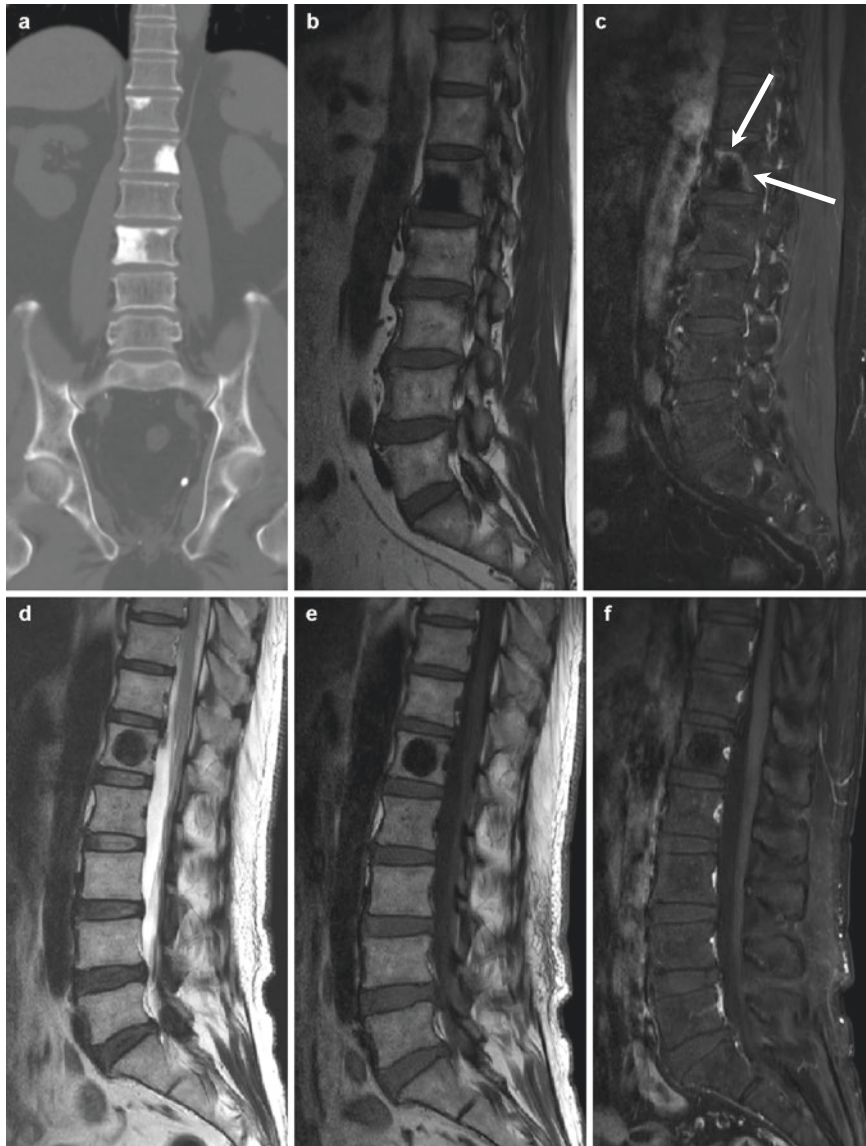


Fig. 8.6

8.7 Ependymoma Versus Astrocytoma

	Ependymoma (Fig. 8.7a, b)	Astrocytoma (Fig. 8.7c, d)
Similarities	Intramedullary tumors	
Differences	Central location Well-defined margin Common cystic change or hemorrhage (cap sign)	Eccentric location Poorly-defined margin Cystic change or hemorrhage is uncommon

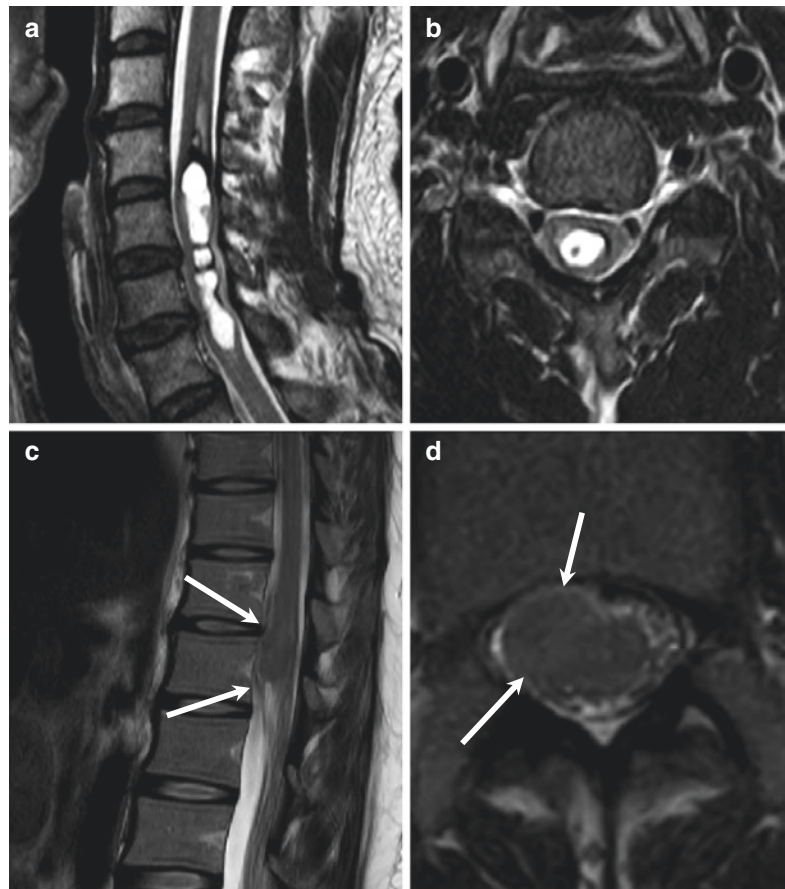


Fig. 8.7

8.8 Multiple Myeloma Versus Lymphoma

	Multiple myeloma (Fig. 8.8a, b)	Lymphoma (Fig. 8.8c, d)
Similarities	Extensive bone marrow signal change	
Differences	Diffuse bone marrow signal change Small variable-sized intraosseous masses ("variegated appearance") Multiple compression fractures (osteoporotic – pattern) Older ages No epidural or paravertebral mass	Multi-compartment involvement – epidural, leptomeningeal involvement T2-isointensity Young adult



Fig. 8.8

8.9 Intramedullary Metastasis Versus Ependymoma

	Intramedullary metastasis (Fig. 8.9a, b)	Ependymoma (Fig. 8.9c, d)
Similarities	Intramedullary round or ovoid mass Strong enhancement	
Differences	Extensive longitudinal spinal cord edema No syrinx Less hemorrhage	Syrinx Hemosiderin cap



Fig. 8.9

8.10 Hemangioblastoma Versus Vascular Malformation

	Hemangioblastoma (Fig. 8.10a, b)	Vascular malformation (Fig. 8.10c, d)
Similarities	Hypervascul ar intramedullary mass or mass-like lesion with prominent perimedullary venous plexus	
Differences	Subpial location Strong enhancement Large syrinx	Abnormal tangled vascular mass Venous dilatation (T2-dark signal) No syrinx Intramedullary T2-hyperintensity



Fig. 8.10

8.11 Schwannoma Versus Meningioma

	Schwannoma (Fig. 8.11a, b)	Meningioma (Fig. 8.11c, d)
Similarities	Intradural extramedullary located tumors	
Differences	<p>Nerve sheath origin</p> <p>No calcification</p> <p>Very high signal intensity on T2-weighted image</p> <p>Heterogeneous enhancement (cystic change, hemorrhage)</p> <p>No dural attachment</p> <p>Variable vascularity</p>	<p>Dura matter origin</p> <p>May have intratumoral calcification</p> <p>Isointense to spinal cord on T1- and T2-weighted images</p> <p>Homogeneous enhancement</p> <p>Dural tail sign</p> <p>Hypervascular tumor staining on conventional angiography</p>



Fig. 8.11

8.12 Herniated Intervertebral Disc (Sequestration) Versus Schwannoma

	Herniated intervertebral disc (sequestration) (Fig. 8.12a, b)	Schwannoma (Fig. 8.12c, d)
Similarities	Epidural mass Can be similar signal on T2-weighted image (high or low signal in both) Can be enhanced	
Differences	Peripheral enhancement (with inner T2-low signal area) Inner low signal on T2-weighted image (commonly) Radial tear or protrusion in the near side of parent intervertebral disc	Homogeneous enhancement or peripheral enhancement (with inner T2-high signal) High signal on T2-weighted image (commonly) Dumbbell shape, bone erosion

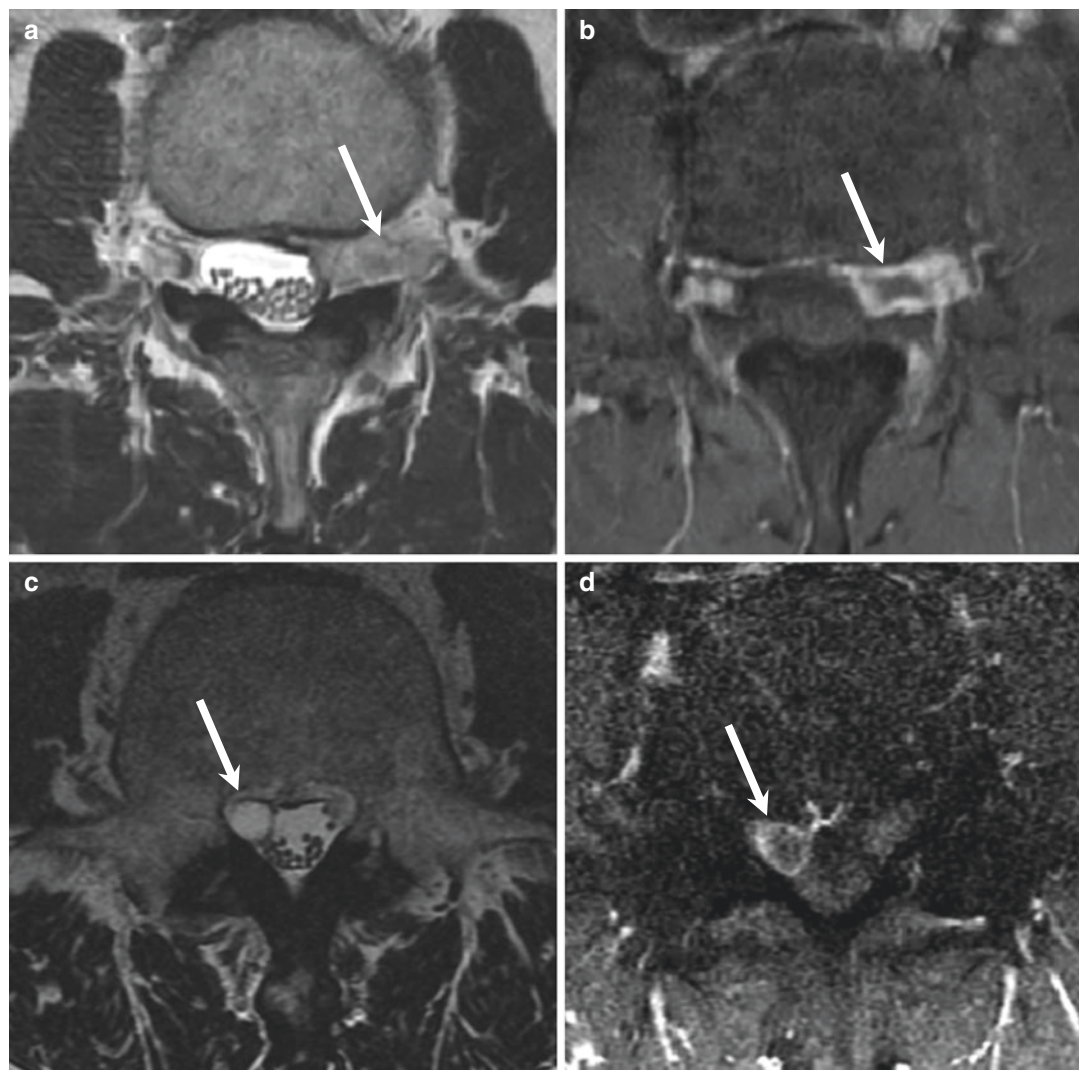


Fig. 8.12

8.13 Sacral Tumors: Chordoma Versus Giant Cell Tumor

	Chordoma (Fig. 8.13a,b)	Giant cell tumor (Fig. 8.13c,d)
Similarities	Sacral tumors Bony destructive tumors	
Differences	Malignancy	Benign
	Midline or paramedian location	Eccentric location
	Intratumoral calcification	No calcification
	Very high signal intensity on T2-weighted image	Low to intermediate signal intensity on T2-weighted image
	Homogeneous enhancement	Heterogeneous enhancement
	Myxoid and mucin contents	Cystic change and hemosiderin contents

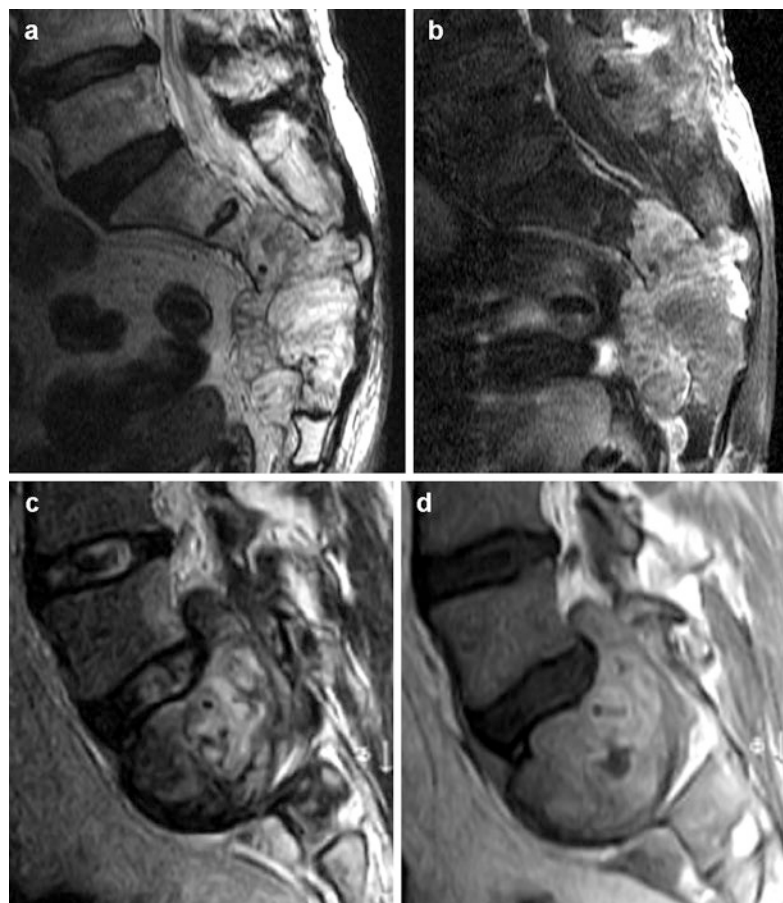


Fig. 8.13

8.14 Spinal Cord Tumor Versus Non-tumorous Myelopathy

	Spinal cord tumor (Fig. 8.14a, b)	Non-neoplastic myelopathy (Fig. 8.14c, d)
Similarities	Intramedullary T2-hyperintensity Enhancement within spinal cord	
Differences	Usually single lesion	Can be multiple lesions with skip areas
	Always spinal cord expansion	Sometimes normal caliber of spinal cord
	Mostly enhanced	Sometimes nodular, sometimes absent enhancement
	Hypointense solid area on T2WI	Usually homogeneous T2-hyperintensity
	Increased size of the lesion on follow-up	Variable changes on follow-up



Fig. 8.14

8.15 Osteoblastoma Versus Osteosarcoma

	Osteoblastoma (Fig. 8.15a, b)	Osteosarcoma (Fig. 8.15c, d)
Similarities	Osteolytic mass with inner osteoid matrix	
Differences	Osteolytic mass in the posterior element Surrounding edema Posterior element Narrow zone of transition	Aggressive bony destruction Irregular inner ossification Wide zone of transition Cortical breakage with soft tissue mass formation

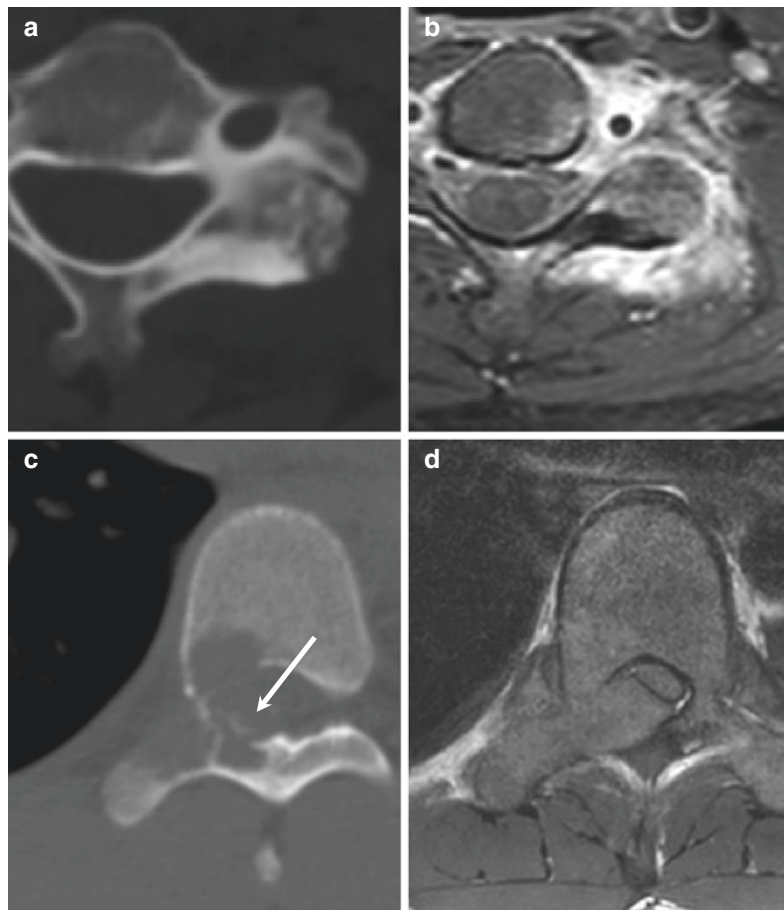


Fig. 8.15

8.16 Chondrosarcoma Versus Osteosarcoma

	Chondrosarcoma (Fig. 8.16a, b)	Osteosarcoma (Fig. 8.16c, d)
Similarities	Osteolytic mass	
Differences	Ring and arc type calcification T2 bright high signal	Inner ossification Heterogeneous T2 signal



Fig. 8.16

8.17 Primary Versus Secondary Aneurysmal Bone Cyst (ABC)

	Primary ABC (Fig. 8.17a, b)	Secondary ABC (Fig. 8.17c, d)
Similarities	Osteolytic mass with inner fluid-fluid level Ballooning appearance with cortical thinning	
Differences	No solid enhancement No cortical destruction	Portion of solid enhancement Cortical destruction with soft tissue mass formation

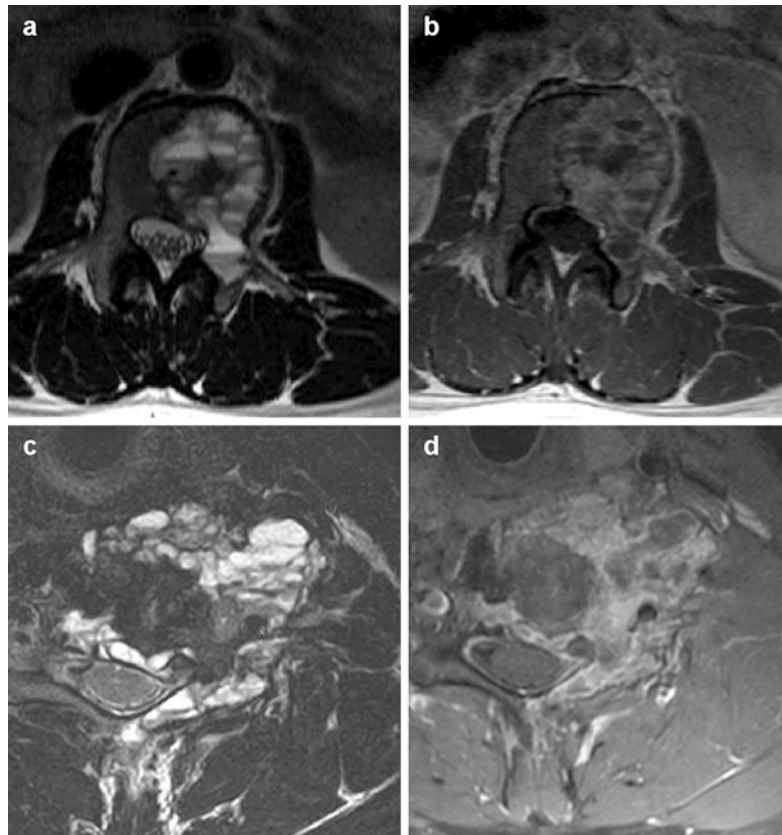


Fig. 8.17